This is to certify that the
dissertation entitled

FLEXURAL RESPONSE OF REINFORCED CONCRETE BEAMS EXPOSED TO FIRE

presented by

MONTHER B.M. DWAIKAT

has been accepted towards fulfillment
of the requirements for the

Ph.D. degree in Civil Engineering

Major Professor's Signature

5/13/2009

Date

FLEXURAL RESPONSE OF REINFORCED CONCRETE BEAMS EXPOSED TO FIRE

VOLUME I

By

Monther B.M. Dwaikat

A DISSERTATION

Submitted to
Michigan State University
in partial fulfillment of the requirements
for the degree of

DOCTOR OF PHILOSOPHY

Civil Engineering

2009

ABSTRACT

FLEXURAL RESPONSE OF REINFORCED CONCRETE BEAMS EXPOSED TO FIRE

BY

Monther B.M. Dwaikat

Reinforced concrete (RC) structural systems are quite frequently used in high-rise buildings and other built infrastructure due to a number of advantages they provide over other materials. When used in buildings, the provision of appropriate fire safety measures to structural members is an important aspect of design since fire represents one of the severe environmental conditions to which structures may be subjected in their life time.

There is very limited information on the fire performance of RC beams, especially under realistic loading and fire conditions. Further, the current fire resistance (FR) provisions in codes and standards are prescriptive and of limited scope, and thus may not be applicable in a performance-based code environment. To overcome these knowledge gaps, the current study focuses on developing a fundamental understanding of the flexural response of RC beams under fire conditions.

A numerical model, in the form of a computer program, is developed for tracing the fire response of RC beams. The model, based on macroscopic finite element approach, undertakes the FR analysis in three steps, namely, evaluating fire temperature, thermal, and structural analyses. The model accounts for fire induced spalling (through a hydro-thermal sub-model derived based on the principles of mechanics and thermodynamics), fire induced axial restraint, various strain components, and high temperature material properties. At each time step, fire induced axial restraint force is evaluated by satisfying compatibility, equilibrium and convergence criteria along the span of the beam.

The numerical model is validated by undertaking fire tests on six RC (two normal strength concrete and four high strength concrete) beams under realistic loading, restraint and fire scenarios. The validated model is utilized to conduct a series of parametric studies to investigate the effect of various influencing parameters on the FR of RC beams. Results from the parametric studies and FR experiments indicate that fire scenario, load ratio, span-to-depth ratio, and support restraints have significant influence on the FR of RC beams. Other factors such as sectional dimensions, aggregate type, axial restraint stiffness, concrete type and spalling, and failure criteria have moderate influence on the fire response.

Results from the parametric studies are utilized to develop a design approach for evaluating fire resistance of RC beams. The proposed approach comprises of evaluating FR under standard fire conditions and then establishing equivalency between standard and design fire scenarios. The empirical relationship for FR under standard fire conditions is expressed as a function of governing parameters. The equivalency between standard and design fire scenarios is derived based on the equal energy (resulting from fire exposure) concept. The proposed approach expresses FR in terms of commonly used structural parameters and thus can easily be integrated into structural design. The validity of the proposed design approach is established by comparing the FR predictions of RC beams with those obtained from detailed finite element analysis, fire test data, and current code provisions. The proposed approach provides better FR estimates than current code provisions and thus can facilitate rational fire design under performance-based code environment.

DEDICATION

I dedicate this dissertation to my parents. Without their caring support and encouragement, I would have never been in the graduate school pursuing the graduate studies.

I also dedicate this work to my brothers and sisters who are always happy for me and my success.

ACKNOWLEDGMENT

I wish to express my most sincere gratitude to my advisor Dr. Venkatesh Kodur, Professor of Civil Engineering, Michigan State University, for the encouragement and guidance received throught the course of this study. It is very hard to appreciate, in few words, his patience and perseverance which made my graduate studies very educational.

I would also like to thank Prof. Ronald Harichandran, Prof. Parviz Soroushian and Prof. Indrek Wichman for joining my Ph.D committee, and for the valuable advice and discussions we had throughout my stay at MSU.

For many reasons that I cannot count, I am thankful to my friends Mohammad Sharief, Mahmoud Dwaikat, and Mohammad Halloush. Although a few words are not enough to do so, but this is the available space I have.

I would like to thank the lab manager, Mr. Siavosh Ravanbakhsh for his support and help during the experimental program in this research.

Obviously, I would like to extend my thanks to Laura Taylor, Mary Mroz, and Margaret Conner for all the help they offered to go through the complications I faced.

I would like to thank Aqeel Ahmad, Goli Nossoni, Kashinath Telsang, Mahmoud Haq, Megan Vivian, Nnaemeka Ezekwmba, Nickolas Hatinger, Nikhil Raut, Nishan Harichandran, Purushutham Pakala, Rustin Fike, Syed Haider, Shahid Iqbal, Spencer Cain and Wasim Khaliq for their support, particularly in the experimental part of this study.

There are many people I have met during my academic and social life, and the conversations we had affect me in one way or another, therefore, I would like to extend my sincere thanks to them, Yaser Aladam, Ahmad Daraghmeh, Rami Halloush, Fuad Abu-Jarad, Hassan Abdelkareem, Mahmood Khassawneh, Ahmad Masa'deh, Qasem Al-Zoubi, Salama Fayyad, Nizar Lajnef, Kavita Kamat, Sonali Kand, Nikhil Choudry, Kishore Balasubramanian, and Lensir Gu.

Finally, I would like to thank all the faculty members and students at the civil and environmental engineering department at Michigan State University for their help and support during my Ph.D. study.

TABLE OF CONTENTS

LIST OF TABLES

LIST OF FIGURES

NOTATION

A = area of boundary exposed to fire

A_d = the area under the heat flux curve of a design fire

A_m = area of each element

A_s = the area under the heat flux curve of ASTM E119 standard fire

ax = axial restraint ratio

b = beam width

b_t = thermal inertia

B = calibration parameter for permeability

c = clear concrete cover

C_t = total compressive force in the beam cross section

C_T = factor to account for the increase in concrete permeability at elevated temperatures

d = effective depth of the beam

D = extent of damage

D_0 = diffusion coefficient of water vapor at the boundaries of the beam

E = mass of evaporated water

E_c = modulus of elasticity of concrete

E_d = total energy under the heat flux curve of the design fire

E_s = total energy under the heat flux curve of the standard fire, and

E_t = total energy

F = equivalent nodal heat flux

$f_{c,20}$ = concrete strength at room temperature

$f_{c,T}$ = concrete strength at temperature, T

f_t = tensile strength of concrete at room temperature

f_{tT} = tensile strength of concrete for temperature, T

F_v = ventilation factor

f_y = yield strength of steel

F_n and F_{n+1} = equivalent nodal heat flux at the beginning and the end of time step, respectively

h = time step

H = total depth of concrete section

h_f and h_c = heat transfer coefficient of the fire side and the cold side, respectively

h_{rad} and h_{con} = radiative and convective heat transfer coefficient

J = mass flux of water vapor

k = thermal conductivity

K = global stiffness matrix

k_0 = initial intrinsic permeability of concrete at room temperature

k_2 = a constant for transient strain calculations and it ranges between 1.8 and 2.35

$k_{damaged}$ and $k_{undamaged}$ = permeability of damaged and undamaged concrete, respectively

K_g = global stiffness matrix for strength analysis

K_{geo} = geometric stiffness matrix

k_r = axial restraint stiffness

k_T = intrinsic permeability of concrete at any temperature

k_{top} = initial permeability in the top surface of the concrete section

L = length of the beam

l_i = projected length of deformed segment i

L_i = length of segment i in the undeformed beam

LR = load ratio

L_s = length of the beam segment

M = molar mass of water (or global mass matrix)

m_0 = mass of water for saturation at 25 °C per unit volume of concrete

m_c = moisture content

m_D = mass of liquid water formed due to dehydration

m_L = mass of liquid water at any time

m_{L0} = mass of water for saturation at any temperature per unit volume of concrete,

m_{LW0} = initial mass of liquid water

m_V = mass of water vapor

n = porosity of concrete

N = vector of the shape functions

n_y and n_z = components of the vector normal to the boundary in the plane of the cross section

n_V = number of moles of water vapor

P_0 = standard atmospheric pressure

P_f = equivalent nodal load vector due to applied loading

P_i, ε_{0i} and κ_i = the axial force, central total strain, and curvature in segment i

P_s = equivalent nodal load vector due to P-δ effect

P_S = saturation pressure

P_{S0} = initial saturation pressure

P_V = vapor pressure

q = heat flux

q_{rad} and q_{con} = radiative and convective heat fluxes.

Q = heat source

r = cooling rate

R = gas constant (or fire resistance)

R_0 = initial estimate of fire resistance

RH = initial relative humidity in the concrete

s = distance along the boundary Γ

s_i = length of deformed segment i

SF = section factor = heated parameter/ cross sectional area

t = time

t^* = fictitious time in Eurocode parametric fire

T = temperature

T_0 = initial temperature

t_d = burning duration of fire

t_e = time equivalent between a design and a standard fire

T_E = temperature of the environment surrounding the boundary

$t_{e(energy)}$ = time equivalent computed from equivalent energy method

$t_{e(FE)}$ = time equivalent computed from maximum deflection method (or finite element analysis)

t_h = time (hours)

T_f = fire temperature

t_s = time at which the area under the heat flux curve is being evaluated

t_t = total duration of fire

T_t = total tensile force in the beam cross section

T_∞ = fire or ambient temperature depending on the boundary

T_{max} = maximum fire temperature

u = variable in finite element analysis which can be temperature or pore pressure

$\dot{u}$ = the derivative of u with respect to time

u_n and u_{n+1} = values of u at the beginning and the end of time step, respectively

V_D = volume fraction of dehydrated liquid water

V_L = volume fraction of liquid water

V_{S0} = initial volume fraction of solid

V_V = volume fraction of water vapor

w = applied distributed load

w_{i1}^{n-1} and w_{i2}^{n-1} = deflections at the beginning and the end of the beam segment which were computed in the $(n\text{-}1)^{th}$ time step

w_{i1}^{n} and w_{i2}^{n} = deflections at the beginning and the end of the beam segment in the n^{th} time step

x = depth of neutral axis under service loads

y = the distance from the geometrical centroid of the beam

y_{top} = distance from the top most fibers of the concrete section

Y = location of axial restraint force from the top most fibers of the concrete section

Z = Zener-Hollomon parameter for creep strain

α and β = calibration constants for permeability to be determined from experiment

χ = number of corner bars/total number of bars.

δ = nodal displacements

Δ = total expansion in the beam length

$\Delta\varepsilon_{th}$ = change in thermal strain

$\Delta\varepsilon_{tr}$ = change in transient strain

ε = emissivity

ε_0 = total strain at the geometrical centroid of the beam cross section

ε_c = strain at the top most fibers of concrete

ε_{cr}, ε_{me}, ε_t, ε_{th} and ε_{tr} = creep strain, mechanical strain, total strain, thermal strain, and transient strain

ε_{crs}, ε_{mes}, ε_{ths} and ε_{ts} = creep strain, mechanical strain, thermal strain and total strain in steel.

ε_{t0} = creep strain parameter

ϕ = structural modification factor in evaluating the fire resistance of reinforced concrete beams

ϕ_{agg} and ϕ_s = factors in evaluating the fire resistance of reinforced concrete beams to account for aggregate type and concrete strength, respectively.

ϕ_{SS} = structural modification factor for fire resistance of simply supported beams

ϕ_{AR} = structural modification factor for fire resistance of axially restrained beams

ϕ_{ER} = structural modification factor for fire resistance of eccentrically axially restrained beams

ϕ_{RR} = structural modification factor for fire resistance of rotationally restrained beams

ϕ_{FR} = structural modification factor for fire resistance of axially and rotationally restrained beams

Γ = boundary of the beam (or time modification factor)

κ = curvature

λ = Darcy's coefficient of permeability

μ_V = dynamic viscosity of water vapor

ψ_0 = section characteristic factor

θ = temperature-compensated time (or an iterative procedure parameter between 0 and 1)

ρ = steel ratio = area of tension steel/effective area of cross section

ρc = heat capacity

ρ_C = mass of cement per unit volume of concrete,

ρ_L = density of liquid water

ρ_V = density of water vapor in the concrete boundaries

$\rho_{V\infty}$ = density of water vapor in the surrounding environment

ρ_w = density of water.

σ = current stress in concrete or steel (or Stevan-Boltzman constant).

σ_m = stress at the center of each element in the cross sectional mesh.

Chapter 1

1. Introduction

1.1 General

Concrete is a widely used construction material, and finds a wide range of applications in buildings, dams, bridges, electric power stations and pavement. Concrete competes extremely well with other construction materials because of its versatility in application. Concrete generally provides excellent fire resistance properties. It does not burn (non combustible) and it does not emit any toxic fumes, smoke or drip molten particles when exposed to fire. These excellent fire resistance properties are due to concrete's constituents (i.e. cement and aggregates) which, when chemically combined, form a material that is essentially inert and has a poor thermal conductivity and low strength loss properties. It is this slow rate of heat transfer and strength loss that enables concrete to act as an effective shield between adjacent spaces and also to continue to perform load bearing functions under fire conditions.

Over the last three decades, there has been significant research and development activity in improving properties of concrete. This has led to new types of concrete which are often

referred to as high strength concrete (HSC), fiber reinforced concrete (FRC), high performance concrete (HPC), and ultra HPC. HPC is typically characterized by high strength, good workability and durability, and HSC is a subset of HPC. HSC, which was widely used in applications such as bridges, off-shore structures, and infrastructure projects, has been extended to columns and beams in reinforced concrete (RC) buildings. This is due to the improvements in durability, which it can provide, compared to the conventional normal strength concrete (NSC).

The classification of HSC continues to change as advances in concrete technology make it easier to obtain increasingly higher strength using conventional construction practice (Mindess et al. 2003). In general, concrete up to a compressive strength of 70 MPa (10 ksi) is referred to as NSC, while concrete with compressive strength in excess of 70 MPa is classified as high strength concrete (HSC) (Kodur et al. 2004).

Similar to other structural members, concrete structural members when used in buildings have to satisfy relevant fire safety requirements. This is because fire represents one of the most severe hazards to which structures are subjected during their life time and hence the provision of appropriate fire safety measures is an important aspect of building design to enhance the safety of occupants, control the spread of fire, and minimize damage to property and environment. Fire safety design can be achieved by active and passive fire protection systems. Active systems are generally self-activated once the fire is triggered and they include fire detectors, smoke control systems, and sprinklers. Passive systems are built into the structures, and do not require specific operation to control the fire. The basis for passive fire protection systems, or what is commonly referred to as fire resistance, can be attributed to the fact that structural integrity is the last line of defense

when other measures for containing the fire fail. Fire resistance is defined as the duration during which a structural member (system) exhibits resistance with respect to structural integrity, stability, and temperature transmission when exposed to fire (Buchanan 2002). Fire resistance can play a crucial role on the performance of a structure in the event of fire as seen in the collapse of the WTC twin towers and the damage to the Euro-tunnel (FEMA 2002, Fire Prevention 1997).

1.2 Design for Fire Hazard

Fires cause significant loss of life and property damage throughout the world. In 2007, fires in the US caused about 3430 deaths, 97,800 injuries and property damage with $14 billion. The total cost of fire (including direct and indirect losses) was estimated to be around $70 billion in 2007 (Karter 2008).

Design for fire safety has been significantly improved in the last century. This improvement mainly focused on reducing the loss of life by introducing active fire safety systems (which are self-triggered in the event of fire) such as sprinklers and fire detections systems. In 1913, the death rate due to fire in the United States was 9.1% per 100,000 people. However, the use of fire resistant material and the improvements in design (including smoke detectors) reduced that rate to 2% per 100,000 people in 1988 (Williams 2004). Generally, the major cause of most fatalities and injuries is toxic smoke evolving during a fire event. However, some of these deaths and injuries, particularly among first responders, were due to structural collapse/damage under fire conditions (FEMA 2008).

The following realistic incident illustrates the catastrophic consequences that may result from fire incidents:

- On May 13, 2008, a serious fire occurred in the school of architecture building, at Delft Technical University in Netherlands (Dutchnews 2008). The fire, which was caused by a short circuit in a coffee machine, spread quickly in the fourteen-story RC building. A large amount of wood that was left over from formwork, and also wood that was used for architectural design studios fueled the catastrophic fire. Fortunately, the fire did not cause any fatalities in the building. This was mainly due to the fast and efficient evacuation of occupants and also due to withdrawal of firefighters from the building after about 3 hours of firefighting. However, six stories of the building collapsed and this resulted in the dismantling of the entire building. While full reasons for the collapse are currently being investigated, this incident exposed the vulnerability of concrete buildings in fire and also the potential danger to firefighters.
- On November 18, 1996, a serious fire in a shuttle train transporting trucks destroyed a section of the south side of the railroad tunnel connecting England and France (Fire Prevention 1997, Ulm et al. 1999). Nine trucks, ten train wagons and one locomotive burned for about 10 hours with temperatures up to 1000°C. Eight people were injured. The cost due to damage to trains, track and tunnel, as well as disruption to services, was estimated to be as high as £50M ($100M). The fire caused severe damage to the tunnel rings in the form of thermal spalling over a length of a few hundred meters. A post analysis of this fire incident indicated that the concrete employed in the Chunnel had typical features of HSC: a compressive strength of 80 to 100 MPa, and a low

permeability (Ulm et al. 1999). Based on the detailed investigation, major work had to be undertaken to repair the damage due to the spalling of the concrete.

- Another fire incident occurred in the Eurotunnel (tunnel connecting France and England) on September 11, 2008 (BBC 2008). The fire occurred in a lorry on board the shuttle train about 11 km from the French entrance. The fire was contained after about 4 hours of the incident but all trains were suspended and thousands of passengers were stranded. The fire did not cause any fatality but it caused 14 injuries.

The above incidents clearly illustrate the role of structural fire safety in minimizing the catastrophic collapse of buildings and built-infrastructures. To minimize the possibility of structural failure during fire, building codes specify fire resistance requirements for structural systems in buildings. The required fire resistance varies based on the importance, number of stories and floor area of the building, and also on the type of the structural members (such as slab, beam or column). As an illustration, the fire resistance requirement for an RC beam in a typical building can vary from 1 to 3 hours.

These fire resistance requirements are determined based on tabulated values in codes and standards (such as ACI 216.1 (2008) and Eurocode 2 (2004)). These provisions are prescriptive and do not account for the critical parameters that govern the behavior of RC structural members under fire conditions. As an illustration, the failure of an RC beam in a standard fire test is based on the temperature attained in the steel reinforcement (just prior to failure), under a predefined standard fire exposure, without any consideration to a number of critical factors such as compartment characteristics, loading, restraints, etc.

An alternative to tabulated values of fire resistance, empirical equations for evaluating fire resistance can be used. However, these equations incorporate only the thickness of concrete cover to the reinforcement and the overall dimensions of the structural member and do not take into consideration important factors such as load level, type of fire exposure, and failure criteria (ACI 216.1 2007). The cover thickness specifications are primarily determined based on corrosion control requirements and then checked for limiting temperature transmission to rebars. This limiting temperature, which is often called the critical temperature, is defined as the temperature at which steel (reinforcement) loses 50% of its strength. For steel reinforcing rebars, it is 593°C, and for prestressing steel it is 426 °C (Kodur and Harmathy 2008). Therefore, the current design approaches are not applicable for design under performance-based codes, which provide rational, cost-effective and innovative fire safety solutions.

One of the main reasons for the lack of rational design approach is the lack of calculation methods for evaluating fire response of RC structural members in general, particularly beams. The lack of understanding of the fire response of RC structural systems under realistic conditions and the absence of reliable calculation methods for evaluating fire resistance are hindering the application of an engineering approach for the fire design of concrete structures.

1.3 Reinforced Concrete Beams under Fire Hazard

When an RC beam is exposed to fire, the temperature increases in both the concrete and reinforcing steel. This increase in temperature is generally associated with the degredation in the constituent materials, which leads to reduction in strength and stiffness of the beam. With the progression of fire exposure time, the beam experiences increasing

mid-span deflection due to the reduction in the beam stiffness and also due to high temperature creep which becomes significant particularly during the later stages of fire exposure. Once the applied load reaches the strength capacity of the beam, the beam is considered to have failed. The duration from the start of fire exposure to the failure is defined as the fire resistance of the beam. The fire resistance of an RC beam is influenced by a number of factors such as high temperature material properties (and spalling), applied loading, support conditions (restraint effects), and type of fire exposure.

In addition to degradation in strength and stiffness, under some conditions, chunks of concrete might break up from the RC beam during exposure to fire (particularly for HSC and HPC beams). This break up of concrete is termed fire induced spalling and primarily results from the buildup of pore pressure within the concrete. The occurrence of spalling is dependent on a number of factors including fire conditions. HSC, due to its high compactness and low permeability, is believed to be more susceptible to spalling than NSC. Fire induced spalling, which was observed in several experimental studies (Diederichs et al. 1988, Castillo and Durrani 1990, Hertz 1991, Hammer 1995, Phan 1996, Phan et al. 2000, Kodur and McGrath 2003, and Sullivan 2004), may have a detrimental effect on the fire resistance of RC beams.

The applied loads on the beam during fire condtions also have an influence on the fire reponse of RC beams. The higher the applied loads, the lower the fire exposure time required to attain failure and thus the lower the fire resistance of the beam.

Another phenomenon that arises during a fire event and may have a significant influence on the fire response of RC beams is the development of fire induced restraint forces. The degree of restraint is dependent on the support conditions and the beam boundaries. The

effect of axial restraint on the fire resistance of RC beams depends on the vertical location of the restraint force which may change with fire exposure time. Generally, the axial restraint force in an RC beam is expected to improve the fire resistance of the beam through an arch action associated with axial restraints, which increases the strength and the stiffness of the beam. However, axial restraint forces may lead to buckling of the beam (particularly for slender beams) which in turn might reduce the fire resistance of RC beams. Rotational restraint, under fire conditions, also influences the fire response of an RC beam through moment redistribution between span (positive moment) and support (negative moment) sections within the length of the beam. Thus, it is essential to account for the fire induced restraint effects for evaluating a realistic response of RC beams. At present, design codes, such as ACI 216.1 (2007), do not fully account for fire induced restraint effects in RC beams.

In addition, the fire response of RC beams is influenced by the type of fire exposure. The temperature profile of a fire in a building compartment is dependent on the characteristics of the compartment and fuel and there always exists a decay phase. This decay phase has a significant influence on the fire response of an RC beam as the beam might recover part of its strength and stiffness during the cooling phase.

For simplicity, standards such as ASTM E119a (2008) and ISO 834 (1975) use standard time temperature curves which are independent of the compartment characteristics and fuel properties and do not include a decay phase. Thus, the standard fire exposure may not sufficiently represent the behavior of actual compartment fires. Such fire scenarios are generally used in standard fire tests for evaluating the fire resistance of RC beams.

The results of these tests comprise much of the current knowledge on the fire response of RC beams.

There have been very limited research studies on evaluating the fire performance of RC beams under realistic (design) fire scenarios. In addition, the current approaches base the fire resistance of RC beams only on the concrete cover thickness and the beam width without any consideration given to important factors such as fire, load, restraint condition, and fire induced spalling. This is mainly due to the fact that the fire resistance of RC beams is based on limited fire tests which are carried out on specimens of standard sizes, service loads (50 % of room temperature capacity) and standard fire exposure. Therefore, the current prescriptive approaches for evaluating fire resistance do not represent realistic fire, loading and restraint scenarios as encountered in practice and may not be applicable for use under the recently introduced performance-based codes that facilitate innovative, cost-effective and rational designs.

Realistic fire resistance assessment can be achieved through a rational engineering approach in which a realistic fire scenario, support conditions (restraint) and material properties can be accounted for based on actual (rather than standard) scenarios. Currently, there is a lack of knowledge on the fire response of RC beams. In addition, there is a dearth of available calculation methods for evaluating the fire resistance of RC beams under realistic fire, loading and support conditions. Thus, there is an urgent need for the development of rational engineering approaches for evaluating the fire response of RC beams.

1.4 Research Objectives

From the above discussion, it is clear that there is lack of knowledge on the fire response of RC beams under realistic fire, loading, and restraint scenarios. To address this knowledge gap, it is proposed to undertake a comprehensive study of the flexural behavior of RC beams under fire conditions with the ultimate objective of developing a rational methodology for evaluating the fire resistance of RC beams. The specific objectives of the research are:

- Conduct a detailed state-of-the-art review on the fire response of RC beams. The comprehensive review will cover experimental and numerical studies, provisions in codes and standards, and high temperature material properties.
- Develop a macroscopic finite element model for tracing the flexural response of rectangular RC beams under realistic fire, loading, and failure conditions. The model will account for nonlinear high temperature material properties, various strain components, fire induced restraint effects, and fire induced spalling of concrete.
- Conduct fire resistance tests on RC beams under realistic fire, loading and restraint scenarios to generate data for the validation of the model.
- Verify the computer program using data from fire resistance tests on NSC and HSC beams.
- Carry out parametric studies to quantify the influence of various factors on the fire resistance of RC beams.
- Develop, using data from fire tests and parametric studies, a design approach for evaluating the fire resistance of RC beams.

1.5 Scope

The research, undertaken to address the above objectives, is presented in eight Chapters. Chapter 1 provides a general background to the fire response of RC beams and presents the objectives of this study. Chapter 2 provides a state-of-the-art review on the behavior of RC beams exposed to fire. A critical review of experimental and analytical studies, as well as the fire design provisions for RC beams in current codes of practice, is provided. Chapter 2 also contains a review of the high temperature material properties and associated constitutive relationships for NSC, HSC, and reinforcing steel.

Chapter 3 deals with fire resistance experiments on six RC beams under realistic fire, loading and restraint scenarios. Results from the fire tests are used to discuss the response of RC beams under these realistic conditions. Chapter 4 presents the development of a numerical model for predicting the fire response of RC beams. The procedure for calculating the fire response, including the axial restraint force in restrained RC beams and fire induced spalling is outlined. The validation of the numerical model is presented in Chapter 5, where predictions from the model are compared with available test data from literature, and also results from the fire tests presented in Chapter 3.

In Chapter 6, results from the parametric studies are discussed and the influence of various parameters on the fire resistance of RC beams is discussed. In Chapter 7, results from the parametric studies are applied to develop a rational approach for evaluating the fire resistance of RC beams under different realistic conditions. Finally, Chapter 8 summarizes the main findings arising from the current study and lays out recommendations for further research.

Chapter 2

2. State-of-the-Art Review

2.1 General

Reinforced concrete beams, when used in buildings, have to satisfy fire resistance requirements specified in building codes. To develop such fire resistance information, a number of studies have been undertaken on RC beams since 1960's. Most of these studies were limited fire resistance tests under standard fire scenarios. A limited number of analytical studies have been reported which focused on the behavior of RC beams under standard fire exposure. This chapter provides a state-of-the-art review on the fire resistance of RC beams. The typical fire behavior of RC beams is first discussed followed by a critical review of different design provisions in codes and standards for evaluating their fire resistance. A review of previous experimental and analytical studies on the fire performance of RC beams is presented. In addition, a review of high temperature material properties (concrete and reinforcing steel) that are critical for modeling the fire response of RC beams is presented.

2.2 Behavior of RC Beams under Fire

The behavior of RC beams under fire is quite different from that at room temperature mainly due to the fact that, under fire conditions, applied loads generally remain constant, but the strength and the stiffness of the beams degrade with fire exposure time. RC beams, when exposed to fire, experience a temperature rise with time due to the transmission of heat from the fire to the exposed surface of the beam through radiation and convection processes. The increasing temperatures lead to gradual loss of strength and stiffness properties in concrete and reinforcing steel which in turn reduces the strength and stiffness of the beam as shown in Figure 2.1. With the progression of fire exposure time, this rise in temperature extends to the inner layers of concrete leading to further reduction in the beam strength and stiffness. This degradation in strength and stiffness may continue until the applied load reaches the strength capacity of the beam as shown in Figure 2.1. At this point in time the beam is considered to have failed and the fire exposure time is considered to be the fire resistance of the beam.

The behavior of RC beams under fire is largely dependent on the support conditions, the type of fire exposure, and the high temperature properties of the constituent materials (concrete and reinforcing steel). Support conditions, which are dependent on the boundary conditions of the beam, have a significant influence on the behavior of RC beams under fire. This effect of support conditions on fire response is illustrated in the following three examples:

- The fire behavior of a simply supported RC beam is demonstrated in Figure 2.2 where the bending moment resulting from the factored loads as well as two different load levels (20 kN/m and 25 kN/m) under fire conditions is plotted. The

load levels under fire conditions are selected to be lower than the applied ultimate load at room temperature as shown in Figure 2.2. This is mainly because fire is a rare event and it is very unlikely to have ultimate loads in a fire event. It can be seen from the figure that the moment capacity of the beam decreases with fire exposure time. At later stages of fire exposure, the beam experiences a significant mid-span deflection (mainly due to the high temperature creep strains which become significant at later stages of fire exposure) as illustrated in Figure 2.2. The failure of the beam occurs when the moment capacity of the beam drops so low that it is exceeded by the applied moment on the beam (see Figure 2.2). It can be seen from Figure 2.2 that the failure of the beam is achieved after 120 and 180 minutes of fire exposure time for loads of 20 and 25 kN/m, respectively.

- Support conditions may prevent thermal expansion and induce axial restraint forces on the beam exposed to fire. The behavior of an axially restrained beam exposed to fire is illustrated in Figure 2.3 where the axial restraint force is assumed to pass through the geometrical centroid of the cross-section of the beam. The vertical location of the restraint axial force in RC beams is generally below the neutral axis of any cross-section along the span of the beam (see Figure 2.3) as a result of cracking of concrete and thermal gradients. This will develop an arch action moment (Pa) which counters the effect of the applied loading, as shown in Figure 2.3. However, when the beam deflects downward, the axial restraint force creates a secondary moment ($P\delta$) that increases the effect of the applied loading. The net moment for the beam shown in Figure 2.3 is the sum of the three moments, namely:

$$M_{net} = \frac{wL^2}{8} - Pa + P\delta \qquad [2.1]$$

where: M_{net} = net bending moment in the beam. The definition of other variables in Eq. [2.1] can be seen in Figure 2.3.

Figure 2.3 and Eq. [2.1] show that when the deflection of the beam (δ) is small, the behavior is governed by the arch action which reduces the effect of the applied loading and increases the fire resistance. However, when the deflection of the beam is large, the secondary moment resulting from P-δ effect (which increases the effect of the applied loading) becomes the governing factor and reduces the fire resistance of the beam. Thus, the effect of axial restraint on the fire resistance of an RC beam depends on the overall response and may not always be beneficial for the fire resistance of the beam. It should be noted that in current code provisions, as well as in much of previous research, axial restraint is assumed to have a positive effect on the fire resistance of RC beams (ACI 216.1 2008, Buchanan 2002).

- Support conditions may also induce rotational restraint on the ends of the beam. Such rotational restraints can improve the fire response of an RC beam through redistribution of moment between span (positive moment) and support (negative moment) sections. This effect is illustrated in Figure 2.4 for the case of a fixed ended RC beam. The figure shows that there is a larger reduction in the span (positive) moment capacity of the beam as compared to the support (negative) moment capacity after 120 minutes of fire exposure. This can be attributed to the fact that the tension rebars for the critical support section (top reinforcement) are

closer to the unexposed surface of the beam than the tension rebars for the critical span section (bottom reinforcement). Thus, some of the span moment is redistributed to the support moments once the span moment capacity is exceeded as shown in Figure 2.4. Consequently, rotational restraint may delay the time to reach failure and increases the fire resistance of RC beams. Even if the moment redistribution has been considered in the design at room temperature, rotational restraint is expected to have a positive influence on the fire resistance of an RC beam (Dwaikat and Kodur 2008a). The effect of rotational restraint on the fire response of RC beam depends mainly on the amount of moment redistributed from the span critical section to the support section.

Another factor that has a significant influence on the behavior of RC beams exposed to fire is the high temperature properties of concrete and reinforcing steel. Concrete and reinforcing steel experience loss of strength and stiffness at high temperatures. This degradation in material properties leads to large deflections, cracking, and discontinuities and may lead to failure of the beam. In addition, some concrete types under certain conditions experience fire induced spalling. Spalling is theorized to be caused by the build-up of pore pressure during heating (Diederichs et al. 1995, Kodur 2000). HSC is believed to be more susceptible to this pressure build-up because of its low permeability as compared to NSC. The extremely high water vapor pressure, generated during exposure to fire, cannot escape due to the high density of HSC and this pressure often reaches the saturation vapor pressure. At 300°C, the pressure might reach about 8 MPa. Such internal pressures are often too high to be resisted by the HSC mix having a tensile

strength of about 5 MPa (Diederichs et al. 1995). Spalling results in reduced cross-section and rapid strength loss, thereby lowering the fire resistance of an RC beam.

The response of an RC beam also depends on the type of fire exposure, which varies significantly based on compartment characteristics, lining materials, ventilation, and fuel characteristics. Details on the temperature course for typical fire scenarios in building compartments are given in Section 2.3.4.1.

Other factors that may have influence on the fire performance of RC beam are span length and cross-sectional dimensions including concrete cover thickness to the reinforcing steel. Concrete cover thickness and cross-sectional dimensions influences the rate of heat transmission to concrete and reinforcing steel and this in turn influences the overall response of an RC beam. Span length significantly affects the flexural and axial stiffness of an RC beam and thus it has an effect on the overall fire response of the beam. In addition, span length influences the magnitude of the fire induced restraint force in restrained RC beams, which will determine the fire resistance of that beam.

In summary, the fire response of RC beams is governed by a number of factors. Many of these factors are interdependent. Accounting for them is critical in tracing the fire response and evaluating the fire resistance of RC beams. The following section provides an overview on various approaches for evaluating the fire resistance of RC beams.

2.3 Approaches for Evaluating Fire Resistance

2.3.1 Standard Fire Test

Fire resistance of RC beams, similar to other structural members, is generally evaluated by subjecting the structural member to fire in a specially constructed furnace. The

purpose of the standard fire test is to determine the failure time at which the structure loses the ability to withstand fire exposure while maintaining function as a load-bearing element and as a barrier to the spread of fire. The standard fire test is a comparative test that does not reflect actual performance of the member.

Standard fire resistance tests are generally carried out on building elements such as walls, floors, or columns in accordance with national standards such as ASTM E119a (2008) and ISO 834 (1975). The standards require test specimens be constructed in a similar manner as the building elements in practice. ASTM E119 specifies the dimensions of the test specimen and the size of the furnace being used for the standard fire test. Further, the furnace chamber is heated by liquid fuel or gas such that the furnace follows the specified standard temperature-time curve shown in Figure 2.5.

During the fire test, load bearing members, such as an RC beam, are loaded with service loads (dead load + live load). A common practice in standard fire tests is to apply a service load level (about 50% of the room temperature capacity) to the tested member.

The test continues until a prescribed failure criterion is exceeded. Fire resistance of the assembly is then recorded as the duration of fire exposure until this failure point. The limiting criteria used for evaluating fire resistance depend on the structural member in question. As an illustration, for an RC beam, the fire resistance is the time at which the rebar (tension steel) temperature exceeds 593°C, or the beam fails to sustain the applied load (ASTM E119a 2008). Different failure limit states are specified for columns, beams and slabs. More details on the failure criteria for RC beams are discussed in Section 2.3.5.3.

Whereas fire resistance provisions in the past were created primarily based on full-scale

tests, the recent trend is moving toward calculation methods. This is mainly because standard fire tests are very expensive and time consuming. Advances in numerical models are facilitating the application of calculation methodologies for evaluating fire resistance.

2.3.2 Provisions in Codes and Standards

Provisions for evaluating the fire resistance of concrete members are generally specified in codes and standards. These prescriptive provisions are derived based on results from standard fire tests. The specifications are in the form of tables or charts, where the fire resistance is often related to member dimensions or other influencing factors. The fire resistance specification for RC beams in three widely used codes, namely, ACI 216.1 (2007), Eurocode 2 (2004), and AS 3600 (2001), are reviewed below.

In the USA, concrete structures are designed in accordance with ACI 318 (2008). ACI 318 does not contain any fire provisions, but refers to the ACI 216.1 standard (2007) which gives specifications for fire resistance design of concrete and masonry structures. Accordingly, ACI 216.1 specifies minimum width and concrete cover thickness requirements for achieving a required fire resistance rating in an RC beam. These requirements differ for restrained and unrestrained support conditions as can be seen in Table 2.1. However, the definition of support conditions (restrained or unrestrained) is not clearly addressed in the code. Thus, it is not clear whether the restrained case refers to the provisions of rotational restraint, axial restraint or both rotational and axial restraints. In addition, specifications are for NSC beams only and there are no clear guidelines for evaluating the fire resistance of HSC beams. Canadian provisions for fire resistance design, which are available in NBCC (2005), are similar to those of ACI 216.1.

Eurocode 2 (2004), Part 1–2: Structural fire design, gives a choice of advanced, simplified or tabular methods for determining the fire resistance of RC beams. Tables provide the fastest and most direct method for determining the minimum width and nominal axis distance for RC beams. The nominal axis distance is the distance from the center of the main reinforcing bar to the surface of the member exposed to fire. Different values have been specified based on the support conditions and the continuity of the beam. Table 2.2 shows fire resistance ratings as specified in Eurocode 2 for continuous beams. The code suggests different possible combinations of axis distance and beam width to achieve the required fire resistance ratings (reproduced in Table 2.2). However, the tables do not provide different values of fire resistance for axially restrained beams.

The simplified method in Eurocode 2 is mainly based on the sectional analysis approach. This method may give more economical design and/or high fire resistance periods for some scenarios. Eurocode 2 (2004) also permits the use of advanced methods for evaluating the fire resistance of RC beams. These methods are generally based on detailed thermal and structural analysis and require the use of sophisticated numerical models.

In the Australian code, AS 3600 (2001), charts that relate the fire resistance of an RC beam to that of concrete cover thickness, and width are presented. There are two charts, one for simply supported beams and the other for continuous beams. Figure 2.6 illustrates the chart for the fire resistance rating of simply supported RC beams as per AS 3600. The code provides required values of concrete cover thickness and beam width for fire resistance rating in the range of 30 minutes to 240 minutes. However, similar to Eurocode

2 (2004), AS 3600 (2001) does not specify any guidelines for the case of axially restrained beams.

Thus, the fire resistance provisions in current codes and standards do not clearly specify the boundary conditions of the RC beam (for the case of restrained end conditions of the beam) for which the tables or charts are applicable. In addition, the degree of axial restraint, represented by the axial restraint stiffness, for RC beams has not been fully addressed in the three codes. It can also be seen that the three codes relate the fire resistance of an RC beam to cross-sectional dimensions and concrete cover thickness without any due consideration to other important factors such as fire scenario, concrete strength, and fire induced restraint effects.

Further, the application of different code provisions produces different and varying fire resistance values for similar RC beams. As an illustration, for a simply supported RC beam with a cross-sectional dimension of 300 mm × 500 mm and a concrete cover thickness of 40 mm (axis distance of 50 mm), the fire resistance based on ACI 216.1, Eurocode 2, and AS 3600 is 210 minutes, 110 minutes, and 113 minutes, respectively. For this beam ACI 216.1 predicts a much higher fire resistance than the other two codes. This clearly indicates that current codes of practice cannot be considered to be reliable tools for evaluating the fire resistance of RC beams.

Until recently, design for fire has been based on prescriptive building codes, with little or no opportunity for designers to apply engineering approaches to the fire safety design. Many countries such as, New Zealand and UK, have recently adopted performance-based building codes which allow designers to use alternate fire safety strategies, provided that adequate safety can be demonstrated. However, there is a lack of calculation methods for

evaluating fire resistance of RC beams and this limits the applicability of the performance-based approach to fire design.

2.3.3 Detailed Calculation Methods

In recent years, several mathematical models to calculate fire resistance of structural members in buildings have been developed. The flowchart in Figure 2.7 illustrates the general calculation procedure employed in such methods (Kodur 2007, Buchanan 2002). The fire resistance calculation is performed in three steps (Kodur 2007):

- Calculation of the fire temperature.
- Calculation of the temperatures in the fire-exposed structural member.
- Calculation of the strength of the member during exposure to fire, including an analysis of the stress and strain distributions.

2.3.3.1 Fire Temperature

The fire temperature can be computed knowing the characteristics of the compartment. At present, in most fire resistance calculations, the fire temperatures is assumed to follow the standard time-temperature curve specified in ASTM E119a (2008).

2.3.3.2 Structural Member Temperature

The next step in the analysis is the calculation of the temperatures of the fire-exposed member. These temperatures are generally calculated using a finite difference or finite element method (Kodur 2007). In these methods, the cross-section of the member is divided into a number of elemental regions, which may have various shapes such as squares, triangles or layers, depending on the geometry of the member (Kodur and

Harmathy 2008). For each element or layer, a heat balance equation can be derived. By solving the heat balance equations for each element or layer, the temperature history of the member can be calculated.

The heat transfer analysis should consider changes in material properties (thermal properties) with increasing temperature for all materials in the structural system (Kodur and Harmathy 2008). Heat transfer by radiation and convection to the boundary of the structural member should be considered in the thermal analysis.

2.3.3.3 Strength Calculations

In the third step, a stress-strain analysis can be conducted to determine the strength of the member during exposure to fire. This strength decreases with increasing temperature and duration of fire exposure. The fire resistance can be derived by determining the time at which the strength of the member reaches the load to which the member is subjected.

2.3.3.4 Critical Factors in Fire Resistance Calculations

To achieve a reliable fire resistance estimate through detailed calculations, the following factors must be accounted for (Kodur et al. 2009a):

- **High temperature material properties:** The temperature-dependent properties that are important for establishing the fire response of RC structures include: thermal, mechanical and special properties such as fire induced concrete spalling. These properties vary as a function of temperature. They are crucial for modeling the fire response of RC structural members.
- **Strain components:** In addition to mechanical and thermal strains, two other components of strain, namely, creep and transient strains must be considered in

computing concrete strains at elevated temperatures. For reinforcing steel, the strains that must be considered for realistic analysis are thermal, mechanical and creep strains. Creep and transient strain, which are often ignored, may have a significant influence on the fire response of RC structural members.

- **Fire scenarios:** In most fire scenarios, there always exists a growth phase followed by a decay (cooling) phase. Further, the fire scenario is a function of compartment characteristics such as fuel load, ventilation and lining material. Therefore, it is essential, in modeling the fire response of RC structural members, to account for realistic fire scenario including the decay phase.
- **Restraint effects:** Fire induced restraint is believed influence the fire response of RC structural members. Thus, restraint effects must be accounted for in tracing the response of RC structural members.
- **Spalling:** Under fire conditions, spalling of concrete can occur because of the development of water vapor pore pressure inside the concrete core. Spalling leads to loss of concrete cross-section and faster heat penetration to the steel reinforcement. Therefore, spalling should be incorporated into fire resistance analysis.
- **Geometrical nonlinearity:** Structural members generally experience large deformations under fire conditions because of the deterioration in strength and stiffness of the members. It is important to account for geometrical nonlinearity in tracing the fire response of RC structural members.
- **Softening effect:** Materials undergo significant softening when exposed to fire. Such softening facilitates redistribution of moment within the structural member under fire

conditions. This should be considered in fire resistance analysis of RC members through the use of a displacement-controlled iterative procedure.

- **Failure limit states:** Currently, the failure of RC structural members under fire conditions is evaluated based on thermal and strength failure limit states. Other failure criteria such as deflection and rate of deflection may be critical under some conditions. Details on different failure limit states are provided in Section 2.3.4.3

It should be noted that some of the above mentioned factors are not fully accounted for in finite element models such as SAFIR (Franssen et al. 2004). Thus, the fire resistance predictions obtained from such models may not yield the actual performance of the beam. More details on currently available computer models are presented in Section 2.4.2.

2.3.4 Performance-Based Design Approach

In recent years, there has been an increased focus in moving toward performance-based fire safety design from the current prescriptive-based approaches (Meacham and Custer 1992, Kodur 1999, and AISC 2005). This is mainly due to cost-effective and rational fire safety solutions that can only be arrived at using the performance-based design approach. One of the key aspects in any performance-based design is the fire resistance design of structural members. At present, there is limited information or tools (design equations) that can be applied for performance-based fire safety design of RC beams. This is due to the lack of both experimental and analytical studies on the fire response of RC beams. In the development of the performance-based approach for evaluating the fire resistance of RC beams, three main factors must be considered, namely, (1) fire scenario, (2) loading conditions and (3) failure criteria. These three factors are discussed in the following sections.

2.3.4.1 Fire Scenarios

The development of a fire scenario in a building compartment, which is commonly referred to as "a room fire" involves three stages; namely, growth, burning, and decay stages as shown in Figure 2.8. In the growth stage, the temperature of the fire gradually increases and the fire spreads slowly over combustible surfaces within the room. Generally, in this stage, the structural integrity is not significantly influenced because the fire temperature does not reach high levels. However, once the fire temperature reaches about 600°C, flashover occurs and the fire enters the intense burning stage, where the temperature may exceed 1000°C. In the burning stage, the temperatures and the radiant heat flux are so high within the room that all exposed surfaces will ignite and burn. The structural integrity may be severely damaged at this stage. Fires that pass the flashover threshold are commonly referred to as "post flashover" fires. Eventually, the fire enters the decay stage where the fire temperature drops once the fuel burns out or there is a lack of ventilation (oxygen) (Buchanan 2002). Often for structural analysis, the fire growth is represented through time-temperature relationships.

The fire growth in a compartment depends on a number of factors including:

- Fuel load that is related to the quantity of combustible materials.
- Opening factor that is related to the degree of ventilation.
- Dimensions of the compartment.
- Thermal properties of the lining materials.
- The amount of volatile combustibles released within the room per unit time.
- The boundaries of the compartment.

- The nature of the fuel (of cellulose or thermoplastic nature). Cellulosic materials are generally charring materials where a layer of char is created at the fire-material interface. The char layer protects the inner core of the material and slows down the burning process. Thermoplastic materials do not generally experience charring when they are subjected to fire.

The development of a fire scenario is quite complex since it is dependent on a number of factors. For ease of calculation, a standard time temperature curve is often used to represent a room fire scenario in various standards (ASTM E119a 2008, ASTM 1529 1993, Eurocode 1 2002, ISO 834 1975). Such standard fires are used to define the temperature profile that is generally used in standard fire tests as discussed earlier. While standard fire resistance tests are useful benchmarks to establish the relative performance of different RC beams under the standard fire condition, they should not be relied upon to determine the survival time of RC beams under realistic fire scenarios. Nor does the standard heating condition bear any relation to the often less severe heating environments encountered in real fires.

Figure 2.5 illustrates the time-temperature curves for a standard and two realistic design fire scenarios. In the standard fire (ASTM E119a 2008), the fire size is the same (irrespective of compartment characteristics), temperature increases with time throughout the fire duration, and there is no decay phase. This standard fire does not represent an actual fire scenario in a building. However, in real fires, the fire size is a function of compartment characteristics, and there is a decay phase as shown in Figure 2.5 (severe and moderate design fires). During the decay phase, the cross-section of the beam enters

the cooling phase, in which the reinforcing steel recovers parts of its strength and stiffness, and thus the fire resistance of the beam might increase.

2.3.4.2 Loading Conditions

The provisions in current codes of practice for evaluating fire resistance are generally based on a load ratio of about 50%. Load ratio is defined as the ratio of the applied load on the beam under fire conditions to the strength capacity of the beam at room temperature. The load ratio depends on many factors including type of occupancy of the building, dead-load-to-live-load ratio, safety factors (load and capacity factors) used for design under both room temperature and fire conditions. The loads that are to be applied on RC beams, in the event of fire, can be estimated based on the guidance given in the ASCE-07 (2005) standard (1.2 dead load + 0.5 live load) or through actual calculation based on different load combinations. Based on ASCE-07 (2005) and ACI 318 (2008), and for typical dead-load-to-live-load ratios (in the range of 2 to 3), the load ratio ranges between 65% and 70%.

The load level has a significant influence on the fire resistance of RC beams. This fact was demonstrated in experimental and analytical studies (Kodur and Dwaikat 2008b, Dwaikat and Kodur 2009). Thus, for innovative, realistic and cost effective fire safety design, it is important to evaluate the fire resistance of RC beams based on actual load levels.

2.3.4.3 Failure Criteria

The conventional approach of evaluating fire resistance (defining failure under fire conditions) is based on thermal and strength failure criteria as specified in ASTM E119a (2008). Accordingly, the thermal failure of an RC beam is said to occur when:

- The temperature in steel rebars (tension reinforcement) exceeds the critical temperature, which is 593°C for reinforcing steel.

Strength failure is said to occur when:

- The beam is unable to resist the applied service load.

The deflection and rate of deflection can play a crucial role on the response of RC beams exposed to fire. In fact, a deflection limit is often applied to check the status of RC beams (serviceability limit state) at ambient conditions. This criterion should be considered to determine failure under fire conditions. The resulting deflections in fire scenarios are generally higher than those at room temperature due to deterioration of member stiffness and also due to temperature-induced creep. The British Standard (BS 476 1987) contains deflection and rate of deflection criteria for defining failure of an RC beam tested in a furnace. Although these deflection limit states might have been set to limit damage to the furnace during fire tests, deflection and rate of deflection can be important under certain fire conditions. This is because the integrity of the structural member cannot be guaranteed with excessive deformations. Moreover, fire resistance based on limiting deflection will help to facilitate the safety of fire fighters and also to safely evacuate occupants prior to structural collapse (Kodur and Dwaikat 2008a). According to BS 476, failure is assumed to occur when:

- The maximum deflection of the beam exceeds $L/20$ at any fire exposure time, or

- The rate of deflection exceeds the limit given by the following expression:

$$\frac{L^2}{9000d} \text{ (mm/min)} \qquad [2.2]$$

where L = span length of the beam (mm), and d = effective depth of the beam (mm).

Other failure limit states that are relevant for fire resistance evaluation are the loss of bond strength or loss of shear strength. However, RC beams generally fail through loss of flexural strength or excessive deformation and thus other modes of failure such as shear and bond failure are not critical for the fire response of RC beams as observed in a number of fire tests (Lin et al. 1981, Lin and Ellingwood 1987, Dwaikat and Kodur 2009).

2.3.4.4 Other Factors

Other major components that should be considered for evaluating the failure of RC beams under fire exposure include spalling and the effect of restraints. Although spalling may not be an important factor for NSC, excessive spalling might occur in HSC under certain conditions due to the low permeability and presence of silica fume(a by-product in the manufacturer of silicon metal and alloys), which generates high pore pressure (Diederichs et al. 1995, Kodur 2000). Spalling reduces the cross-sectional area of the beam, and increases the heat transmission to the steel reinforcement. Thus, spalling might result in a significant reduction in the strength and stiffness of the beam, which in turn might cause early failure. However, spalling may not be required as a separate failure criterion, since excessive spalling leads to loss of strength and higher deflection which in turn dictate the failure of the beam.

One other key parameter to be included in performance-based design is end restraints. End restraints (axial or rotational) may have a significant influence on the fire response of RC beams as discussed earlier in this chapter. Axial restraint can improve the fire resistance of the RC beam through arch action, which increases the strength of the beam under fire exposure. However, axial restraint when associated with large deflection of the beam may lead to the development of significant secondary moments (through the P-δ effect) which may lead to buckling and early failure of the beam. The rotational restraint can enhance the fire resistance of RC beams through the redistribution of the moment between the span and support sections of the beam. Further discussion on the effect of end restraints on the fire response of RC beams was presented in Section 2.2.

2.3.4.5 Summary

The fire resistance of RC members is currently evaluated through prescriptive-based approaches. The prescriptive approaches are derived based on standard loading and fire scenarios and thus have limited application. Realistic fire resistance assessment can be obtained through a performance-based approach in which the fire scenario, load level, restraint effects, and failure criteria, can be accounted for based on actual (rather than standard) scenarios. Presently, there is a lack of design approaches for undertaking performance-based fire design of RC beams. Applying the performance-based approach to fire design can produce design challenges since numerous fire scenarios must be considered, and it is not possible to undertake fire resistance tests for all possible fire scenarios. One way of overcoming this problem is by establishing an equivalency between standard and design fire exposures. In this way, the fire scenario, which is one of the key factors, can be accounted for in the fire design.

2.3.5 Time Equivalent Methods

As discussed above, one way to account for design fire scenarios in evaluating the fire resistance of RC beams is through establishing equivalency between standard and design fire scenarios. A review of the literature indicates that there are few time equivalent methods to establish such equivalency. These methods include: maximum temperature method, minimum load carrying capacity method, maximum deflection method, equal area method, and empirical formulae such as CIB, Law and Eurocode formulae. More details on these methods are presented in Kodur et al. (2009b). Many of these methods have limitations and are more applicable to protected steel structural members. Further, the current time equivalent empirical formulae such as the CIB formula, the Law formula, and the Eurocode formula are not validated for RC members and thus cannot be applied for establishing equivalency in RC beams. There is an appreciable amount of data on the fire resistance of RC beams under standard fire exposures, which can be used for members under design fire exposures if a reliable time equivalent approach is available. Thus, development of a reliable time equivalency approach can facilitate the evaluation of fire resistance under design fire scenarios.

Kodur et al. (2009b) compared the computed time equivalency values from equal area method and the empirical formula (CIB, Law and Eurocode) with those from the maximum deflection method (since the maximum deflection method provides the most accurate time equivalent due to the fact that the failure of an RC beam is generally controlled by the deflection limit state). Their comparative study did not include the minimum load capacity and the maximum temperature methods since these methods may not be as accurate as the maximum deflection method and also because these methods

require detailed finite element analysis which limits their use for design purposes. Results from their comparative study are plotted in Figure 2.9 which shows a comparison of the estimated time equivalent values based on various methods with that predicted by finite element analysis. The safety line, as well as the safe and unsafe regions, for the data points are also shown in Figure 2.9.

It can be seen from Figure 2.9, that there is a significant variation in the time equivalency values predicted by various methods and empirical formulae. Further, the time equivalent values computed based on various methods are unconservative. This comparative study clearly indicates that the current methods for evaluating time equivalency are generally unconservative. Thus, there is an urgent need to develop a conservative and reliable time equivalency approach which will facilitate fire resistance evaluation under design fire scenarios.

2.4 Previous Studies on RC Beams

A review of the literature indicates that there is only a limited number of experimental and numerical studies on the fire response of RC beams. This is in contrast with the fire behavior of RC columns which was the focus of a number of studies. This section provides an overview of experimental and analytical studies that were undertaken to study the fire performance of RC beams.

2.4.1 Experimental Studies

The most notable fire tests were carried out by Lin et al. (1981), Dotreppe and Franssen (1985), and Lin and Ellingwood (1987). Lin et al. (1981) tested eleven 305 mm × 355 mm RC beams under ASTM E119 standard fire exposure. The beams were reinforced

with ϕ25 mm and ϕ19 mm bars having a yield strength 435 MPa. Ten beams were made with normal weight carbonate aggregate concrete, while the remaining beam was fabricated from lightweight aggregate concrete. The concrete strength ranged between 26-33 MPa. The beams were moist cured for 7 days and then stored in air maintained at 21°C - 27°C and 30% - 40% relative humidity.

Lin et al. (1981) investigated the influence of a number of factors including beam continuity, moment redistribution and aggregate type on the behavior of RC beams under standard fire conditions. One of the tested beams had simple support conditions at both ends, whereas the remaining beams had cantilever spans on one or both ends. The applied loading on the cantilever was chosen to reflect the continuity effect in RC beams. Lin et al. (1981) concluded that the fire resistance of continuous beams is much higher than that of simply supported beams due to the occurrence of moment redistribution under fire conditions.

The second experimental study, reported by Dotreppe and Franssen (1985), involved testing a simply supported RC beam under ISO 834 fire exposure to assess its fire resistance rating. The beam had cross-sectional dimensions 200 mm × 600 mm and a span length 6.5 m. The beam was fabricated with siliceous aggregate concrete having a compressive strength of 15 MPa. The beam was reinforced with 3 ϕ22 mm bars as tension reinforcement and 2 ϕ12 mm bars as compression reinforcement. The beam was tested under two concentrated loads located at a distance of 1.625 m from the support. No explosive spalling was observed in the tested RC beam. The study concluded that RC beams experience a large deformation prior to failure under fire conditions.

Lin and Ellingwood (1987) tested six full scale RC beams to study the flexural and shear behavior of RC beams under fire conditions. Five of the six beams had cross-sectional dimensions of 239 mm × 533 mm, while the remaining beam was of 254 mm × 610 mm. All beams were 8.2 m in length, with a 6.1 m span exposed to fire and an unexposed cantilever loaded so as to provide continuity over one support. The beams were fabricated with normal-weight concrete. Four beams were exposed to the standard (ASTM E119) fire, while the remaining two beams were tested under a design fire having the time temperature curve shown in Figure 2.10. During the tests, applied load, furnace pressure and temperature, concrete and steel temperatures, deflection, axial deformation, and slope were measured. Flexural failure occurred in all beams. The measured fire resistance ranged between 3:26 to 4 hours for the six beams. The study concluded that shear failure is not likely to occur in RC beams exposed to fire. Another finding from the study was that the temperature history in the tension reinforcement is the most critical factor that influences the fire resistance of an RC beam.

Other experimental studies reported in the literature include the fire resistance tests carried out by Sanjayan and Stocks (1993), Saito et al. (1992) (cited in Phan 1996), Hansen and Jensen (1995), and Shi et al. (2004). Sanjayan and Stocks (1993) tested two T-beams; one made of NSC (25 MPa), the other made of HSC (92 MPa). The study aimed to investigate the fire induced spalling in HSC beams, thus the beams were not subjected to any mechanical loading during the fire tests. The beams had a length of 2.5 m and a flange width of 1.2 m. Two flange thicknesses; namely, 200 mm, and 150 mm were used, and the overall depth of the beams was 450 mm. Three values of concrete cover, namely, 25 mm, 50 mm, and 75 mm were used. During the fire test, the weight of

the beam was measured to gauge the extent of concrete spalling. Significant spalling was observed in HSC when the concrete cover was large. No spalling was observed with a concrete cover of less than 75 mm. The main finding from these tests was: that HSC beams are more susceptible to spalling than NSC beams.

Siato et al. (1992) tested six RC beams made with different concrete strengths to assess the residual strength of beams exposed to a maximum temperature of 550°C. The beams were heated in accordance with the standard time-temperature curve prescribed by JIS A1304 (2002) and allowed to cool down before loading was applied. The beams were loaded with two concentrated loads until failure. The study concluded that changing the compressive strength of concrete did not have a significant effect on the residual strength of RC beams.

Hansen and Jensen (1995) tested three series of 150 × 200 × 2850 mm RC beams under standard fire exposure (ISO 834 and hydrocarbon) to investigate the extent of fire induced spalling in concrete and the residual strength of RC beams. The beams were reinforced with 20 mm and 32 mm longitudinal bars. The varied test parameters were concrete strength (cube compressive strength varied from 50 to 95 MPa), aggregate type (normal weight and lightweight aggregates), prestressing effects, addition of fibers, and concrete density. The study concluded that light weight aggregate and HSC is more prone to spalling than other types of concrete. Further, the study reported that the extent of spalling in RC beams could be reduced through the addition of polypropylene fibers.

Shi et al. (2004) tested five beams to study the influence of concrete cover thickness on the behavior of RC beams exposed to fire. The temperature in the furnace was controlled so that it followed the time-temperature curve shown in Figure 2.11. The beams had a

width of 100 mm, a length of 1300 mm and a depth ranging from 180 to 200 mm. The concrete cover varied between 10 and 30 mm and the concrete compressive strength was about 40 MPa. The supported length of the beam was 1200 mm, and the beam was subjected to two concentrated loads. The main conclusion of this study was that the fire response of RC beams can be improved by increasing the concrete cover thickness to the reinforcement.

The above review infers that most of the previous experimental studies were aimed at evaluating the fire resistance of RC beams or the extent of spalling of HSC beams. The fire tests considered only a limited number of parameters, generally followed standard fire conditions. No realistic conditions, such as actual fire exposure (with a cooling phase), the restraint effect, loading, and strength/deflection failure criteria, were considered. Most of the fire tests were undertaken using small-scale beams which may not reflect the behavior of large-scale beams used in practical applications.

2.4.2 Analytical Studies

The most notable analytical studies are those reported by Dotreppe and Franssen (1985), Ellingwood and Lin (1991), Kang and Hong (2004), and Shi et al. (2004). Dotreppe and Franssen (1985) developed a finite element based numerical model to trace the behavior of RC beams under fire. The Newton-Raphson procedure was used to perform the iterative nonlinear structural analysis. The model did not consider critical factors such as concrete spalling, creep and transient strains and axial restraint that significantly influence the behavior under fire conditions.

Ellingwood and Lin (1991) developed a mathematical model for tracing the thermal and structural response of RC beams exposed to fire. The finite element method was applied

for both thermal and structural analysis. The model accounted for different strain components in concrete, but did not account for creep of reinforcing steel. Also, the model ignored concrete spalling, axial restraint force, strain hardening in steel reinforcement and tensile strength of concrete. In addition, the model was not fully validated over the whole range of behavior.

Kang and Hong (2004) proposed a numerical model for tracing the fire response of RC beams. Thermal analysis was performed using the finite element method. For structural analysis, to obtain the sectional response, the model assumed the thermal strain to vary linearly across the depth of the beam. The effect of a nonlinear thermal stain distribution was accounted for by introducing an additional self-equilibrating strain. Then Bernoulli-Navier beam theory was applied to trace the response of the whole beam. Their model does not consider different fire scenarios, concrete spalling, axial restraint force, tensile strength of concrete, and various strain components. Also, the model was not fully validated for various scenarios.

Shi et al. (2004) developed a simplified model to predict the behavior of RC beams exposed to fire. This model was developed based on a sectional analysis approach. The load carrying capacity of the beam was estimated by analyzing the critical section. The model included only structural analysis, and thus a heat transfer analysis was not considered. For the structural analysis, the temperatures were assumed similar to the values measured in fire tests conducted by Shi et al. (2004). The model does not account for important factors such as restraint effects, concrete spalling, and fire scenario. In addition, the model is unable to predict the temperature distribution within the cross-section or the deflections in the beam.

Finite element based special purpose computer models such as SAFIR, which was developed at the University of Liège in Belgium (Franssen et al. 2004), can be applied for fire resistance analysis of RC beams. SAFIR, which undertakes coupled or uncoupled thermal and structural analysis, is capable of modeling the behavior of one, two and three-dimensional structures under fire conditions. Although SAFIR can be used to predict the fire response of RC beams, the model does not account for fire induced spalling of concrete. In addition, various strain components for concrete and reinforcing steel are not considered in the analysis. Further, the model does not allow for material constitutive relationships other than those specified in the Eurocodes.

Detailed fire response of structural members can also be assessed through the use of general purpose commercially available microscopic finite element based computers models such as ANSYS and ABAQUS. In all these microscopic finite element models, RC structural members are generally discretized in a one, two or three dimensional mesh. Coupled (or uncoupled) thermal and structural analyses are carried out to trace the fire behavior of RC members. However, the level of analysis associated with these microscopic finite element models is complex, requires significant effort and the results are difficult to interpret. Although such methods are capable of accounting for high temperature material properties, various strain components and different failure criteria (strength and deflections), none of the microscopic finite element models is capable of modeling fire induced spalling of concrete. Further, the constitutive relationships for concrete at elevated temperature in more than one dimension are not well established. This makes the three dimensional modeling of limited use.

The above review of the reported analytical studies and the currently available computer programs reveals a number of limitations and drawbacks. Specifically, most of the models are not fully validated over the entire range of behavior. Also, they do not account for important factors such as fire scenario, failure criterion, concrete strength and load level. Also, the above analytical studies focused only on the behavior of RC beams fabricated with NSC. They were not validated for HSC beams.

2.5 Material Properties at Elevated Temperatures

2.5.1 General

The fire response of RC members is influence by the characteristics of constituent materials, namely, concrete and reinforcing steel. These include: (a) thermal properties (b) mechanical properties (c) deformation characteristics and (d) material specific characteristics such as spalling in concrete. The thermal properties determine the extent of heat transfer to the structural member, whereas the mechanical properties determine the extent of strength loss and stiffness deterioration of the member. The deformation properties (in conjunction with the mechanical properties) determine the deformations and strains in structural members. In addition, fire induced spalling can play a significant role in the performance of RC members fabricated with some types of concrete. All of these material properties and characteristics vary as a function of temperature and depend on the composition and characteristics of concrete as well as those of the reinforcing steel (Kodur et al. 2008).

The thermal properties that influence the temperature rise and distribution in an RC member are thermal conductivity, specific heat, and mass loss for concrete and

reinforcing steel. The mechanical properties that determine the fire performance of RC members are strength, and modulus of elasticity of the constituent materials. The deformation properties are thermal expansion, creep of concrete and steel, and transient strain of the concrete. Creep, often referred to as creep strain, is defined as the time-dependent plastic deformation of the material. At normal stresses and ambient temperatures, the deformation due to creep may not be significant. At higher stress levels and extreme temperatures, however, the rate of deformation caused by creep can be substantial. The main factors that influence creep are temperature, stress level, and their duration.

In addition to thermal, mechanical, and deformation properties, fire induced spalling in concrete influences the fire performance of a concrete structure. For predicting such spalling, additional properties such as porosity and permeability of concrete are required.

All of the above material properties vary as a function of temperature and must be properly accounted for in tracing the fire response of RC members. Further, the variation of many of properties and material characteristics at high-temperatures is often quite sensitive to small changes in the concrete ingredients and environmental conditions (e.g., humidity and temperature rise). As an illustration, the thermal properties are influenced by the type of aggregate and composition of the concrete mix (Flynn 1999). This section provides a review on high temperature properties of concrete and reinforcing steel.

2.5.2 Concrete Properties

2.5.2.1 Thermal Properties

Thermal properties that influence on the thermal response of concrete structures are thermal conductivity, specific heat (or heat capacity), and mass loss. There have been limited test programs for characterizing high temperature thermal properties of concrete (Kodur and Sultan 2003, Shin et al. 2002, Van et al. 1996, Van et al. 1997, Lie and Kodur 1995a, Lie and Kodur 1996 and Saad et al. 1996). Based on the test data, empirical formulae for thermal properties of different types of concrete have been developed (ASCE 1992, Kodur and Sultan 2003, Lie and Kodur 1996, Eurocode 2 2004).

Figure 2.12 illustrates the variation in thermal conductivity of NSC plotted as a function of temperature, while Figure 2.13 shows heat capacity of NSC. The test data is compiled from different studies (Kodur and Sultan 2003, Shin et al. 2002, Lie and Kodur 1995a, Lie and Kodur 1996, Harada et al. 1972, Harmathy and Allen 1973, Harmathy 1970). The large variation in this data can be attributed to the differences in test methods, conditions, procedures and measurement techniques. It can be seen from Figure 2.13 that the aggregate type has a significant influence on the thermal capacity of concrete. The high heat capacity for carbonate aggregate concrete in the temperature range 600 -800°C is caused by the endothermic reaction, which results from the decomposition of dolomite and absorbs a large amount of energy. This high heat capacity in carbonate aggregate concrete helps to minimize spalling and enhance fire resistance.

Very few studies have been carried out to characterize other high-temperature properties of concrete, such as density variations and porosity structure. These tests usually came along with elemental tests, and were not characterized for performance-based design (due

to the fact that test conditions, heating rates and other parameters were not well reported for these tests). Therefore, such properties were not addressed properly in the literature.

Test data generated from the above studies have been used to develop constitutive models, such as those specified in the ASCE manual (1992) and Eurocode 2 (2004), for the temperature dependent thermal properties of concrete. Thermal conductivity and heat capacity from the available constitutive models in Eurocode 2 (2004) and the ASCE Manual of Practice (1992) are also plotted in the Figures 2.12 and 2.13. The high-temperature constitutive models for thermal properties of concrete are presented in Table A.1 in the Appendix. These properties are generally expressed as a function of temperature in the Eurocode, and as a function of aggregate type and temperature in the ASCE Manual. While the ASCE constitutive model accounts for the increase in heat capacity that occurs for carbonate aggregate concrete in the range 600-800°C, the Eurocode constitutive model ignores this effect and has the same heat capacity constitutive model for both siliceous and carbonate aggregate concrete. The ASCE constitutive model describes NSC only, whereas the Eurocode constitutive model was derived for both NSC and HSC. Based on experimental studies, Kodur et al. (2004) extended the ASCE constitutive model, applicable for NSC, to HSC (see Appendix A, Table A.1).

Recent studies have shown that the thermal conductivity and heat capacity of concrete are also dependent on moisture content and concrete porosity, not on temperature alone (Naus 2006, Flynn 1999). Such interdependencies are not taken into consideration in most constitutive models. Therefore, the current high temperature constitutive models may not fully represent realistic thermal properties of concrete.

2.5.2.2 Mechanical Properties

Mechanical Properties during Heating Phase

High-temperature mechanical properties of concrete have been studied more widely than thermal properties. The property tests were carried out in two ways, namely, (1) high temperature tests, and (2) residual tests. In the high temperature tests, the response was measured during exposure to elevated temperatures (Lie and Kodur 1996, Khoury 2006a, Khoury 2006b, Khoury 2006c, Cheng et al. 2005, Wang et al. 2003, Balendran et al. 2003, Lawson et al. 2000, Chan et al. 1999, Khoury 1996, Lie and Kodur 1995b, Furumura et al. 1995, Castillo and Durrani 1990). In these tests, the specimens were subjected to various temperature increments. After attaining a specific target temperature in concrete, the specimen was loaded to failure in order to measure the mechanical response. In the residual tests, the response was measured after exposure to elevated temperatures (Lau and Anson 2006, Chang et al. 2006, Nassif 2006, Xiao et al. 2006, Fu et al. 2005, Savva et al. 2005, Li et al. 2004, Felicetti et al. 1996, Morita et al. 1992). In such tests, the specimens were subjected to various temperature increments. After attaining a specific target temperature in the concrete, the specimen was cooled to room temperature and then loaded to failure to measure its mechanical response. There is a good amount of high-temperature test data on the strength properties of both NSC and HSC with different types of aggregates.

Figures 2.14 and 2.15 show the variation of concrete compressive strength with temperature for NSC and HSC, respectively. Figure 2.14 shows a large but uniform variation of the compiled test data for NSC throughout the temperature range. However, Figure 2.15 shows a larger variation in the compressive strength with temperature for

HSC in the range 200°C to 500°C, and less variation above 500°C. This is mainly because fewer test data points were reported for temperatures higher than 500°C either due to the occurrence of spalling or due to limitations in the test apparatus. However, a wider variation is observed for NSC in this temperature range (above 500 °C) when compared to HSC as seen from Figures 2.14 and 2.15. This is mainly because of the higher number of test data points reported for NSC in the literature and also due to the lower tendency of NSC to spall under fire. The variations in the mechanical properties of concrete at high-temperatures are quite high. These variations from different tests can be attributed to using different heating or loading rates, specimen curing, condition at testing (moisture content and age of specimen), and the use of admixtures.

Among the factors that directly affect the high-temperature mechanical property test results are the initial curing, moisture content at the time of testing and the addition of admixtures and silica fume to the concrete mix. These factors are not addressed in the literature, and there is no test data that shows the influence of these factors on the high-temperature mechanical properties of concrete.

Another main reasoning for the significant variation in the high-temperature properties of concrete is the use of different testing conditions (such as heating rate and strain rate) and test procedures (hot strength test and residual strength test) due to a lack of standardized test methods for carrying out property tests. Further, much of the data reported in the literature does not provide full details on the type of aggregate, moisture content, and heating or loading rates under which the tests were conducted. Therefore, the constitutive models developed from such test data may not be reliable.

Based on the data from mechanical property tests, researchers have proposed different constitutive models for high temperature mechanical properties of concrete. The most widely used constitutive models present in the Eurocode 2 (2004), ASCE Manual of Practice (1992), and Kodur et al. (2004) are reproduced in Appendix A Table A.1. The ASCE model is valid for NSC, the Eurocode model is valid for both NSC and HSC, and the Kodur et al. (2004) model is valid for HSC. These relations give the rate of degradation of concrete as a function of temperature only, and without any consideration to variations in other significant parameters such as rate of loading, heating, and material composition. Figures 2.14 and 2.15 show the variation of concrete strength with temperature for NSC and HSC, respectively, according to the models in Eurocode 2, ASCE 1992 and Kodur et al.(2004) and from test data reported in the literature.

It can be seen from Figures 2.14 and 2.15 that there is a large variation in the reported test data and also from the different models present in ASCE, Eurocode and Kodur et al. (2004). For example, the reduction in NSC compressive strength with temperature based on the ASCE model (1992) seems to be closer to the upper bound of the reported experimental data. However, the Eurocode 2 (2004) curve for the strength reduction of NSC is closer to the lower bound of the reported test results.

Phan and Carino (2003) reviewed the current high-temperature constitutive models for the compressive strength of HSC and proposed a lower bound model for the compressive strength of HSC (shown in Figure 2.15). However, even this model is not conservative throughout the temperature range 100-500°C as can be seen from Figure 2.15. Overall, the model proposed in Eurocode 2 (2004) for Class 3 of HSC gives conservative values for concrete compressive strength reduction with temperature.

The above review clearly illustrates the large variation in the available test data and constitutive relationships in codes and standards for high-temperature strength properties. Consequently, performance-based design using these models is expected to produce diverse fire resistance predictions. However, Kodur et al. (2008) showed that using the ASCE model (which is most commonly used for fire resistance evaluation in North America) produces better fire resistance predictions for NSC columns when compared to the Eurocode model.

Mechanical Properties during Cooling Phase

Upon cooling (in the decay phase of the fire scenario), concrete continues to lose its strength and stiffness. This can be mainly attributed to the hydration of some of the dehydrated cement components upon cooling. The products of such hydration are of larger volumes than those of the original components. This leads to further cracking in the concrete. Thus, the residual strength of concrete is generally less than the strength of heated concrete (provided both are heated to the same temperature). The residual strength of concrete is important in modeling RC members exposed to design (or real) fire scenarios where a cooling phase always exists. The literature review shows that there is a large variation in the residual strength of concrete as shown in Figure 2.16. This large variation can be attributed to using different heating (or cooling) or loading rate, specimen and test conditions, and the use of admixtures. Codes and standards, such as Eurocode 2 and ASCE manual, do not specify relationships for the residual strength of concrete after fire exposure. Thus, the best fit of the reported test data, which is generally used for evaluating the residual strength of concrete, is plotted in Figure 2.16 (Kumar 2004).

2.5.2.3 Deformation Properties

Deformation properties are highly dependent on the chemical composition, the type of aggregate and the chemical and physical reactions that may occur in the concrete during heating (Schneider 1988). Deformation properties include thermal expansion, creep strain and transient strain.

Thermal Expansion

The coefficient of thermal expansion represents the change in length of a material due to temperature changes. The coefficient of thermal expansion, which is defined as the change in a unit length of a material caused by a unit (degree) increase in temperature, is important as a measure of the structural movement and thermal stresses resulting from temperature changes (Kodur et al. 2008).

Data from the literature indicates that there is large variation in the measured thermal expansion of concrete as shown in Figures 2.17. This can be attributed to the fact that the coefficient of thermal expansion of concrete is affected by the aggregate type and its composition, moisture content and many other factors. The thermal expansion of siliceous aggregate concrete is greater than that for carbonate aggregate concrete. At high temperatures (600°C to 800°C) most concretes no longer exhibit any expansion and in some cases contract as shown in Figure 2.17.

Creep and Transient Strain

Creep is defined as the time-dependent plastic strain under constant stress and temperature. Creep strains generally occur due to the movement of moisture in concrete and thus are largely influenced by concrete temperature. At room temperature, the

movement of moisture in concrete is limited, and therefore creep deformations occur at a very slow pace. However, at elevated temperatures, significant moisture movement occurs in concrete resulting in larger creep strains. Because creep affects strain, deflection, and stress redistribution, it plays an important role in the fire response of structural members. Since high temperature causes degradation of the concrete properties, creep properties will also be affected.

A review of the literature shows that high temperature creep of concrete depends on many factors including temperature, loading, and mix proportions. The review indicates that creep generally increases with temperature. It also shows that low-modulus aggregates exhibited increased creep deformation. Creep rates were found to be significantly higher at elevated temperatures than under ambient conditions. In addition, it was found that creep increases with increasing load level.

Compared to creep strain, transient strain occurs during the first time that concrete is heated under load, but not upon subsequent heating (Khoury et al. 1985), and is independent of time. Transient strain is essentially caused by the thermal incompatibilities between the aggregate and the cement paste (Purkiss 2007). During heating of concrete, there are complex changes in the moisture content and chemical composition of the cement paste, and there is also a mismatch in thermal expansion between the cement paste and the aggregate. Such mismatches lead to internal stresses and micro-cracking in the concrete constituents (aggregate and cement paste) and results in transient strain in the concrete (Schneider 1988).

A review of the literature shows that there is very limited information on creep and transient strain of concrete at elevated temperature (Kodur et al. 2008). However, based

on the limited available data in the literature, Anderberg and Thelandersson (1976) developed constitutive models for creep and transient strain in concrete at elevated temperatures (Harmathy 1993). According to them, the creep strain and transient strain of concrete at elevated temperatures are given by the following two equations, respectively:

$$\varepsilon_{cr} = \beta_1 \frac{\sigma}{f_{c,T}} \sqrt{t}\, e^{d(T-293)} \qquad [2.3]$$

$$\varepsilon_{tr} = k_2 \frac{\sigma}{f_{c,20}} \varepsilon_{th} \qquad [2.4]$$

where ε_{cr} = creep strain, ε_{tr} = transient strain, $\beta_1 = 6.28\times10^{-6}$ $s^{-0.5}$, $d = 2.658\times10^{-3}$ K^{-1}, T = concrete temperature (K) at time t (s), $f_{c,T}$ = concrete strength at temperature T, and σ = stress in the concrete at the current temperature, k_2 = a constant ranges between 1.8 and 2.35, ε_{th} = thermal strain, and $f_{c,20}$ = concrete strength at room temperature. These formulae generally produce reasonable estimates for high temperature creep and transient strains in concrete (Anderberg and Thelandersson 1976, Harmathy 1993).

2.5.2.4 Fire Induced Spalling

General

The occurrence of spalling in concrete members can broadly be classified into three stages, namely, early spalling, intermediate spalling, and late spalling. In typical RC members (beams and columns), early spalling can start immediately after fire exposure (5 to 10 minutes) and can continue up to 30 to 45 minutes. This type of spalling is generally an explosive in nature and often results due to the development of high thermal gradients within parts (surfaces close to fire exposure) of the concrete members. Early spalling

results in the break-up of large chunks of concrete and thus may have a detrimental influence on the fire resistance of RC members, particularly when spalling reduces the concrete cover thickness to the main reinforcement.

Intermediate spalling occurs mid-way through fire exposure (about 30 to 45 minutes) and results in surface scaling (breaking off of small pieces of concrete). This can continue through the final stages of fire exposure. Such spalling has less effect on the fire resistance of RC members since it generally results in a break-up of the thin layers of concrete. Late spalling occurs just prior to failure of structural members and primarily results from a significant loss of strength and stiffness of the structural member due to prolonged fire exposure. This spalling has a minor influence on the overall fire response of RC members. Such type of spalling occurs even in room temperature conditions prior to failure of concrete members.

Spalling generally results in reduced cross-sections and rapid strength loss, thereby lowering the fire resistance of a concrete member. A review of the literature indicates that the main factors influencing fire induced spalling in concrete are moisture content, concrete permeability, concrete strength, fire scenario (rate of heating) and stress levels (Phan 1996, Phan et al. 2000, Kodur and Phan 2007). Compared to NSC, HSC has a higher susceptibility to fire induced spalling. This is probably because the low permeability and the high density of HSC prevent water vapor from escaping at elevated temperatures and leads to high pore pressure buildup, producing spalling. In addition, HSC is normally subjected to higher stress levels than NSC which may enhance the conditions for fire induced HSC spalling.

Causes of Spalling

A review of the literature presents a conflicting picture on the occurrence of spalling and also on the exact mechanism. While some researchers reported explosive spalling in concrete structural members, a number of other studies reported little or no significant spalling. One possible explanation for this confusing trend of observations is the large number of factors that influence spalling and their inter-dependency. However, most researchers agree that the major causes for spalling in concrete are low concrete permeability of concrete and moisture migration at elevated temperatures.

There are two broad theories by which the spalling phenomenon can be explained (Kodur 2000):

- **Pressure build-up:** Spalling is believed to be caused by the build-up of pore pressure during heating. HSC is believed to be more susceptible to this pressure build-up than NSC because of its low permeability. The extremely high water vapor pressure, generated during exposure to fire, cannot escape due to the high density (and low permeability) of HSC. When the effective pore pressure (porosity times pore pressure) exceeds the tensile strength of concrete, chunks of concrete fall off from the structural member as shown in Figure 2.18. This falling off can often be explosive depending on the fire and concrete characteristics (Harmathy 1993, Anderberg 1997).
- **Restrained thermal dilatation:** This hypothesis considers that spalling results from restrained thermal dilatation close to the heated surface, which leads to the development of compressive stresses parallel to the heated surface as shown in Figure 2.19. These compressive stresses are released by brittle fractures of concrete (spalling). The pore pressure can play a significant role in the onset of instability in the form of explosive thermal spalling (Bazant 1997).

Previous Studies on Fire Induced Spalling

Experimental Studies

In the last two decades, there have been several experimental studies to investigate fire induced spalling in HSC. Some of these studies were conducted on small scale specimens (cylinders) (Phan 2007, Han et al. 2005, Hertz 2003, Kalifa et al. 2001, Phan et al. 2000). Other studies were conducted on building components (columns and concrete blocks) such as those reported by Park et al. (2007), Kodur (2003b), Kodur and McGrath (2003), Kodur et al. (2003), and Bilodeau et al. (2004). All these studies have shown that HSC is more susceptible to spalling than NSC.

Phan (2007) investigated the effect of temperature induced pore pressure buildup and potential for explosive spalling in concrete. The pore pressure measurements were conducted on 100 × 200 × 200 mm blocks heated to 600°C at two heating rates, namely, 5°C/min and 25°C/min. Other factors such as water-to-cementitious-material ratio (w/cm), curing condition, and addition of polypropylene fibers, on the buildup of pore pressure in heated concrete were also investigated. The study concluded that spalling occurs in HSC at temperatures between 220-245°C. The study also showed that specimens with high water-cement ratio and with lower initial moisture content developed lower pore pressure (and thus were less prone to spalling) than those with low water-cement ratio or low initial moisture content. Furthermore, the addition of polypropylene (PP) fibers caused a significant reduction in maximum pore pressure and thus prevented explosive spalling in HSC specimens.

Han et al. (2005) conducted fire tests to study the spalling resistance of HPC, reinforced with PP fibers or sheet material as lateral confinement. The concrete specimens were 100

mm × 200 mm cylinders reinforced with metal fabrics of 0.6 mm and 1.6 mm in thickness, or with glass fiber sheets. The study concluded that the PP fibers mitigated spalling of HSC. Metal fabrics increased the resistance to spalling by the confinement effect, whereas glass fiber sheets were ineffective to reduce spalling of the HSC specimens.

Hertz (2003) conducted fire tests to illustrate the influence of thermal stresses on spalling of dense concrete. Ten 600 × 600 × 20 mm^3 tiles made of dense concrete were heated over a limited area of 200 × 200 mm^2 at the center of one side of each specimen. All specimens were heated using a sudden exposure from a hole in an oven at a constant temperature. Hertz (2003) concluded that spalling of concrete is not expected if the concrete does not contain small particles such as silica fume and if the moisture content is lower than 3%. He also found that spalling occurs at temperatures near the critical temperature of water (temperature at which all evaporable water in concrete becomes vapor) which is about 374 °C. Further, thermal stresses significantly influenced spalling of dense concrete. In addition, he concluded that PP fibers are effective in mitigating spalling of dense concrete.

Kalifa et al. (2001) tested 120-mm thick RC slabs by exposing them to rapid heating from one side to investigate fire induced HSC spalling in a PP-HSC mix. A heating rate of 5°C/sec was used for the first two minutes and then the temperature was kept at 600°C. Temperature and pore pressure were measured at different locations within the slab. The study concluded that pp fibers increased the permeability and thus decreased the pore pressure in concrete at the elevated temperatures. The lower pore pressure reduces the potential of fire induced spalling in concrete.

Phan et al. (2000) reported the results of a study on the residual strength and spalling of HSC and NSC. Cylinders of 102 mm × 204 mm were fabricated from concrete with compressive strength ranging from 51 to 93 MPa. The specimens were heated at a 5°C/minute rate so that their internal temperature reached 450°C and cooled down to be tested for residual strength. Spalling was observed in the specimens. It was found that HSC is more susceptible to spalling than NSC.

Park et al. (2007) conducted fire resistance tests on HSC columns to investigate the effect of tie spacing and section size on fire induced spalling. They tested five RC columns (three of 305 mm × 305 and two of 500 mm × 500 mm cross-section). Two concrete batches with compressive strength of 69 MPa and 138 MPa, respectively, were used in fabricating the columns. Both concrete batches were made of siliceous aggregate. The columns were loaded with 55% of their room temperature capacity and exposed to the ISO 834 (1971) standard time temperature curve. The main finding was that fire induced HSC spalling is significantly influenced by cross-sectional size and tie spacing.

Kodur (2003b) carried out fire resistance tests on a number of full-scale RC columns. The test variables included column dimensions, concrete strength, aggregate type, tie configuration, addition of fiber reinforcement, type of fiber, load intensity and eccentricity of loading. All columns were of 3810 mm long. The compressive strength of concrete was between 34 MPa and 110 MPa, with most columns being in the range of 80–100 MPa. The study showed HSC columns are more prone to spalling than NSC columns. This study also showed that spalling of concrete is influenced by many factors including moisture content, concrete density, heating rate, specimen dimensions, tie spacing and configuration, fiber reinforcement, aggregate type and load intensity.

Kodur and McGrath (2003) investigated the fire performance of HSC by testing six RC columns. The main factors varied in the test included cross-sectional size, aggregate type, and tie configuration. The main findings in this study were that HSC was more prone to spalling than NSC and that carbonate aggregate concrete experienced less spalling than siliceous aggregate concrete. The study also showed that the tie configuration (bending of ties at 135°, and provision of cross ties), and closer tie spacing reduced HSC spalling.

Kodur et al. (2003) carried out fire tests on fifteen RC columns to evaluate the influence of strength and fiber reinforcement on the fire resistance of HSC columns. The variables considered included concrete strength, aggregate type, and fiber reinforcement (steel and polypropylene fibers). HSC was found to be more susceptible to spalling than NSC. The study showed that PP and steel fibers reduced concrete spalling. In addition, carbonate aggregate concrete was more resistant to spalling than siliceous aggregate concrete.

Bilodeau et al. (2004) investigated the optimum amount of PP fibers to be added in lightweight HSC to mitigate spalling. Twelve concrete blocks with 610 × 425 × 770 mm^3 size were cast from twelve different batches of concrete. The concrete compressive strength ranged between 59.1-70.8 MPa. The blocks were tested under hydrocarbon fire exposure in a furnace in accordance with ISO 834 (1975). After the test, spalling of concrete in the blocks was evaluated and cores were taken from the blocks to determine the residual compressive strength. The study showed that about 3.5 kg (0.75% by weight of cement) of 20 mm PP fibers was required per cubic meter of concrete to mitigate spalling in low water/cement ratio concrete. However, only 1.5 kg (0.35% by weight of cement) was required to mitigate spalling if 12.5 mm PP fibers were used. Thus, the study showed that 12.5 mm fibers were more effective in mitigating spalling of HSC.

Further, spalling of HSC largely increased with the degree of absorption of light weight aggregate used in the concrete.

From these experimental studies it is clear that spalling of concrete is a complex phenomenon that depends on the following factors:

- Concrete strength: HSC is more susceptible to spalling than NSC.
- Concrete moisture content: moisture content increases the potential for spalling in concrete.
- Concrete density: the extent of spalling is much greater when the lightweight aggregate is used.
- Heating rate: a higher heating rate increases fire induced concrete spalling.
- Specimen dimensions: the risk of explosive thermal spalling increases with specimen size.
- Tie configuration and spacing: spalling in HSC columns can be minimized by providing an improved tie configuration (provision of bent ties at 135° back into the core of the column and increased lateral reinforcement) and with a closer tie spacing (at 0.75 times that required for the NSC columns).
- Fiber reinforcement: addition of PP or steel fibers reduces fire induced HSC spalling.
- Type of aggregate: carbonate aggregate concrete is less prone to spalling than siliceous aggregate concrete.

Analytical Studies

Most of the analytical studies reported in the literature indicate that fire induced spalling occurs when the internal pore pressure exceeds the tensile strength of concrete.

Calculation of the pore pressure in concrete requires a hydro-thermal or hydro-thermo-mechanical analysis. Models for hydro-thermal analysis were developed by Tenchev et al. (2001), Qian et al. (2005), Tenchev and Purnell (2005), Gawin et al. (1999, 2005) and Witek et al. (2006).

The Tenchev et al. (2001) model is based on conservation of mass and energy in a control volume of concrete. It accounts for the dehydration of cement paste at high temperatures. Movement of both air and water vapor is assumed to follow Darcy's law. Their model is capable of predicting the buildup of pore pressure inside concrete exposed to fire. However, the model is not extended to account for spalling or the updated boundary conditions of the cross-section once spalling occurs in concrete. The model also ignores the mobility of liquid water and the variation of concrete permeability with temperature.

Qian et al. (2005) suggested a simple hydro-thermal model to predict the vapor pressure inside concrete. Their model assumed diffusion to be the driving force for moisture movement inside concrete. The model ignored dehydration of cement paste at elevated temperatures, mobility of liquid water and air, air pressure, and variation of concrete permeability with temperature. In addition, the isotherms (the relations between the amount of liquid water and pore pressure at constant temperature) used in the model were not reported.

Similar to the model developed by Tenchev et al. (2001), Tenchev and Purnell (2005) developed a hydro-thermo-mechanical model to predict fire induced spalling. The model was derived based on the principles of mechanics and thermodynamics and it accounts for coupling between stress analysis and pore pressure calculations. Moisture migration and the effect of concrete damage are also included in the model. However, in this model,

to accurately predict fire induced spalling in concrete, material properties such as the concrete permeability tensor, diffusion coefficients, material stiffness tensor, must be provided as input data. These properties vary as a function of temperature and many of them are not well defined, even at room temperature.

Gawin et al. (1999, 2005) and Witek et al. (2006) developed a hydro-thermo-mechanical model to predict spalling in concrete. The model applies the conservation of mass, momentum and energy principles for pore pressure calculations in heated concrete. The model accounts for the mobility of water and the variation of the permeability as a function of temperature and pore pressure. For such models to accurately predict the spalling of concrete, material properties such as the concrete permeability tensor, diffusion coefficients, and the material stiffness tensor must be precisely known. These properties vary as a function of temperature.

In lieu of complex hydro-thermo-mechanical models, Kodur et al. (2004) suggested a simplified "rule-of-thumb" approach for estimating spalling in HSC columns. This approach was developed based on actual observations in a large number of fire tests on RC columns and correlates the pore pressure development with the temperature rise. Accordingly, the extent of spalling in HSC can be computed based on the following guidelines:

- Spalling occurs when the temperatures in a layer of an HSC column exceed 350 °C.
- The extent of spalling is influenced by the stirrup configuration adopted for the beam as follows:
  - Spalling occurs throughout the cross-section when the stirrups are bent in a conventional pattern (no hooks).

- Spalling occurs only outside the reinforcement cage when the stirrups are bent at 135° into the concrete core.

- No spalling occurs when PP fibers are present in the concrete mix.
- No spalling occurs inside the reinforcement core when the stirrup spacing is 0.7 times the standard spacing.
- When spalling occurs, its extent depends on:
  - Type of aggregate: the extent of spalling is higher (100%) in siliceous aggregate HSC than that for carbonate aggregate HSC (40%).
  - Presence of steel fibers in the concrete mix: the extent of spalling in HSC columns with steel fiber is about 50%.

Due to significant approximations associated with monitoring spalling during fire tests, this approach may not provide a reliable prediction of spalling. Further, the approach was developed specifically for RC columns and may not be applicable for RC beams. Thus, the currently available spalling models (hydro-thermo-mechanical models and simplified approaches) are of limited practical use.

Codes and Standards

A review of the literature also indicates that there are limited guidelines in current codes and standards to predict fire induced spalling. The specifications in Eurocode 2 (2004) state that spalling is unlikely to occur when the moisture content in concrete is lower than 3% without any due considerations to concrete permeability and the tensile strength of concrete. ACI 216.1 standard (2007) does not have any specifications for predicting concrete spalling. However, this standard provides some guidelines for mitigating spalling through the addition of PP fibers. It should be noted that the guidelines on fire

induced spalling in current codes are mainly derived from fire tests on small specimens. They do not account for moisture migration and pore pressure buildup. The lack of calculation methodologies for predicting spalling is one of the main reasons for slow progress in developing effective spalling mitigation measures in concrete structures.

2.5.3 Reinforcing Steel Properties

High temperature properties of reinforcing steel that influence the fire response of concrete structures are: thermal properties, mechanical properties, deformation properties and specific properties such as bond strength.

2.5.3.1 Thermal Properties

The thermal properties of reinforcing steel depend on the type and temperature of the steel. These properties include thermal conductivity and thermal capacity. The thermal conductivity of reinforcing steel is high in comparison with concrete and thus heat is distributed through steel rebars quite rapidly. In addition, steel reinforcement is embedded in concrete and is of very small area as compared to concrete. For these reasons, in fire resistance calculations steel reinforcement is generally assumed to be a perfect conductor, which implies that temperature is uniform within the steel area, and thus do not separately account for steel reinforcement in a thermal analysis. As temperature rises, the thermal properties of steel become more dependent on temperature and are influenced less by the steel composition (Williams 2004). However, it has been shown that reinforcing steel has a small influence on the temperature distribution within the RC cross-section (Lie and Irwin 1993). Thus, thermal properties of reinforcing steel are not very important for predicting temperature distributions in RC members.

2.5.3.2 Mechanical Properties

Mechanical properties of reinforcing steel include yield strength, ultimate strength and modulus of elasticity. These properties are generally represented by the stress-strain-temperature relationships of steel. The literature review shows that there is a large variation in the yield and ultimate strength of steel as shown in Figure 2.20 (Harmathy 1993). Some of this variation is due to the variation of steel composition and the lack of definition of the yield strength of steel (Buchanan 2002). The variation of yield and ultimate strength of reinforcing steel as a function of temperature, specified in the ASCE Manual (1992) are also shown in Figure 2.20. It can be seen that the ASCE model follows the lower bound yield strength of steel. However, for ultimate strength, the ASCE model is overly conservative for temperatures below 500°C and unconservative for temperatures above 700°C.

A review of the literature indicates that reinforcing steel recovers nearly all of its original yield strength upon cooling as long as heating temperatures do not exceed 500°C (Neves et al. 1996). However, for steel heated to temperatures above 500°C the residual strength starts to decrease gradually as shown in Figure 2.21. The behavior of reinforcing steel in the cooling phase is crucial for modeling the response of RC structural members exposed to real (design) fire scenarios. The high-temperature constitutive models for mechanical properties of reinforcing steel are presented in the Appendix Table A.3.

2.5.3.3 Deformation Properties

Deformation properties of reinforcing steel include thermal strain and creep strain. The thermal strain of reinforcing steel at elevated temperatures is directly related to the temperature rise and generally increases with temperature. Between 650-815°C thermal

strain decreases, due to a phase transformation in the steel, before increasing again. The variation for the thermal strain as a function of temperature as per the ASCE Manual (1992) is shown in Figure 2.22.

Creep strain is the gradual increase in strain with time under a constant stress. Creep strain occurs due to the movement of dislocations in the slip plane (in the microstructure of steel). Normally, steel (metal) composition contains a variety of defects, for example solute atoms, that act as obstacles to dislocation movement. At room temperature, the amount and distribution of these defects remains almost uniform and thus creep strains occur at a very rate. However, at high temperatures, vacancies in the crystal structure can diffuse to the locations of a dislocation and cause the dislocations to move faster to an adjacent slip plane thereby allowing further deformation to occur. Thus, creep strain becomes significant at elevated temperatures, particularly above 450°C, and should be included in modeling the fire response of RC members. A review of the literature indicated that there is very little information on high temperature creep strain of reinforcing steel. The available creep models, such as the one proposed by Harmathy (1967), are based on Dorn's theory, which relates the creep strain to the temperature, stress, and time. More information on Harmathy's creep model is provided in Chapter 4. The high-temperature constitutive models for deformation properties of reinforcing steel are presented in the Appendix Table A.3.

2.5.3.4 Other Properties

Other properties of reinforcing steel that may influence the fire response of concrete structures include bond between concrete and reinforcing steel, which arises primarily from friction and adhesion between concrete and steel. Generally, bond strength is a

function of: (1) mix proportions of concrete (cement type, admixtures, water-cement ratio), (2) mechanical properties of the steel (size and spacing of the ribs if any), and (3) rebar position within the concrete member (under tension or compression). Permissible bond stresses are generally specified as percentages of concrete's compressive strength (Naus 2006).

The bond between concrete and steel at room temperature has been well studied. However, there are limited studies on the effect of elevated temperatures on the bond properties between steel and concrete. The most notable study is that reported by Harmathy (1993), which showed that in the case of deformed bars, the bond strength degrades at elevated temperatures in a trend similar to that of the compressive strength of concrete. Thus, the reduction in bond strength is similar to the reduction in concrete compressive strength at elevated temperature for deformed bars (which are the most widely used steel bars in concrete structures). Thus, bond failure is not likely to occur in RC beams at elevated temperatures due to the fact that the degradation in the strength of reinforcing steel is faster than the degradation in the bond strength (which is similar to that of the concrete compressive strength).

2.6 Summary

This chapter presents an overview of the behavior of RC beams under fire. The current approaches for evaluating the fire resistance of RC beams were reviewed. In addition, the main findings and drawbacks of experimental and analytical studies on the fire response of RC beams were discussed. Previous experiments and analytical studies investigated the influence of only a limited number of parameters on the fire response of RC beams. Critical factors such as different fire scenarios, axial restraint effects, and spalling were

not addressed in many of the reported experiments and analytical studies. The material properties of concrete and reinforcing steel at elevated temperature that are crucial for predicting the fire response of RC beams are also reviewed in this chapter. The high temperature properties of concrete and reinforcing steel show large variations. This may result in large variations in the predicted fire response of RC beams. Consequently, there are few guidelines and calculation methods for evaluating the fire resistance of RC beams. The available provisions in codes and standards are generally prescriptive and may not be applicable for performance-based design. Thus, there is a critical need for further analytical and experimental research leading to the development of rational approach for the fire resistance design of RC beams.

Table 2.1 - ACI Minimum Width and Cover Thickness Requirements for Achieving Fire Resistance in RC Beams (ACI 216.1 2007)

Support Conditions	Minimum Beam Width (mm)	Cover Thickness for Fire Resistance in Minutes (mm)				
		60	90	120	180	240
Unrestrained	127	19	25	32	Not permitted	Not permitted
	178	19	19	19	44	76
	≥ 254	19	19	19	25	44
Restrained	127	19	19	19	25	32
	178	19	19	19	19	19
	≥ 254	19	19	19	19	19

Table 2.2 - Eurocode Specifications for Fire Resistance Rating of Continuous RC Beams (Eurocode 2 2004)

Beam Dimensions/Fire Resistance (minutes)		30	60	90	120	180	240
Possible Combinations of Beam Width and Axis Distance (mm)	Beam Width	80	120	150	200	240	280
	Axis Distance	15	25	35	45	60	75
	Beam Width	160	200	250	300	400	500
	Axis Distance	12	12	25	35	50	60
	Beam Width	****	****	****	450	550	650
	Axis Distance	****	****	****	35	50	60
	Beam Width	****	****	****	500	600	700
	Axis Distance	****	****	****	30	40	50

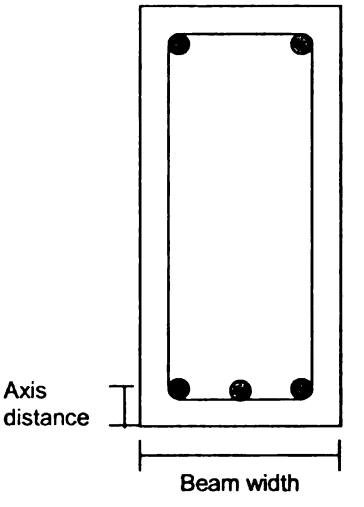

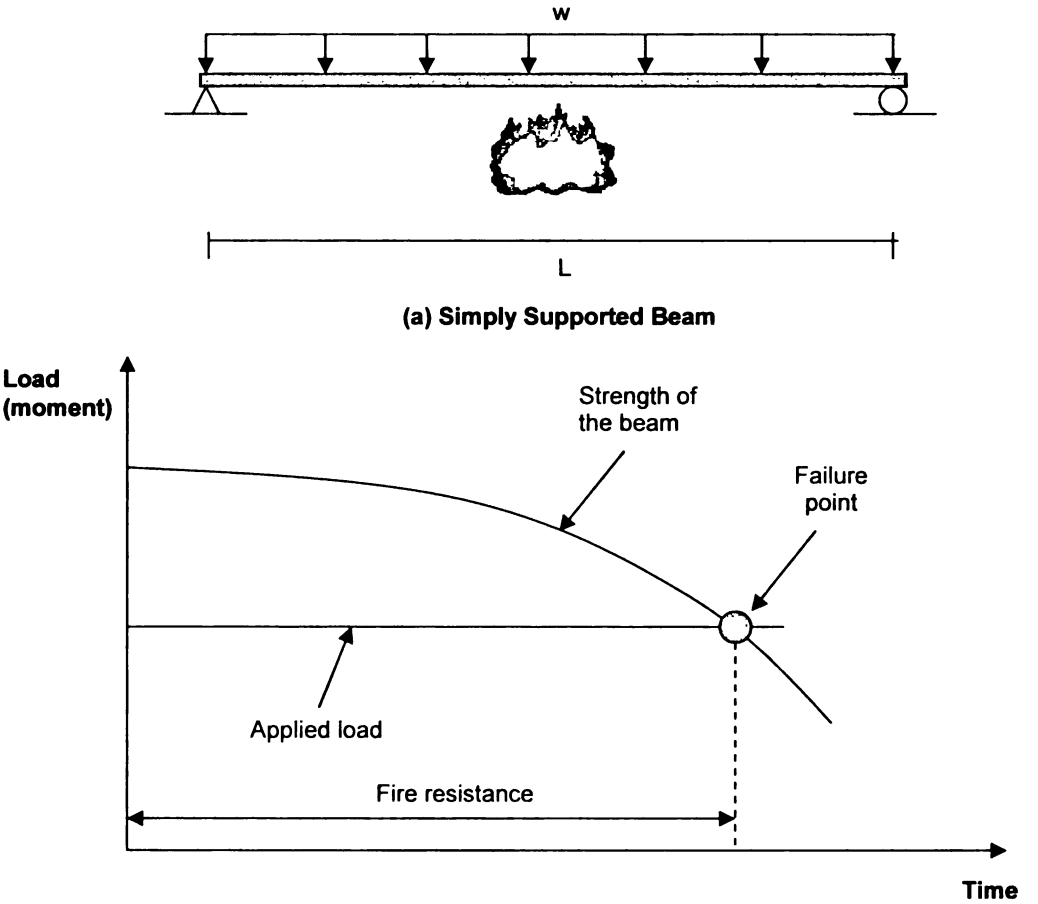

Figure 2.1 – Degradation of Strength of RC Beam Exposed to Fire

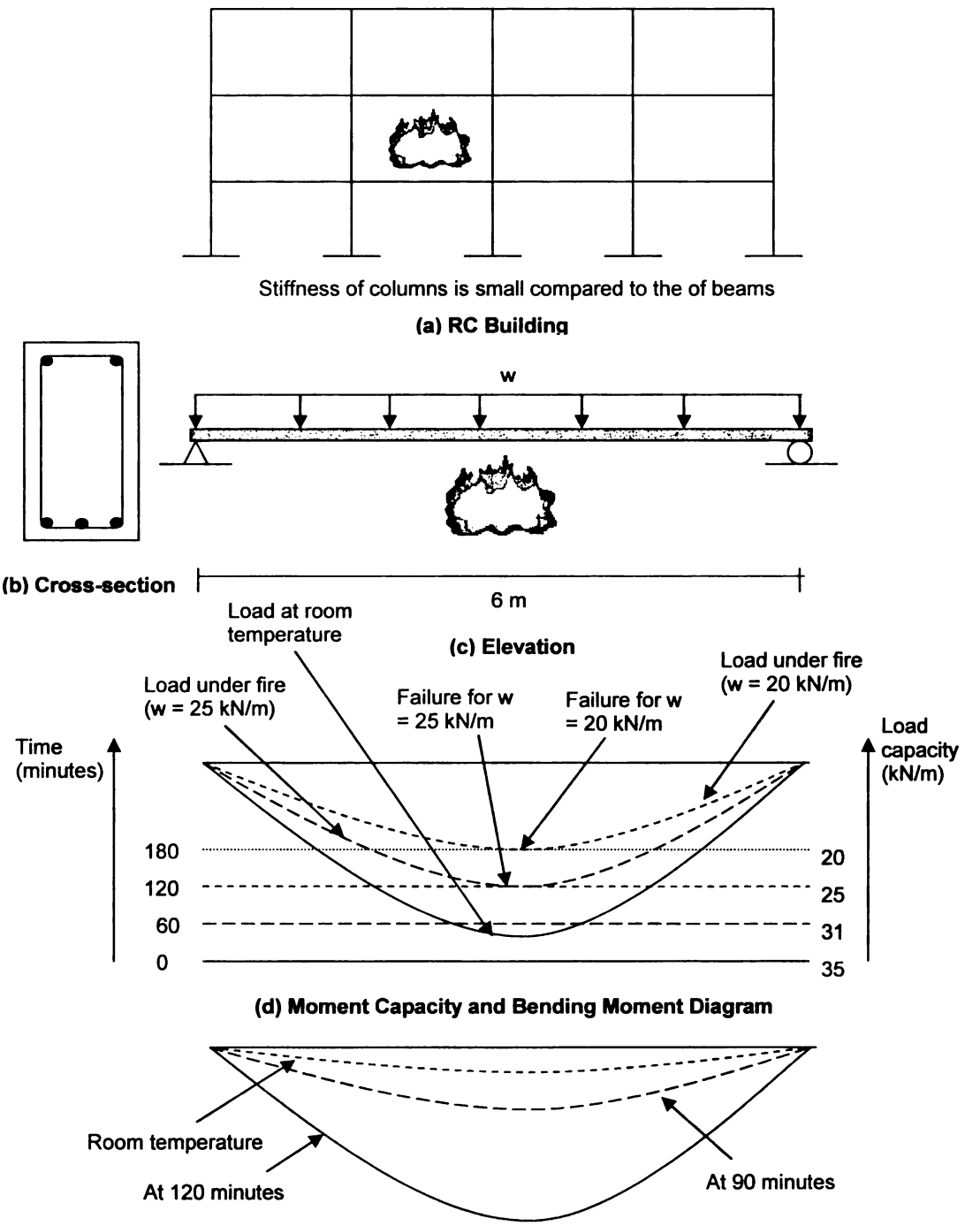

Figure 2.2 – Illustration of Degradation of Load Carrying Capacity for an RC Beam Exposed to Fire

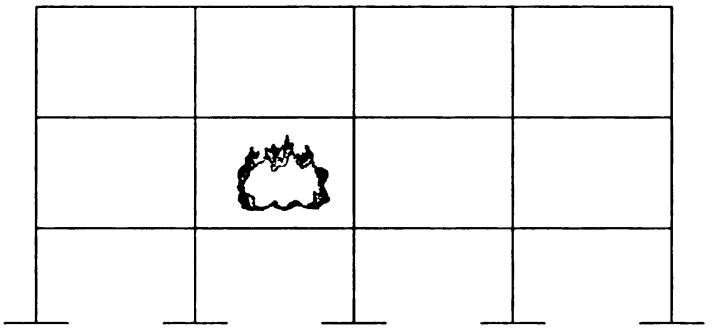

(a) RC Building

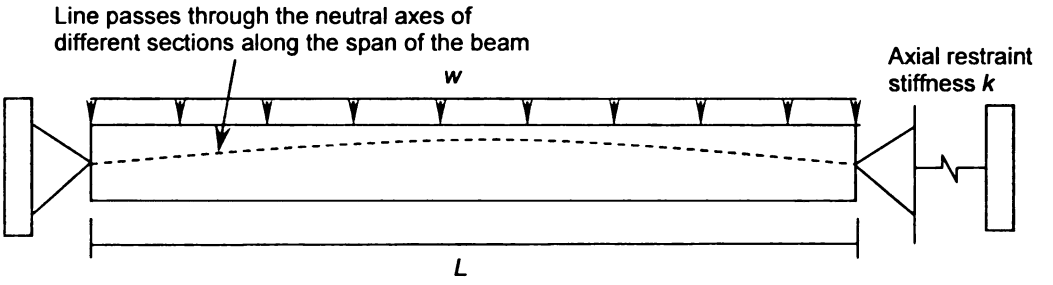

(b) Elevation

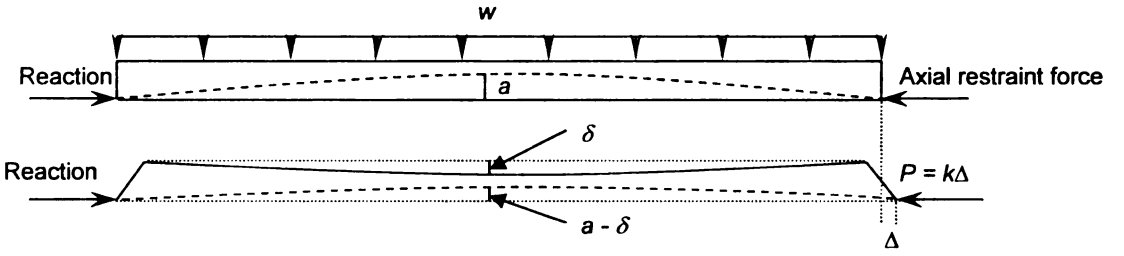

(c) Illustration of Arch Action

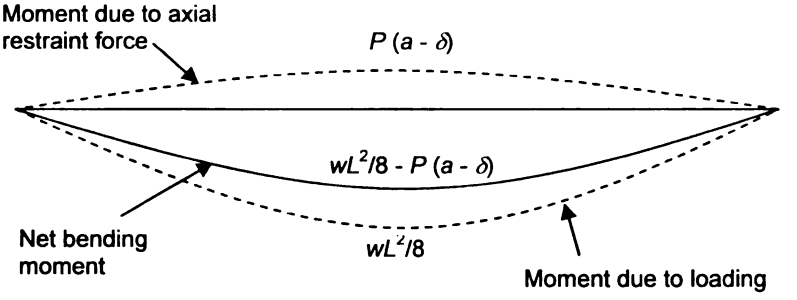

(d) Bending Moment Diagram

Figure 2.3 – Illustration of the Effect of Axial Restraint on the Fire Response of an RC Beam

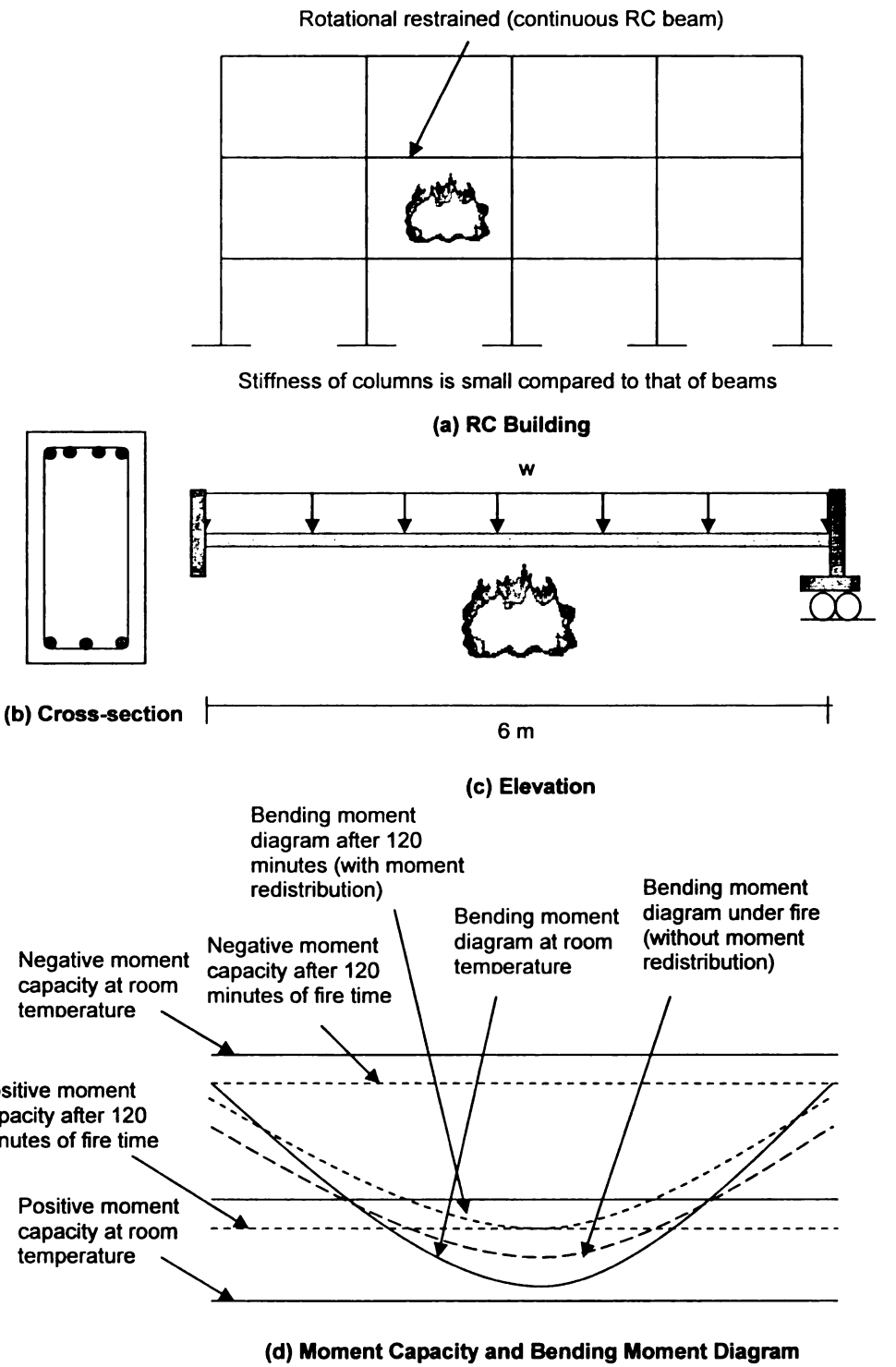

Figure 2.4 – Illustration of the Effect of Rotational Restraint on the Fire Response of an RC Beam

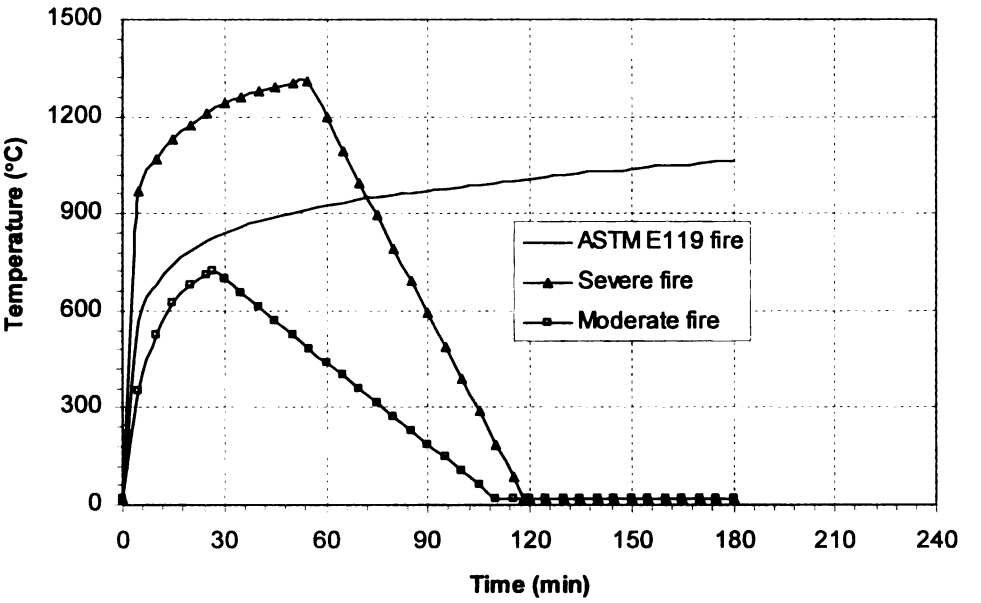

Figure 2.5 - Time-Temperature Curve for ASTM E119 Standard Fire and Two Design Fire Exposures

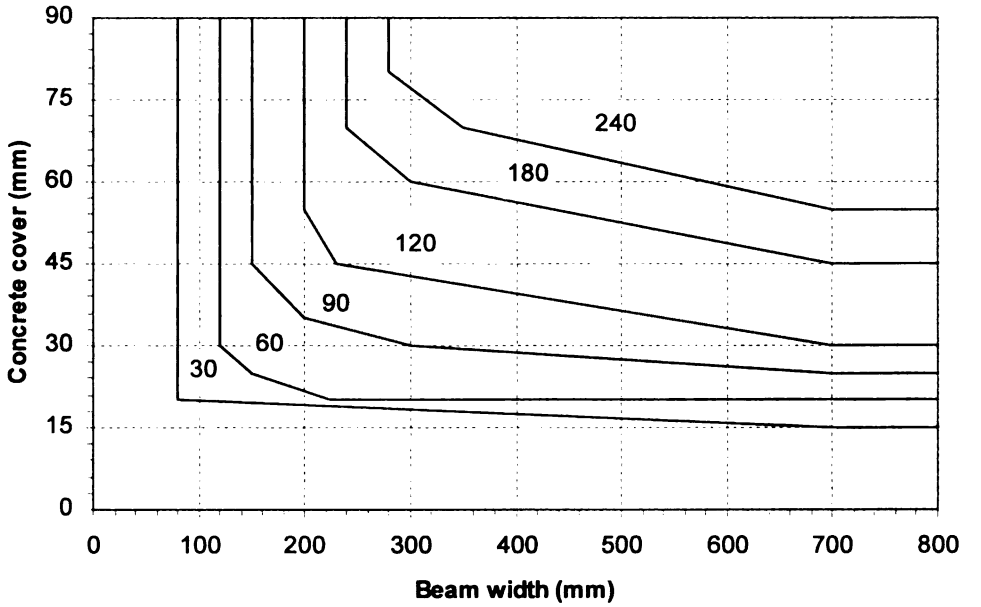

Figure 2.6 - Fire Resistance (in minutes) of Simply Supported RC Beam as per AS 3600 (2001)

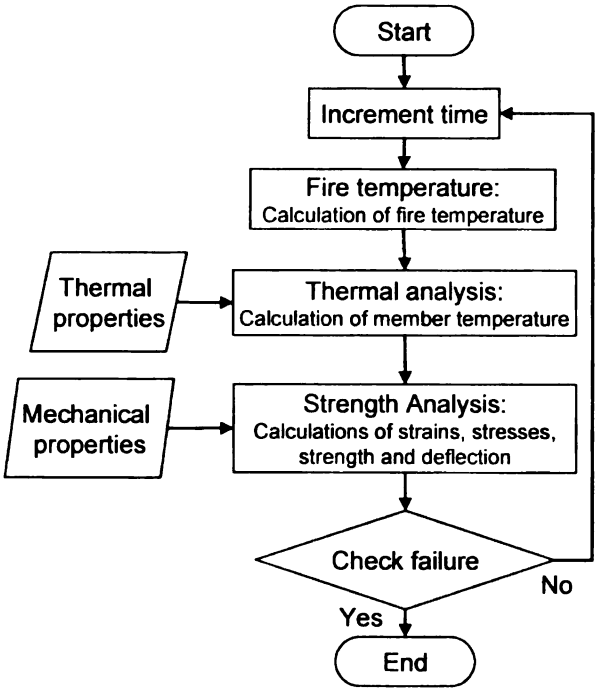

Figure 2.7 – Flowchart for Calculating the Fire Resistance of a Structural System (Reporduced from Kodur 2007)

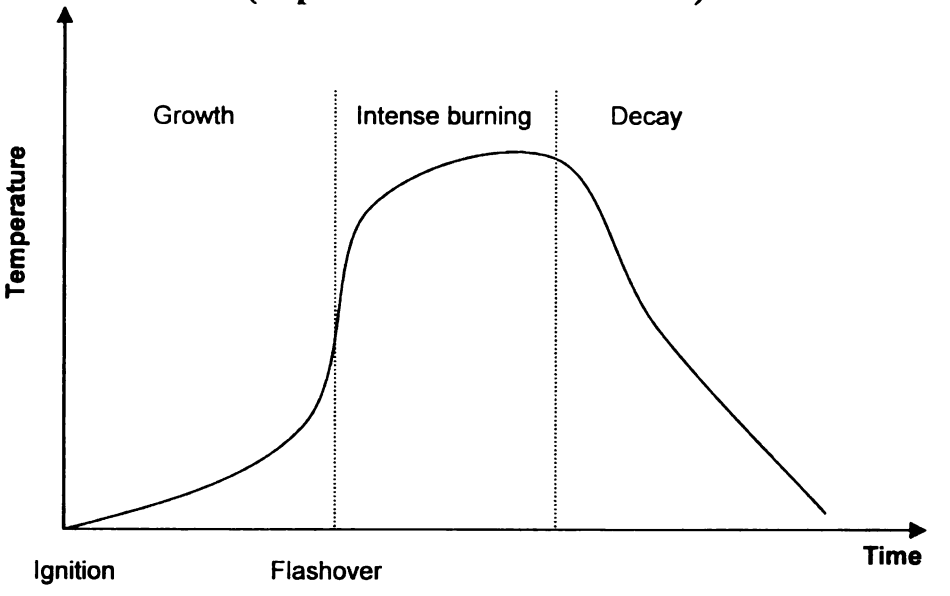

Figure 2.8 – Various Stages of Fire in a Typical Compartment

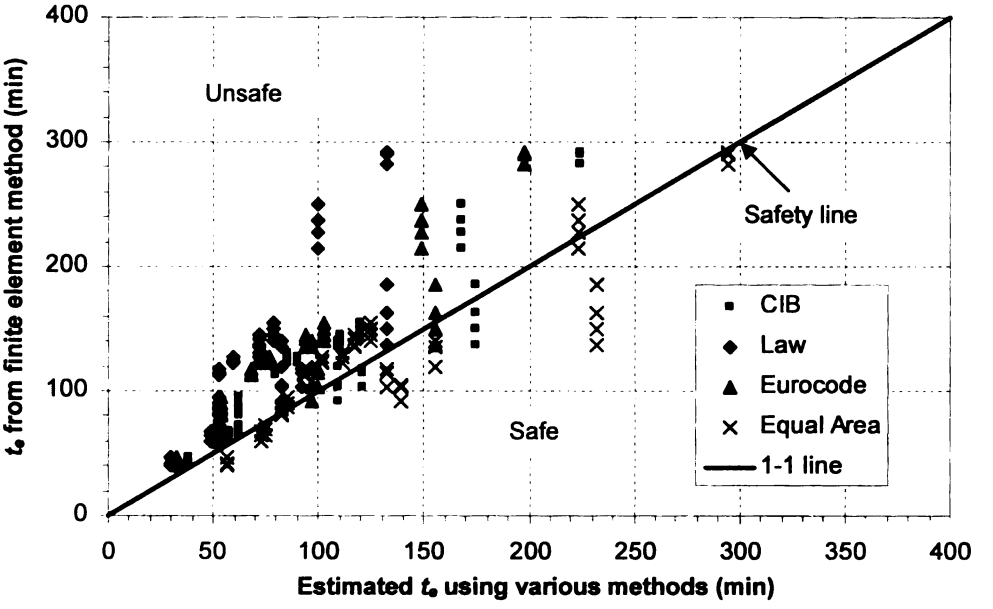

Figure 2.9 – Comparison of Time Equivalency Computed based on FE Analysis with that from Empirical Methods (Kodur et al. 2009b)

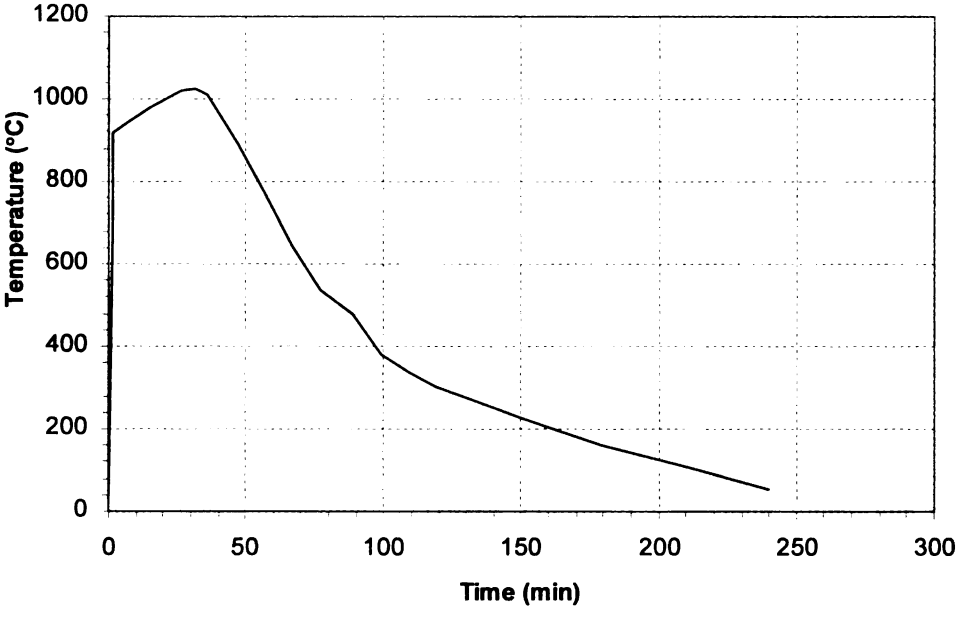

Figure 2.10 - Time-Temperature Curve for Design Fire (Reproduced from Lin and Ellingwood 1987)

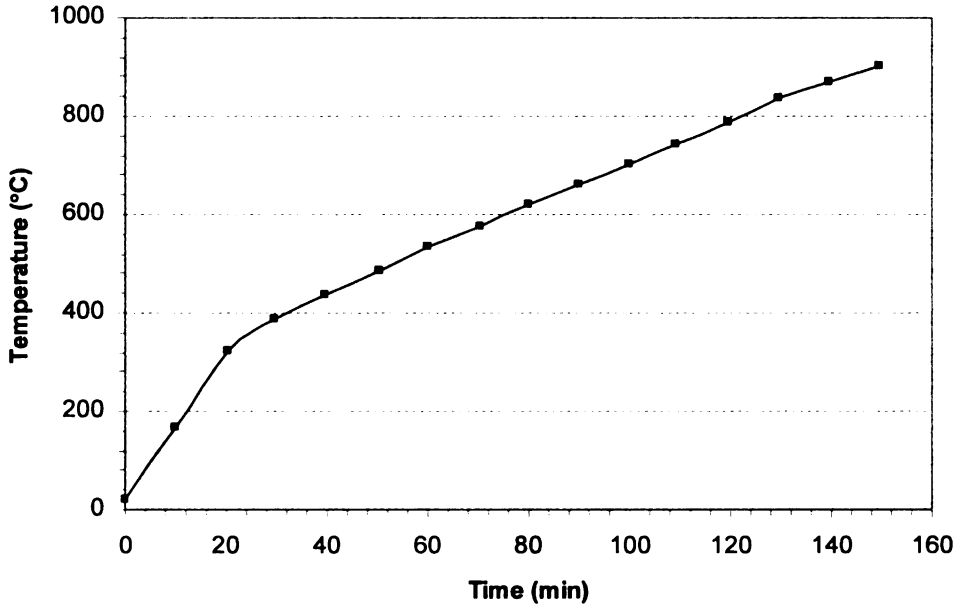

Figure 2.11 - Time-Temperature Curve used in Fire Resistance Tests by Shi et al. (2004)

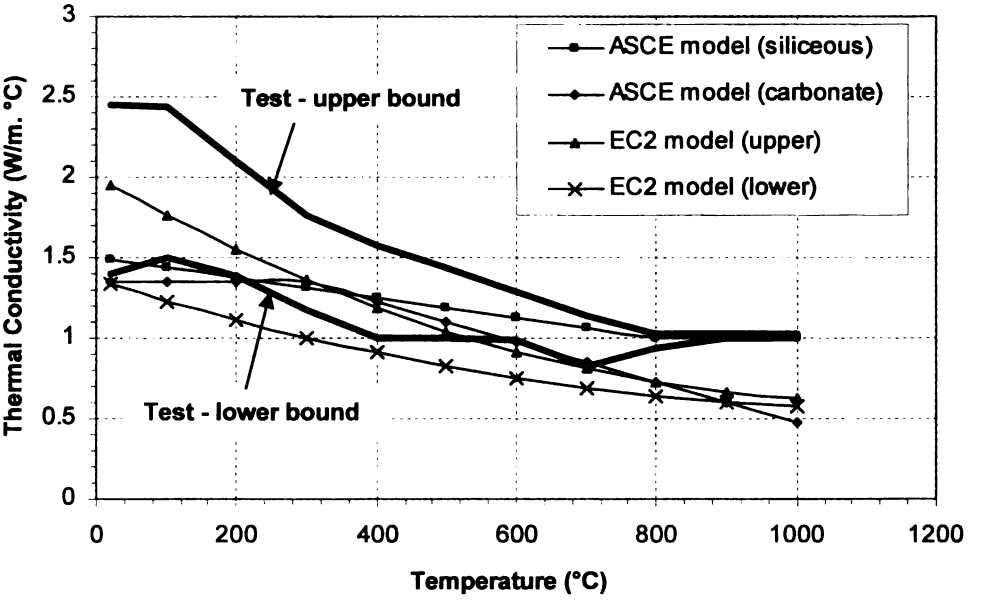

Figure 2.12 - Variations of Measured and Predicted of Thermal Conductivity for NSC as a Function of Temperature

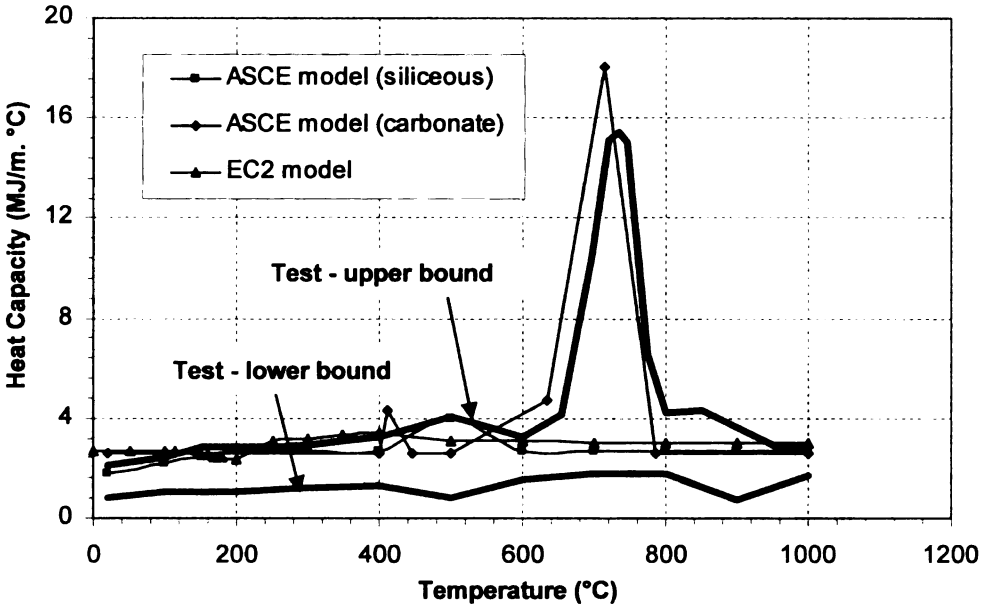

Figure 2.13 - Variations of Measured and Predicted of Thermal Capacity for NSC as a Function of Temperature

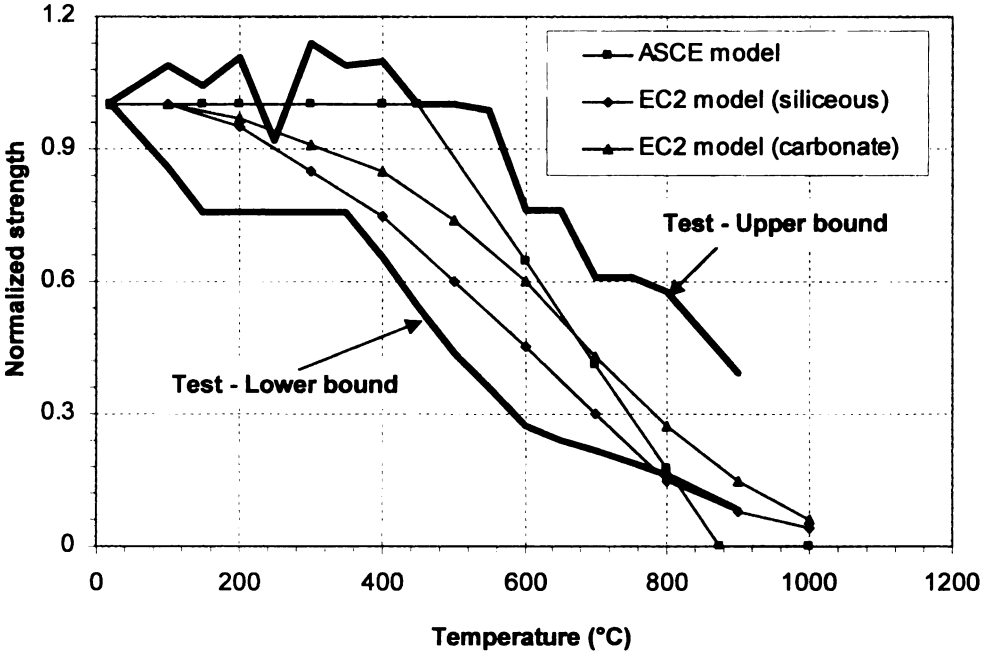

Figure 2.14 - Variation of Compressive Strength as a Function of Temperature for NSC

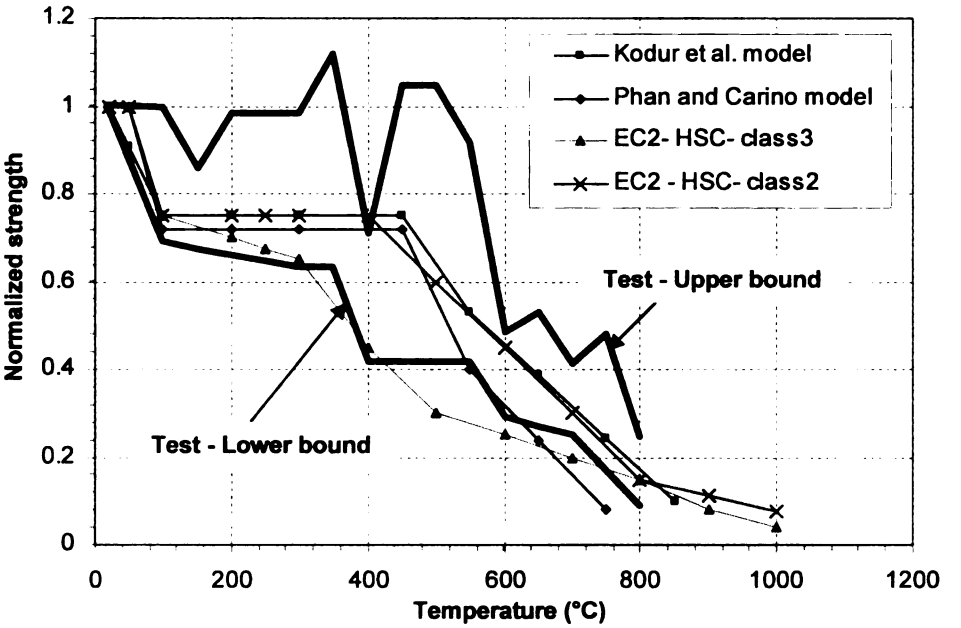

Figure 2.15 - Variation of Compressive Strength as a Function of Temperature for HSC

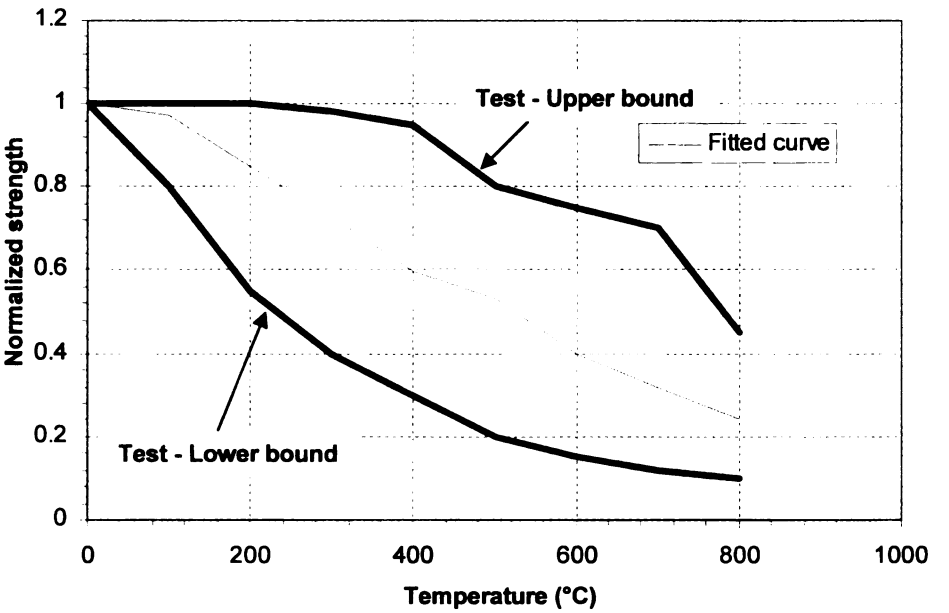

Figure 2.16 - Variation of Residual Compressive Strength as a Function of Temperature (Reproduced from Kumar 2003)

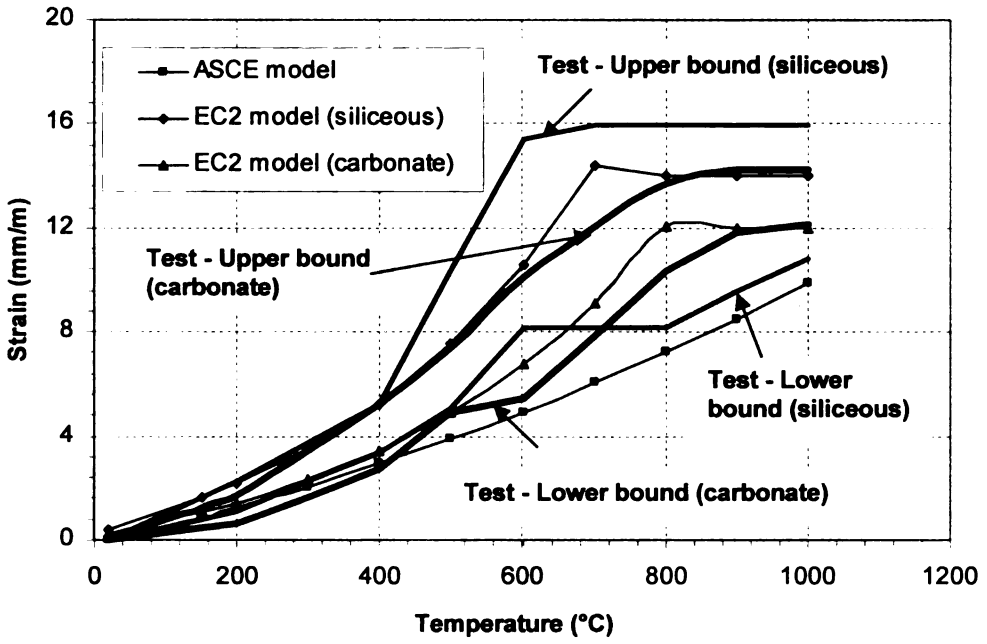

Figure 2.17 - Variations of Measured and Predicted of Thermal Expansion for Concrete as a Function of Temperature

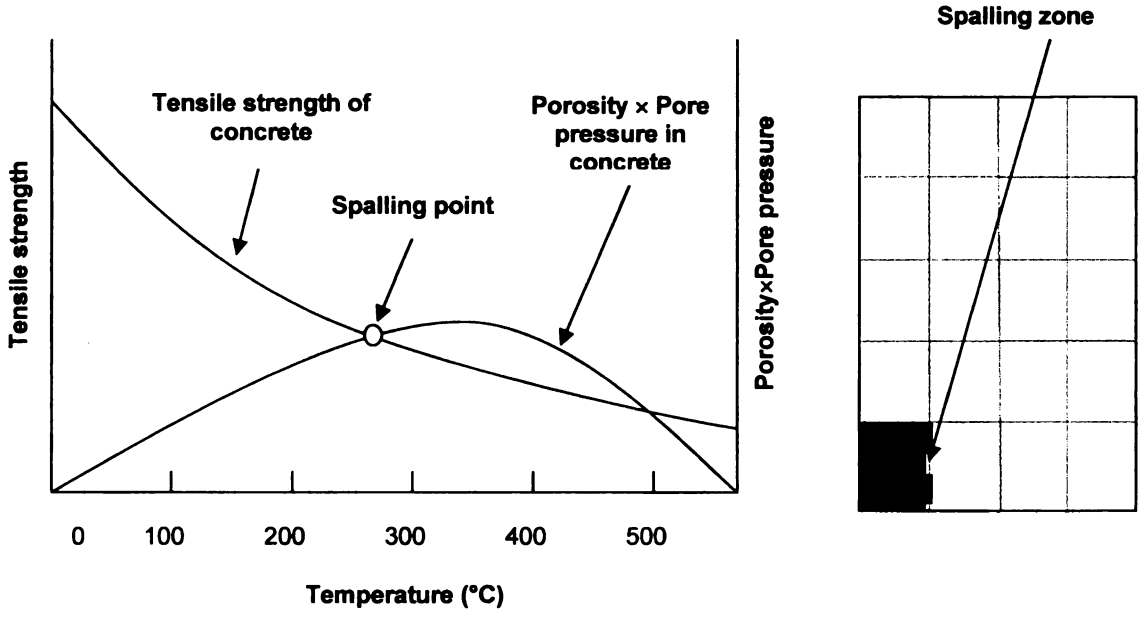

Figure 2.18 – Illustration of Spalling Prediction in the Model

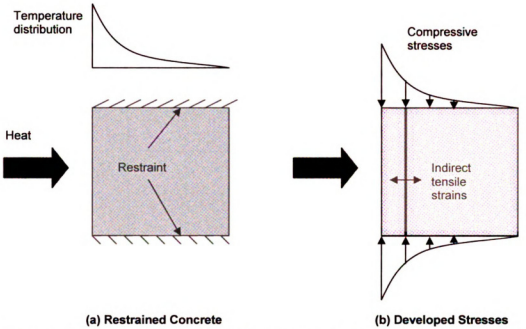

Figure 2.19 – Illustration of Thermal Dilation Mechanism for Fire Induced Spalling

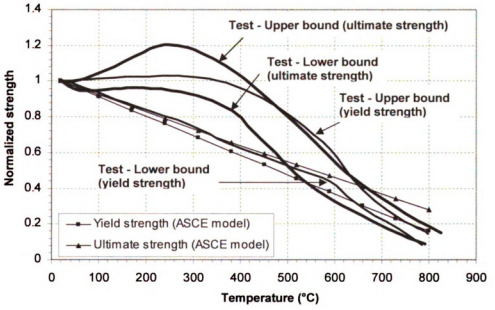

Figure 2.20 – Variations of Measured and Predicted Ultimate and Yield Strength of Reinforcing Steel as a Function of Temperature

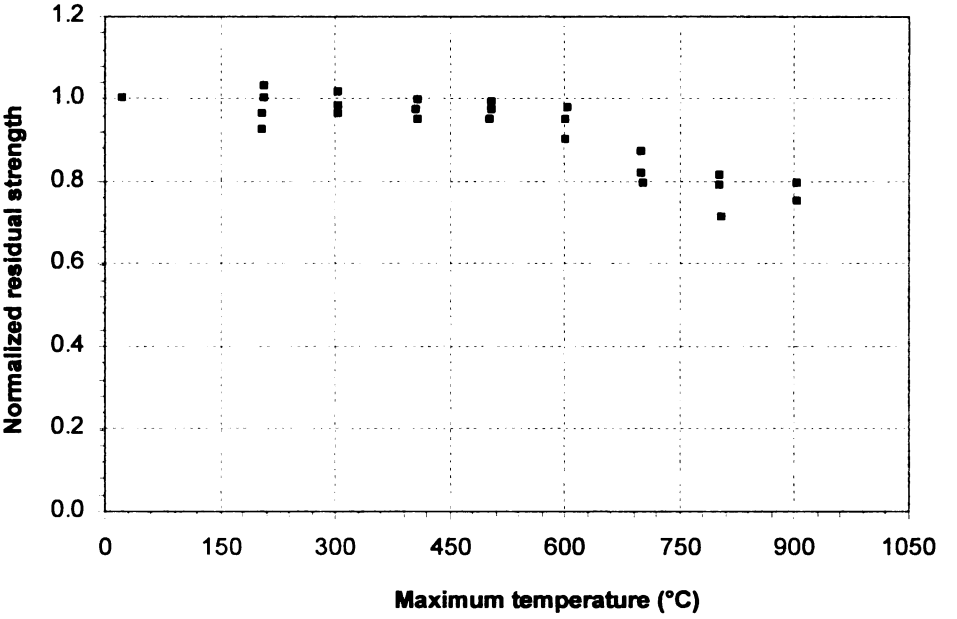

Figure 2.21 – Measured Residual Yield Strength of Reinforcing Steel (Reproduced from Neves et al. 1996)

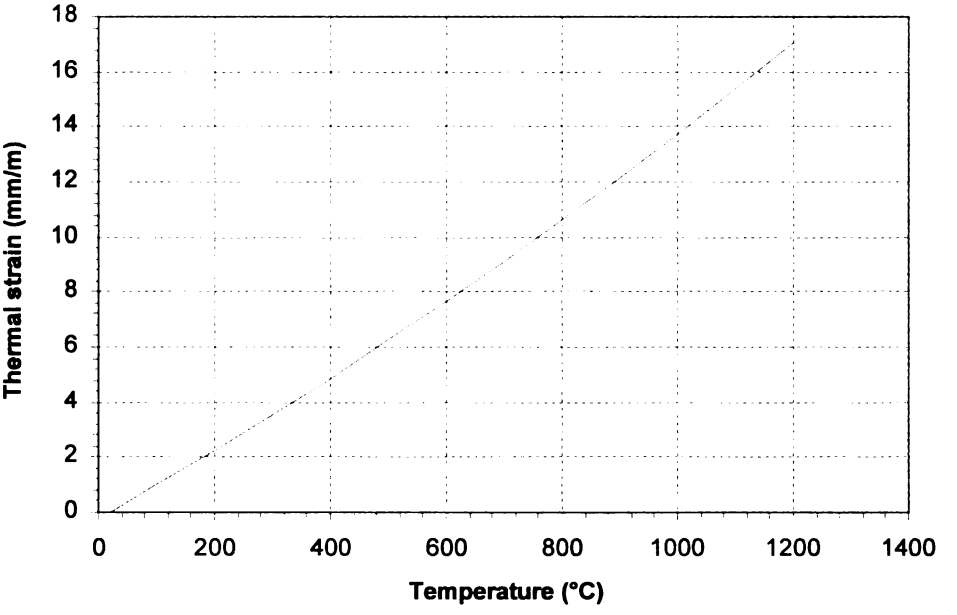

Figure 2.22 – Variation of Thermal Strain as a Function of Temperature (ASCE Manual 1992)

Chapter 3

3. Experimental Program

3.1 General

The review (Chapter 2) indicates that there are few experimental studies on the fire resistance of RC beams. Further, most of the experimental studies were carried out under 'standard' conditions that did not cover important factors such as the fire scenario, fire induced spalling, and axial restraint, which will influence the fire response of RC beams. For these reasons, experiments were carried out on NSC and HSC beams under realistic fire, loading, and axial restraint conditions. Two of the beams were tested under standard fire exposure. The remaining four beams were tested under typical design fire scenarios. A significant amount of data was collected from these fire experiments for validating a numerical model. Full details of the fire experiments, including fabrication of beams, fire tests procedure and measured parameters are presented in this chapter.

3.2 Test Specimens

The experimental program consisted of conducting fire resistance tests on six RC beams designated B1 to B6. Four of these beams, B3, B4, B5 and B6, were made of HSC. The other two beams, B1 and B2, were made with NSC. All beams were 3960 mm long and of rectangular cross-section of 406×254 mm. These beams were designed as per ACI 318 specifications (2008). Design details of these beams are presented in Section B.1 in Appendix B. A summary of the test parameters and results for these beams are given in Table 3.1.

The beams were designed with 3 ϕ19 mm bars as tensile reinforcement and 2 ϕ13 mm bars as compressive reinforcement. The shear reinforcement consisted of ϕ6 mm stirrups spaced at 150 mm over the length of the beam and bent at 135° into the concrete core. The steel used for the main reinforcing bars and stirrups had specified yield strengths of 420 MPa and 280 MPa, respectively. Figure 3.1 shows the elevation and cross-sectional details of the beams together with the location of the stirrups.

In each beam, the bars were tied with the stirrups to form a steel cage as shown in Figure 3.2. Then, each steel cage was placed horizontally in a wooden formwork which was properly designed and fabricated to have the same internal dimensions as those of the tested beams. To achieve good quality control, the concrete mix was ordered from a local concrete plant.

Two batches of concrete were used for fabricating the beams. Beams B1 and B2 were fabricated from an NSC mix (Batch 1). Beams B3 through B6 were fabricated from an HSC mix (Batch 2). Both batches of concrete were made with general purpose, Type I Portland cement. The coarse aggregate in both batches were of carbonate aggregate

(predominantly limestone). The mix proportions per cubic meter of concrete in the two batches are given in Table 3.2.

Silica fume was added to Batch 2 in order to obtain the target high strength concrete. The HSC beams were moist cured in the forms for 7 days by covering them with burlap soaked with water (see Figure 3.3). The NSC beams were sealed in the forms for 7 days. All the specimens were removed from the forms and stored in air maintained at about 25°C temperature and 40% relative humidity.

The average compressive cylinder strength of the concrete, measured at 28 days and on the day of the testing, was 52.2 MPa and 58.2 MPa for NSC, and 93.3 MPa and 106 MPa for HSC, respectively. Beams B1 through B4 were tested about 16 months after casting, while beams B5 and B6 were tested 8 months after casting.

The moisture condition (relative humidity) was measured on the day of the test using a "Sensirion" relative humidity sensor (probe) at a depth of 100 mm and at two different locations of the beam. For relative humidity measurements, ½ inch holes were drilled at two different locations in each beam. The probe was then placed in each hole and the hole was sealed for about 5 minutes until equilibrium of relative humidity and temperature was achieved. Once equilibrium was reached, the relative humidity was recorded for each location in the concrete. The average relative humidity from different locations for each beam is given in Table 3.1. The moisture content in each beam is computed from the measured relative humidity values using the following equation (Bazant and Thonguthai 1978):

$$m_c = RH \times \rho_w \times n \qquad [3.1]$$

where m_c = moisture content, RH = relative humidity, n = porosity of concrete, and ρ_w = density of water.

The porosity of concrete was computed using the concrete mix proportions and the approach presented by Mindess et al. (2003). The moisture content was also computed as a percentage (by weight) of concrete. The measured relative humidity and the computed moisture content are tabulated in Table 3.1. It can be seen from the tabulated values in Table 3.1 that the relative humidity of the HSC beams was slightly higher than that of the NSC beams. This can be attributed to the low permeability of the HSC beams. Further, the relative humidity in beams B5 and B6 was higher than that in the remaining HSC beams (B3 and B4). This can be attributed to the fact that beams B3 and B4 were eight months older than beams B5 and B6 on the day of testing.

3.3 Instrumentation

The beams were instrumented with thermocouples, high temperature strain gages, and displacement transducers. Type-K Chromel-alumel thermocouples, 0.91 mm thick, were installed at three different cross-sections (A, B and C as shown in Figure 3.1) in each beam for measuring concrete and rebar temperatures. Section B was instrumented with 9 thermocouples for each of the tested beams. Sections A and C were instrumented with 5 and 6 thermocouples for beams B1 through B4, and 4 for beams B5 and B6, respectively. Also, five thermocouples were installed at the top side of the beam to monitor the unexposed surface side temperature. High temperature "ZFLA-6-11 strain gages" (specified by the manufacturer to be reliable up to 300°C) were installed to measure strains in the reinforcing bars. Four beams, B1 through B4, were instrumented with 20

thermocouples and 4 high temperature strain gages. The remaining two beams (B5 and B6) were instrumented with 17 thermocouples and 2 high temperature strain gages. Figure 3.4 shows thermocouples and strain gage after being installed in position within the reinforcement cage. The location and numbering of the thermocouple and strain gages in the cross-section are shown in Figure 3.1. The deflection of each beam is measured, using "Linear Variable Differential Transducers" with gage length 375 mm, at mid-span as well as at the location of one of the two point loads.

3.4 Test Apparatus

The fire resistance tests on RC beams were carried out using the structural fire testing facility recently commissioned at Michigan State University. The test facility has been specially designed to produce conditions, such as temperature, loads and heat transfer, to which a structural member might be exposed during a fire. The test furnace, shown in Figure 3.5, has the capacity to supply both heat and applied loads that are present in a typical building exposed to fire.

The furnace consists of a steel framework supported by four steel columns, with a fire chamber that is 2.44 m wide, 3.05 m long, and 1.68 m high. The maximum heat power the furnace can produce is 2.5 MW. Six natural gas burners located within the furnace provide thermal energy. Six thermocouples, distributed throughout the test chamber, monitor the furnace temperature during a fire test. During the fire test, these furnace temperatures are used to manually adjust fuel supply, and maintain a temperature profile consistent with a pre-determined standard or realistic fire scenario. In this way, the furnace temperature can be maintained along a desired curve. Two small view ports on either side of the furnace wall are provided for visually monitoring the fire-exposed

specimens during a test. The furnace accommodates two beams at a time as shown in Figure 3.6 and different load levels can be applied for each beam. One of the two beams can be tested with axial restraint support conditions, while the other beam has to be tested with simply supported end conditions. The axial restraint stiffness of the loading frame and the axial restraint system (restraining the beam axially) is about 13 kN/mm. To minimize damage to the loading frame, the stiffness of the axial restraint system is set to adjust (automatically) to zero (using a relief valve) when the axial restraint force exceeds a value of about 120 kN. During a fire test, the loading is applied through a hydraulic system that utilizes a pneumatically driven hydraulic pump. The pump has two pressure zones which allow the application of two different loads on the tested beams.

Data from fire tests, which include temperatures, displacements, forces and strains, are collected using a "Darwin Data DA100/DP120-13" acquisition system. This system contains 70 thermocouple channels, 10 voltage channels for measuring displacements and forces, and 10 strain-gage channels. These channels are connected to the data acquisition system, which transfers the data to a personal computer that stores it in a ".CSV" file using the "DAQ 32" computer program.

3.5 Test Conditions and Procedure

The fire resistance tests were carried out by placing two RC beams in the furnace and exposing them to a targeted fire scenario. The beams were exposed to fire from three sides (bottom and two sides). The top surface of the beam was insulated with a 50 mm layer of insulation (ceramic fiberfrax material) to prevent heat penetration from the top. This is similar to the conditions encountered in practice where the top side of the beam is

generally covered with a concrete slab. The beams had 3.66 m span length, with 2.44 m of the beam length exposed to fire.

To investigate the effect of the fire scenario on the response of RC beams, the beams were tested under three fire scenarios. Beams B1 and B3 were tested under ASTM E119 standard fire exposure (ASTM E119a 2008). The remaining four beams were tested under two design fire exposures. Beams B2 and B4 were tested under short severe design fire exposure (SF). Beams B5 and B6 were tested under long severe design fire exposure (LF). The two design fire scenarios have similar time-temperature curves to the parametric time-temperature curve proposed in Eurocode 1 (2002). These design fire scenarios were assumed in such a way that fire SF represents a short design fire in a lightly furnished office where there is a small quantity of combustible materials (about 800 MJ/m^2 floor area), and fire LF represents a long severe design fire in a library room with a large quantity of combustible materials (about 1600 MJ/m^2 floor area). The time-temperature curves for the three fire scenarios (ASTM E119 standard fire, SF, LF) are shown in Figure 3.7.

All beams were tested under two point loads, each of which was placed at 1.4 m from the end supports. For all beams, except beam B5, each of the two point loads was 50 kN, which is about 54% of the beam capacity according to ACI 318 (2008). Beam B5 was subjected to two point loads of 60 kN or 65% of beam capacity. The type of fire exposure and the load ratio, defined as the ratio of applied load to beam capacity, for the various beams are tabulated in Table 3.1. Detailed load calculations for the RC beams are given in Appendix B. Beams B1, B3, B4 and B5 were tested under simple support conditions, while beams B2 and B6 were axially restrained during the fire tests.

The load was applied for approximately 30 minutes before the start of the fire test and was maintained until a static condition was reached at which no further increase in the deflection could be measured. This was the initial condition for the deflection of the beam. During the test, the beam was exposed to heat controlled in such a way that the average temperature in the furnace followed, as closely as possible, the targeted time-temperature curve (ASTM E119 standard fire, SF, or LF). The load was maintained constant throughout the test. The test data including furnace temperatures, specimen temperatures, strains, deflections, and loading were recorded every 5 seconds by the data acquisition system. Observations were made every 5 minutes through the view ports in the furnace to record any major changes in the specimens such as fire induced spalling or visible cracks. The beams were considered to have failed and the tests were terminated when the hydraulic jack, with a stroke of 250 mm, could no longer maintain the load.

After the fire tests, post-fire inspection was carried out to record any fire induced spalling, rupture of reinforcement and concrete cracking in the tested beams. In addition, the beams were stored to conduct volumetric measurements to quantify the volumes of spalled concrete from each beam during the tests. The exposed length of each beam was divided into a number of segments and the volume of each segment was computed by taking measurements with respect to a reference axes system. The total volume of a damaged beam was then computed as the sum of the volumes of all the segments, and used to compute the spalled volume of concrete.

3.6 Material Tests

Material tests on concrete and reinforcing steel specimens were carried out to obtain strength properties of the materials used in the beam fabrication. Concrete cylinders from

the two batches (Batch 1 and Batch 2) were tested to obtain the compressive strength at 28 days and on the day of corresponding fire test. Also, split tensile tests were conducted on concrete cylinders at 28 days to measure the tensile strength. Results from the compression tests are given in Table 3.3. The 28-day design compressive strength of the two mixes (NSC and HSC) was 41.3 MPa and 103.3 MPa, respectively. The split tensile strength, measured 28 days after casting, was found to be 3.7 MPa and 5.1 MPa for NSC and HSC, respectively.

Tensile tests were performed on ϕ19 mm steel bars similar to those used as tensile reinforcement in the concrete beams. The yield strength, ultimate strength, and ultimate strain were found to be about 450 MPa, 705 MPa and 0.17, respectively. The stress strain curves for the tested bars are shown in Figure B.3 in Appendix B.

3.7 Test Results

Data generated from the above fire tests was utilized to evaluate the fire behavior of RC beams under different conditions. The test variables included concrete strength, axial restraint, type of fire exposure, and load level. The evaluation is carried out by comparing the thermal response, structural response, fire induced spalling, and failure patterns as well as fire resistance time.

3.7.1 Thermal Response

The thermal response of NSC and HSC beams is compared in Figures 3.9 and 3.10 by plotting rebar and concrete temperatures as a function of fire exposure time. While beams B1 and B3 were exposed to ASTM E119 standard fire exposure (no decay phase) as shown in Figure 3.8, beams B2 and B4 were exposed to a short design fire, with a well

defined decay phase as shown in Figure 3.9. Data presented in these two figures show that there is a temperature plateau at about 100°C for rebar and concrete temperatures. This temperature plateau can be mainly attributed to the evaporation of water in concrete which consumes a significant amount of energy. After the plateau, the temperatures in the rebar and concrete increase with fire exposure time. The two figures also show that the measured temperatures in concrete decrease with increasing distance from the bottom surface. This is due to the low thermal conductivity and high thermal capacity of concrete which slows down heat penetration to the concrete inner layers.

The plotted temperatures in Figures 3.9 and 3.10 can be used to gage the effect of concrete strength on the thermal response of NSC and HSC beams. Figure 3.8 shows the comparison of temperatures in the rebar and two concrete locations (TC10 and TC11, which are located at depths of 200 and 300 mm, respectively, as shown in Figure 3.1) for NSC (B1) and HSC (B3) beams exposed to the ASTM E119 standard fire. Except for the strength, the NSC and HSC beams had similar characteristics and were subjected to comparable load levels. It can be seen from Figure 3.8 that the measured temperatures in rebars and concrete (at 100 mm concrete depth) in the NSC beam (B1) are lower than the corresponding temperatures in the HSC beam (B3) throughout the fire exposure. The variation in temperature profiles can be partly attributed to differences in thermal properties of the two concretes resulting from higher compactness (lower porosity) of HSC and also due to the occurrence of "minor" spalling in the HSC beam. The higher thermal conductivity of HSC, resulting from lower porosity, increases the rebar and concrete temperatures in the HSC beam. Also, in the case of the HSC beam there was some surface spalling in the "intermediate stage" of fire exposure. This loss of concrete

also led to a faster rise in temperature. This variation in concrete temperature almost disappears at larger depths and can be explained by the large distance from the exposed surface which reduces the effect of compactness and spalling on the temperature distribution in the HSC beam.

Figure 3.9 shows the variation of rebar and concrete (TC10 and TC11) temperatures as a function of fire exposure time for NSC beam B2 and HSC beam B4 exposed to SF. The fire temperature rises rapidly in the first 10 minutes, then remains constant up to about 60 minutes, before following a decay curve in the cooling phase. The rebar and concrete temperatures in the NSC beam are slightly higher than those of the HSC beam particularly in the heating phase of the fire exposure time. This is contrary to what was observed for beams B1 and B3 (exposed to ASTM E119 standard fire) and can be partly attributed to the fact that less spalling was observed for the HSC beam B4 (exposed to SF) as compared to HSC beam B3 (exposed to ASTM E119 standard fire). The decreased spalling is mainly due to the presence of a decay (cooling) phase in the design fire which caused lower temperature rise in beam B4. In addition, the steep time-temperature increase in the early stages of fire exposure (see Figure 3.7) produced a high thermal gradient in the beam cross-section. Such high thermal gradients induced higher damage and microcracking in the HSC beam (which in turn increased the porosity of HSC) due to the high compactness and low permeability of HSC. The higher damage and microcracking (porosity) reduced the thermal conductivity and hence slowed the temperature rise in HSC.

Overall, the temperatures measured in the HSC beams followed closely those in the NSC beams. It may therefore be concluded that the strength of concrete does not significantly influence the thermal response of RC beams under fire conditions.

The effect of the type of fire exposure on the thermal response of RC beams can be illustrated by comparing the temperature profiles in Figure 3.8 with those in Figure 3.9. It can be seen from Figure 3.8 that for the beams exposed to the standard ASTM E119 fire (B1 and B3), the rebar and concrete temperature increases throughout the fire exposure time. However, Figure 3.9 shows that for beams B2 and B4 (exposed to the SF), the measured temperatures in concrete and steel rebars increased to a maximum value and then decrease. This is attributed to the decay (cooling) phase in the time-temperature curve of the design fire which leads to cooling in the RC beam.

A comparison of test data for the two HSC beams (B5 and B6) exposed to the long severe design fire (LF) is shown in Figure 3.10, wherein the variation of rebar and concrete (TC9 and TC10) temperatures is plotted as a function of fire exposure time. The locations of TC9 and TC10 (at 200 and 300 mm depths) in these two beams are identical to those of thermocouples TC10 and TC11 in beams B1 through B4 as can be seen by comparing Figure 3.1(b) with Figure 3.1(c). A comparison of Figure 3.9 and Figure 3.10 indicates that the higher rebar and concrete temperatures were recorded in the two HSC beams (B5 and B6) compared with the measured temperatures in HSC beam B4. This can be attributed to the longer burning duration of the design fire LF. Also, the extent of surface spalling was higher in beams B5 and B6 than that in HSC beam B4, mainly resulting from different loading, fire and support conditions. This led to a higher temperature rise in HSC beams B5 and B6. However, the cooling in the rebar and concrete temperatures is

found to be faster for the beams exposed to the 'LF' fire (beams B5 and B6). This is attributed to the faster cooling rate in the LF in the decay phase, see Figure 3.7.

The plotted temperatures in Figure 3.10 can be used to gage the effect of axial restraint on the thermal response of HSC beams. From Figure 3.10, the rebar and concrete temperature in beam B6 is higher than in beam B5, particularly at the late stages of fire exposure. This can be attributed to the axial restraint effects which increased the fire induced spalling in beam B6 as compared to beam B5.

Generally, load level and axial restraint have only a minor influence on the thermal response of RC beams. The effect of these factors on the thermal response generally arises through their influence on spalling and cracking of concrete. The recorded temperatures in all thermocouples as a function of fire exposure time for all tested beams are given in Appendix B (Figures B.4 to B.27).

3.7.2 Structural Response

3.7.2.1 Deflection

The measured mid-span deflection for the six tested beams is shown in Figure 3.11 as a function of fire exposure time. For all six beams the mid-span deflection gradually increases with time at the early stages of fire exposure as a result of thermal expansion and the deterioration of strength and stiffness properties of concrete and reinforcing steel with increased temperature. The initial deformation of the beam results mainly from thermal gradients developed within the beam cross-section and also the applied loading. However, the effect of creep becomes pronounced in the later stages of fire exposure due to higher temperatures in concrete and steel, and also due to significant deterioration in

the stiffness of the beam. This is one of the main reasons for the increase in the deformations in beams B1, B3 and B5 towards the later stages of fire exposure. These beams experienced very high temperatures (in concrete and steel) prior to failure resulting in high stress levels which produce high creep deformations. However, due to the cooling phase, beams B2, B4 and B6 did not attain such high temperatures and thus significant creep deformation might not have occurred in these beams.

The effect of concrete strength on the fire response of RC beams can be illustrated by comparing the deflection-time curves of beams B1 and B3 (subjected to the ASTM E119 fire) in Figure 3.11. The mid-span deflection of beam B3 (HSC beam) is higher than that of beam B1 (NSC beam) throughout the range of standard fire exposure. The higher deflection in beam B3 (HSC beam) resulted from the higher rebar temperature in that beam and also the faster degradation of strength and stiffness of the HSC. The larger deflection led to early failure of HSC beam (B3) resulting in lower fire resistance. The failure of the HSC beam was brittle as compared to that of the NSC beam.

The effect of fire scenario on the structural response of RC beams can be gauged by reviewing the deflection trends in Figure 3.11. It can be seen that the deflection of the two beams (B1 and B3) exposed to the ASTM E119 standard fire increases throughout the fire exposure time. However, except for beam B5, the figure shows recovery in the mid-span deflection for the beams exposed to the design fire scenarios. This can be attributed to the recovery in the strength and stiffness once the beam enters the cooling phase. Because of the high loading levels and the longer duration of the 'growth phase' of the fire, beam B5 failed before the rebar temperature entered the cooling phase. Thus no deflection recovery was observed for B5.

The effect of axial restraint on the fire response of RC beams can also be gauged by looking at the deflection response in Figure 3.11. Although the rebar and concrete temperatures in beam B4 are lower than those in beam B2, beam B4 experienced a higher mid-span deflection. This can be attributed to the fact that B2 was axially restrained. As explained in Section 2.2, the axial force resulting from restraining the thermal expansion of an RC beam produces a counteracting bending moment, a mechanism similar to that of an arch action (Dwaikat and Kodur 2008a). This axial force induced bending moment counteracts the moment due to the applied (gravity) load resulting in reduced deflections. The effect of load on the structural response of HSC beams can be gauged by comparing the deflections in HSC beams B5 and B6 exposed to the severe design fire (LF). In Figure 3.11, the load ratio has a significant effect on the deflection of RC beams exposed to fire. Beam B5, which was exposed to a higher load ratio (65%), also experienced a higher mid-span deflection compared to beam B6 which had a 55% load ratio. This is mainly because an increased load ratio caused early yielding of the steel reinforcement and thus increased the mechanical and creep strains. This led to lower stiffness in the beam and resulted in a significant increase in deflection leading to early failure of beam B5 as can be seen in Figure 3.11.

3.7.2.2 Axial Restraint Force

The measured axial restraint force for the two tested axially restrained beams (NSC beam B2 and HSC beam B6) is shown in Figure 3.12 as a function of fire exposure time. The axial force in both beams increased with fire exposure time in the first 100 minutes. This can be attributed to restraining the thermal expansion of the beam which increased with fire exposure time due to the increase in concrete and rebar temperatures. The rate of

increase in the axial restraint force is lower in beam B6 compared to beam B2. This can be mainly attributed to the severe spalling that occurred at the early stages of fire exposure in HSC beam B6 which reduced the axial stiffness and resulted in the development of smaller axial restraint forces, see Figure 3.12.

Figure 3.12 also shows that after 100 minutes, the axial force was almost constant in beam B2 for about 40 minutes. This was followed by a gradual decrease in the axial restraint force. The plateau in the axial restraint force between 100 minutes and 140 minutes (in beam B2) can be attributed to the relief valve in the restraint system which reduces the axial restraint stiffness to zero. This plateau in the axial restraint stiffness is mainly to avoid possible damage of the test facility and loading frame as discussed above. The reduction in the axial restraint force at the later stages of fire exposure for this beam can be attributed to the decay phase in the time-temperature curve of the fire exposure in which the beam started cooling.

However, for beam B6, a reduction in the axial restraint force occurred between 100 and 140 minutes of fire exposure. This is attributed to the severe long design fire to which this beam was exposed. Severe spalling occurred in B6 and the faster degradation of strength and stiffness of HSC contributed to the reduction in the axial force. At the later stages of fire exposure, the axial force started to decrease gradually due to the decay phase in the design fire where B6 enters the cooling phase.

The results presented in Figure 3.12 show that HSC beams may develop smaller axial restraint forces under fire conditions when compared with NSC beams. This can be primarily attributed to the fact that HSC is more prone to spalling than NSC and to the faster degradation of strength and stiffness in HSC compared to NSC. It can also be

attributed to the differences in the thermal strain of HSC from that of NSC. This result suggests that HSC might have a lower thermal strain than that of NSC

3.7.2.3 Strain in Longitudinal Reinforcement

The strains in the longitudinal reinforcement of the beams were monitored using high temperature strain gages. The measured strain in the tension reinforcement of the central section in the six tested beams is plotted as a function of time in Figure 3.13. It can be seen that there is a variation among the measured strains at room temperature in the six beams. This can be mainly attributed to the variation in concrete strength among the beams, axial restraint force (which is slightly higher than zero at room temperature as can be seen from Figure 3.12), variation of cracks developed in the different beams, and malfunction of the strain gages themselves.

Despite the fact that the tested beams experienced relatively large deflections during fire exposure, Figure 3.13 shows that there is a slight and irregular variation of strains measured in the rebars with fire exposure time. This can be attributed to the de-bonding of the strain gage from the reinforcing steel due to the increase in rebar temperature during exposure to fire.

It can also be seen from Figure 3.13 that three of the six strain gages (particularly in HSC beams B4, B5, and B6) started to record nonsensical strains in the first 10 minutes of fire exposure. This can be mainly attributed to the cracking and spalling in these beams which left the strain gage wire directly exposed to fire.

It should be noted that high temperature strain gages are generally unreliable due to the many complex physical and chemical processes that occur at elevated temperatures. The problem associated with the reliability of high temperature strain gages was also

encountered by other researchers (Williams 2004, Bisby 2003). Some previous researcher attributed the problem in strain gages to the electrical interference from the operation of the high voltage ignition and the control systems (Williams 2004). One other reason for this problem could be that the strain gages were designed for a low heating rate compared to the high rate of heating encountered (about 10°C per minute for rebars) in fire exposure. Due to the lack of consistency, the strain gage data cannot be confidently used to infer any strain trends in the tested RC beams. The measured strains from other strain gages are plotted as a function of fire exposure time in Appendix B Figures B.28 through B.30.

3.7.3 Spalling Pattern and Failure Mode

Of the six tested beams, three beams, namely, B1, B3 and B5 failed in the flexural mode followed by a longitudinal crack at the level of the tension rebars. This cracking resulted in significant spalling at the bottom surface prior to failure. However, this type of spalling in concrete did not greatly influence the fire response of the RC beam since it occurred just prior to failure. The HSC beams B3 and B5 failed in a brittle mode as compared to the NSC beam B1.

The remaining three beams (B2, B4, and B6) exposed to design fires, did not fail since the fires had a well defined decay phase. This resulted in recovery of some strength and stiffness of those beams. These three beams were tested after they cooled to obtain the residual strength after the fire test. In addition, a lower concrete strength in beam B2 and the presence of axial restraint in beam B6 provided some beneficial effect.

The extent of early and moderate spalling during the fire test was recorded through observations in the windows of the furnace. Also, volumetric measurements were made

after fire resistance tests to determine the extent of spalling. The volumetric measurements and test observation did not account for late spalling, which occurred just prior to failure, and did not influence the fire response of RC beams as discussed in Chapter 2. Volumetric measurements of spalled concrete in each beam after the fire tests are tabulated in Table 3.1. The spalled volume ratio was computed as the ratio of the spalled volume to the total original volume of concrete. Based on these volumetric measurements, the extent of spalling for the six tested beams was classified as minor, moderate, or severe and is given in Table 3.1. Spalling is said to be 'minor' when small amounts of concrete chip off of the surface of the RC beam. Spalling is said to be 'moderate' when the extent of spalling does not reach the steel reinforcement, while it is said to be 'severe' when the extent of spalling reaches the reinforcement. In the NSC beams (B1 and B2), the extent of spalling was minimal or almost negligible throughout the fire exposure. However, in the HSC beams the extent of spalling was moderate and severe, and some of the spalling occurred at early stages of fire exposure. The extent of spalling was influenced by test conditions and beam characteristics.

The level of spalling reported in Table 3.1 can be used to gauge the effect of different parameters on fire induced spalling. Minor spalling in the form of surface scaling occurred in NSC beams B1 and B2. However, the extent of spalling was higher for HSC beams B3, B4, B5, and B6. This can be attributed to the higher compactness (low permeability) and faster degradation of HSC compared to NSC. The low permeability of HSC increased the pore pressure buildup in HSC beams. When this pressure exceeded the tensile strength of concrete, chunks of concrete fell from the surface.

In addition to permeability, load ratio and initial relative humidity were found to significantly influence the spalling in RC beams. Observations in the fire tests indicated that, for beam B4, spalling was not explosive and most of it occurred at intermediate stages of fire exposure or just prior to the failure of this beam. In contrast, there was significant and random explosive spalling for HSC beam B5 in the first 35 minutes of fire exposure. The severe spalling observed in HSC beam B5 can be partly attributed to the higher load ratio applied to the beam compared to B4. It can also be attributed to the slightly higher relative humidity (moisture content) of beam B5 compared to B4.

Between the HSC beams B5 and B6, more severe spalling occurred for the axially restrained beam B6 as compared to the simply supported beam B5. This can be mainly attributed to the fact that the development of axial forces in restrained beams altered the internal stresses (including higher tensile stresses in the lateral direction of the beam) and enhanced the conditions for spalling.

Figure 3.14 shows a picture of a typical beam before the fire resistance tests as well as pictures of the tested beams after the fire tests. Figure 3.14(b) illustrates the extent of spalling after fire resistance tests. In addition, damage in beam B6 during the fire test and after the residual testing is shown for beam B6. Also shown is a sketch of the beam section to illustrate the spalling that occurred during the early stages of fire exposure for HSC beam B6. Significant spalling occurred in the HSC beam as compared to the NSC beam. Although the HSC beam (B5) was exposed to fire from three sides, much of the early spalling was mainly observed on the upper area (compression zone) of both sides of the beam. The lack of spalling on the bottom face of the beam can be attributed to the cracking in the tension zone caused by the applied loading. Cracking facilitates the

escape of steam and thus reduces the buildup of pore pressure under fire conditions (Dwaikat and Kodur 2008b). In addition to cracking, curing conditions also influence the permeability of concrete. The top surface of the beams was covered with burlap that was soaked with water (common practice for curing RC beams). This results in better curing conditions for the top part of the beam which enhances hydration of concrete leading to reduced porosity (permeability) in the top part of the beam. The significant damage at the central part of beam B6, which can be seen in Figure 3.14, is not due to fire induced spalling. This damage is mainly from the residual test (through higher loads) where the top part of the beam (concrete) experienced crushing.

3.7.4 Fire Resistance

A comparison of fire resistance of the six beams is given in Table 3.1. The time to reach failure is defined as the fire resistance and failure occurs when the strength of the beam decreased to a level at which the beam cannot sustain the applied load. Only three of the six tested beams, two of which were exposed to the ASTM E119 standard fire and the remaining one exposed to LF, attained failure. Beams B2, B4, and B6 did not attain failure and survived burnout conditions. These failure patterns can be attributed to variations in test conditions (fire) and beam characteristics (loading, concrete strength, restraint).

The effect of concrete strength on the fire resistance of RC beams can be illustrated by comparing the failure time (fire resistance) of HSC beam B3 with that of NSC beam B1. The fire resistance of HSC beam B3 (160 minutes) was found to be lower than that of NSC beam B1 (180 minutes). This can be attributed to the faster degradation of strength properties of HSC and also due to 'moderate' fire induced spalling in the HSC beam.

The type of fire exposure influences the fire resistance of RC beams. Although beams B1 and B3, under the ASTM E119 fire exposure, failed, three of the beams (1 NSC and 2 HSC) exposed to the design fire scenarios did not fail. This can be attributed to the presence of the decay phase in the design fire in which the beams recover a large fraction of their original strength and stiffness. The failure of beam B5 after 146 minutes of severe fire exposure can be attributed to the higher load level and also to the simple support (no restraint effect) conditions. The reduced fire resistance of B5 as compared to the similar beam B3 can mainly be attributed to the severe load and fire conditions to which beam B5 was exposed compared to B3.

Test data showed that the axial restraint and load ratio affected the fire resistance of RC beams. Although B5 experienced less spalling than B6, B5 failed after 146 minutes of fire exposure. This can be attributed to the fact that B5 was not axially restrained (the beam was simply supported) and was loaded with a higher load level (63%). The effect of axial restraint in HSC B6, enhanced its fire resistance (despite higher spalling as compared to B5) and contributed to sustaining burnout conditions.

3.8 Summary

Details of fire resistance tests on six RC beams were presented in this chapter. The test variables included concrete strength (permeability), support conditions, fire scenario, and load ratio. Data from fire tests was utilized to illustrate the comparative performance of HSC and NSC beams under different fire, restraint and loading conditions. Results from the tests showed that HSC beams have a lower fire resistance than NSC beams. Also, test data revealed that HSC beams exhibited higher levels of spalling, which is largely influenced by the permeability of concrete, type of fire exposure, load level, restraint

conditions, and initial moisture content. Similarly, the type of fire scenario, axial restraint, and load level were found to influence the overall fire resistance of RC beams. Results from the fire tests provide a better understanding of the response of RC beams under realistic fire, load, and restraint conditions. These tests provide valuable data for validating computer models for tracing the fire response of RC beams.

Table 3.1 - Summary of Test Parameters and Results for RC Beams

Beam designation	Test #	Fire exposure	Concrete type	Support conditions*	P (kN)	Relative humidity %	Moisture content		Measured fire resistance (min)	Predicted fire resistance (min)	Spalled volume ratio+ (%)	Extent of spalling
							(kg/m3)	% by weight				
B1	I	ASTM E119	NSC	SS	50	81.5	74.7	3.1	180	180	1.7	minor
B2	II	SF	NSC	AR	50	81.1	74.4	3.1	NF**	NF	1.5	minor
B3	I	ASTM E119	HSC	SS	50	87.5	61.9	2.5	160	153	3.3	moderate
B4	II	SF	HSC	SS	50	86.6	61.3	2.5	NF	NF	3.2	moderate
B5	III	LF	HSC	SS	60	91.8	65	2.6	146	147	7	severe
B6	III	LF	HSC	AR	50	92.5	65.5	2.7	NF	NF	8.7	severe

* SS = simply supported AR = axially restrained ** No failure
+ computed as the ratio of spalled volume to the original volume of the beam

Table 3.2 – Concrete Mix Design Proportions used in Fabrication of RC Beams

Mix Parameter	Batch 1 (NSC)	Batch 2 (HSC)
Beams fabricated	B1, B2	B3, B4, B5 and B6
Total cement (kg/m^3)	389.9	512.5
Silica fume (kg/m^3)	NA	42.7
Water (kg/m^3)	156.4	129.8
Coarse aggregate (kg/m^3)	1036.9	1078.4
Fine aggregate (kg/m^3)	830.1	684.3
Water reducing agent (kg/m^3)	1.9	15.0
Slump (mm)	100	100
Water/cement ratio	0.4	0.25
Air content %	1.7	2.7
Unit weight (kg/m^3)	2415	2463

Table 3.3 – Measure Concrete Strength in Test Beams

Beam	Concrete batch	Design compressive strength (MPa)	28-day compressive strength (MPa)	28-day tensile strength (MPa)	Test day compressive strength (MPa)
B1	1	41.3	52.2 ± 0.6	3.7 ± 0.5	58.2 ± 3.1
B2	1				
B3	2	103	91.0 ± 0.3	5.1 ± 0.3	106.5 ± 2.6
B4	2				
B5	2				
B6	2				

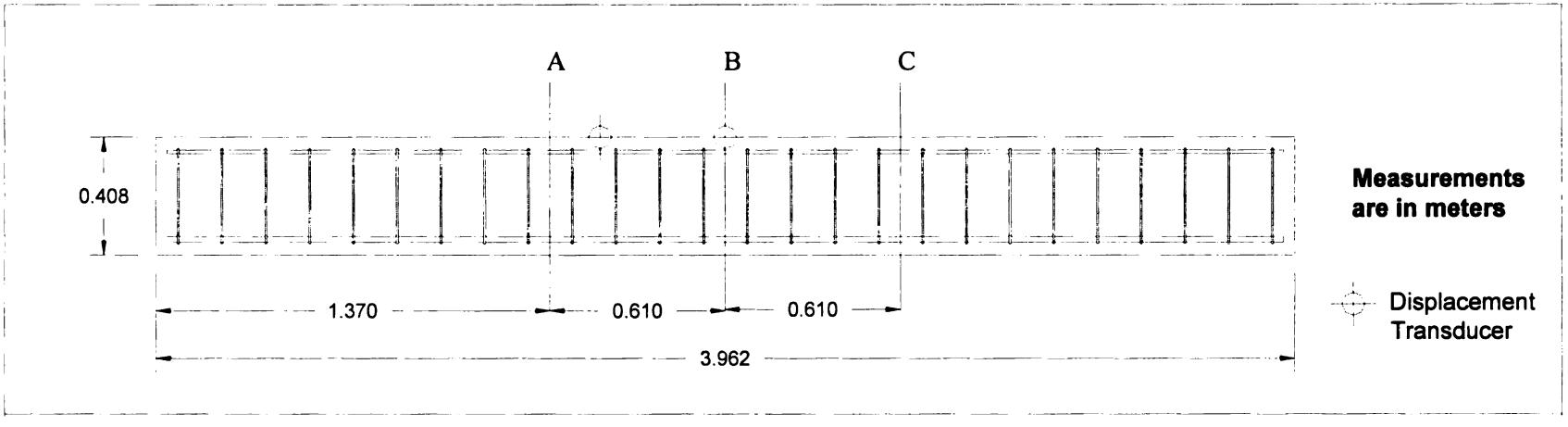

Figure 3.1(a) – Elevation and Location of Displacement Transducer in Tested Beams

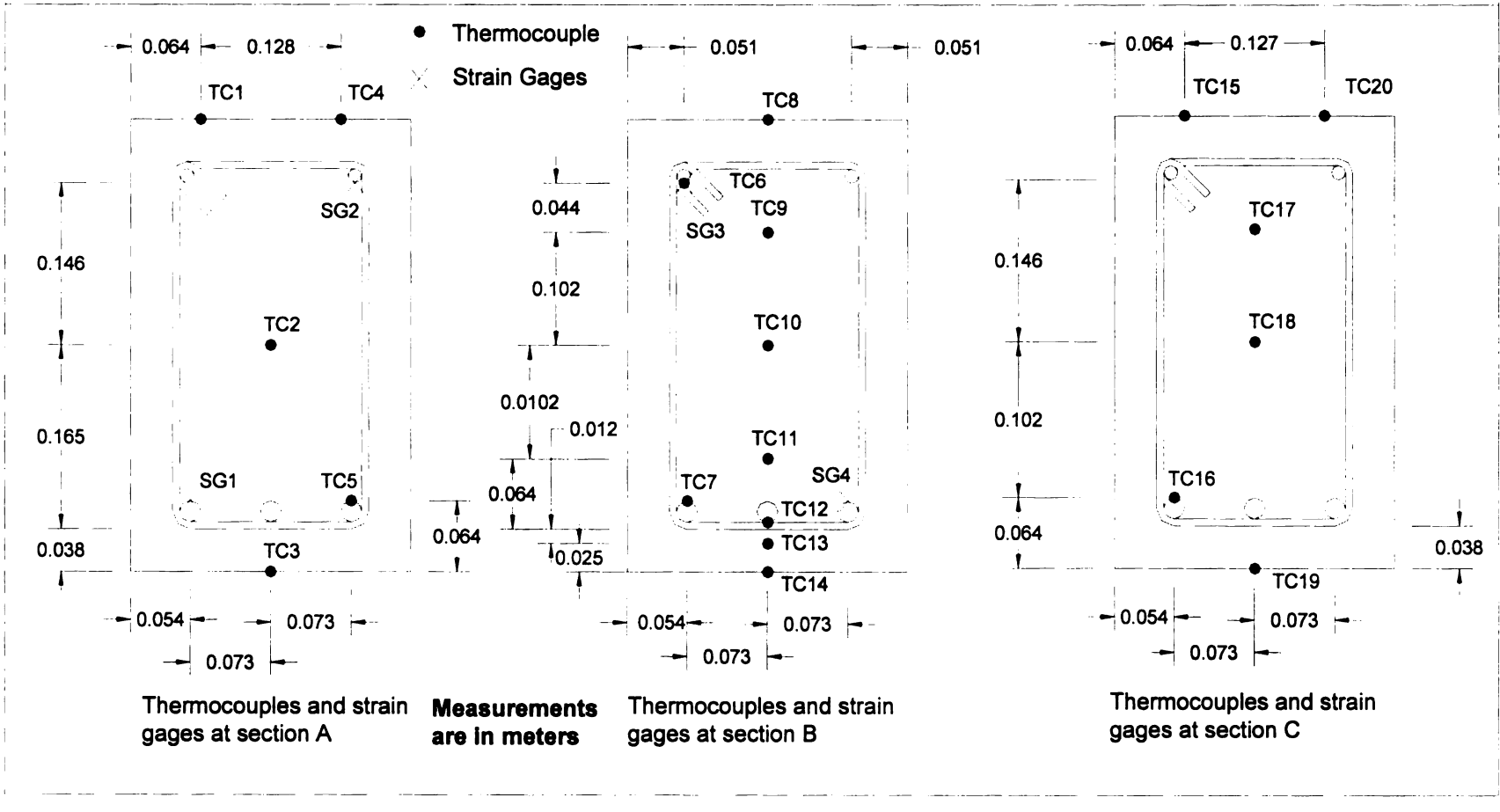

Figure 3.1(b) – Cross-section and Location of Thermocouples and Strain Gages in Beams B1 through B4

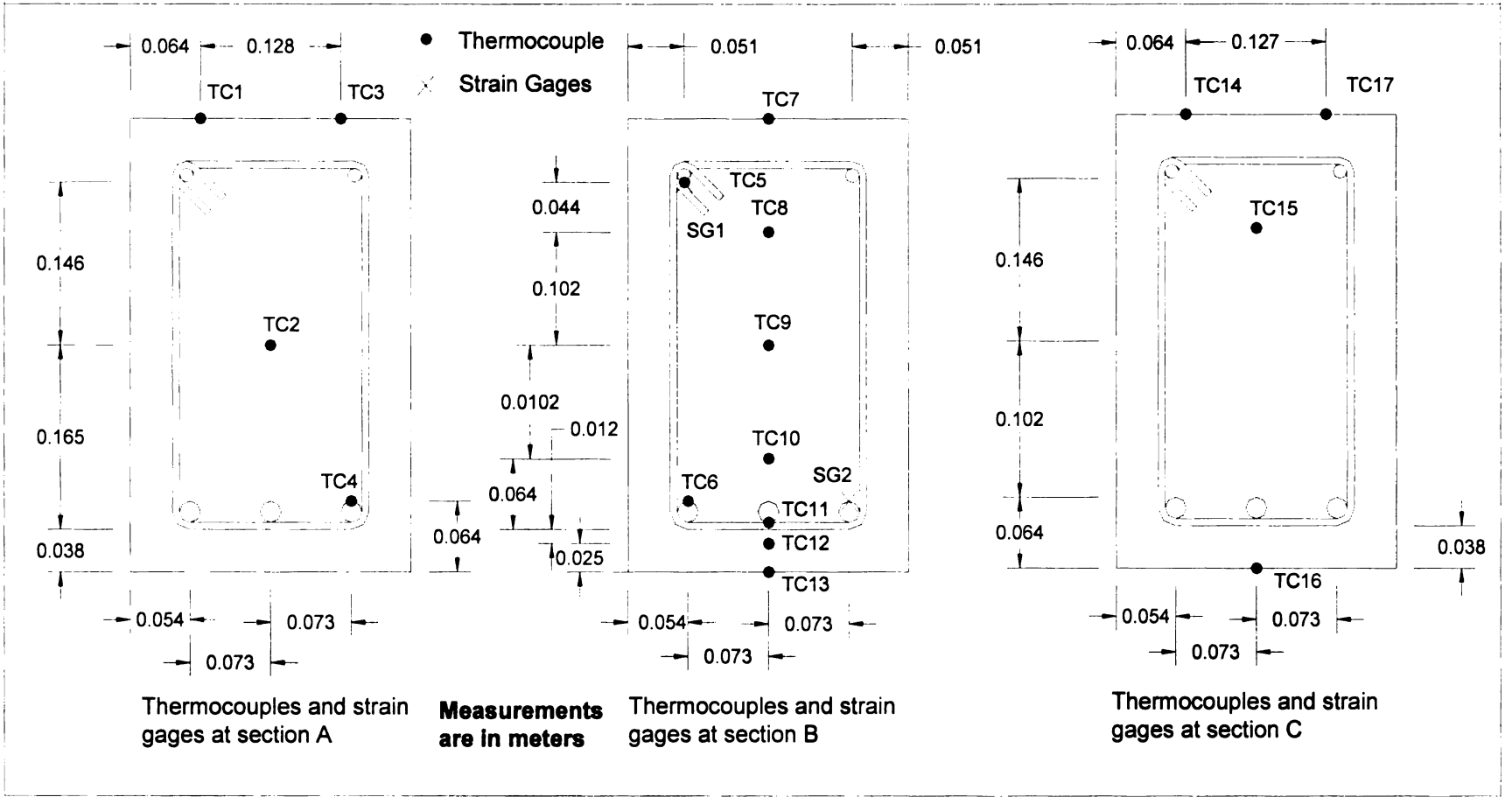

Figure 3.1(c) – Cross-section and Location of Thermocouples and Strain Gages in Beams B5 and B6

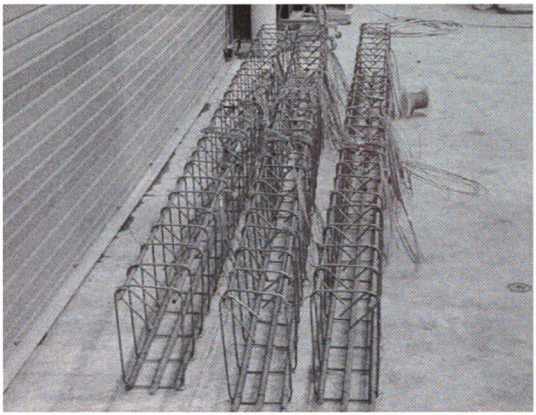

Figure 3.2 – Layout of Steel Reinforcement before Concrete Placement

Figure 3.3 – View of HSC Beams after Fabrication

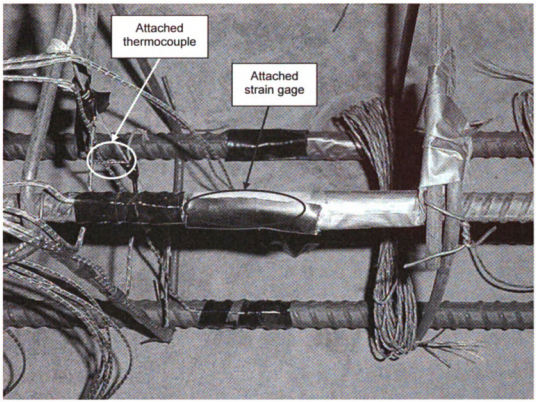

Figure 3.4 – View of a Thermocouple and a Strain Gage attachment to Beams

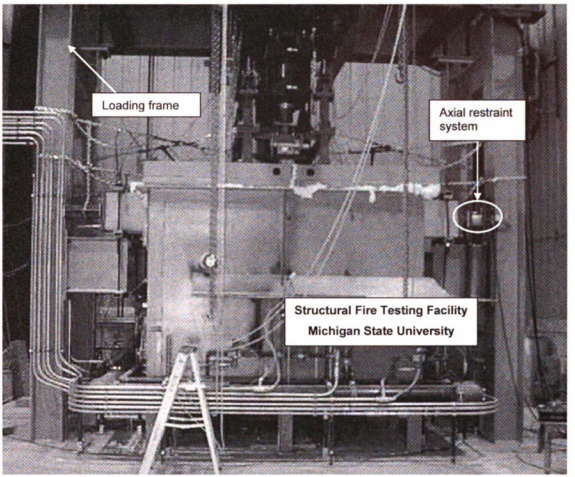

Figure 3.5 – Structural Fire Test Facility at MSU's Civil Infrastrcuture Laboratory

A: 8' x 10' x 5' furnace B: 3' x3' external column
C: Removable support D: Beam column specimen to be tested
E: Load cell to measure restraint force
F: Two point loading G: Flexible insulated filling

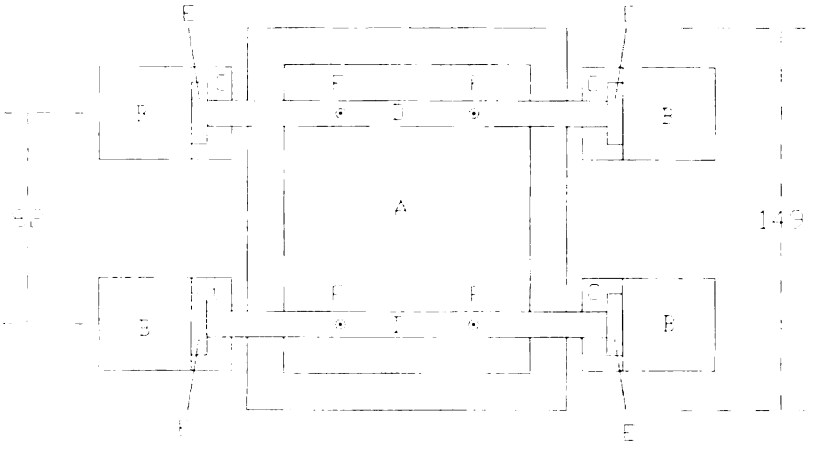

(a) Plan

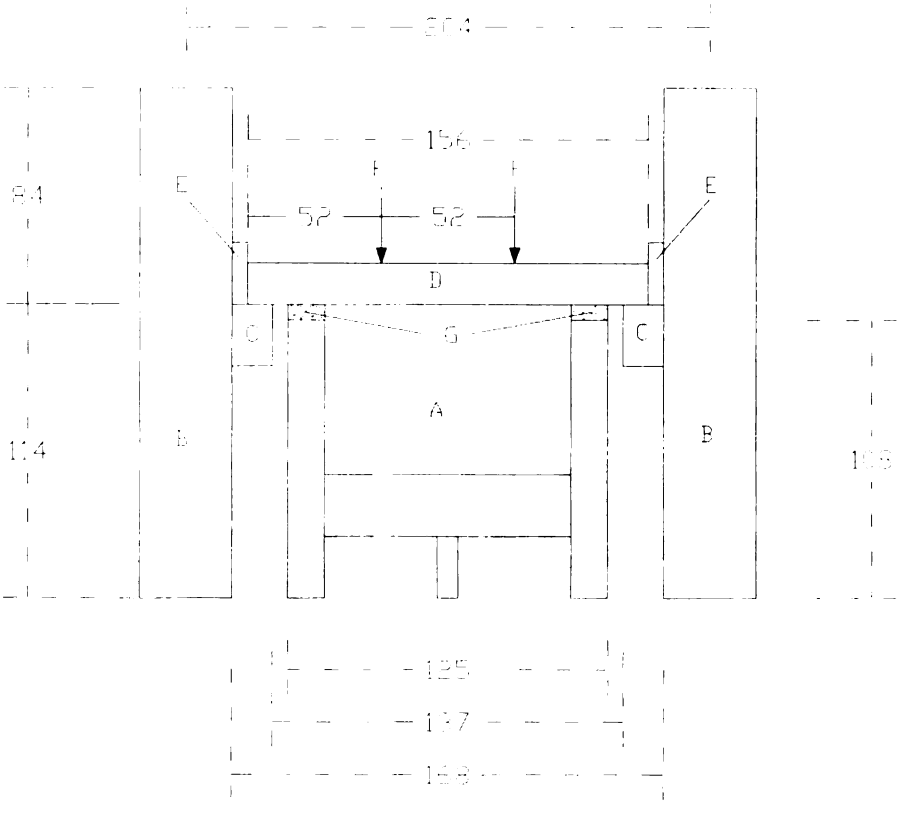

All measurements are in inches

(a) Elevation

Figure 3.6 – Test Setup Showing RC Beams in the Furnace

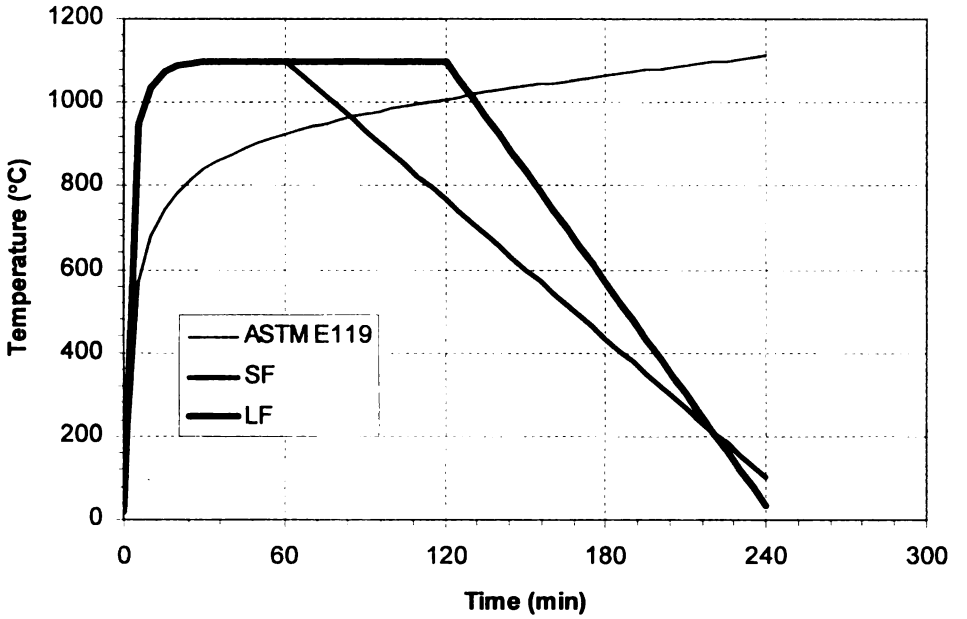

Figure 3.7 – Time Temerpature Curves for Fire Scenarios used in the Fire Tests

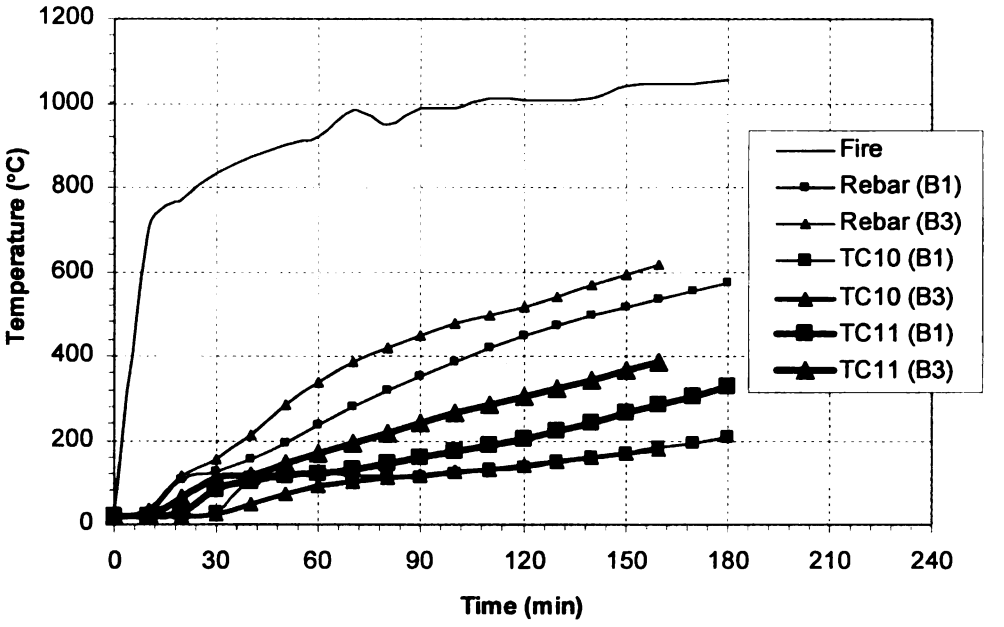

Figure 3.8 – Measured Rebar and Concrete Temperatures as a Function of Time for NSC Beam B1 and HSC Beam B3

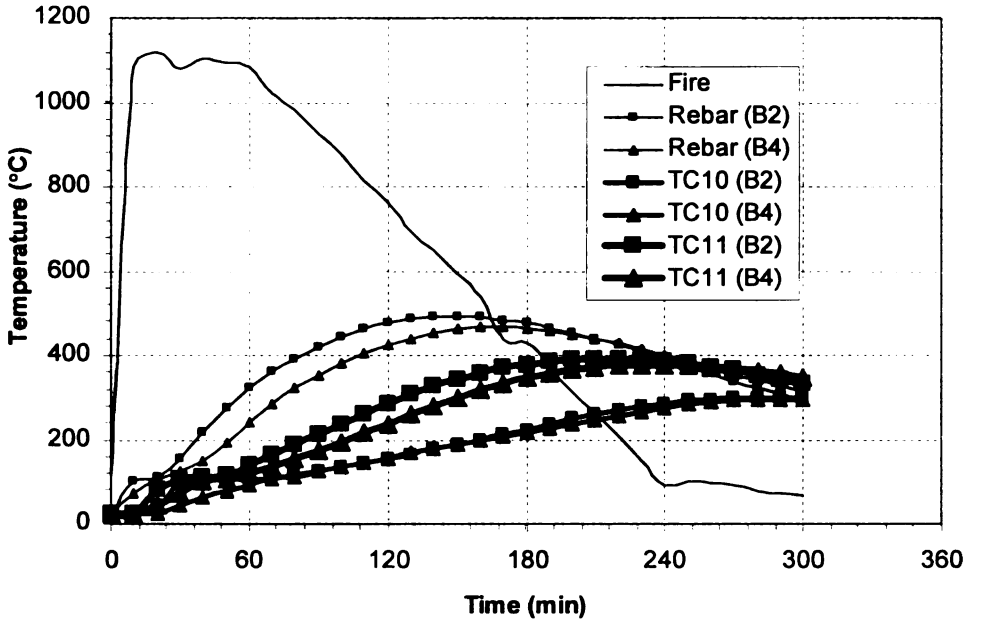

Figure 3.9 – Measured Rebar and Concrete Temperatures as a Function of Time for NSC Beam B2 and HSC Beam B4

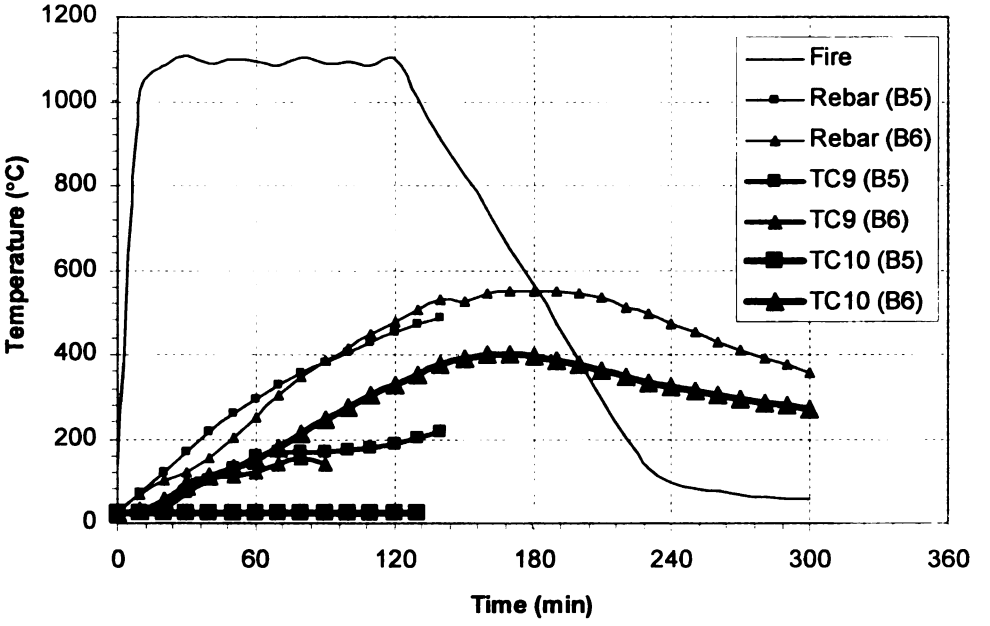

Figure 3.10 – Measured Rebar and Concrete Temperatures as a Function of Time for HSC Beams B5 and B6

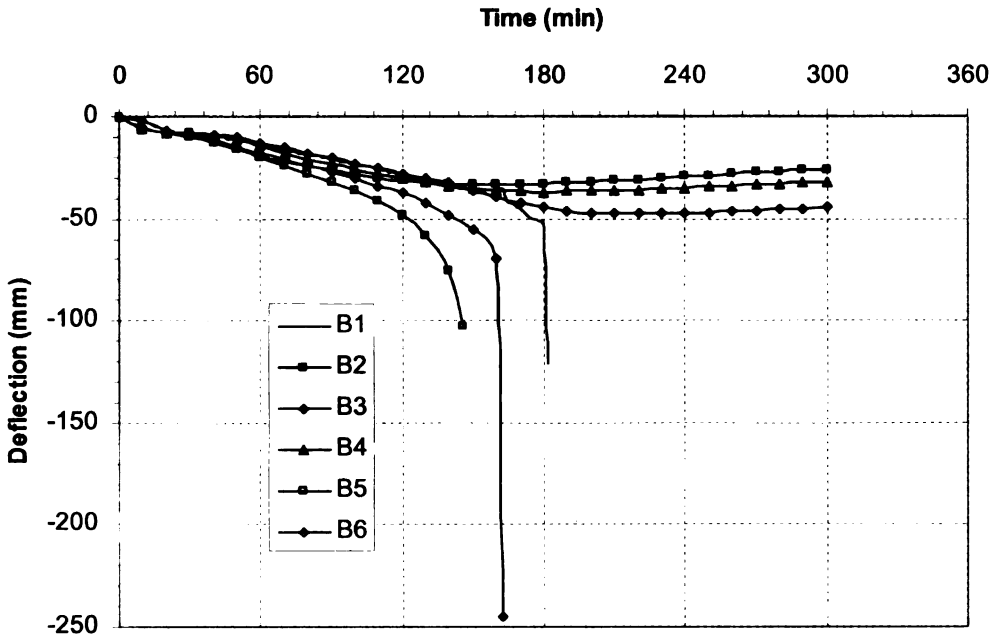

Figure 3.11 – Measured Mid-span Deflection as a Function of Time for RC Beams

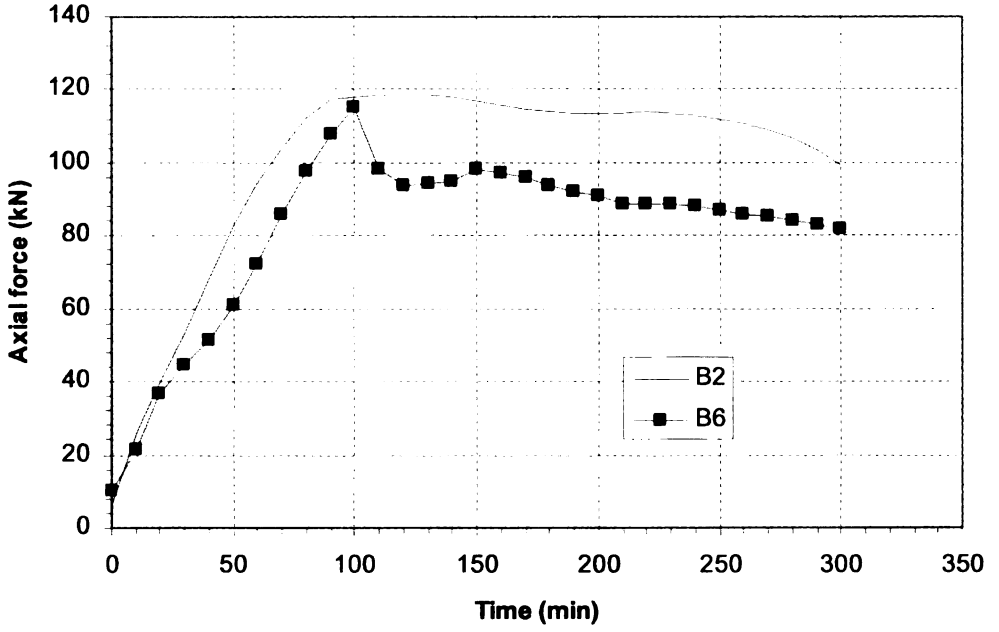

Figure 3.12 – Measured Axial Force as a Function of Time for Axially Restrained RC Beams B2 and B6

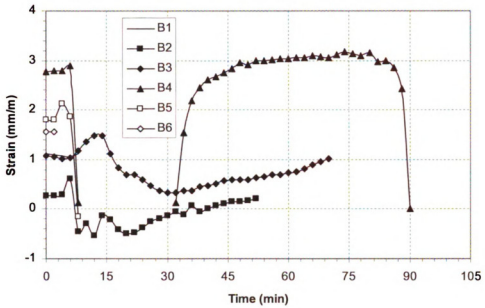

Figure 3.13 – Measured Strain as a Function of Time in the Tensile Reinforcement in the Central Section of the Test Beams

(a) Typical Beam before Fire Test

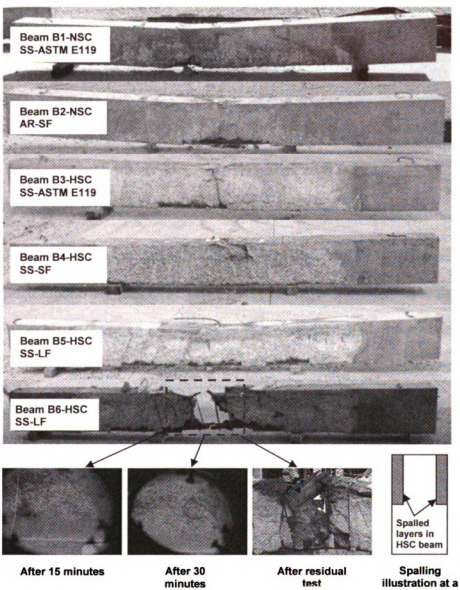

(b) Beams B1 to B6 after Fire Test

Figure 3.14 – Photographs of Beams after Fire Resistance Tests

Chapter 4

4. Numerical Model

The behavior of RC beams under fire can be simulated by using advanced numerical models. Such models are generally based on microscopic or macroscopic finite element formulations. In the case of microscopic finite element based models (eg. ANSYS, ABAQUS and SAFIR), a structural member is discretized into a three dimensional mesh, and coupled (or uncoupled) thermal and structural analyses are carried out to trace the fire behavior. However, such an analysis is complex, requires significant effort and the results are often difficult to interpret. Although, such models are capable of accounting for high temperature material properties and different strain components, and can generate detailed output parameters, most of the commercial finite element programs are not capable of modeling fire induced spalling of concrete. Also, some of the sophistication and complexity used in three dimensional modeling is of limited use since high temperature constitutive relationships for concrete in more than one dimension are not available.

An alternative to complex microscopic finite element methods is the use of a macroscopic finite element approach for tracing the fire behavior of RC members (beams, columns etc.). In the macroscopic finite element method, a sectional analysis is carried out at a number of cross-sections along the length of the structural member. The sectional response generated at various cross-sections is utilized to predict the fire response of the RC member. Strain components, high temperature constitutive relationships, fire induced spalling, and restraint effects can be accounted for in such models. In this way, the necessity of three dimensional material properties is avoided and the model results are easier to interpret and use. However, such macroscopic models are not currently available for modeling the fire response of concrete structures. A macroscopic finite element based model for tracing the response of RC members exposed to fire is developed in this dissertation.

4.1 General Approach

The numerical model uses moment curvature (M-κ) relationships to trace the response of an RC beam in fire over the entire range of loading up to collapse. The RC beam is divided into numerous segments along its length (see Figure 4.1). The mid-section of each segment is assumed to represent the behavior of the whole segment. The fire resistance analysis is carried out by incrementing time in steps. At each time interval, the analysis is performed through three main stages, namely:

- Establishing the fire temperature due to fire exposure;
- Carrying out a coupled heat transfer-spalling analysis in each segment to predict cross-sectional temperature and spalling; and
- Performing a strength and deflection analysis through three sub-stages, namely:

- Calculating the fire induced axial restraint force in the RC beam;
- Generating M-κ relationships (utilizing the axial restraint force computed above) for each beam segment; and
- Performing structural analysis of the entire beam to compute deflections and internal forces.

The first stage of the analysis is to establish the fire temperature using standard or design fire scenarios. Following this, a hydro-thermal analysis is performed to evaluate cross-sectional temperatures and any fire induced spalling in each segment of the beam.

The fire induced restraint is then accounted for in the analysis through the axial restraint force, which involves a large computational effort. The axial restraint force, at each time interval, is computed based on an iterative approach by satisfying the equilibrium and compatibility criteria along the span of the beam.

Once the axial restraint force in the beam is computed, the next step is the generation of M-κ relationships for each segment of the beam. It has been well established that M-κ relationships appropriately represent the behavior of an RC beam at ambient conditions (Campbell and Kodur 1990). In the current model, M-κ relationships are established as a function of time for various segments and they are used to trace the response of the beam under fire conditions. Material nonlinearity and fire induced restraint effects are implicitly accounted for in the moment curvature generation.

Using the M-κ relationships, the load (moment) the beam can carry at a particular time step is evaluated. Also, the deflection at that time step can be calculated through a stiffness approach by evaluating the average stiffness of the beam. This is computed using segmental stiffnesses, which are estimated by means of known M-κ relationships.

A flowchart showing the numerical procedure for fire resistance calculations is given in Figure 4.2.

The model generates various output parameters, such as temperatures, stresses, strains, axial restraint force, deflections, and moment capacities at various fire exposure times. The temperatures and strength capacities for each segment, and computed deflections in the beam, are used to evaluate failure of the beam at each time step. At every time step, each beam segment is checked against pre-determined failure criteria, which include prescriptive thermal criterion, and performance-based strength and deflection considerations. Details of the analysis procedure are presented in the following sections.

4.2 Fire Temperatures

The fire temperatures are calculated by assuming that three sides of the beam are exposed to a fire, whose temperature follows that of the standard fire exposure such as ASTM E119a (2008) or any other design fire scenario (SFPE 2004, Eurocode 1 2002). The time-temperature relationship for the ASTM E119 standard fire can be approximated by the following equation:

$$T_f = T_0 + 750\left(1 - \exp\left(-3.79553\sqrt{t_h}\right)\right) + 170.41\sqrt{t_h} \qquad [4.1]$$

where t_h = time (hours), T_0 = initial temperature (°C), and T_f = fire temperature (°C).

For design fires, the time-temperature relationship specified in Eurocode 1 (2002) for typical fuel load and ventilation factor are built into the model. Also, to simulate hydrocarbon fire scenarios, the time-temperature relationship specified in ASTM E1529 (1993) is incorporated into the model.

4.3 Hydro-thermal Analysis and Spalling Prediction

The hydro-thermal analysis is performed to compute the temperature and pore pressure distributions within the beam cross-section. At each time step, a hydro-thermal analysis is carried out in two steps, namely, thermal analysis and pore pressure calculations.

4.3.1 Thermal Analysis

The temperatures within the cross-section of each segment are computed using the finite element approach. The fire temperature established in Section 4.2 forms the input into the thermal analysis. The cross-sectional area of each segment is subdivided into a number of elements and the temperature rise in a beam segment is derived by establishing a heat balance for each element. Detailed equations for the calculation of segment temperatures are derived.

The temperature is assumed to be uniform along the length of the segment and thus the calculations are performed for a unit length of each segment. Steel reinforcement is not specifically considered in the thermal analysis because it does not greatly influence the temperature distribution in the beam cross-section (Lie and Irwin 1993). More details on the governing equations for the calculations of the vapor pressure are given below.

Based on the conservation of energy, the following equation can be obtained for one dimensional heat transfer problems:

$$\rho c \frac{dT}{dt} = -\frac{dq}{dx} + Q \qquad [4.2]$$

Using Fourier's Law, which relates the heat flux to the temperature gradients as $q = -k\frac{dT}{dx}$, Eq. [4.2] can be written as:

$$\rho c \frac{dT}{dt} = \frac{d\left(k \frac{dT}{dx}\right)}{dx} + Q \qquad [4.3]$$

Thus, the governing heat transfer equation within a beam cross-section, which represents a two dimensional problem, can be written as:

$$\rho c \frac{dT}{dt} = \nabla(k \nabla T) + Q \qquad [4.4]$$

where k = thermal conductivity, ρc = heat capacity, T = temperature, t = time, Q = heat source, and q = heat flux.

At the fire-beam interface, the mechanism for heat transfer is through radiation and convection. The heat flux on the boundary due to convection and radiation can be given by the following two equations:

$$q_{rad} = h_{rad}\left(T - T_E\right) \qquad [4.5]$$

$$q_{con} = h_{con}\left(T - T_E\right) \qquad [4.6]$$

where

q_{rad} and q_{con} = radiative and convective heat fluxes,

h_{rad} and h_{con} = radiative and convective heat transfer coefficients,

$h_{rad} = 4\sigma\varepsilon\left(T^2 + T_E^2\right)\left(T + T_E\right)$,

T_E = temperature of the environment surrounding the boundary,

σ = Stefan-Boltzman constant = 5.67×10^{-8} (W/m^2.°K^4), and

ε = emissivity.

Hence, the total heat flux on the beam boundaries (q_b) can be given by:

$$q_b = \left(h_{con} + h_{rad}\right)\left(T - T_E\right) \qquad [4.7]$$

Using Fourier's Law, the governing heat transfer equation on the boundary of the beam can be written as:

$$k\left(\frac{\partial T}{\partial y}n_y + \frac{\partial T}{\partial z}n_z\right) = -h\left(T - T_f\right) \qquad [4.8]$$

where

n_y and n_z = components of the vector normal to the boundary in the plane of the cross-section, and

$h = h_{con} + h_{rad}$

Since the beam is exposed to fire from three sides, two types of boundary equations must be considered for thermal analysis, namely:

- Fire exposed boundaries where the heat flux is governed by:

$$k\left(\frac{\partial T}{\partial y}n_y + \frac{\partial T}{\partial z}n_z\right) = -h_f\left(T - T_f\right) \qquad [4.9]$$

- Unexposed boundary where the heat flux equation is given by:

$$k\left(\frac{\partial T}{\partial y}n_y + \frac{\partial T}{\partial z}n_z\right) = -h_c\left(T - T_0\right) \qquad [4.10]$$

where

h_f and h_c = heat transfer coefficient of the fire side and the cold side, respectively, and

T_f and T_0 = fire and cold side temperatures, respectively.

4.3.2 Pore Pressure Calculations

To evaluate the possible occurrence of fire induced spalling, pore pressure calculations are carried out for each segment at each time step.

Assumptions

The following assumptions are made in the development of the spalling sub-model:

- Concrete is a continuum. This assumption is based on the fact that the heterogeneity scale (length over which the medium changes from one phase to another) of concrete is much smaller than the length over which a change can be observed in the temperature, moisture content, and pressure.
- Water vapor is an ideal gas, which is valid for most engineering applications (Harmathy 1969, 1971 and Huang 1979).
- Mobility of liquid water is ignored. This assumption is reasonable because Darcy's coefficient (permeability) for liquid water in concrete is much smaller than for water vapor (Harmathy 1969 and Sahota 1979).
- The effect of air is ignored in the analysis. This assumption is considered to be reasonable because the mass of air in concrete is much smaller than the mass of water.
- The solid skeleton (concrete structure) is assumed to be undeformable. This is because the mechanical and thermal deformation of the solid phase is small when compared with the volume changes due to other processes such as evaporation.
- Water is an incompressible liquid. This assumption is valid because the volumetric deformation of liquid water due to pressure is much smaller than the volumetric changes due to other processes such as evaporation.
- The applied loading is assumed not to influence the hydro-thermal analysis. The applied loading generally causes damage in the concrete, which increases the

concrete permeability. Thus, this assumption leads to conservative spalling predictions.

- Latent heat and heat of dehydration are not accounted for in the analysis. Accounting for them will slightly reduce predicted temperatures. Thus, latent heat and heat of dehydration can be conservatively ignored in the analysis.

Governing Equations

The governing equations for the calculation of vapor pressure in concrete are derived using four main principles, namely:

- Conservation of mass for liquid water,
- Ideal gas law,
- The total volume of all different components in a unit volume of concrete equals unity, and
- Conservation of mass for water vapor.

Additional details on the governing equations for the calculation of vapor pressure are provided in the following discussion.

- The basic equation that governs the conservation of mass for liquid water is given by:

$$E = m_{LW0} - m_L + m_D \qquad [4.11]$$

Differentiating with respect to time, Eq. [4.11] can be written as:

$$\frac{dE}{dt} = -\frac{dm_L}{dt} + \frac{dm_D}{dt} \qquad [4.12]$$

Using the chain rule to expand $\frac{dm_L}{dt}$, Eq. [4.12] can be written as:

$$\frac{dE}{dt} = -\frac{dm_L}{dP_V}\frac{dP_V}{dt} - \frac{dm_L}{dT}\frac{dT}{dt} + \frac{dm_D}{dT}\frac{dT}{dt} \qquad [4.13]$$

where E = mass of evaporated water, m_{LW0} = mass of liquid water at t = 0, (initial mass of liquid water), m_L = mass of liquid water at any subsequent time, t, m_D = mass of liquid water formed by dehydration, T = temperature, P_V = vapor pressure, and t = time.

- The ideal gas law is used to relate the pressure, the volume, the mass, and the temperature for water vapor as follows:

$$P_V V_V = n_V RT \qquad [4.14]$$

$$n_V = \frac{m_V}{M} \qquad [4.15]$$

Hence, $$P_V = \frac{R}{M}\frac{m_V T}{V_V} \qquad [4.16]$$

$$\frac{dP_V}{dt} = \frac{R}{M}\left(\frac{TV_V \dfrac{dm_V}{dt} + m_V V_V \dfrac{dT}{dt} - m_V T \dfrac{dV_V}{dt}}{V_V^2}\right) \qquad [4.17]$$

Rearranging Eq. [4.17] gives:

$$\frac{dm_V}{dt} = \frac{V_V M}{RT}\frac{dP_V}{dt} - \frac{m_V}{T}\frac{dT}{dt} + \frac{m_V}{V_V}\frac{dV_V}{dt} \qquad [4.18]$$

where m_V = mass of water vapor, R = gas constant, n_V = number of moles of water vapor, M = molar mass of water, V_V = volume fraction of water vapor, and T = temperature (°K).

- For a unit volume of concrete, the sum of the volume fractions of all phases equals unity, which leads to the following equation:

$$V_V + V_L + (V_{S0} - V_D) = 1 \qquad [4.19]$$

Eq. [4.19] can be written as:

$$V_V = 1 - V_L - (V_{S0} - V_D) \qquad [4.20]$$

Using the volume-mass-density relationship, Eq. [4.20] can be written as:

$$V_V = 1 - \frac{m_L}{\rho_L} - \left(V_{S0} - \frac{m_D}{\rho_L}\right) \qquad [4.21]$$

Differentiating both sides of Eq. [4.21] with respect to time yields:

$$\frac{dV_V}{dt} = \frac{1}{\rho_L}\left(\frac{dm_D}{dt} - \frac{dm_L}{dt}\right) - \frac{1}{\rho_L^2}\frac{d\rho_L}{dT}\frac{dT}{dt}(m_D - m_L) \qquad [4.22]$$

Substituting Eq. [4.12] in Eq. [4.22] results in:

$$\frac{dV_V}{dt} = \frac{1}{\rho_L}\frac{dE}{dt} - \frac{1}{\rho_L^2}\frac{d\rho_L}{dT}\frac{dT}{dt}(m_D - m_L) \qquad [4.23]$$

By substituting Eq. [4.23] in Eq. [4.18], Eq. [4.24] can be obtained.

$$\frac{dm_V}{dt} = \frac{V_V M}{RT}\frac{dP_V}{dt} - \frac{m_V}{T}\frac{dT}{dt} + \frac{m_V}{V_V \rho_L}\left(\frac{dE}{dt} - \frac{1}{\rho_L}\frac{d\rho_L}{dT}\frac{dT}{dt}(m_D - m_L)\right) \qquad [4.24]$$

where V_L = volume fraction of liquid water, V_{S0} = initial volume fraction of solid, V_D = volume fraction of dehydrated liquid water, and ρ_L = density of liquid water.

- Based on the conservation of mass of water vapor, the following equation can be obtained for one dimensional problems:

$$\frac{dm_V}{dt} = -\frac{dJ}{dx} + \frac{dE}{dt} \qquad [4.25]$$

Using Darcy's Law, which relates the mass flux to the pressure gradients as $J = -\lambda\frac{dP_V}{dx}$, Eq. [4.25] can be written as:

$$\frac{dm_V}{dt} = \frac{d\left(\lambda\frac{dP_V}{dx}\right)}{dx} + \frac{dE}{dt} \qquad [4.26]$$

Darcy's coefficient, λ, can be written as:

$$\lambda = m_V \frac{k_T}{\mu_V} \tag{4.27}$$

Substituting for λ, Eq. [4.26] can be written as:

$$\frac{dm_V}{dt} = \frac{d\left(\left(m_V \frac{k_T}{\mu_V}\right)\frac{dP_V}{dx}\right)}{dx} + \frac{dE}{dt} \tag{4.28}$$

For two dimensional problems, Eq. [4.28] can be written as:

$$\frac{dm_V}{dt} = \nabla\left(m_V \frac{k_T}{\mu_V}\right)\nabla P_V + \frac{dE}{dt} \tag{4.29}$$

By substituting Eq. [4.24], Eq. [4.29] can be written as:

$$\begin{aligned}&\frac{V_V M}{RT}\frac{dP_V}{dt} - \frac{m_V}{T}\frac{dT}{dt} + \frac{m_V}{V_V \rho_L}\left(\frac{dE}{dt} - \frac{1}{\rho_L}\frac{d\rho_L}{dT}\frac{dT}{dt}(m_D - m_L)\right)\\ &= \nabla\left(m_V \frac{k_T}{\mu_V}\right)\nabla P_v + \frac{dE}{dt}\end{aligned} \tag{4.30}$$

Hence, the governing differential equation for pore pressure is given by:

$$\begin{aligned}&\frac{V_V M}{RT}\frac{dP_V}{dt} = \nabla\left(m_V \frac{k_T}{\mu_V}\right)\nabla P_V + \left(1 - \frac{m_V}{V_V \rho_L}\right)\frac{dE}{dt}\\ &+ \frac{m_V}{T}\frac{dT}{dt} + \frac{m_V}{V_V \rho_L^2}\frac{d\rho_L}{dT}\frac{dT}{dt}(m_D - m_L)\end{aligned} \tag{4.31}$$

Using Eq. [4.13], Eq. [4.31] can be written as:

$$\begin{aligned}&\frac{V_V M}{RT}\frac{dP_V}{dt} = \nabla\left(m_V \frac{k_T}{\mu_V}\right)\nabla P_V + \left(1 - \frac{m_V}{V_V \rho_L}\right)\left(-\frac{dm_L}{dP_V}\frac{dP_V}{dt} - \frac{dm_L}{dT}\frac{dT}{dt} + \frac{dm_D}{dT}\frac{dT}{dt}\right)\\ &+ \frac{m_V}{T}\frac{dT}{dt} + \frac{m_V}{V_V \rho_L^2}\frac{d\rho_L}{dT}\frac{dT}{dt}(m_D - m_L)\end{aligned} \tag{4.32}$$

which can be rearranged as:

$$\left[\left(1-\frac{m_V}{V_V\rho_L}\right)\frac{dm_L}{dP_V}+\frac{V_V M}{RT}\right]\frac{dP_V}{dt}=\nabla\left(m_V\frac{k_T}{\mu_V}\right)\nabla P_V$$
$$+\left[\left(1-\frac{m_V}{V_V\rho_L}\right)\left(-\frac{dm_L}{dT}+\frac{dm_D}{dT}\right)+\frac{m_V}{T}+\frac{m_V}{V_V\rho_L^2}\frac{d\rho_L}{dT}(m_D-m_L)\right]\frac{dT}{dt} \quad [4.33]$$

where J = mass flux of water vapor, λ = Darcy's coefficient of permeability, k_T = intrinsic permeability of concrete at temperature, T, and μ_V = dynamic viscosity of water vapor.

Equation [4.33] can be simplified by introducing three parameters, A, B, and C as follows:

$$A\frac{dP_V}{dt}=\nabla B\nabla P_V+C \quad [4.34]$$

where

$$A=\left[\left(1-\frac{m_V}{V_V\rho_L}\right)\frac{dm_L}{dP_V}+\frac{V_V M}{RT}\right]$$

$$B=m_V\frac{k_T}{\mu_V}$$

$$C=\left[\left(1-\frac{m_V}{V_V\rho_L}\right)\left(-\frac{dm_L}{dT}+\frac{dm_D}{dT}\right)+\frac{m_V}{T}+\frac{m_V}{V_V\rho_L^2}\frac{d\rho_L}{dT}(m_D-m_L)\right]\frac{dT}{dt}$$

Initial and Boundary Conditions

The initial and boundary conditions for pore pressure calculations are assumed as follows:

- The initial pore pressure (P_{V0}) can be computed as

$$P_{V0}=RH\cdot P_{S0} \quad [4.35]$$

where RH = initial relative humidity in the concrete and P_{S0} = initial saturation pressure which can be computed based on the initial temperature of concrete.

- On the boundaries (surface) of the beam the water vapor is assumed to be transferred through diffusion. Thus, the governing mass transfer equation of water vapor at the beam boundaries can be written as

$$\lambda\left(\frac{\partial P_V}{\partial y}n_y + \frac{\partial P_V}{\partial z}n_z\right) = -D_0\left(\rho_V - \rho_{V\infty}\right) \qquad [4.36]$$

where D_0 = diffusion coefficient of water vapor at the boundaries of the beam, ρ_V = density of water vapor in the concrete boundaries, and $\rho_{V\infty}$ = density of water vapor in the surrounding environment. By assuming $\rho_{V\infty}$ to be constant during fire exposure (due to the lack of information on the changes that take place in the surrounding environment of the beam), Eq. [4.36] can be written as

$$\lambda\left(\frac{\partial P_V}{\partial y}n_y + \frac{\partial P_V}{\partial z}n_z\right) = -\frac{D_0 M}{RT}\left(P_V - \frac{RT\rho_{V\infty}}{M}\right). \qquad [4.37]$$

4.3.3 Finite Element Solution

The Galerkin finite element formulation is applied to solve Eq. [4.4] and Eq. [4.34]. Both equations can be written in the following form:

$$A_1\frac{du}{dt} = \nabla B_1 \nabla u + C_1 \qquad [4.38]$$

The governing equation at the beam boundaries for both heat and mass transfer can be written as:

$$A_{11}\left(\frac{\partial u}{\partial y}n_y + \frac{\partial u}{\partial z}n_z\right) = -B_{11}\left(u - C_{11}\right) \qquad [4.39]$$

The cross-section of an RC beam is divided into elements as shown in Figure 4.3. According to the finite element formulation, the material property matrices and the equivalent nodal heat or mass flux (stiffness matrix K_e, mass matrix M_e, and nodal heat or mass flux F_e) are generated for each element. These matrices are given by the following equations (William 1990):

$$K_e = \int_A \left[B_1 \frac{\partial N}{\partial x}\frac{\partial N^T}{\partial x} + B_1 \frac{\partial N}{\partial y}\frac{\partial N^T}{\partial y} \right] dA + \int_\Gamma N B_{11} N^T ds \qquad [4.40]$$

$$M_e = \int_A A_1 N N^T dA \qquad [4.41]$$

$$F_e = \int_A N C_1 dA + \int_\Gamma N B_{11} C_{11} ds \qquad [4.42]$$

where N = vector of the shape functions, A_1, B_1, C_1, A_{11}, B_{11} and C_{11} = parameters computed by comparing equations [4.4], [4.9], [4.10], [4.34] and [4.37] with equations [4.38] and [4.39] for heat and mass transfer, Γ = boundary of the beam, and s = distance along the boundary Γ.

Once the element matrices are computed, they are assembled into a system of differential equations which can be written as

$$M\dot{u} + Ku = F(t) \qquad [4.43]$$

where K = global stiffness matrix, M = global mass matrix, F = equivalent nodal heat flux, and $\dot{u}$ = the derivative of u with respect to time.

A finite difference procedure (θ algorithm) in the time domain is used to solve Eq. [4.43] (William 1990). The algorithm assumes

$$u_{n+1} = u_n + h(\theta \dot{u}_{n+1} + (1-\theta)\dot{u}_n) \qquad [4.44]$$

Multiplying both sides of Eq. [4.44] by M and using Eq. [4.43] at the beginning and the end of the time interval (t_n, t_{n+1}), the following equation can be obtained

$$(M + h\theta K)u_{n+1} = (M - h(1-\theta)K)u_n + h(\theta F_{n+1} + (1-\theta)F_n) \quad [4.45]$$

where h = time step, u_n and u_{n+1} = values of u at the beginning and the end of time step, respectively, F_n and F_{n+1} = equivalent nodal heat flux at the beginning and the end of time step, and θ = a constant between 0 and 1.

For unconditional stability of numerical calculations, θ has to be greater than or equal to 0.5 (William 1990). By knowing the values of u at ambient conditions, Eq. [4.45] can be applied to obtain the time history for temperature or pressure at the following time step, and this can be repeated for subsequent time steps. For each time step, an iterative process is required to solve Eq. [4.45] due to the nonlinearity of both the material properties and the boundary conditions. Details on the finite element formulation for solving the heat and mass transfer equations are provided in Appendix C.

4.3.4 Spalling Prediction

Once the pore pressure in various concrete elements is calculated, a simplified approach is applied to determine spalling. The computed effective pore pressure (pore pressure multiplied by the porosity of concrete) is compared against the temperature dependent tensile strength of concrete as shown in Figure 4.4. When the effective pore pressure exceeds the temperature dependent tensile strength at that time step, spalling is assumed to occur in that concrete element; i.e.:

$$nP_V > f_{tT} \quad [4.46]$$

where n = porosity of concrete = $V_V + V_L$ and f_{tT} = tensile strength of concrete for temperature, T.

Once spalling occurs, that concrete element is assumed to be lost and the reduced concrete section and new boundary surface is considered in the subsequent hydro-thermal and strength analyses. In this way, the coupling between spalling and hydro-thermal analysis will be accounted for in the model.

4.3.5 Constitutive Relationships

Isotherms

Isotherms are used to predict the mass of liquid water inside concrete as a function of pore pressure and temperature. The isotherms, used in the analysis, are assumed to follow the semi empirical isotherms developed by Bazant and Thonguthai (1978). The main assumption in Bazanat's isotherms is that water in concrete is capillary water (adsorbed water is ignored). This assumption may not be applicable for HSC at room temperature where adsorbed water is a large portion of water in concrete. However, Bazant showed that the adsorbed water decreases at elevated temperatures and thus capillary water becomes the dominant state of water in HSC. According to Bazant's isotherms, the mass of liquid water is given as:

$$m_L = \begin{cases} \rho_C \left(\dfrac{m_0}{\rho_C} \dfrac{P_V}{P_S} \right)^{1/m(T)} & , \dfrac{P_V}{P_S} \le 0.96 \\ m_{0.96} + \left(\dfrac{P_V}{P_S} - 0.96 \right) \dfrac{m_{1.04} - m_{0.96}}{0.08} & , 0.96 < \dfrac{P_V}{P_S} < 1.04 \\ m_{L0} \left[1 + 0.12 \left(\dfrac{P_V}{P_S} - 1.04 \right) \right] & , \dfrac{P_V}{P_S} \ge 1.04 \end{cases} \qquad [4.47]$$

The case of relative humidity (P_V/P_S) exceeding 100% represents the case of condensation of water vapor. According to Bazant's isotherms, the mass of liquid water (m_L) exceeds the saturation mass of liquid water (m_{L0}) at room temperature when the relative humidity exceeds 100%. This can be attributed to the condensation of water vapor transferred to the high pressure region.

Thus, the derivatives of m_L with respect to pore pressure and temperature (which are essential to compute A and C in Eq. [4.34]) are:

$$\frac{dm_L}{dP_V} = \begin{cases} \dfrac{m_0}{m(T)P_S}\left(\dfrac{m_0}{\rho_C}\dfrac{P_V}{P_S}\right)^{1/m(T)-1} & ,\dfrac{P_V}{P_S} \le 0.96 \\ \dfrac{m_{1.04} - m_{0.96}}{0.08} & ,0.96 < \dfrac{P_V}{P_S} < 1.04 \\ 0.12\dfrac{m_{L0}}{P_S} & ,\dfrac{P_V}{P_S} \ge 1.04 \end{cases} \qquad [4.48]$$

$$\frac{dm_L}{dT} = \begin{cases} -m_L\left[\dfrac{\dfrac{dm(T)}{dT}}{m(T)^2} ln\left(\dfrac{m_0 P_V}{\rho_C P_S}\right) + \dfrac{\dfrac{dP_S}{dT}}{m(T)P_S}\right] & ,\dfrac{P_V}{P_S} \le 0.96 \\ \dfrac{dm_{0.96}}{dT} - \dfrac{P_V\dfrac{dP_S}{dT}}{P_S^2}\left(\dfrac{m_{1.04} - m_{0.96}}{0.08}\right) + X & ,0.96 < \dfrac{P_V}{P_S} < 1.04 \\ \dfrac{dm_{L0}}{dT}\left[1 + 0.12\left(\dfrac{P_V}{P_S} - 1.04\right)\right] - 0.12\dfrac{m_{L0}P_V\dfrac{dP_S}{dT}}{P_S^2} & ,\dfrac{P_V}{P_S} \ge 1.04 \end{cases} \qquad [4.49]$$

where:

ρ_C = mass of cement per unit volume of concrete,

m_0 = mass of water for saturation at 25 °C per unit volume of concrete,

m_{L0} = mass of water for saturation at any temperature per unit volume of concrete,

P_S = saturation pressure,

$$m(T) = 1.04 - \frac{(T+10)^2}{22.3(T_0+10)^2 + (T+10)^2},$$

$$m_{0.96} = \rho_C \left(0.96 \frac{m_0}{\rho_C}\right)^{1/m(T)},$$

$$m_{1.04} = m_{L0} = \rho_L (1 - V_{S0}) + m_D,$$

$$\frac{dm(T)}{dT} = -\frac{2(T+10)\left(22.3(T_0+10)^2 + (T+10)^2\right) - 2(T+10)^3}{\left(22.3(T_0+10)^2 + (T+10)^2\right)^2},$$

$$\frac{dm_{0.96}}{dT} = -m_{0.96} \frac{ln\left(0.96 \frac{m_0}{\rho_{cem}}\right) \frac{dm(T)}{dT}}{(m(T))^2},$$

$$\frac{dm_{1.04}}{dT} = \frac{dm_{L0}}{dT} = (1 - V_{S0}) \frac{d\rho_L}{dT} + \frac{dm_D}{dT},$$

$$X = \left(\frac{P_V}{P_S} - 0.96\right) \frac{\frac{dm_{1.04}}{dT} - \frac{dm_{0.96}}{dT}}{0.08}, \text{ and}$$

T = temperature (°C).

Permeability Model

The permeability of concrete varies with temperature and pore pressure. However, even to date, thin variation is not well understood. Thus, in the spalling sub-model, the variation of permeability as a function of pore pressure and temperature is assumed to follow the relationship developed by Gawin et al. (1999) based on the experimental results conducted by Schneider and Herbst (1989). Accordingly, the intrinsic permeability of concrete at any temperature is given as:

$$k = k_0 10^{C_T(T-T_0)}\left(\frac{P_V}{P_0}\right)^{0.368} \quad [4.50]$$

where k_T = intrinsic permeability of concrete at temperature T (°C), k_0 = initial intrinsic permeability of concrete at room temperature, P_0 = 101,325 Pa, P_V = pore pressure (Pa), T_0 = initial temperature (°C), and C_T = factor to account for the increase in concrete permeability at elevated temperatures.

Mechanical and thermo-chemical damage increases the permeability of concrete which leads to the development of lower pore pressure and in turn less spalling. Thus, the effect of mechanical and thermo-chemical damage on permeability of concrete is conservatively ignored.

Gawin et al. (1999) suggested a value of 0.005 $°C^{-1}$ for C_T. However, this value of C_T seems to overestimate the increase in permeability of concrete at elevated temperatures (especially for concrete with high initial permeability) when compared with test results reported by Kanema et al. (2007) as can be seen from Figure 4.5. The higher the permeability at elevated temperatures, the lower the (developed) vapor pressure and this will reduce the fire induced spalling in concrete. A review of the literature indicates that there is lack of test data on the variation of permeability as a function of temperature. Thus, the factor C_T in Eq. [4.50] is conservatively assumed to be 0.0025 $°C^{-1}$, which is lower than all values obtained from test results.

However, for RC beams, the concrete room temperature permeability (k_0) may vary within the cross-section due to cracking patterns resulting from variation in bending

moment and also due to curing conditions. The variation in the permeability of concrete can be assumed to change with the depth of the beam as given by the following equation:

$$k_0 = k_{top}\left\{\begin{array}{ll} 10^{\alpha y_{top}/H} & y \le x \\ \underbrace{\left(10^{\alpha y_{top}/H}\right)}_{I}\underbrace{\left(10^{\beta\left(\frac{y_{top}-x}{H-x}\right)}\right)}_{II} & y > x \end{array}\right\} \qquad [4.51]$$

Here k_0 = initial permeability of concrete, k_{top} = initial permeability in the top surface of the concrete section, H = total depth of concrete section, y_{top} = distance from the top most fibers of the concrete section, and x = depth of neutral axis under service loads, α and β = calibration constants to be determined from experiments.

The first and second terms in Eq. [4.51] (terms I and II) account for the variation of permeability due to curing conditions and cracking in the concrete section, respectively. Equation [4.51] is developed based on the effect of cracking and damage on the permeability of concrete which can be generally given by (Gawin et al. 2005, Gawin et al. 1999):

$$k_{damaged} = k_{undamaged} \times 10^{\beta D} \qquad [4.52]$$

where $k_{damaged}$ and $k_{undamaged}$ = permeability of damaged and undamaged concrete, respectively, B = calibration parameter, and D = extent of damage.

Figure 4.6 shows the spatial variation of permeability for an RC beam with a cross-section 300 mm × 500 mm. The permeability at the top of the beam (k_{top}) and the depth of the neutral axis were assumed to be 10^{-19} m^2, and 100 mm, respectively. In the tension

zone of the beam the cracks in concrete become wider leading to higher values of the permeability as seen in Figure 4.6.

Dehydration

Two types of water, namely, evaporable and nonevaporable water, are present in cement paste. Evaporable water is lost when cement paste is oven-dried at 110°C, while nonevaporable water is lost when oven-dried cement paste is heated to a temperature of about 800°C in a process called dehydration. Dehydration of cement paste is a complex phenomenon that depends on many factors including temperature and chemical composition of the cement paste itself. Even to date, this phenomenon is not completely understood. The amount of nonevaporable water, which is chemically bound with cement, increases with the degree of hydration of the concrete mix. Thus, for spalling predictions, it will be conservative to assume that the concrete is fully hydrated. In the spalling model, dehydration of cement paste is considered based on the simplified approach suggested by Bazant and Kaplan (1996). In this approach (where concrete is assumed to be fully hydrated at room temperature) the mass of dehydrated water, m_D, is given as:

$$m_D = \begin{Bmatrix} 0 & T \le 100°C \\ 0.04\rho_C \dfrac{T-100}{100} & 100°C < T \le 700°C \\ 0.24\rho_C & T > 700°C \end{Bmatrix} \qquad [4.53]$$

Tensile Strength of Concrete

The tensile strength of concrete, at elevated temperatures, is assumed to vary as per Eurocode 2 (2004) but with some modifications to avoid the convergence conditions when the tensile strength becomes zero at relatively low temperatures (600 °C). In such

conditions, the model might predict spalling to occur at very low values of the pore pressure, which is unrealistic as observed in fire tests. Thus, the variation of tensile strength of concrete with temperature is assumed to follow the expression:

$$f_{tT} = \begin{cases} f_t & T \le 100°C \\ f_t \dfrac{600 - T}{500} & 100°C < T \le 550°C \\ f_t \dfrac{1200 - T}{6500} & 550°C < T \le 1200°C \\ 0 & T > 1200°C \end{cases} \qquad [4.54]$$

where f_{tT} = tensile strength of concrete at temperature T (°C) and f_t = tensile strength of concrete at room temperature.

It should be noted that the modifications to the Eurocode equation for the temperature dependent tensile strength is to avoid numerical instability, which has a very small effect on the accuracy of the spalling predictions. This is because, according to Eq. [4.54], more than 90% of the room temperature tensile strength will be lost for concrete heated to above 600°C.

4.3.6 Limitations

The spalling sub-model presented here is capable of predicting early and intermediate stages of spalling. "Late" stage spalling, which occurs just prior to failure, is not considered in the analysis since it primarily results from significant loss of strength and stiffness. However, such type of spalling, due to the fact that it occurs just prior to failure, does not significantly influence the overall fire resistance of RC beams.

4.4 Strength Analysis

4.4.1 General Analysis Procedure

The third step in the numerical model is the strength analysis at the mid-section of each segment. The cross-sectional temperature distribution generated from hydro-thermal analysis is used as input to the strength analysis. For the strength analysis, the following assumptions are made:

- Plane sections before bending remain plane after bending.
- There is no bond-slip between steel reinforcement and concrete.
- Concrete of strength higher than 70 MPa is considered to be HSC.

Additionally, for fire induced axial force calculations, the following assumptions are made:

- The fire induced axial force is constant along the span of the beam, at a given time step.
- The curvature and displacements from the preceding time step can be used to compute the fire induced axial restraint force.

At each time step, the strength analysis is performed in three sub-steps, namely, estimating the axial force in each segment of the restrained beam, generating the M-κ relationship for each segment, and carrying out a nonlinear stiffness analysis to trace the response of the beam under fire conditions. The axial force, due to fire induced restraint, is computed based on the curvature distribution along the span of the beam. This axial force is assumed to be zero at the first time step (room temperature). For the subsequent time steps, the curvature distribution from the preceding time step is utilized to compute

the axial force. The use of the curvatures from the preceding time step does not have a significant influence on the restraint force provided the time increments are small.

The M-κ relationships, at various time steps, are generated using the calculated axial restraint force and the constitutive relationships for concrete and reinforcement. The interaction between axial force and bending moment capacity (and stiffness of the beam) is automatically accounted for in the generated M-κ relationships. In the nonlinear stiffness analysis, the deflection of the beam at each time step can be calculated through a stiffness approach which utilizes generated M-κ relationships to compute the stiffness for each beam segment.

Various strain components including mechanical strain, thermal strain, and creep strain for both concrete and reinforcing steel, and transient strain for concrete are accounted for in the model. The creep and transient strains, which are often not accounted for in fire resistance calculations, might play a role on the fire response of RC beams, particularly deflections. Spalling of concrete is incorporated into fire resistance calculations through the pore pressure predictions as discussed above.

The strength calculations are carried out using the same rectangular network described above and shown in Figure 4.3(b). The temperatures, deformations and stresses in each element are represented by those at the center of the element. The temperature at the center of the concrete element is obtained by averaging the temperatures of the nodes of that element in the network. The same procedure is used for steel reinforcement, with the values of stress, strain components, and temperature of each bar represented by those at the center of the bar. The temperature at the center of a steel bar is approximated by the temperature at the location of the center of the bar cross-section (in the concrete).

The total strain in a concrete element, at any fire exposure time, is taken as the sum of the thermal expansion, the mechanical strain, the creep strain, and the transient strain:

$$\varepsilon_t = \varepsilon_{th} + \varepsilon_{me} + \varepsilon_{cr} + \varepsilon_{tr} \qquad [4.55]$$

where ε_t = total strain, ε_{th} = thermal strain, ε_{me} = mechanical strain, ε_{cr} = creep strain, and ε_{tr} = transient strain.

Thermal strain is directly dependent on the temperature in the element and can be obtained by knowing the temperature and thermal expansion of the concrete. Creep strain is assumed to be a function of time, temperature, and stress level, and is computed based on Harmathy's (1993) approach using the following expression:

$$\varepsilon_{cr} = \beta_1 \frac{\sigma}{f_{c,T}} \sqrt{t}\, e^{d(T-293)} \qquad [4.56]$$

where $\beta_1 = 6.28\times10^{-6}$ $s^{-0.5}$, $d = 2.658\times10^{-3}$ K^{-1}, T = concrete temperature (°K) at time t (s), $f_{c,T}$ = concrete strength at temperature T, and σ = stress in the concrete at the current temperature.

The transient strain, which is specific for concrete under fire conditions, is computed based on the relationship proposed by Anderberg and Thelandersson (1976). The transient strain is related to thermal strain as follows:

$$\Delta\varepsilon_{tr} = k_2 \frac{\sigma}{f_{c,20}} \Delta\varepsilon_{th} \qquad [4.57]$$

where k_2 = a constant ranging between 1.8 and 2.35 (a value of 2 will be used in the analysis), $\Delta\varepsilon_{th}$ = change in thermal strain, $\Delta\varepsilon_{tr}$ = change in transient strain, and $f_{c,20}$ = concrete strength at room temperature.

For steel reinforcement, the total strain, at any fire exposure time, is calculated as the sum of three components, as given by the following equation:

$$\varepsilon_{ts} = \varepsilon_{ths} + \varepsilon_{mes} + \varepsilon_{crs} \qquad [4.58]$$

where ε_{ts}, ε_{ths}, ε_{mes} and ε_{crs} are total strain, thermal strain, mechanical strain, and creep strain in the steel reinforcement, respectively.

Similar to concrete, thermal strain in steel can be directly calculated from the knowledge of rebar temperature and the thermal expansion coefficient of the reinforcing steel. Creep strain is computed based on Dorn's theory and the model proposed by Harmathy (1967) with some modifications made to account for different values of yield strength of steel. According to Harmathy's model, creep strain in steel is given by the following expression:

$$\varepsilon_{crs} = \left(3Z\varepsilon_{t0}^{2}\right)^{1/3}\theta^{1/3} + Z\theta \qquad [4.59]$$

where

$$Z = \begin{Bmatrix} 6.755\times10^{19}\left(\dfrac{\sigma}{f_y}\right)^{4.7} & \dfrac{\sigma}{f_y} \le \dfrac{5}{12} \\ 1.23\times10^{16}\left(e^{10.8\left(\sigma/f_y\right)}\right) & \dfrac{\sigma}{f_y} > \dfrac{5}{12} \end{Bmatrix},$$

$$\theta = \int e^{-\Delta H/RT}\,dt,$$

$$\frac{\Delta H}{R} = 38900°\text{K},$$

t = time (hours),

$$\varepsilon_{t0} = 0.016\left(\frac{\sigma}{f_y}\right)^{1.75},$$

σ = stress in steel, and

f_y = yield strength of steel.

Figure 4.7 shows the distributions of total strain, stress, and internal forces for the beam cross-section at any fire exposure time. The total strain in any element (concrete or rebar) can be related to the curvature of the beam by the following expression:

$$\varepsilon_t = \varepsilon_0 + \kappa y \qquad [4.60]$$

where ε_0 = total strain at the geometrical centroid of the beam cross-section, κ = curvature, and y = the distance from the geometrical centroid of the beam cross-section. In the model, Eq. [4.55] to Eq. [4.60] can be used to carry out strain computation of a segment at any given fire exposure time. At any time step, and for an assumed value of ε_0 and κ, the total strain in each element (concrete or rebar) can be determined using Eq. [4.60]. Then the thermal, transient (for concrete only), and creep strains in the concrete and rebars are evaluated using the known temperatures and the corresponding equations derived above. Using the knowledge of total, thermal, transient, and creep strains, the mechanical strain in the concrete or steel element can be evaluated by rearranging Eqs. [4.55] and [4.58]:

$$\varepsilon_{me} = \varepsilon_t - \varepsilon_{th} - \varepsilon_{cr} - \varepsilon_{tr} \qquad \text{for concrete} \qquad [4.61]$$

$$\varepsilon_{mes} = \varepsilon_{ts} - \varepsilon_{ths} - \varepsilon_{crs} \qquad \text{for steel} \qquad [4.62]$$

Then for the estimated mechanical strain, the stress in the element can be established using the stress-strain relationships for steel and concrete.

4.4.2 Calculation of Fire Induced Axial Force

RC beams can develop restraint forces under fire exposure (which can be as high as 30% of the room temperature axial force capacity of the beam). The degree of restraint is dependent on the support conditions and will determine the behavior and fire resistance of an RC beam. Generally, the axial restraint force in an RC beam is expected to be below the neutral axis of the section as a result of higher temperature in the bottom most fibers as shown in Figure 4.8. The calculation of fire induced axial force (P) in a beam segment is analogous to the analysis of prestressed concrete beams, and is the summation of the compressive and the tensile forces. Thus, the axial force can be written as:

$$P = T_t + C_t = \int \sigma \, dA \qquad [4.63]$$

where T_t = resultant tensile force in concrete and reinforcement, C_t = resultant compressive force in concrete and reinforcement, and σ = stress in the infinitesimal area dA within the cross-section of each segment.

The integration of Eq. [4.63] is difficult to compute. Therefore, for an idealized cross-section where the cross-sectional area is divided into a number of elements, Eq. [4.63] can be approximated by:

$$P = T + C = \sum \sigma_m A_m \qquad [4.64]$$

where σ_m = stress at the center of each element and A_m = area of each element

However, the stress distribution in the cross-sectional area of the segment can be computed for a given central total strain (ε_0) and the curvature (κ) using Eqs. [4.55] to [4.62] and the constitutive relationship of the constituent materials. Thus, the axial force

can be related to central total strain (ε_0) and the curvature (κ) through the functional relationship:

$$P = \phi(\varepsilon_0, \kappa) \qquad [4.65]$$

Equation [4.65] shows that the axial force in a beam segment can be calculated if κ and ε_0 are known for that segment.

For beam segment *i*, the axial force can be written as:

$$P_i = \phi(\varepsilon_{0i}, \kappa_i) \qquad [4.66]$$

where P_i, ε_{0i} and κ_i = the axial force, central total strain, and curvature in segment *i*.

As stated in the assumptions above, the axial restraint forces for all segments are equal. Hence, the axial force in segment *i* (P_i) equals a constant value (P).

Based on the assumptions above, the curvature in segment *i*, for the n^{th} time step (κ_i^n), is equal to the curvature in the same segment computed in the $(n\text{-}1)^{th}$ time step (κ_i^{n-1}). Thus, for an assumed value of P, the central total strain in each segment is computed by solving Eq. [4.66], which can be written as:

$$P = \phi(\varepsilon_{0i}, \kappa_i^n) \approx \phi(\varepsilon_{0i}, \kappa_i^{n-1}) \qquad [4.67]$$

The total central strain in each segment is used to check the compatibility conditions. The value of the axial force, P, is modified until the compatibility and equilibrium conditions are satisfied. Figure 4.9 shows an RC beam exposed to fire and its deformed shape at current and preceding time steps of fire exposure. The columns restraining the beam are modeled as a spring of stiffness (k_r). The compatibility conditions along the span of the beam require that the following equation is to be satisfied:

$$\sum l_i - L - \Delta = 0 \qquad [4.68]$$

where l_i = projected length of deformed segment i, L = beam length, and Δ = total expansion in the beam length.

Figure 4.9 (b) shows that the projected length of a beam segment is given by the following formula:

$$l_i = \sqrt{(s_i)^2 - \left(w_{i2}^n - w_{i1}^n\right)^2} \approx \sqrt{(s_i)^2 - \left(w_{i2}^{n-1} - w_{i1}^{n-1}\right)^2} \qquad [4.69]$$

where s_i = length of deformed segment i, w_{i1}^{n-1} and w_{i2}^{n-1} = deflections at the beginning and the end of the beam segment which were computed in the $(n\text{-}1)^{\text{th}}$ time step, and w_{i1}^n and w_{i2}^n = deflections at the beginning and the end of the beam segment in the n^{th} time step.

Also, the length of the deformed segment i (s_i) can be computed from the definition of strain as:

$$s_i = (1 + \varepsilon_{0i}) L_i \qquad [4.70]$$

where L_i = length of segment i in the undeformed beam.

Combining Eq. [4.68], Eq. [4.69] and Eq. [4.70], the compatibility conditions require that:

$$\sum \sqrt{(1 + \varepsilon_{0i})^2 L_i^2 - \left(w_{i2}^0 - w_{i1}^0\right)^2} - L - \Delta = 0 \qquad [4.71]$$

Further, the equilibrium of node B in Figure 4.9 requires that:

$$P = k_r \Delta \qquad [4.72]$$

Thus, for an assumed value of axial force (P), an iterative procedure is used to solve Eq. [4.69] in order to compute the axial strain in each segment. Then, Eq. [4.71] is checked to ensure the compatibility requirements with Δ being calculated using Eq. [4.72]. The value of P is modified until Eq. [4.71] is satisfied within a pre-determined tolerance. The error involved in the estimation of Eq. [4.69] and Eq. [4.67] becomes smaller if shorter time steps are used.

4.4.3 Generation of *M*-κ Relationships

The M-κ generation, at elevated temperatures, is carried out using the same rectangular network described above and shown in Figure 4.3. Once the axial restraint force in the beam is computed, the M-κ relationships are generated through an approach analogous to the method used for the analysis of prestressed concrete beams. In this approach, M-κ relationships are established by iterating the central total strain (ε_0) and the curvature (κ).

At the beginning of the analysis, values for curvature and central total strain (in concrete) are assumed. Then, the total strain in each of the rebars and concrete elements is computed from the assumed strain and curvature. The stresses in the rebars and the concrete elements are determined using the constitutive laws of the materials. The temperature of a rebar is assumed to be equal to the temperature at the location of the center of the rebar. Once the stresses are known, the forces are computed in the concrete and the rebars. The curvature is then iterated until equilibrium of forces is satisfied (internal force equal to the fire induced axial restraint force). Once the equilibrium is satisfied, the moment and the corresponding curvature are calculated. Thus, the values of moment and curvature are stored to represent a point on the M-κ curve.

The value of the central total strain is incremented to generate subsequent points on the moment curvature curve. This procedure is repeated for each time step of fire exposure. The generated M-κ curves are used for tracing the behavior of the beam through nonlinear structural analysis. The generation of M-κ relationships is an important part of the numerical model since these relationships form the basis for the fire resistance analysis of the beam.

4.4.4 Beam Analysis

The M-κ relationships and the axial restrained force generated for various segments are used to trace the response of the whole beam exposed to fire. At each time step the deflection of the beam is evaluated through a stiffness approach. The secant stiffness for each segment is determined from the M-κ relationships, based on the moment level reached in that particular segment.

Each node in the idealized beam is assumed to have two degrees of freedom, namely, rotation and vertical displacement. Axial deformations are accounted for in the calculation of the axial restraint force. The deflection of the beam is computed using an iterative procedure described by Campbell and Kodur (1990). Accordingly, the first step in the analysis is to conduct a linear analysis using the initial rigidity of the beam (EI_0) to determine the moment distribution along the span of the beam. The segment having the maximum bending moment is selected to be the critical segment.

The second step is to increment the curvature in the critical segment and the curvature and moment distributions along the span of the beam (in each segment) are computed for each increment of the curvature. An iterative procedure is employed to obtain the solution

at each increment of curvature such that equilibrium, compatibility, and convergence conditions are satisfied.

The iterative procedure used for the beam analysis is illustrated in Figure 4.10. For each increment, a target curvature is selected for the critical segment. The analysis is carried out using secant stiffness of the beam computed from the generated moment curvature relationships. The beam is analyzed under a unit load and the bending moment and the curvature in each segment are computed. The curvature in each segment is multiplied by a scaling factor that is computed through dividing the target curvature in the critical element by the computed curvature in the same element. The new secant rigidity for the next iteration can be computed from the generated M-κ relationship. The iterative procedure continues until convergence is achieved where the rigidity in each segment is approximately maintained within a certain tolerance.

In the iterative procedure described above, the stiffness matrix and the loading vector are computed for each longitudinal segment. Then these matrices are assembled in the form of a nonlinear global stiffness equation, which can be written as:

$$[K_g][\delta] = [P_f] + [P_s] \qquad [4.73]$$

where $[K_g]$ = global stiffness matrix, $[\delta]$ = nodal displacements, $[P_f]$ = equivalent nodal load vector due to applied loading, and $[P_s]$ = equivalent nodal load vector due to P-δ effect.

The effect of the second order moments, developed due to the axial restraint force, is calculated using the following equation:

$$[P_s] = -[K_{geo}][\delta] \qquad [4.74]$$

where $[K_{geo}]$ = geometric stiffness matrix, $[\delta]$ = nodal displacements, and $[P_s]$ = equivalent nodal load vector due to P-δ effect.

The second order moments are then added to the external loads in the stiffness analysis as given by equation [4.73]

Thus, for any given time step, the temperatures (in concrete and steel), moment capacity and curvatures, as well as deflection and rate of deflection of the beam are known for a given fire exposure. These output parameters are used to evaluate the failure of the beam at local (in each segment) and global (whole beam) levels using four sets of failure criteria which include strength, thermal, and deflection limit states. The analysis is continued until strength failure of the beam is reached. The four sets of failure criteria used to define failure of an RC beam are (Kodur and Dwaikat 2008a):

1) When the temperature in steel rebars (tension reinforcement) exceeds the critical temperature which is 593°C for reinforcing steel.
2) When the beam is unable to resist the specified applied service load.
3) When the maximum deflection of the beam exceeds $L/20$ at any fire exposure time, where L is span length.
4) When the rate of deflection exceeds the limit given by the following expression:

$$\frac{L^2}{9000d}\ (\text{mm/min}) \qquad [4.75]$$

where L = span length of the beam (mm), and d = effective depth of the beam (mm).

4.5 Computer Implementation

4.5.1 Computer Program

The numerical procedures described in Section 4.1 through 4.4 require a large amount of computations since an iterative approach must be used. Therefore, to facilitate the above set of calculations, the numerical procedure was incorporated into a computer program, written in FORTRAN. Figure 4.2(a,b) shows a flowchart of the numerical procedure associated with the computer program.

4.5.2 Beam Idealization

The given RC beam is idealized to be a set of longitudinal beam segments. For hydro-thermal and mechanical analysis of RC beams, the cross-section of the beam is idealized as a mesh of elements as shown in Figure 4.3(b). The number of longitudinal segments and the number of elements and the grid size in each direction must be specified in the input file. The program allows for non-uniform grid size in the cross-sectional mesh. The program determines the element size based on the specified number of elements. The program also allows for any rebar configuration. However, the section must be symmetrical around the vertical centroidal axis, since the model cannot account for the development of torsional forces due to non-symmetrical geometry.

4.5.2 Material Properties

Concrete

Three sets of concrete properties suggested by Eurocode 2 (2004), the ASCE Manual (Lie 1992), and Kodur et al. (2004) are incorporated into the program. In addition, the

program allows for general material properties read from other input files where the material properties should be presented in a tabular format as a function of temperature. The user can specify any of the material models in the input file. The user also has the option of selecting either siliceous aggregate concrete or carbonate aggregate concrete. Relevant formulae for both mechanical and thermal properties of concrete as a function of temperature are built into the program. In the input file the user has to specify the 28-day compressive strength of concrete, initial moisture content, initial concrete permeability, tensile strength of concrete, concrete model (Eurocode, ASCE, or Kodur), and the type of aggregate in the concrete.

Steel Reinforcement

The mechanical properties of reinforcing steel (stress-strain-temperature relationships) that are given in the ASCE Manual (Lie 1992) and in Eurocode 2 (2004) are incorporated into the program. In addition, the program allows for general stress strain relationships as a function of temperature, which should be tabulated in another input file. When the ASCE or Eurocode model is selected, the user must specify the yield strength of steel in the input file and the program automatically uses the built-in stress-strain relationships.

4.5.3 Input Data

The basic input for the program consists of cross-sectional properties, material properties, and general data such as the number of time increments. The sequential order of the input data must be followed. Consistent units must be used throughout.

4.5.4 Output Results

The output from the program includes the results from the hydro-thermal and structural analyses. At each incremental time step, the temperature and pore pressure at each node (see Figure 4.3 (b) is computed. The output results also include the M-κ curves. In addition, the deflection of the beam and the rate of deflection are also recorded for each time step.

4.6 Summary

This chapter presents a numerical model that was incorporated into a computer program, for tracing the response of RC beams exposed to fire. The three stages associated with the fire resistance analysis, namely, fire growth, thermal, and structural analysis, are explained. Equations governing the hydro-thermal and mechanical analyses are derived. The proposed model accounts for high temperature material properties, various fire scenarios, fire induced axial restraint effects, geometrical nonlinearity, and various strain components. In the nonlinear beam analysis, the model uses a curvature controlled iterative procedure in which the softening of the beam is accounted for. Also, a sub-model, which involves pore pressure calculations, is incorporated into the numerical model to account for fire induced spalling. The validity of the computer model will be established in the following chapter.

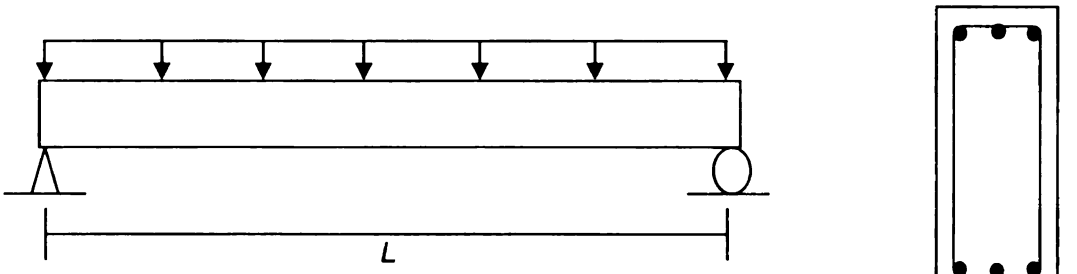

(a) Simply Supported Beam

(b) Cross-section

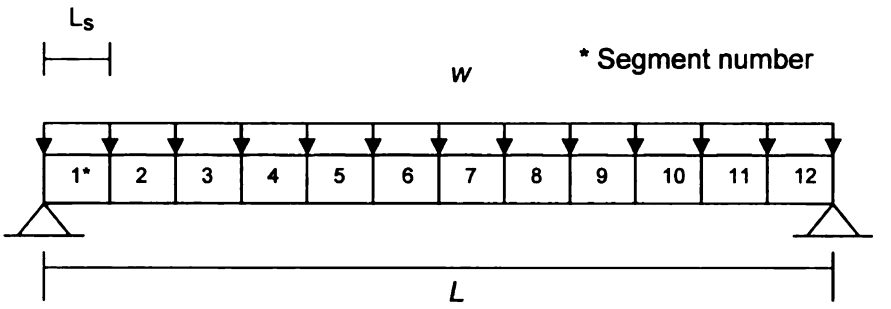

(c) Idealization

Figure 4.1 - Layout of a Typical RC Beam and its Idealization for Analysis

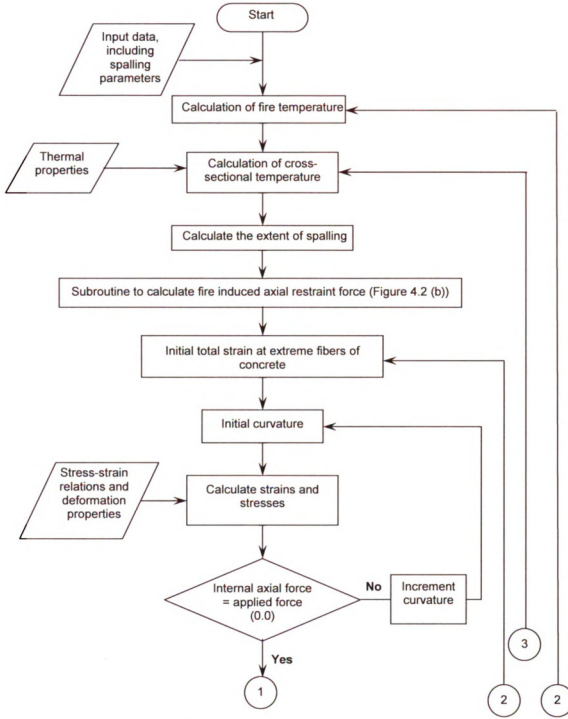

Figure 4.2(a) - Flowchart Showing the Steps Associated with the Analysis of an RC Beam Exposed to Fire

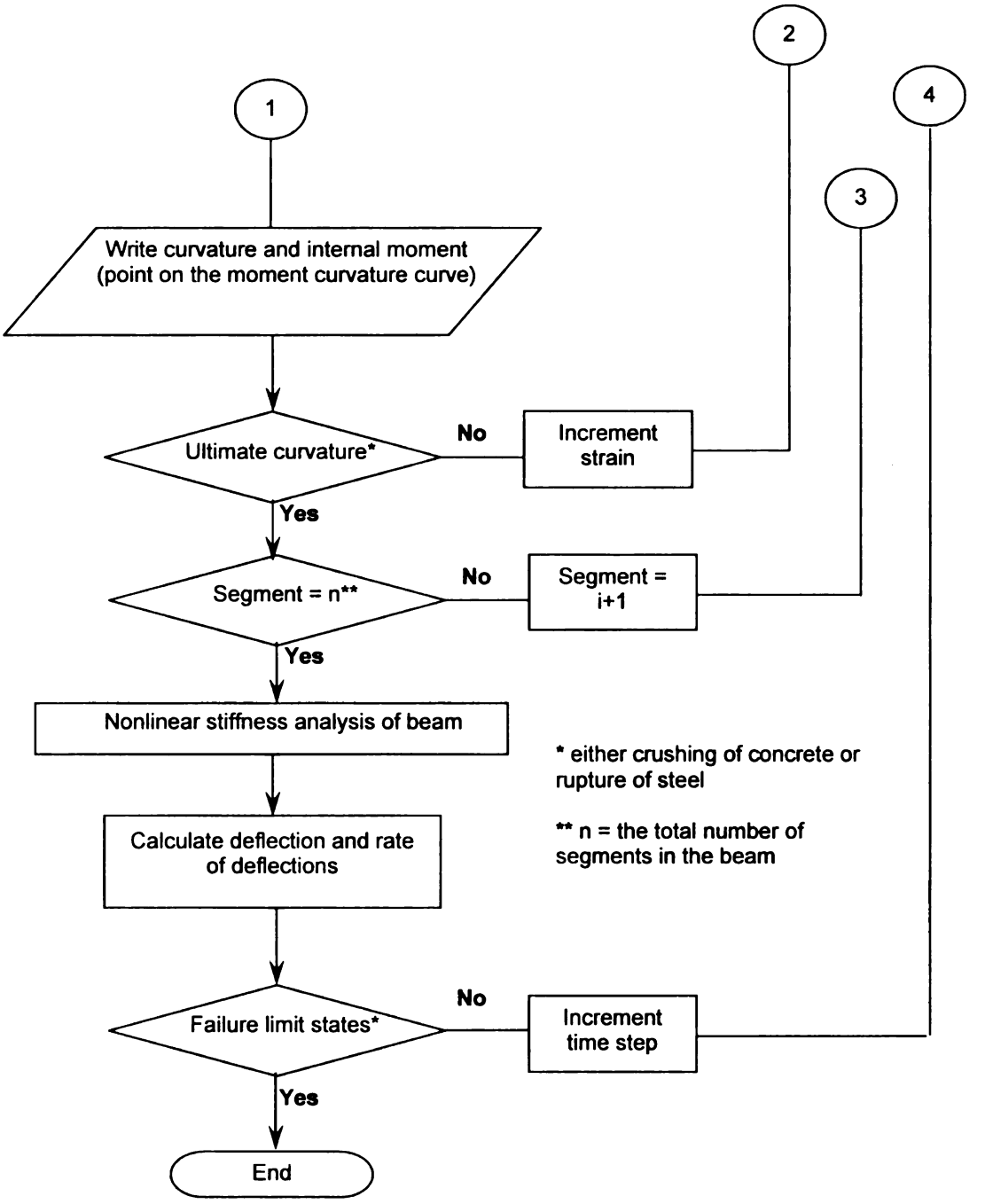

Figure 4.2(a) (Continued) - Flowchart Showing the Steps Associated with the Analysis of an RC Beam Exposed to Fire

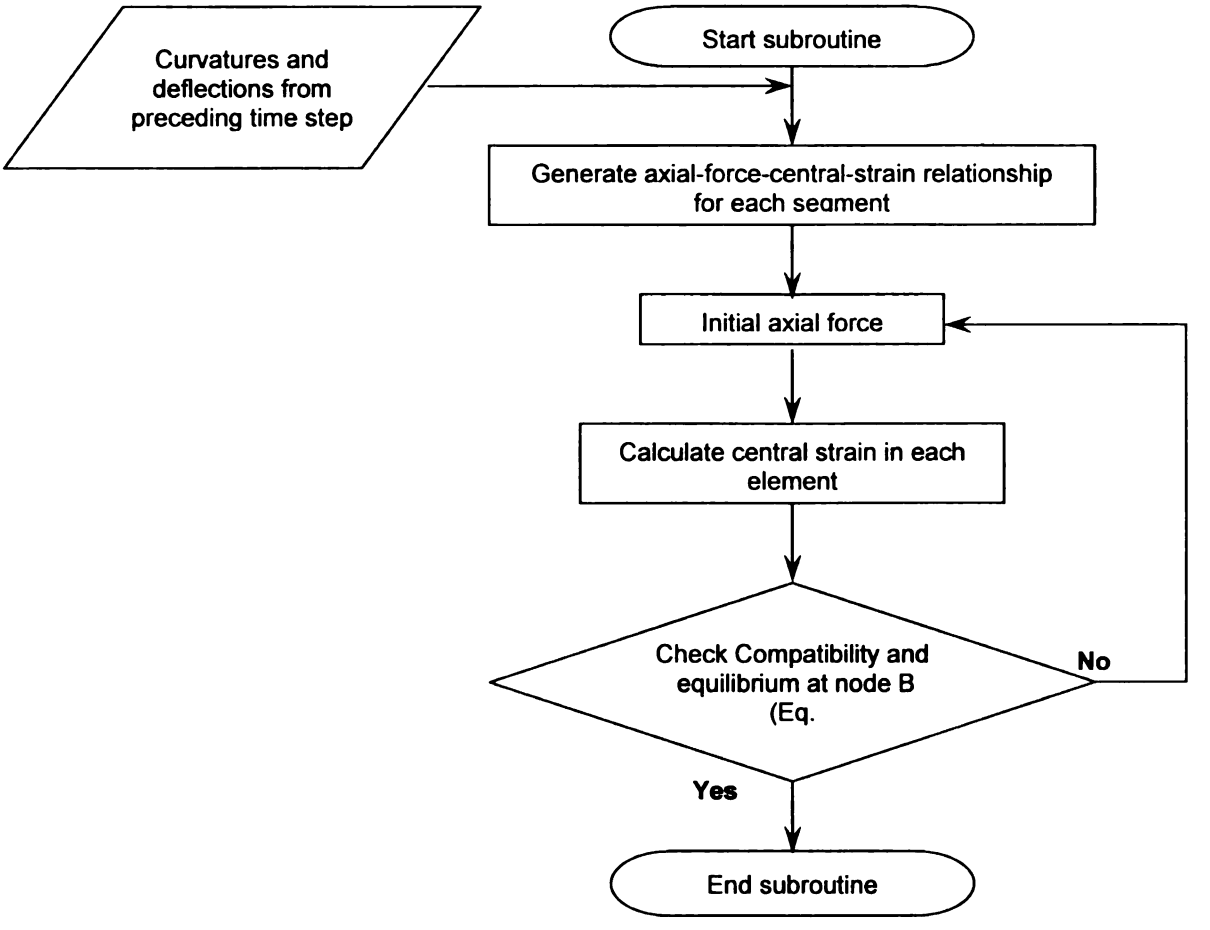

Figure 4.2(b) - Flowchart Showing the Steps Associated with the Axial Restraint Force Calculations

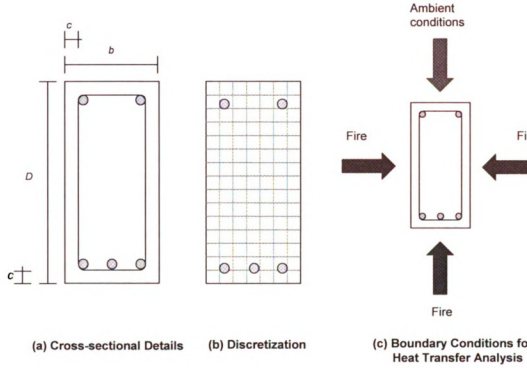

Figure 4.3 - Cross-section of an RC Beam and its Discretization for Analysis

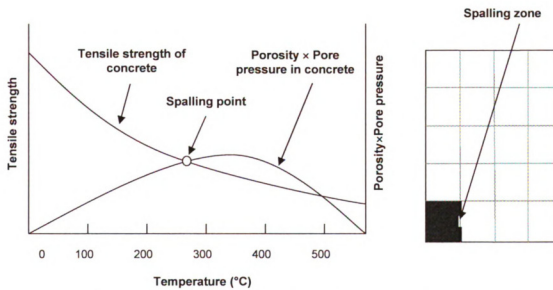

Figure 4.4 - Illustration of Spalling Prediction in a Concrete Segment

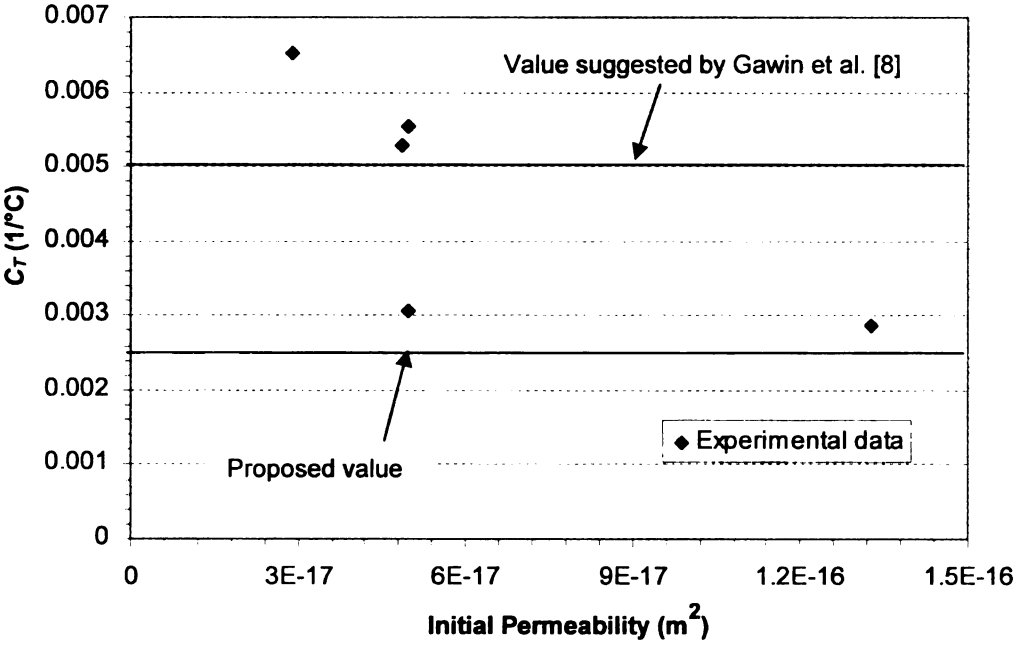

Figure 4.5 – Measured and Suggested Values of Permeability Factor, C_T

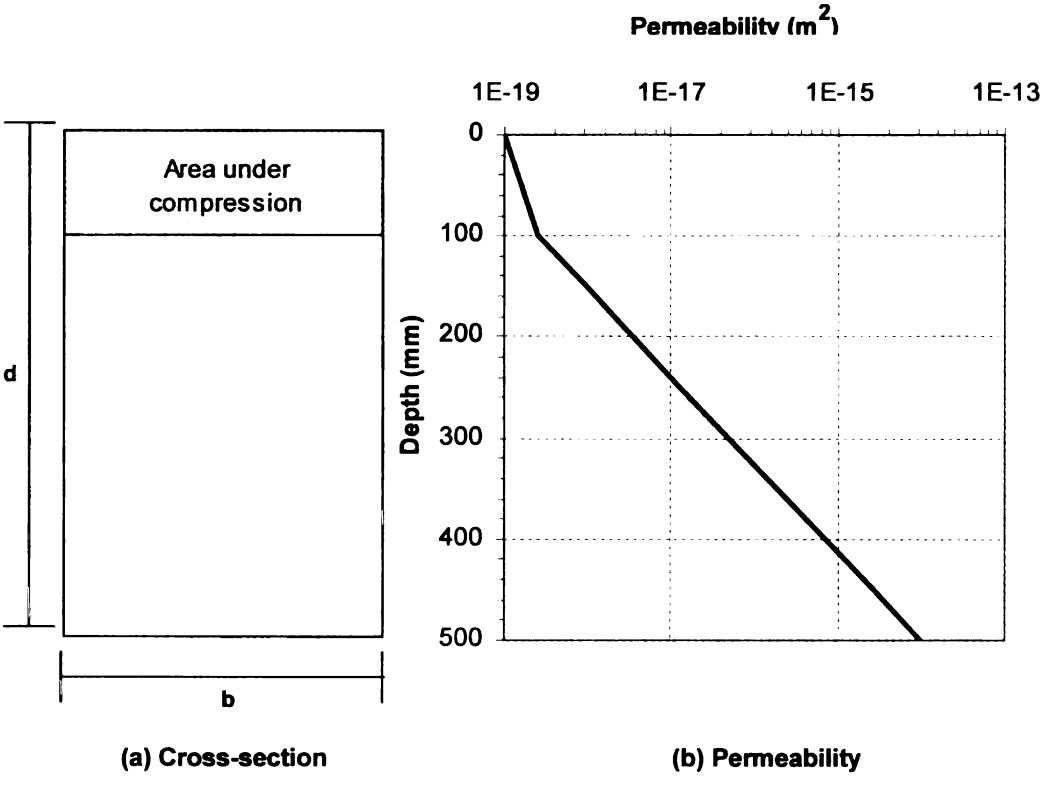

Figure 4.6 – Variation of Concrete Permeabiliy across the Depth of a Typical RC Beam

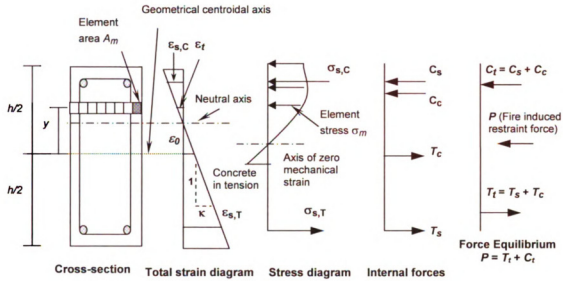

Figure 4.7 - Variation of Strain, Stress and Internal Forces in a Typical Beam Cross-section Exposed to Fire

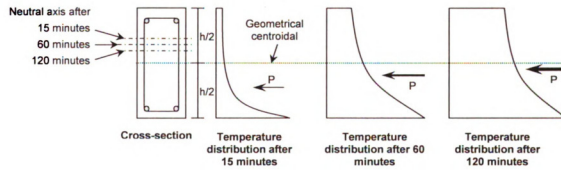

Figure 4.8- Schematic Diagram Showing the Thermal Gradients and the Position of Axial Force (Resulting from Restraining Thermal Expansion) as a Function of Fire Exposure Time

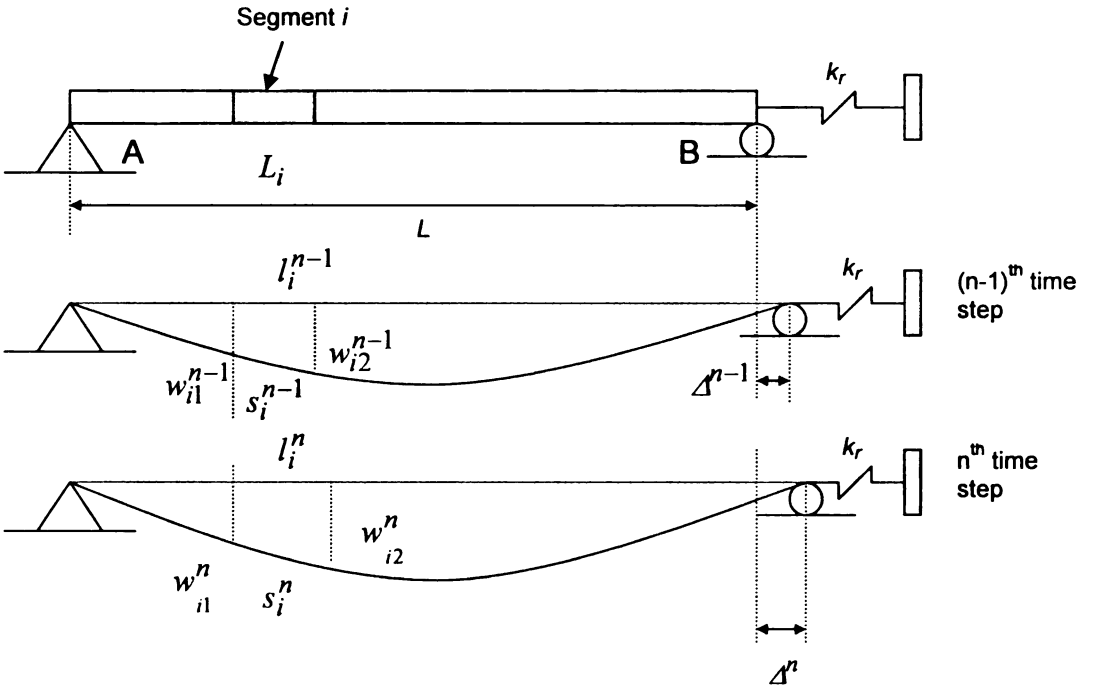

(a) Deflected shape at the (n-1)th and nth time step

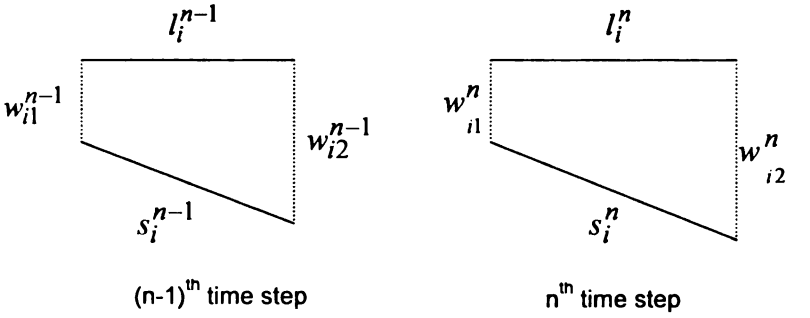

(b) Typical Beam Segment

Figure 4.9 - Illustration of Axial Restraint Force Calculations

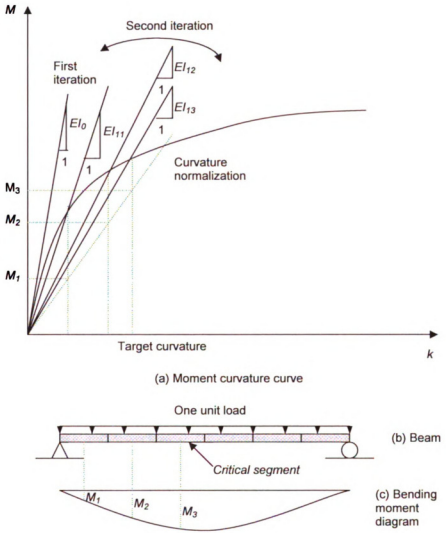

Figure 4.10 - Illustration of Curvature Controlled Iterative Procedure used for Beam Analysis

FLEXURAL RESPONSE OF REINFORCED CONCRETE BEAMS EXPOSED TO FIRE

VOLUME II

By

Monther B.M. Dwaikat

A DISSERTATION

Submitted to
Michigan State University
in partial fulfillment of the requirements
for the degree of

DOCTOR OF PHILOSOPHY

Civil Engineering

2009

Chapter 5

5. Model Validation

5.1 General

In this chapter, the validity of the computer model, presented in Chapter 4, is established by comparing predictions from the model with data from fire tests on RC beams and slabs. The predicted fire response of structural members depends on numerous factors including fire exposure, high temperature material properties, structural parameters (boundary conditions and geometry), and the discretization (idealization of member and time steps) used in the analysis. Many of these parameters vary within their domain and thus the values selected can influence the fire response of RC beams. As an example, the thermal conductivity of a given concrete type can vary by ±20% depending on the measurement techniques, heating rate, sample conditioning, etc. It is not possible to obtain exact high temperature properties of each of the constitutive materials due to the

complexity and effort involved in the process. Therefore, the validation was carried out for upper and lower bound values of material properties. Other important factors that influence the results are the discretization used along the span of the beam and the geometry of the cross-section, and also the time increments (time steps used for the analysis). Thus, this chapter starts with a sensitivity study to identify the upper bound and the lower bound values of material properties and to determine the optimum discretization parameters, including size of cross-sectional mesh, number of segments along the span of the beam, and time increment, to be used in the analysis.

Within the overall fire resistance model, a spalling sub-model is derived based on a number of assumptions and relationships developed from previous studies. Therefore, the validation is carried out in two steps: the spalling sub-model, and the overall numerical model. The spalling sub-model is verified against temperature, pore pressure, and spalling measurements from fire tests reported in the literature, and also from fire tests presented in Chapter 3. The full numerical model is validated against data from fire tests conducted on RC beams and reported in the literature, as well as from the fire tests summarized in Chapter 3. Due to the large variations in the reported high temperature material properties, the test data is compared with two sets of model predictions. The first set of model predictions is computed using the best case scenario of material properties, while the second set is computed using the worst case scenario. This is because it was not possible to measure the exact material properties of the tested beams due to the large amount of resources and effort required for such measurements.

5.2 Sensitivity Analysis

5.2.1 Effect of Material and Meshing Parameters

A sensitivity analysis was conducted to evaluate the influence of various material properties and discretization parameters on the fire response of RC beams. Two RC beams were analyzed, the first beam was simply supported and the second was axially restrained as show in Figure 5.1. The axial restraint stiffness (k) for the axially restrained beam was assumed to be 50 kN/mm. The value of k was selected in such a way that it represented typical boundary conditions commonly encountered in practice.

The beams analyzed were of rectangular cross-section (300 mm × 500 mm) and had a span length of 6 m as shown in Figure 5.1. The beams were made of concrete with a compressive strength of 30 MPa and reinforced with 3 ϕ20 mm steel rebars (both tension and compression) having a yield strength of 400 MPa. The room temperature capacity of the analyzed beams was calculated based on ACI 318 (2008) provisions. The applied loading on the beam shown in Figure 5.1, was calculated for a dead load (DL) to live load (LL) ratio of 2, based on ASCE 07 (2005) provisions (1.2 DL + 1.6 LL for room temperature calculation, and 1.2 DL + 0.5 LL under fire conditions). For load calculations, the ultimate load at room temperature was equated to the room temperature capacity of each beam. The time increment for the hydrothermal analysis was selected to be 10% of that used in the strength analysis. This is because of the high nonlinearity of the constitutive models used for hydrothermal analysis (such as heat capacity and isotherms), which required a smaller time increment to provide a sufficient level of accuracy.

The sensitivity study involved evaluating the effect of six material parameters on the fire response of the analyzed beams. The parameters were: thermal conductivity, heat capacity, thermal strain, creep and transient strain, compressive strength of concrete, and tensile strength of steel. The literature review, presented in Chapter 2, indicated that there is a wide variation in the properties of concrete at high temperatures. Thus, two values for each of the above parameters were used in the analysis (upper bound and lower bound values). The upper bound and lower bound values were selected to be 20% higher and lower than the reference value for the studied parameter, respectively, as given in Table 5.1. It should be noted that the main purpose of this analysis was to study the effect of variation in the material properties and the discretization parameters on the fire resistance of RC beams. Thus, a variation of 20% above and below the reference values was sufficient to determine the sensitivity of fire resistance to each of the studied material parameters.

The sensitivity study also involved evaluating the effect of discretization parameters on the fire response of RC beams. The discretization parameters included mesh size within the beam cross-section, number of segments along the span of the beam, and time increments up to failure. Results for the sensitivity analysis are presented in Figures 5.2-5.10.

Figure 5.2 shows the effect of thermal conductivity variation on the fire response of an RC beam. It can be seen that increased thermal conductivity increased the deflection and thus reduced the fire resistance of the beam. This trend is noted for both simply supported and axially restrained beams. This can be attributed to the fact that a higher thermal conductivity facilitates faster heat transmission to the concrete and the steel

reinforcement leading to early failure of the beam. Thus, for the worst case scenario, the analysis should be carried out using upper bound values of thermal conductivity of concrete reported in the literature, while the lower bound values of thermal conductivity should be used in the analysis for the best case scenario.

A contrary trend can be seen in Figure 5.3 for the effect of heat capacity of concrete. The figure shows that increased heat capacity reduces the deflection and increases the fire resistance for the two analyzed beams. This is due to the fact that a higher heat capacity delays the temperature rise in concrete and rebars, which in turn improves the fire performance of the beam. Thus, for the worst case scenario, the lower bound values of heat capacity of concrete should be used, while the upper bound values of heat capacity should be used in the analysis for the best case scenario.

The effect of variation in thermal strain on the fire response of RC beams is shown in Figure 5.4. It can be seen that the thermal strain has minor influence on the fire behavior of simply supported RC beams. However, this effect is pronounced for axially restrained beams with the upper limit values of thermal strain producing conservative fire resistance. This can be attributed to the fact that, for axially restrained beams, higher values of thermal strain increases the stresses (due to restrained thermal dilation) causing early failure in the beam. Therefore, the upper and lower bound of the thermal strain should be used in the analysis of the worst and best case scenarios, respectively.

Creep and transient strains appear to have a small influence on the overall fire response of an RC beam as shown in Figure 5.5. However, the major influence of creep and transient strain components can be noted for the axially restrained beam. Figure 5.5 shows that the higher the creep and transient strains, the lower the fire resistance of the

beam. This can be attributed to the fact that increased creep and transient strains increase the deflection of the beam leading to early failure, and thus lower fire resistance. This indicates that the upper limit for these strain components should be considered in the analysis for the worst case scenario. However, for the best case scenario analysis, the lower limit of creep and transient strain should be used.

Similar to creep and transient strain, the variation in concrete strength (at high temperatures) has a minor effect on the fire response of RC beams as shown in Figure 5.6. However, as expected, increased concrete strength (at high temperature) leads to higher fire resistance of RC beams. Higher concrete strength contributes to a larger moment capacity and thus enhances the fire resistance of the beam. Hence, the lower and upper bound range of the concrete strength has to be used in the analysis of the worst and best case scenarios, respectively.

Figure 5.7 shows that steel strength influences the fire behavior of RC beams. It can be seen that the higher the steel strength the higher the fire resistance of the beam. This is mainly because increasing the strength of steel reinforcement significantly increases the moment capacity, leading to lower deflection and higher fire resistance of the beam. Thus, for the worst case scenario, the analysis should be carried out using the lower bound steel strength, while the upper bound steel strength should be used in the analysis for the best case scenario.

Due to the very limited information on spalling related properties such as permeability and isotherms, it is not possible to establish an upper and lower limit for these properties, and thus these properties were not included in the sensitivity study. However, the

reported values for these properties were used in the model validation and subsequent analysis.

The effect of structural discretization on the fire response of RC beams is illustrated in Figure 5.8. It is well known that increasing the number of segments (finer discretization) in the beam improves the accuracy of the predicted response. The analysis was carried out using three different idealizations with 10, 20, and 40 longitudinal segments. It can be seen from the Figure 5.8 that increasing the number of longitudinal segments from 10 to 40 does not greatly improve the accuracy of the predicted deflection-time curve. Thus, a sufficient level of accuracy can be obtained by using 40 segments in the analysis.

Figure 5.9 shows the effect of cross-sectional mesh size on the fire response of RC beams. Three cross-sectional discretization patterns, namely, 9 × 15 elements, 15 × 25 elements, and 30 × 50 elements were used in the analysis. It is well known that refining the mesh size generally increases the accuracy of the predicted fire response (Cook et al. 2003). However, it can be seen from Figure 5.9 that varying the mesh size does not significantly influence accuracy of the fire response of the analyzed beam. This result points out that dividing the beam cross-section into 15 × 25 elements will provide sufficient accuracy in the analysis.

The effect of the time increment on the fire response of RC beams is shown in Figure 5.10. The analysis was carried out using three values of time increments namely, 2.5 minutes, 5 minutes and 10 minutes. As discussed in Chapter 4, a smaller time increment improves the accuracy of the model predications. However, it can be seen from Figure 5.10 that the time increment has only a minor influence on the accuracy of the predicted

fire response of the analyzed beams. Therefore, a reasonable level of accuracy can be obtained when a 5 minute time increment is used in the strength analysis.

5.2.2 Proposed Material and Mesh Parameters

The literature review presented in Chapter 2 showed that high temperature properties of concrete and reinforcing, reported from different experimental studies, are highly scattered. The lower and upper bounds of thermal conductivity, heat capacity and thermal strain, interpreted from different experimental results, are shown in Figures 5.11-5.16 for carbonate and siliceous aggregate concrete, respectively. The lower and upper limits of compressive strength variation of NSC and HSC, together with measured test data, are shown in Figures 5.17 and 5.18, respectively. Figure 5.19 shows the upper and lower limits for the yield strength variation of reinforcing steel as a function of temperature (Harmathy 1993). The upper and lower limits for these properties are selected based on the range of test data reported in the literature. As discussed in Chapter 2, there is a large variation in compressive strength of NSC and HSC concrete and in yield strength of reinforcing steel at elevated temperatures. Such variations will have a significant influence on the computed fire resistance of RC beams.

It is not possible to obtain an upper bound for creep strain due to the lack of experimental data on creep strain for both concrete and reinforcing steel. However, lower and upper limits for transient strain of concrete can be obtained by using the minimum and maximum values of the constant k_2 in Eq. [4.51], which ranges between 1.8 and 2.35 (Anderberg and Thelandersson 1976). It should be noted that the combined effect of creep and transient strain on the fire response of RC beams is small as can be seen from

Figure 5.5. The upper and lower limits of the material properties are selected based on the scenario to be analyzed (best case scenario or worst case scenario).

For the sensitivity study, the beam cross-section was discretized using square elements with size in the range of 7 to 20 mm (15×25 to 32×50 elements within the cross section). Since spalling is a concern in HSC, smaller element sizes are used for HSC beams to improve the accuracy of spalling perditions. The span of the beam was discretized into 40 segments for rotationally unrestrained (simply supported and axially restrained) beams and 80 segments for rotationally restrained (and axially and rotationally restrained) beams. To improve the accuracy of the model predictions, shorter segments were used in critical zones where plastic hinges might be formed as shown in Figure 5.20. The discretization was carried out such that the length of the segments forms an arithmetic sequence (the difference between the lengths of two successive segments is constant). The ratio of the length of the longest segments (segments with smaller bending moment) to that of the shortest segments (segments in critical zone) was selected to be 4. The discretization pattern for the analyzed beams is illustrated in Figure 5.20. A summary of the material properties and meshing parameters used in the analysis for the worst and best case scenarios are given in Table 5.2.

5.3 Validation of Spalling Sub-model

The validity of the spalling sub-model is established by comparing temperature, pore pressure and spalling predictions with the measured values from fire tests. Data for this validation is taken from the tests reported in the literature and also the tests carried out as part of the current study (presented in Chapter 3). Full details on the validation of the spalling sub-model are presented in the following sections.

5.3.1 Temperature and Pore Pressure

Due to the lack of test data on fire induced spalling in RC beams, slab tests conducted by Kalifa et al. (2001) were selected for the validation of spalling sub-model. In these tests, Kalifa et al. exposed 120-mm thick RC slabs to elevated temperature through rapid heating from one side. A heating rate of 5°C/sec was used for the first two minutes and then the temperature was kept at 600°C. The cross-sectional temperatures were measured at four different locations within the slab thickness. The pore pressure was measured at three different depths, namely, 20 mm, 30 mm, and 40 mm, from the heated side. The analysis was carried out by using the upper and lower bound values of material properties as given in Table 5.2 and a 2-mm mesh size. Results from the numerical model are compared with test data in Figures 5.21-5.24.

The measured and predicted temperatures at four different depths in the concrete slab are compared in Figure 5.21. The predicted temperatures are computed for both the best and worst case material property scenarios. It can be seen that the measured temperatures are in close agreement with the predicted temperatures (computed based on best case scenario) for the four different locations throughout the temperature range. The minor discrepancies can be attributed to the differences in high temperature material properties such as thermal conductivity and specific heat, since these properties are dependent on the type of concrete mix. These variations are not accounted for in the high temperature constitutive models. Also, the variation in the convective heat transfer coefficient and emissivity might contribute to these discrepancies. It can also be seen from Figure 5.21 that the variation between the temperatures computed based on the worst case scenario and those computed based on the best case scenario becomes more pronounced at

increased depth of concrete from the exposed surface. This can be mainly attributed to the fact that the thermal properties of concrete have higher influence on the temperatures at larger depths of concrete as compared to those at smaller depths. At smaller depths of concrete, the temperatures are governed by the heat flux (convective and radiative) at the boundaries and the thermal properties of concrete. However, the temperatures at larger depths are governed predominantly by the thermal properties of the material. This explains the high sensitivity of the temperatures at larger depths to the variation in the thermal properties of concrete.

The pore pressure predictions were carried out for three values of initial permeability, namely, 20×10^{-18} m^2, 5×10^{-18} m^2, and 2×10^{-18} m^2, for the two cases (worst and best cases) as can be seen in Figures 5.22 to 5.24. The figures show that lower concrete permeability will increase the pore pressure at any fire exposure time. As an illustration, for the three depths where pore pressure was measured, a peak pore pressure of about 2 MPa is predicted for concrete permeability of 20×10^{-18} m^2. However, for a permeability of 2×10^{-18} m^2, a peak pore pressure of about 4 MPa is predicted. It can also be seen from Figures 5.22 to 5.24 that the results from the model in the best case scenario compare well with the experimental results for permeability of 2×10^{-18} m^2. This value of permeability is between the residual permeability reported by Kalifa et al. (2001) for the same concrete heated to 80 °C (4×10^{-18} m^2) and the minimum permeability of concrete at room temperature given by Baroghel-Bouny et al. (1999) (5×10^{-22} m^2). However, Figure 5.23 shows that the pore pressure predicted by the model is higher than the measured values for most of the fire exposure time. This can be attributed to the variation of the permeability of concrete with temperature and pore pressure. Yet, this relationship is not

fully understood (Witek et al. 2006, Dwaikat and Kodur 2008b). The model predicted higher pore pressure in the worst case scenario as compared to that in the best case scenario. This is on the expected lines and can be attributed to the higher temperatures resulting from the high thermal conductivity and low heat capacity in the worst case scenario. Overall, the spalling model seems to overestimate the pore pressure in concrete and this leads to conservative estimates for spalling predictions.

5.3.2 Extent of Spalling

The validity of the spalling sub-model is also established by comparing the quantity of spalled concrete with the measured spalling values in the fire tests conducted by Bilodeau et al. (2004). In their tests, six concrete blocks of 610×425×770 mm size were exposed to ASTM E1529 (1993) hydrocarbon fire for two hours in a furnace. Only one face of each tested block was exposed to fire, while all the other faces are covered with insulation. Of the six blocks, Block 5, which was made without polypropylene fibers, had the largest amount of spalling, and thus this block is used for the validation of the model. The measured and predicted reduction in the block thickness (loss of cross-section) as a function of fire exposure time is presented in Figure 5.25. It should be noted that the extent of spalling was only measured at the end of the fire test and not throughout the test and thus, one measured value of reduced block thickness is plotted as shown in Figure 5.25. Since the permeability in concrete was not reported by the authors, the analysis was carried out by assuming three values of permeability, namely, 20×10^{-18} m^2, 5×10^{-18} m^2, and 1×10^{-18} m^2. The comparisons in Figure 5.25 show that, when concrete permeability of 1×10^{-18} m^2 is used, a good prediction of concrete spalling is obtained in the best case scenario. The figure also shows that the permeability of concrete has a significant

influence on fire induced spalling, with no spalling predicted when concrete permeability is higher than 20×10^{-18} m^2. It can also be seen that the model predicted higher spalling in the worst case scenario as compared to that in the best case scenario. This can be attributed to high temperatures and developed pore pressure in the worst case scenario.

Since the focus of this research is on the response of RC beams under fire, predictions from the spalling sub-model are also compared with spalling measurements from fire tests (conducted as part of the current study) for two HSC beams, B5 and B6, which experienced significant spalling (see Chapter 3). In these two beams significant spalling occurred at early stages of fire exposure (referred to as "early spalling"). In both beams, the nature of spalling including the time at which spalling started and the approximate time at which spalling stopped were recorded during the fire tests. The extent of spalling at the end of the test was computed by measuring the volume of fire damaged beam. The extent of spalling is assumed to vary linearly between the time it started and the time it ended. These two beams experienced some "late spalling" just prior failure. However, most of the "late spalling" occurred close to the mid-span of the beam and is not accounted for in the volumetric measurements and in the analysis ("late spalling" has negligible effect on the overall behavior of the RC beam as discussed earlier in Chapter 2).

The water permeability was measured in both beams as per ASTM C1202 (1997) using "Chloride Penetration" test and was found to be about 10^{-21} m^2. Gas permeability is generally higher than water permeability and can be higher in magnitude up to the order of 10^2 (Neville 1996). Thus, for the analysis, the permeability of water vapor in the top side of the concrete beams (k_{top}), which is required for pore pressure calculations, is

assumed to be 10^{-19} m^2. The spatial variation of permeability in the beam cross-section is assumed as given in Chapter 4 (Eq. [4.51]). For the two beams, the depth of the neutral axis under service loads (x in Eq. [4.51]) was found to be 90 mm. Based on the average spalling thickness measured in the tests, it is assumed in the analysis that the spalling depth (the thickness of spalled concrete) does not exceed 20 mm and 25 mm for beams B5 and B6, respectively. For the analysis, the cross-section of the beam is discretized into 7 mm square elements. With these values as input parameters to the spalling sub-model, the extent of spalling is evaluated as a function of fire exposure time for both beams. The test data for beam B5 are used to calibrate the model and determine the values of α and β in Eq [4.51], and then the test data for beam B6 are used to validate the spalling sub-model.

The predicted quantities and times of spalling are compared with the measured values for beams B5 and B6 in Figures 5.26 and 5.27, respectively. In Figure 5.26, the model is calibrated such that the extent of spalling in the best case scenario matches with the measured spalling, and the values of α and β in Eq [4.51] were found to be 2 and 3, respectively. For this beam, the model predicts spalling to start at about 11 minutes and stop at about 50 minutes after fire exposure in the best case scenario. The visual observations in the test indicated that spalling started and stopped at about 10 and 35 minutes after fire exposure, respectively. The extent of spalling in beam B6 is computed using the calibrated values of α and β and then compared with the measured value as shown in Figure 5.27. It can be seen that there is good agreement between the predicted and measured values in the entire range of fire exposure. For this beam, the measured start and end times of spalling were 5 minutes and 30 minutes, and the predicted times (in

the best case scenario) were 6.5 minutes and 122 minutes. These results indicate that, in the best case scenario, the program predicts well the start time of spalling. In contrast, there is variation between the predicted and the measured end time of spalling. This variation might be acceptable since the model predictions indicate that a small amount of spalling occurs after 35 minutes and 30 minutes of fire exposure for beams B5 and B6, respectively. This can be attributed to the drying of concrete which reduces the developed pore pressure, and hence decreases the spalling at later stages of fire. The model predicts slightly higher extent of spalling in beam B6, which is a conservative estimate.

However, the model predicts higher extent of spalling in both beams in the worst case scenario. This can be attributed to higher temperatures and pore pressures developed in the RC beam in the worst case scenario. Overall, the spalling predictions in the best case scenario match reasonably well with the measured spalling in early and intermediate stages of fire exposure for RC beams. It should be noted that spalling is dependent on a number of variables and accurate test data on these variables is hard to measure or obtain. Nevertheless, reasonable spalling predictions were obtained and thus, for qualitative assessment, the proposed spalling sub-model is deemed to be sufficient.

5.4 Validation of Numerical Model

To establish the validity of the overall fire resistance model, presented in Chapter 4, fire response from the model is compared with measured parameters for nine RC beams. The first beam, designated B0, is analyzed to illustrate the usefulness of the program in tracing the fire response of a typical RC beam in the entire range of loading up to collapse under fire exposure. The second and third beams, designated BL1 and BL2 selected from literature, were analyzed to compare model predictions with fire test data.

The remaining six beams (B1 through B6) are the specimens tested as part of this study. Beam B0 represents typical RC beams used in buildings and is analyzed under ASTM E119 standard fire exposure from three sides. Since Beam B0 is analyzed to illustrate the usefulness of the model, the high temperature material property relations reported by Lie (1992) were used in the analysis. However, for the remaining eight beams, the analysis was carried out using both worst and best case scenario of high temperature material properties since it is not possible to measure actual high temperature material properties. Details of the geometric and material properties and load level for beams B0, BL1 and BL2 are given in Table 5.3.

5.4.1 RC Beam B0

Results from the analysis on beam B0 are utilized to illustrate the fire behavior of a typical RC beam. The temperature variation is plotted as a function of fire exposure time at various locations of the beam cross-section in Figure 5.28. The temperature at various depths of concrete, as well as in rebars, increases with fire exposure time. As expected, the predicted temperature decreases with increasing distance from the fire exposed side. It can be seen that the unexposed side of the beam remains unaffected for the first 60 minutes of the fire exposure. This is due to low thermal conductivity and high thermal capacity of concrete which slows down heat transmission to the inner layers of concrete. Also, it can be seen in the figure that the temperatures in the corner rebar is higher than that for central rebar throughout fire exposure time. This trend is on expected lines and can be attributed to the fact that corner rebars are exposed to fire from two sides, while the central rebar is exposed to fire from the bottom face only.

The moment-curvature curves of the mid-span of the beam, generated by the model, are shown in Figure 5.29 at various time steps. The figure shows that the sectional moment capacity of the beam decreases with time. This is due to deterioration in strength and stiffness properties of concrete and steel as a result of increased temperatures. The figure also shows that ultimate curvature (curvature at collapse) increases with time of fire exposure and is mainly due to softening effect resulting from degradation of the material strength and stiffness, as well as the creep strain which becomes significant prior to failure.

The variations of mid-span moment capacity and deflection in the beam are shown in Figure 5.30 as a function of fire exposure time. It can be noted that the predicted moment capacity of the mid-span at room temperature (179.8 kN.m) is slightly higher than the calculated moment capacity (156.6 kN.m) based on ACI 318 (2008). This is because the program accounts for strain hardening of steel reinforcement which is not accounted for in the ACI 318 (2008) strength equations. Figure 5.30 also shows significant reduction in moment capacity with time of fire exposure. However, the rate of reduction in moment capacity decreases with fire exposure time. This can be attributed to slower rise in rebar temperature towards the end of fire exposure time (due to lower rise in fire temperature after about 30 minutes (1000°C)) as shown in Figure 5.28.

It can be seen from Figure 5.30 that the mid-span deflection gradually increases with time at early stages of fire exposure. The initial deformation of the beam results mainly from thermal gradients developed within the beam cross-section and also due to applied loading. The figure also shows a large increase in deflection prior to failure. This trend is mainly due to yielding of steel and creep strains that become predominant prior to the

collapse of the beam. This is in agreement with reported test results from fire tests on RC members, which clearly show significant increase in deflection at later stages of fire exposure (Kodur and McGrath 2003).

The fire resistance for beam B0 was computed according to the four sets of failure criterion discussed in Chapter 4 and is tabulated in Table 1. The fire resistance values, predicted based on the rebar temperature and strength failure criteria, are approximately similar. However, changing the load ratio or the mechanical properties of the constituent materials can produce different fire resistance values for strength failure criteria. On the contrary, these changes do not affect the rebar temperature failure criterion since it is independent of these factors. Based on the deflection and rate of deflection failure criteria, the program predicts 150 and 159 minutes as fire resistance, which is lower than that predicted for temperature and strength failure criteria. Thus, deflection failure criterion governs the failure of beam B0 and results in fire resistance of 150 minutes for that beam. As explained in Chapter 2, ASTM E119a (2008) does not specify deflection failure criterion, which can be a governing factor in determining the fire resistance of RC beams.

The failure times obtained from the model are also compared with fire resistance values, calculated based on ACI 216.1 (2007) specifications, in Table 5.3. It can be seen that the fire resistance for beam B0, predicted by ACI 216.1 (2007), is higher than that predicted by the program. This is because the prescriptive approach in ACI relates the fire resistance of RC beams to the concrete cover thickness and the width of the beam only, and does not take into consideration factors such as load ratio and concrete strength.

5.4.2 Lin's Test Beams

The validity of the computer model is established by comparing predicted results from the model with the measured values from fire tests on two RC beams tested by Lin et al. (1981). One of the beams (BL1) was simply supported while the other beam (BL2) was tested under continuous support conditions. Both beams were not axially restrained and were tested under ASTM E119 standard fire exposure. The geometric and material properties of the tested beams used in the analysis are taken from the reported data in the tests and are given in Table 5.3. The mesh parameters used in the analysis of these beams are also given in Table 5.3. The fire resistance of the two beams (designated as beam BL1 and beam BL2, respectively) is calculated based on four sets of failure criterion discussed in Chapter 4 and is summarized in Table 5.3. Predicted results from the analysis (for both worst and best case scenarios of high temperature material properties) are compared to measured values from fire tests in Figures 5.31 to 5.34.

In Figures 5.31 and 5.32, the calculated average temperatures in the rebars are compared with the measured values for beams BL1 and BL2, respectively. It can be noted that there is good agreement between the predicted and measured values in the entire range of fire exposure for the best case scenario. The steep increase in rebar temperature in the early stages of fire exposure is due to the occurrence of a high thermal gradient at the beginning of fire exposure time as a result of faster increase in fire temperature. Results from the analysis indicate that predicted temperatures in concrete at various depths follow the expected trend with lower temperatures at larger depths from fire exposed surface. However, predicted concrete temperatures could not be compared with test data since the measured temperatures were not reported by Lin et al. (1981). Figures 5.33 and 5.34

show predicted and measured mid-span deflection as a function of fire exposure time for beams BL1 and BL2, respectively. It can be seen that model predictions for best case scenario are in close agreement with the measured deflections, throughout the fire exposure time. However, the figures show that the test data ends at earlier time as compared to the predicted values. This is mainly because the tests were terminated before the complete failure of the beams to limit any possible damage to the testing facility (Lin et al. 1981).

The fire resistance of the two beams was evaluated based on four failure criteria and its values are given in Table 5.3. The measured fire resistance, for both beams (BL1 and BL2), is lower than that predicted by the program in the best case scenario for all failure criteria. This is mainly because the fire tests were terminated after 80 and 210 minutes of fire exposure for beams BL1 and BL2, and before the beams attained complete failure probably due to severe conditions experienced towards the final stages in fire tests. The fire resistance predicted based on rebar temperature and the best case scenario for beam BL1 (105 minutes) is much lower than that for strength failure criterion (135 minutes). This is because the rebar temperature failure criteria is based on load level of 50% of the room temperature capacity of the beam, however, the load level on this beam is lower than 50% and this results in higher fire resistance based on strength failure criterion. However, for beam BL2, rebar temperature failure criterion is not considered in the analysis because this failure criterion is prescriptive and does not represent the actual failure of restrained beams. As discussed earlier for beam B0, the model predicted lower fire resistance based on deflection (or rate of deflection) failure criteria as compared to the value predicted based on strength failure criterion for both beams.

Although the worst case scenario (material relations) analysis predicts fire resistance values that are closer to the measured ones, there are significant discrepancies between the predicted temperatures and deflections and the measured ones as can be seen from Figures 5.31 to 5.34. Such discrepancies point out that the worst case scenario analysis does not reasonably predict the fire response of the two beams. This can be attributed to the variation of the material relations (used in the worst case scenario analysis) from the actual high temperature material properties of the tested beam. Overall, the minimum fire resistance predicted based on deflection and rate of deflection failure criteria for both beams (105 and 257 minutes) is a reasonable estimate to the measured value in the fire tests (when the test was terminated).

5.4.3 MSU Test Beams

5.4.3.1 Analysis Procedure

The six RC beams tested as part of this study (and reported in Chapter 3) are analyzed in order to further validate the numerical model. The beams include two NSC and four HSC beams that were tested under ASTM E119 standard fire and two design fire scenarios. More details on the characteristics of the beams and the fire scenarios used in the fire tests are given in Chapter 3. For the axially restrained beams (B2 and B6), loading frame and axial restraint stiffness are modeled as a nonlinear axial spring with stiffness of 13 kN/mm when the axial restraint force is below a threshold of 120 kN for beam B2 and 110 kN for beam B6 as measured in the fire tests. The spring stiffness is assumed to be zero when the axial force exceeds this threshold. Each beam is analyzed under corresponding fire scenarios as given in Table 3.1. The analysis was carried out for both

best and worst case scenarios of high temperature material properties in five minute time increments till failure occurred in the beam. Details on the discretization parameters used in the analysis are given in Table 5.4 and Figure 5.20. Failure time is recorded when the strength, deflection or rate of deflection limit states are exceeded. The fire resistance values, obtained from the analysis, are summarized in Table 5.4.

5.4.3.2 Material Properties

The material properties, used in the analysis, are selected as piecewise linear functions from Figures 5.11 to 5.19 for the best and worst case scenarios as discussed in Section 5.2 and given in Table 5.2. Different high temperature mechanical properties are used for HSC than those used for NSC as discussed in Chapter 2. The thermal properties are assumed to be same for both heating and cooling phase. For mechanical properties, linear interpolation between high temperature strength and residual strength is used to estimate the strength of both concrete and reinforcing steel in the cooling phase. The residual strengths for any concrete element or steel rebar are determined based on the maximum temperature attained in that element (or rebar). For concrete, the residual strength is determined for the best and worst case scenarios from the upper and lower limits given in Figure 2.16. However, the residual strength of reinforcing steel is assumed based on the residual strength tests conducted by Neves et al. (1996) on reinforcing steel as shown in Figure 5.35. Up to 500°C, residual strength of reinforcing steel is assumed to be similar to room temperature strength. However, the residual strength is assumed to decrease linearly with temperature till it reaches 0.7 of the room temperature strength at 800°C.

5.4.3.3 Results and Discussion

The validity of the model is established by comparing predictions from the model with measured temperatures, deflections, axial restraint force, and fire resistance in Figures 5.36 to 5.55 and Table 5.4. Figures 5.36 through 5.41 show the predicted and measured average rebar temperature as a function of fire exposure time for tested beams B1 through B6, respectively. It can be seen that there is good agreement between the measured and predicted average rebar temperatures throughout the fire exposure time for the six beams when the best case scenario of material properties is used. However, for HSC beam B6, the model predicts slightly higher temperatures than the measured ones in the cooling phase of fire exposure (after 180 minutes). This may be primarily attributed to the use of lower values of thermal conductivity of concrete in the cooling phase. As discussed above the high temperature thermal properties of concrete in the cooling phase are assumed to be the same as that in the heating phase due to the lack of data on the thermal properties in the cooling phase. In addition, due to severe spalling observed in beam B6, the thermocouple location might have displaced during fire tests and thus measured rebar temperatures may not be fully reliable after 180 minutes of fire exposure. Predicting slightly higher temperature generally leads to conservative fire resistance in an RC beam. The measured and predicted temperatures at two different locations (compression reinforcement and center of beam cross-section) in beams B1 through B6 are shown in Figures 5.42 and 5.47, respectively. It can be seen that the predicted temperatures (for best case scenario) match well with the measured temperatures for the three locations in all beams (both NSC and HSC) except beam B6. For beam B6 there is appreciable difference between the predicted and measured temperatures particularly for compression

reinforcement with the model predicting higher temperatures. This can be attributed to the fact that the model predicts higher extent of spalling (in the top part of the beam) at early stages of fire exposure as can be seen from Figure 5.27. Such high early spalling leads to higher temperature particularly in compression rebars which are close to the spalling zone of the beam cross-section. The large discrepancies in compression rebar temperature have small influence on the overall fire response of an RC beam since contribution of compression reinforcement to moment capacity of an RC beam is small (Nawy 2005). Figures 5.42 to 5.45 show that the thermal response of the HSC beams, B3 and B4, is similar to that in the NSC beam, B1 and B2, respectively. This is due to similar high temperature thermal properties for HSC and NSC and thus the concrete strength does not significantly influence the thermal response of RC beams.

Overall, the model predicts temperatures reasonably well in tension and compression reinforcement and center of the beam for the six tested beams when best case scenario of material properties is used. However, when the worst case scenario of material properties is used, the model predicts significantly higher temperatures than those measured in fire tests.

The predicted and measured deflections are compared in Figures 5.48 to 5.53 for beams B1 through B6. The figures show that there is good agreement between the measured and the predicted deflections for beams B1 to B5 when the best case scenario of material properties is used. However, for beam B6, the model predicted higher deflections than the measured ones after about 180 minutes of fire exposure. This can be mainly attributed to the discrepancy between predicted and measured rebar temperatures after 180 minutes as show in Figure 5.41.

The model predicts higher deflection for HSC beam B3 than that for NSC beam B1 throughout the range of standard fire exposure. The higher deflection in HSC beam resulted from the faster degradation of strength and stiffness of HSC at elevated temperatures. The good agreement between model predictions and test data can be attributed to the fact that the model accounts for high temperature material properties, various strain components, fire induced restraint effects and fire induced spalling.

When worst case scenario of material properties is assumed, the model predicts significantly higher deflections than those measured in the fire tests for the six RC beams. This can be attributed to the higher rebar and concrete temperatures resulting in this case, for the six beams, as can be seen from Figures 5.36 to 5.47. It can also be attributed to the faster degradation of strength and stiffness for concrete and reinforcing steel, which is assumed in the worst case scenario of material properties.

The predicted and measured axial restraint forces are compared in Figures 5.54 and 5.55 for axially restrained beams B2 and B6. The two figures show that there is good agreement between measured and predicted axial restraint forces for beam B2 when best case scenario of material properties is used. However, for beam B6, the model predicted higher axial restraint force for most of the fire exposure duration. This may be primarily attributed to the differences in the thermal strain of HSC from that used in the analysis. This result suggests that HSC might have slightly lower thermal strain (coefficient of thermal expansion) than that of NSC. However, when worst case scenario of material properties is used, the model generally predicts higher axial restraint force in beams due to higher concrete and rebar temperatures arising from these properties (worst case scenario).

The predicted fire resistance values are computed based on strength, deflection and rate of deflection limit states and is tabulated in Table 5.4. The fire resistance is computed using best case scenario and worst case scenario (values given in bracket in Table 5.4) of material properties.

The model predictions, based on the best case scenario of material properties, are in good agreement with measured fire resistance values for the six tested RC beams. Similar to the observations in the tests, no failure was predicted for beams B2, B4 and B6. For the remaining three beams (B1, B3 and B5), the predicted fire resistance values compared well with the measured ones and deflection criterion governed fire resistance. The good agreement between the predicted (deflection criteria) and measured fire resistance can be mainly attributed to fact that when the beam experienced large deflections, wide cracks developed in the beam causing the tension rebars to be directly exposed to fire. This suggests that deflection and rate of deflection limit states may be the governing failure criteria for RC beams. It should be noted that the current fire resistance provisions in ASTM E119 do not specify any deflection or rate of deflection limit states to define failure or RC beams exposed to fire. In agreement with fire test results, the predicted fire resistance for NSC beam B1 is higher than that for HSC beam B3. This can be attributed to the fast degradation in strength and stiffness for HSC as compared to NSC.

The model predicts significantly lower fire resistance than the measured values when worst case scenario of material properties is used. This can be attributed to the higher deflections predicted in this case as compared to measured ones in the fire tests.

5.5 Summary

The validity of the computer model developed as part of the current study is established by comparing perditions from the model with test data. In the validation, predicted spalling, temperatures, deflections, axial restraint force and fire resistance were compared with measured values in fire resistance tests. The analysis was carried out using best and worst case scenarios of high temperature properties of concrete and steel. Fine structural and cross-sectional discretizations and small time steps were used in the analysis to provide sufficient level of accuracy in the obtained results. Based on these comparative studies, it is concluded that the microscopic finite element model is capable of predicting the fire response of RC beams under realistic fire, loading and restraint scenarios. It is also concluded that, when the best case scenario of material properties is used, the model predictions match well with the measured test parameters. In the following chapter, the validated model will be applied to conduct parametric studies to investigate the influence of various parameters on the fire resistance of RC beams.

Table 5.1 – Reference, Upper and Lower Values for the Studied Parameters

Parameter	Reference value	Upper value	Lower value
Thermal conductivity	k_T (Lie 1992)	1.2 k_T	0.8 k_T
Heat capacity	ρC (Lie 1992)	1.2 ρC	0.8 ρC
Thermal strain	ε_{th} (Lie 1992)	1.2 ε_{th}	0.8 ε_{th}
Creep and transient Strain components	$\varepsilon_{cr} + \varepsilon_{tr}$ for concrete ε_{cr} for reinforcing steel (Harmathy 1993, 1967, Anderberg and Thelandersson 1976)	1.2 ($\varepsilon_{cr} + \varepsilon_{tr}$) for concrete 1.2 ε_{cr} for reinforcing steel	0.8 ($\varepsilon_{cr} + \varepsilon_{tr}$) for concrete 0.8 ε_{cr} for reinforcing steel
Deterioration in concrete strength	f_{cT} (Lie 1992)	1.2f_{cT}	0.8f_{cT}
Deterioration in steel strength	f_{yT} (Lie 1992)	1.2f_{yT}	0.8f_{yT}

Table 5.2 – Summary of the Material and Meshing Parameters used in the Analysis

Parameter	Worst case scenario	Best case scenario
Thermal conductivity (Figures 5.11 and 5.12)	Upper limit	Lower limit
Heat Capacity (Figures 5.13 and 5.14)	Lower limit	Upper limit
Thermal strain ((Figures 5.15 and 5.16)	Upper limit	Lower limit
Transient strain in concrete	$k_2 = 2.35$	$k_2 = 1.8$
Concrete strength (Figures 5.17 and 5.18)	Lower limit	Upper limit
Reinforcing steel strength (Figure 5.19)	Lower limit	Upper limit
Creep strain	Equation reported in literature (Harmathy 1967 and 1993) as given by Eqs. [4.56] and [4.59]	
Spalling related properties	Constitutive models reported in the literature as given in Section 4.3.5	
Number of segments along the span of the beam*	40 for rotationally unrestrained and 80 for rotationally restrained beams	
Cross-sectional mesh size*	between 7 and 20 mm depending on the cross-sectional dimension of the beam being analyzed	
Time increment for strength analysis*	5 minutes	

* Only applicable for the analysis used for the validation of the overall response of the beams

Table 5.3 – Properties and Results for RC Beams B0, BL1 and BL2

Property		Beam B0	Beam BL1	Beam BL2
Description		Typical RC beam	Tested by Lin et al. 1981	Tested by Lin et al. 1981
Cross-section		300 mm × 500 mm	305 mm × 355 mm	305 mm × 355 mm
Length (m)		6	6.1	6.1
Reinforcement		2 ϕ 14 mm top bars	2 ϕ 19 mm top bars	6 ϕ 19 mm top bars
		3 ϕ 20 mm bottom bars	4 ϕ 19 mm bottom bars	4 ϕ 19 mm bottom bars
f'_c **(MPa)**		30	30	30
f_y **(MPa)**		400	435.8	435.8
Applied total load (kN)		120	80	200
Concrete cover thickness (mm)		40	25 (bottom) 38 (side)	25 (bottom) 38 (side)
Support conditions		simply supported	simply supported	continuous
Aggregate type		carbonate	carbonate	carbonate
Cross-sectional discretization (elements)		15×25	20×25	20×25
Structural discretization (number of segments)		40	40	80
Fire resistance based on failure criterion:	Rebar temperature	180	105 (85)	NA*
	Strength	185	135 (80)	310 (255)
	Deflection	150	111 (75)	257 (225)
	Rate of deflection	159	105 (67)	305 (245)
Fire resistance based on ACI 216		210	180	180
Fire resistance-test		NA	80	210

* Not applicable

Table 5.4 – Results of MSU Fire Tests on Six RC Beams

Beam designation	Cross-sectional discretization (elements)	Structural discretization (number of segments)	Predicted Fire resistance (minutes) based on failure criterion**:			Fire resistance-test (minutes)
			Strength	Deflection	Rate of deflection	
B1	16×25	40	185 (95)	181 (92)	181 (77)	180
B2	16×25	40	NF* (105)	NF (92)	NF (77)	NF
B3	32×50	40	185 (105)	167 (101)	154 (87)	160
B4	32×50	40	NF (95)	NF (91)	NF (77)	NF
B5	32×50	40	180 (90)	160 (85)	147 (70)	146
B6	32×50	40	NF (115)	NF (106)	NF (102)	NF

* No failure

** Values in bracket are for worst case scenario and other values are for best case scenario

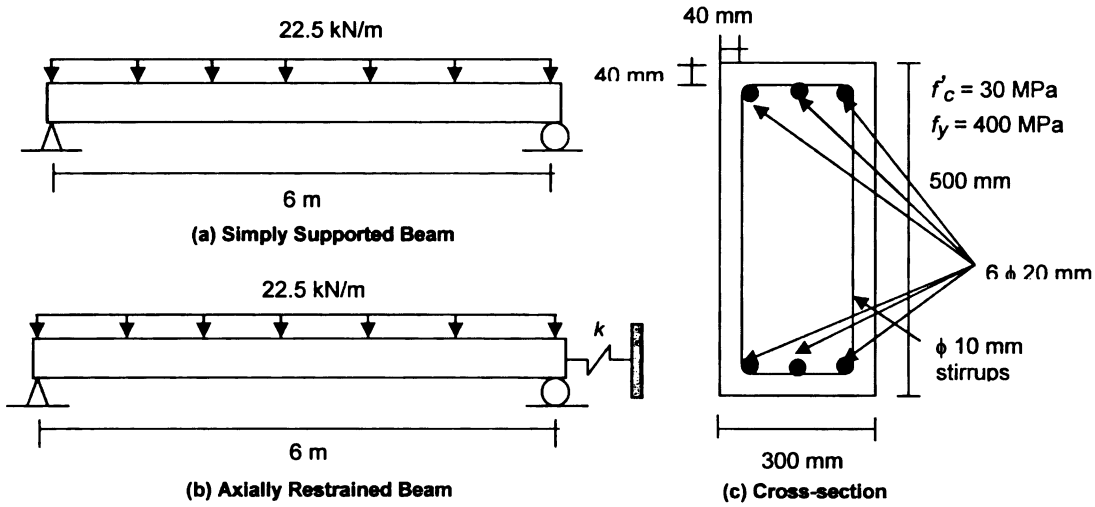

Figure 5.1 – Cross-section and Elevation of RC Beam used in Sensitivity Study

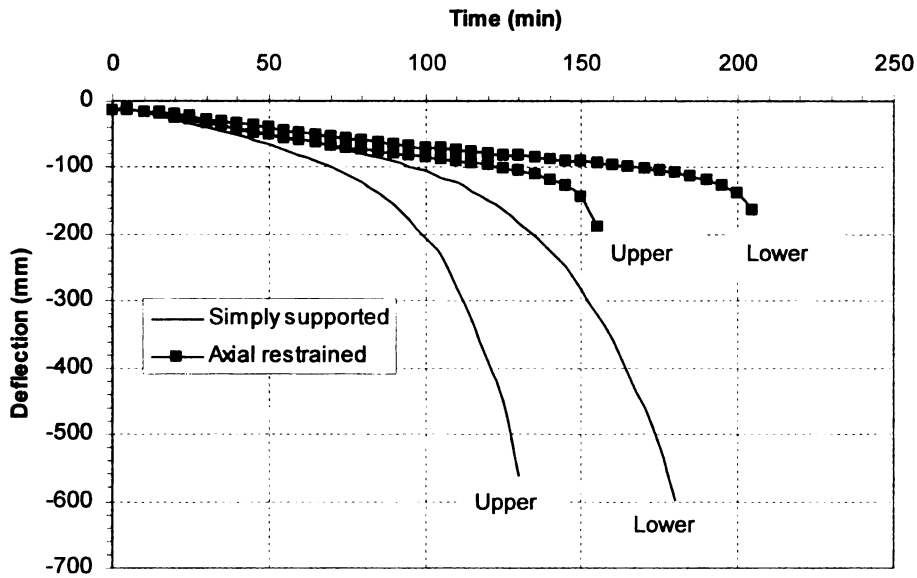

Figure 5.2 – Effect of Variation in Thermal Conductivity on Fire Response of RC Beams

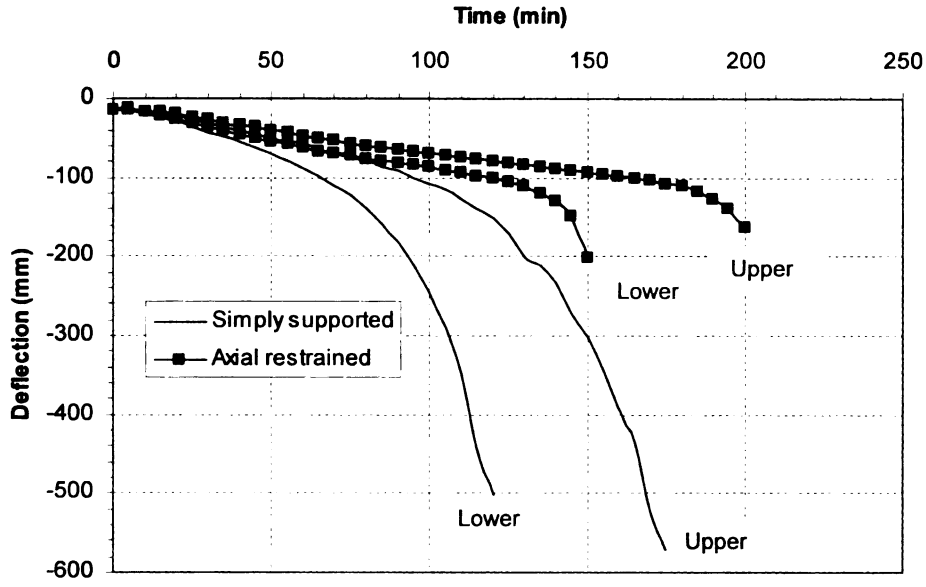

Figure 5.3 – Effect of Variation Heat Capacity on Fire Response of RC Beams

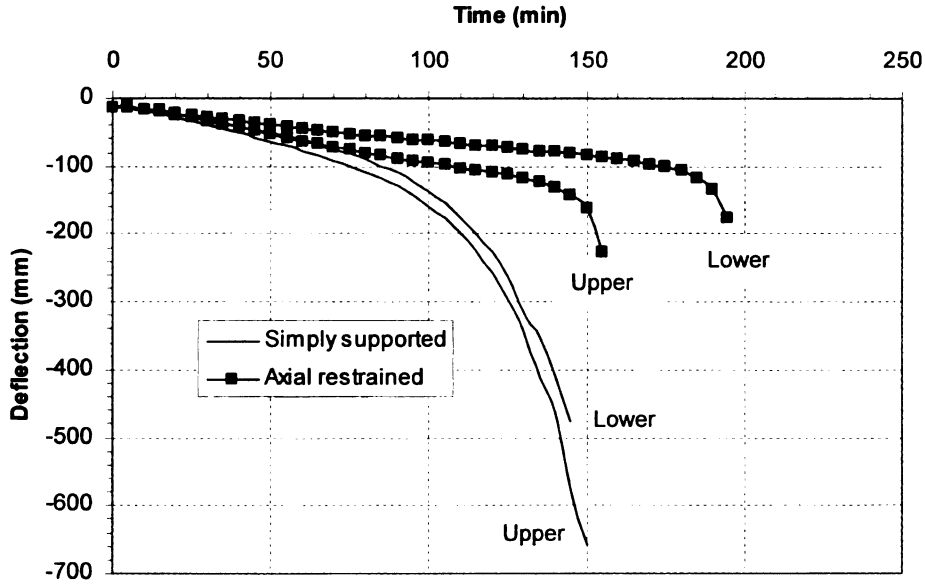

Figure 5.4 – Effect of Variation of Thermal Strain on Fire Response of RC Beams

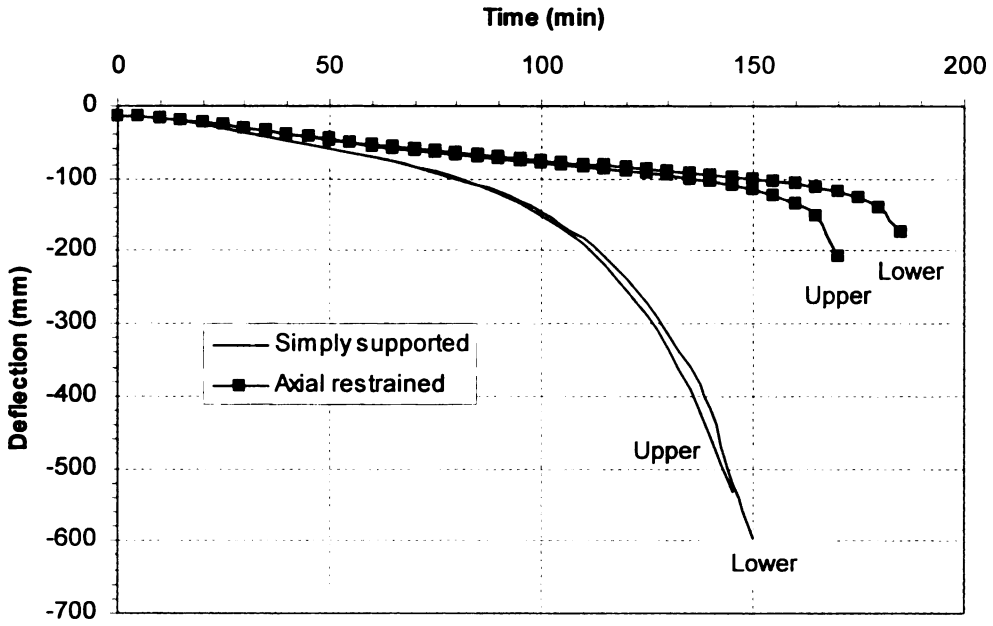

Figure 5.5 – Effect of Variation in Creep and Transient Strain Components on Fire Response of RC Beams

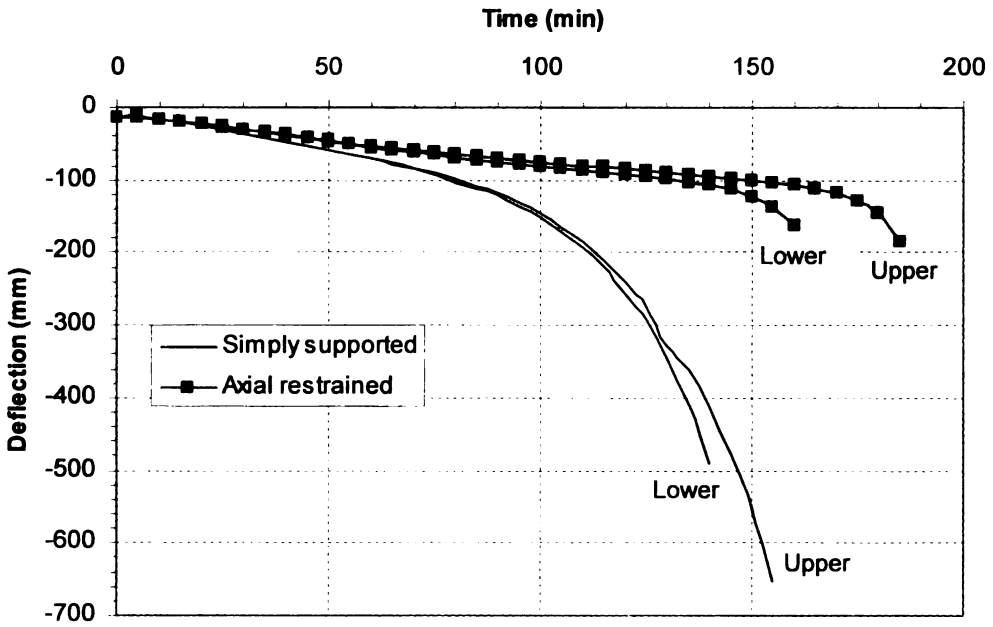

Figure 5.6 – Effect of Variation in Concrete Strength on Fire Response of RC Beams

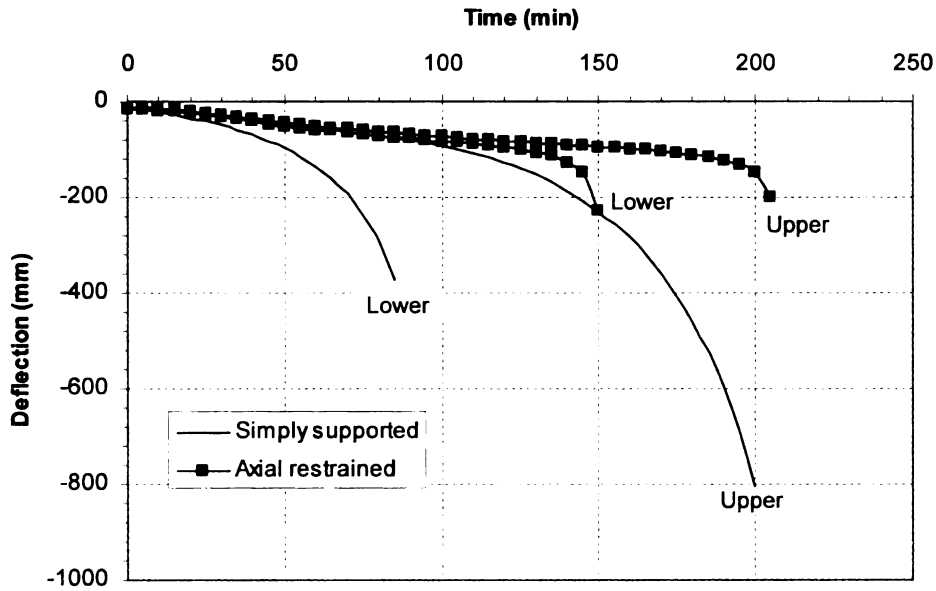

Figure 5.7 – Effect of Variation in Steel Strength on Fire Response of RC Beams

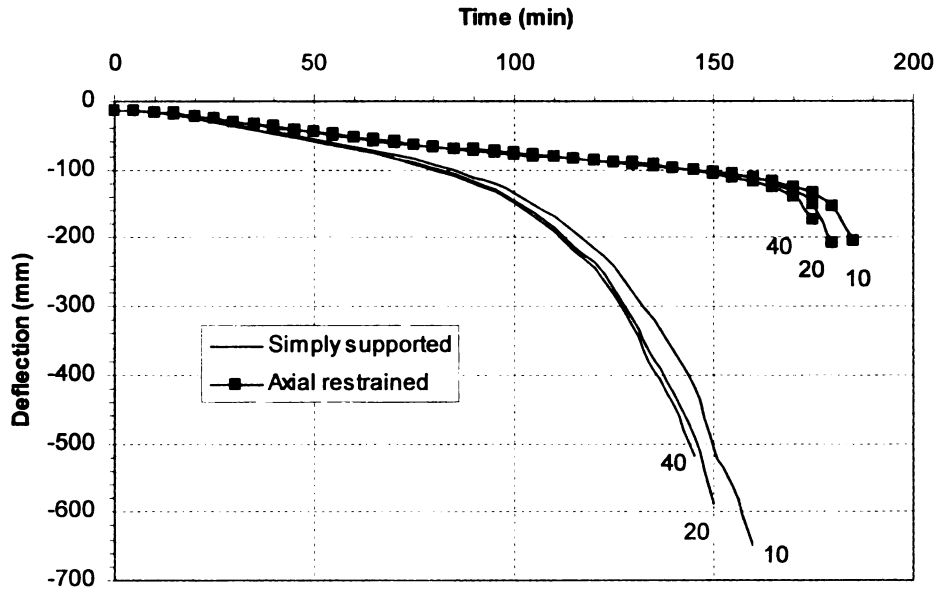

Figure 5.8 – Effect of Segmental Discretization on the Fire Response of RC Beams

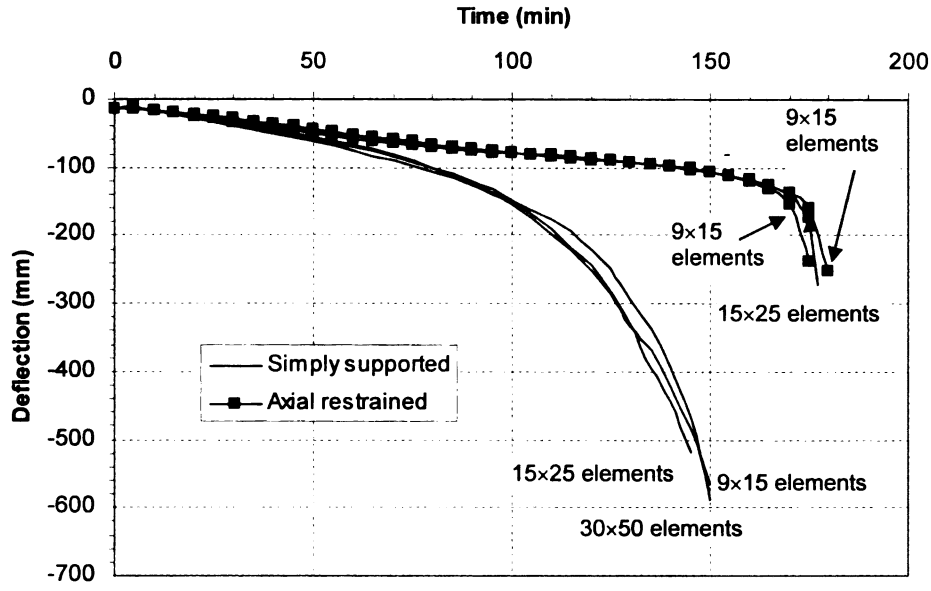

Figure 5.9 – Effect of Cross-sectional Discretization on the Fire Response of RC Beams

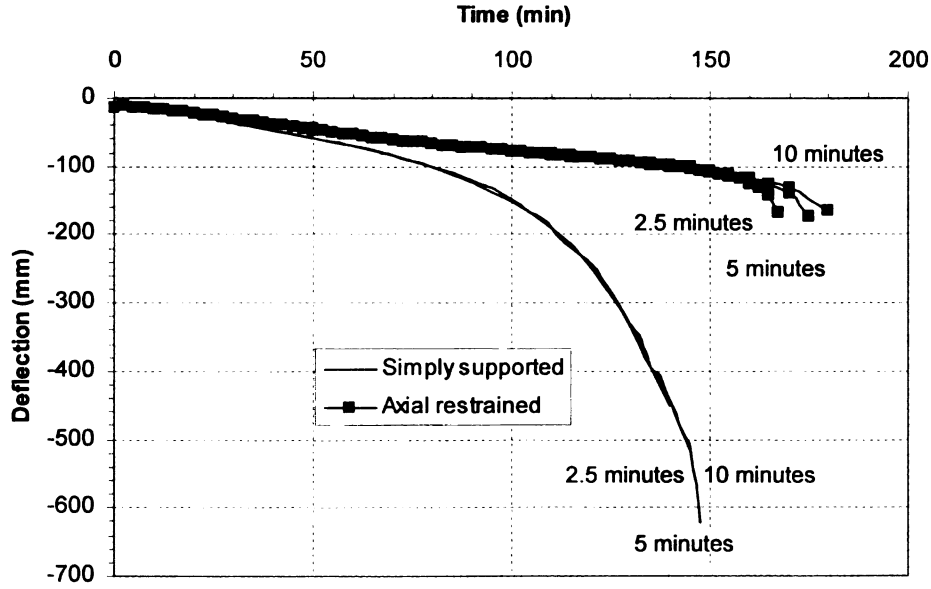

Figure 5.10 – Effect of Time Increment on the Fire Response of RC Beams

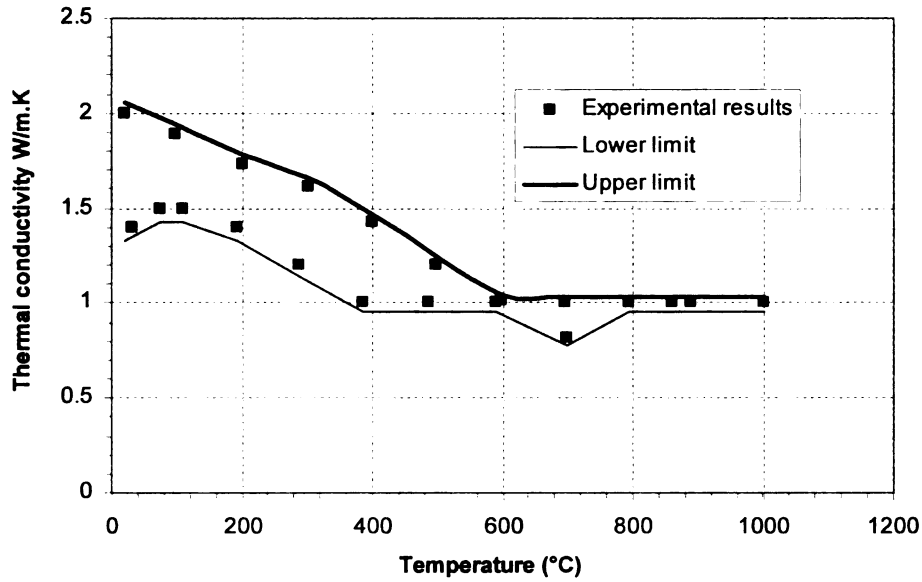

Figure 5.11 – Lower and Upper Limit and Experimental Results for Thermal Conductivity of Carbonate Aggregate Concrete at Elevated Temperatures

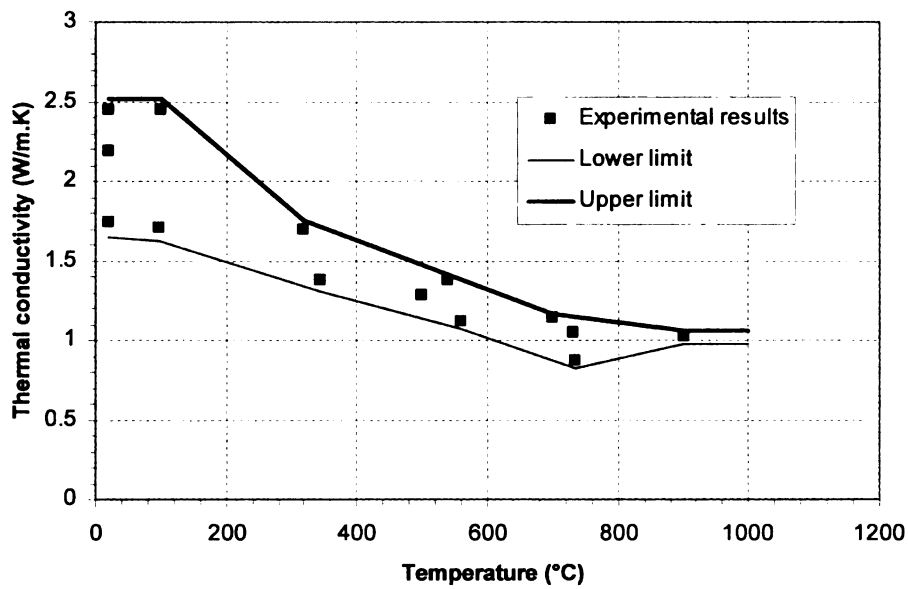

Figure 5.12 – Lower and Upper Limit and Experimental Results for Thermal Conductivity of Siliceous Aggregate Concrete at Elevated Temperatures

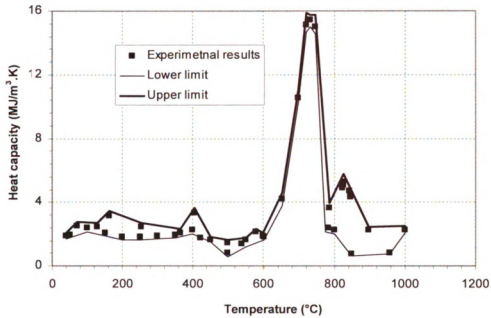

Figure 5.13 – Lower and Upper Limit and Experimental Results for Heat Capacity of Carbonate Aggregate Concrete at Elevated Temperatures

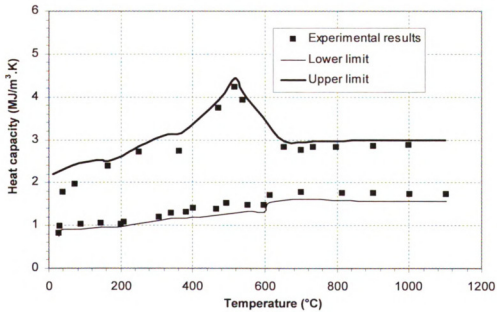

Figure 5.14 – Lower and Upper Limit and Experimental Results for Heat Capacity of Siliceous Aggregate Concrete at Elevated Temperatures

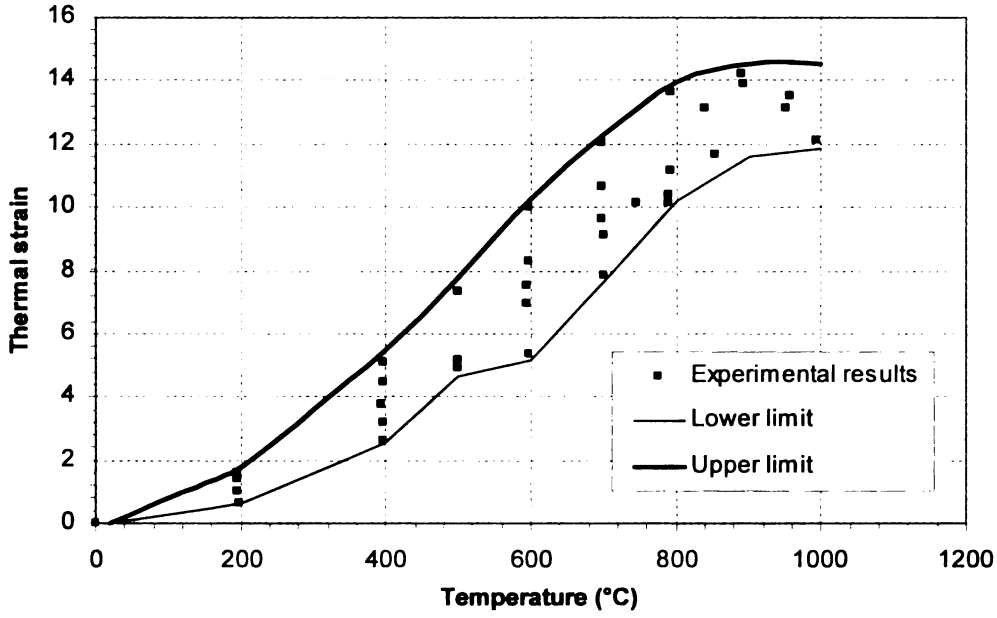

Figure 5.15 – Lower and Upper Limit and Experimental Results for Thermal Strain of Carbonate Aggregate Concrete at Elevated Temperatures

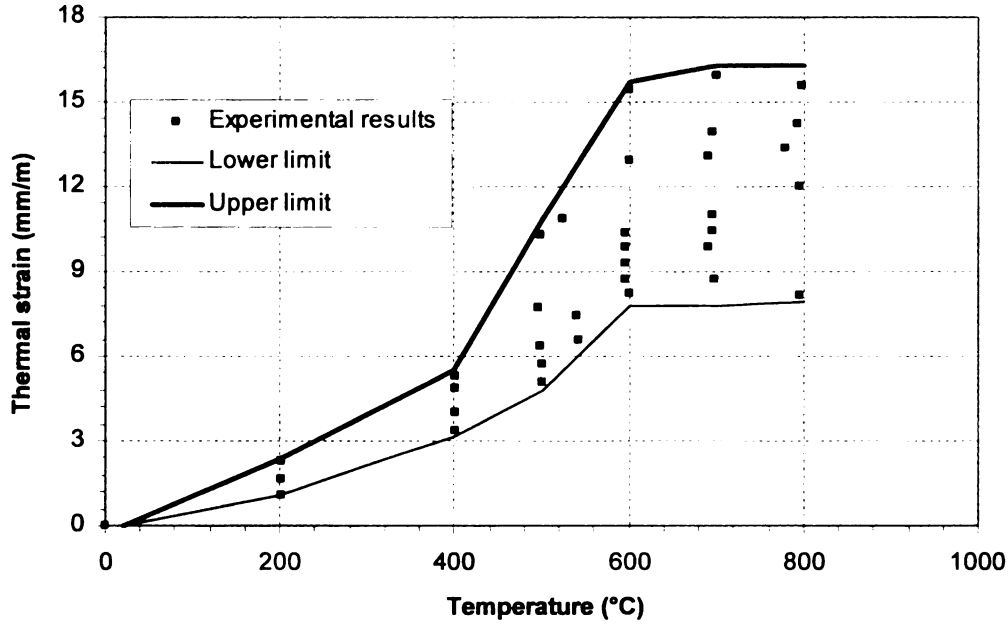

Figure 5.16 – Lower and Upper Limit and Experimental Results for Thermal Strain of Siliceous Aggregate Concrete at Elevated Temperatures

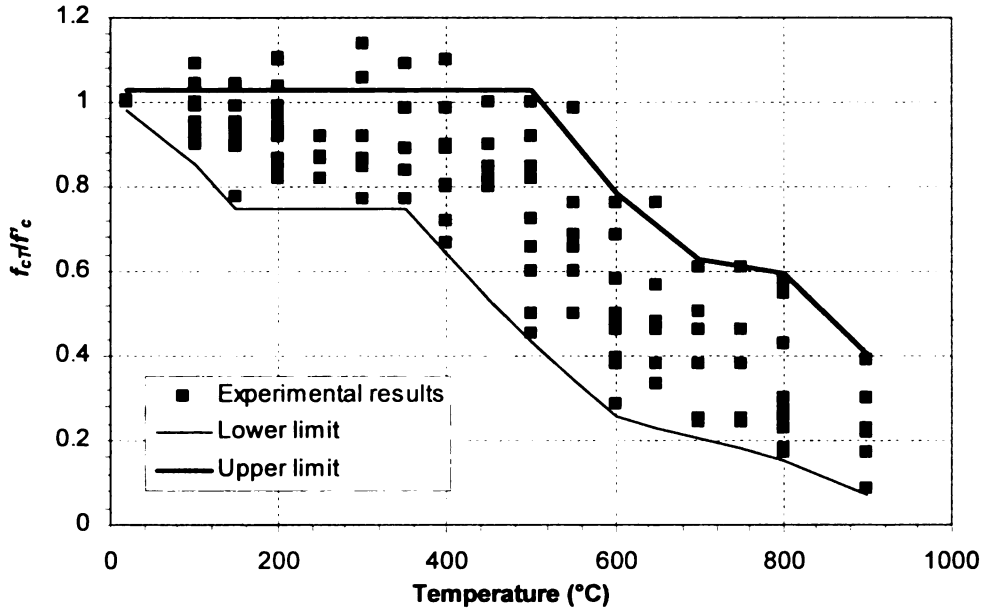

Figure 5.17 – Lower and Upper Limit and Experimental Results for Concrete Compressive Strength of NSC at Elevated Temperatures

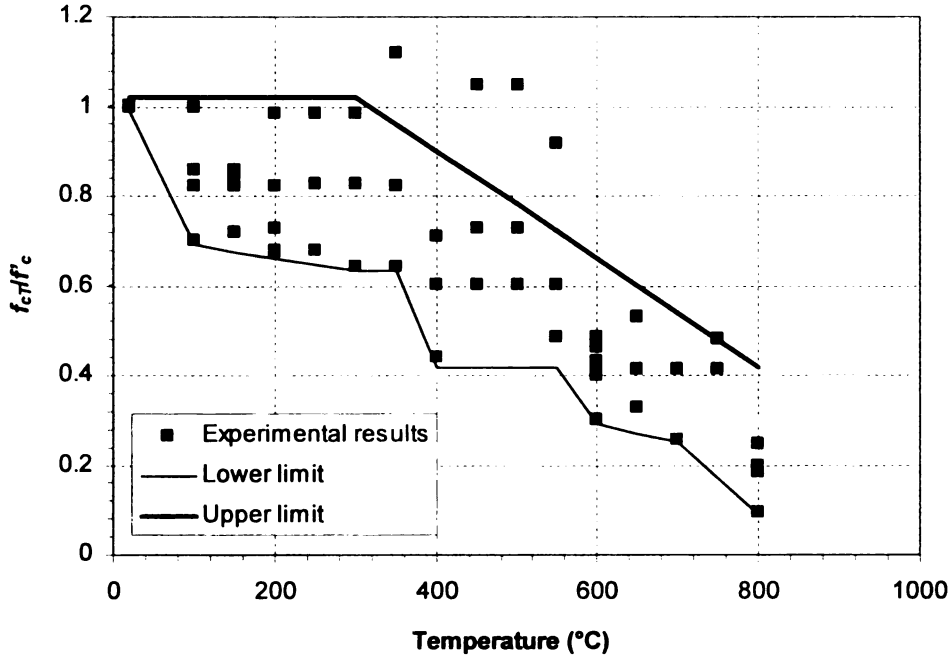

Figure 5.18 – Lower and Upper Limit and Experimental Results for Concrete Compressive Strength of HSC at Elevated Temperatures (Kodur et al. 2007)

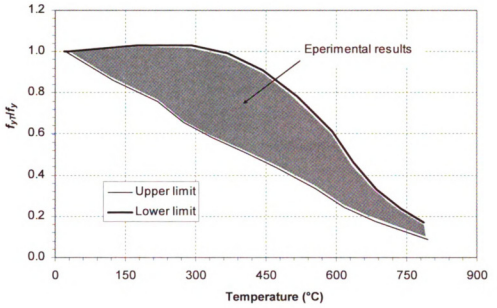

Figure 5.19 – Lower and Upper Limit of Steel Yield Strength at Elevated Temperatures (Reproduced from Harmathy 1993)

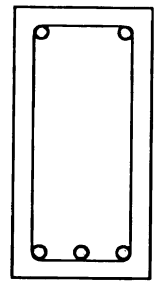

(a) Cross-sectional Details

Uniform mesh size is used with a number of elements within the cross-section of each beam as follows:

- 15×25 elements for beam B0
- 20×25 elements for beams BL1and BL2
- 16×25 elements for beams B1 and B2
- 32×50 elements for beams B3, B4, B5 and B6

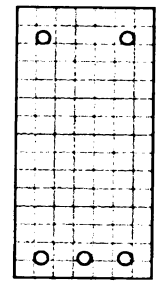

(b) Cross-sectional Discretization

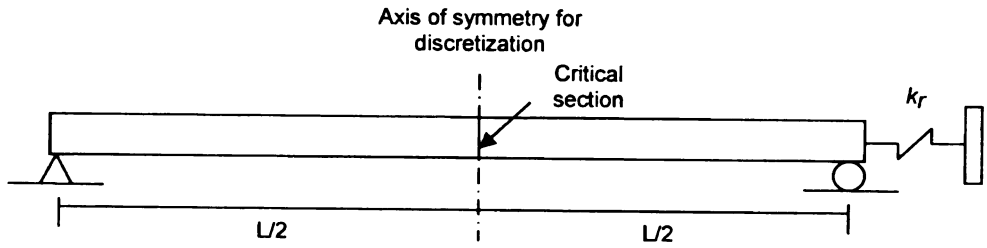

(c) Elevation of a Rotationally Unrestrained Beam

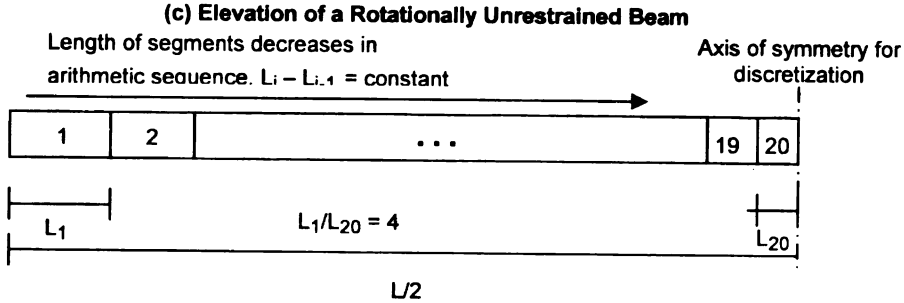

(d) Structural Discretization of Rotationally Unrestrained Beams

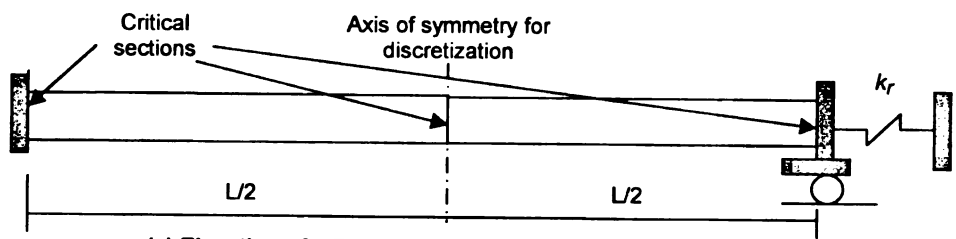

(e) Elevation of a Rotationally Restrained Beam

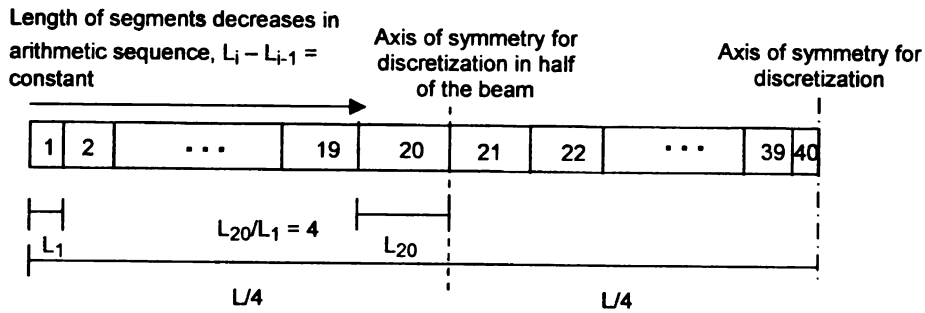

(f) Structural Discretization of Rotationally Restrained Beams

Figure 5.20 – Discretization of the Analyzed Beams

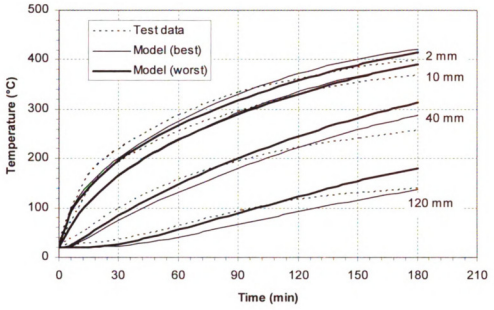

Figure 5.21 –Measured and Predicted Temperatures for Slab Tested by Kalifa et al. (2001)

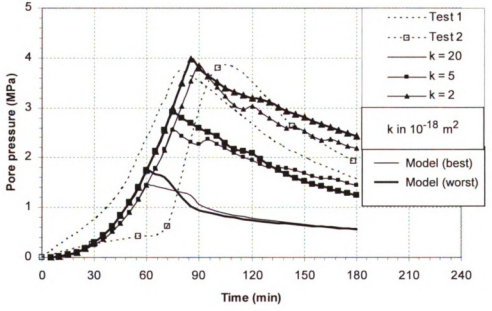

Figure 5.22 – Measured and Predicted Pore Pressure at Depth of 20 mm from Exposed Surface

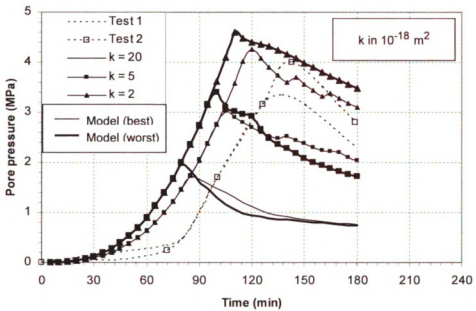

Figure 5.23 – Measured and Predicted Pore Pressure at Depth of 30 mm from Exposed Surface

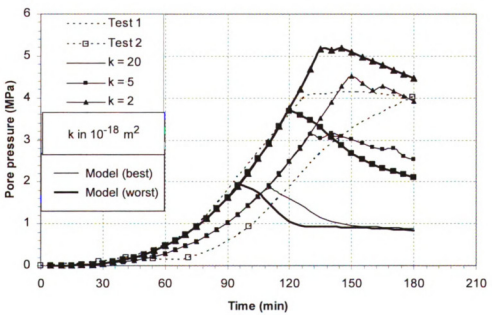

Figure 5.24 – Measured and Predicted Pore Pressure at Depth of 40 mm from Exposed Surface

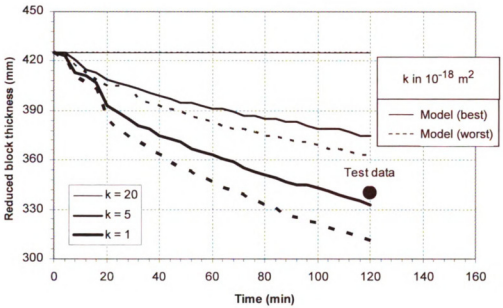

Figure 5.25 – Measured and Predicted (Leftover) Block Thickness as a Function of Time

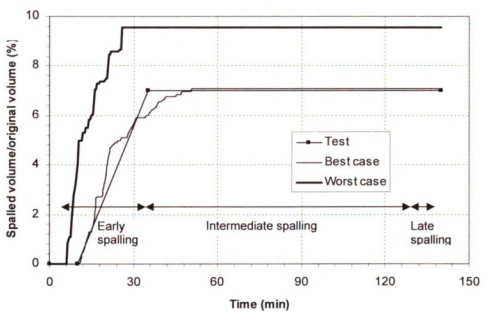

Figure 5.26 – Measred and Predicted Extent of Spalling as a Function of Time for Beam B5

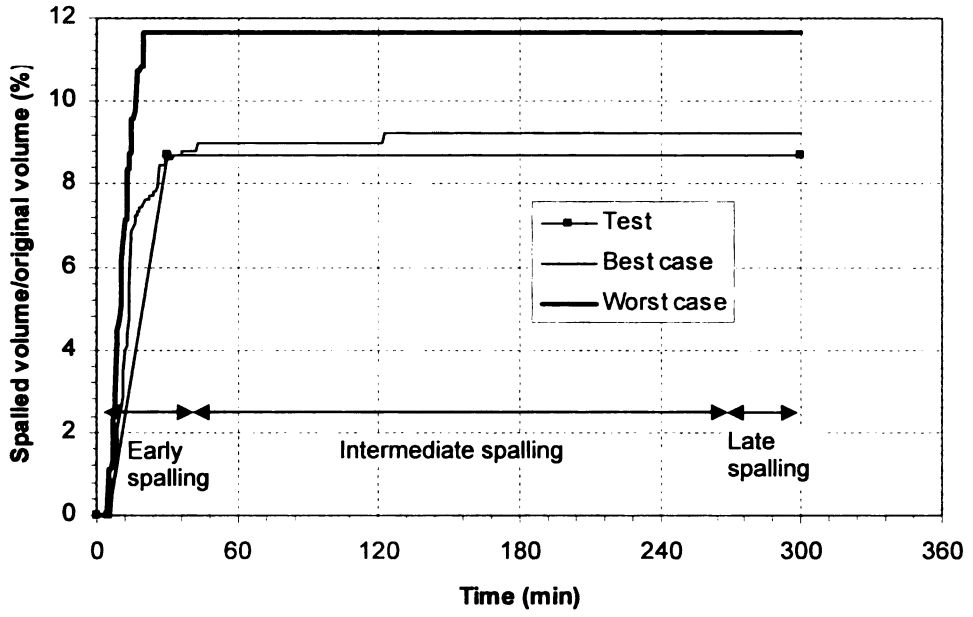

Figure 5.27 – Measred and Predicted Extent of Spalling as a Function of Time for Beam B6

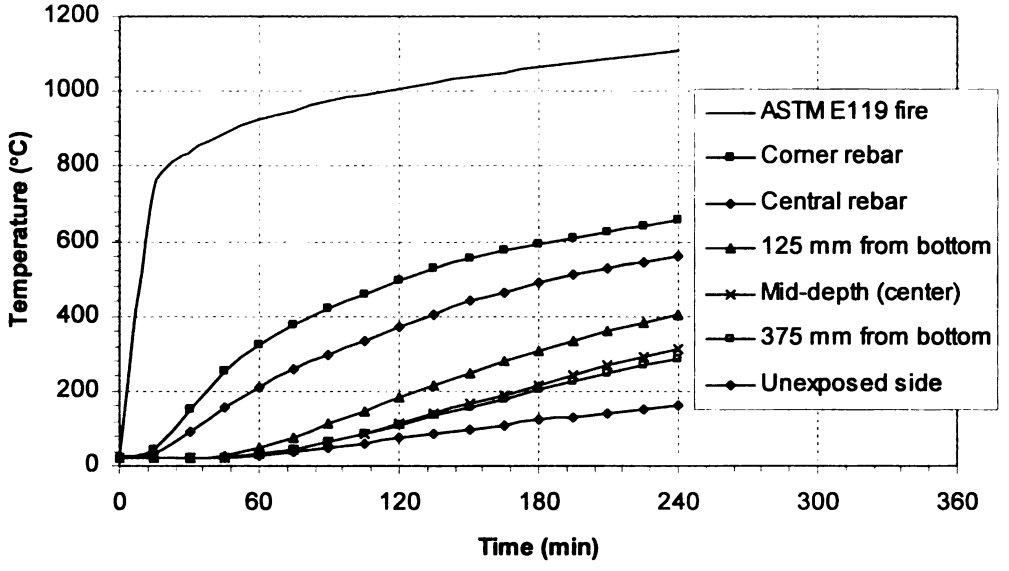

Figure 5.28 - Temperature as a Function of Time at different Locations of Cross-section in Beam B0

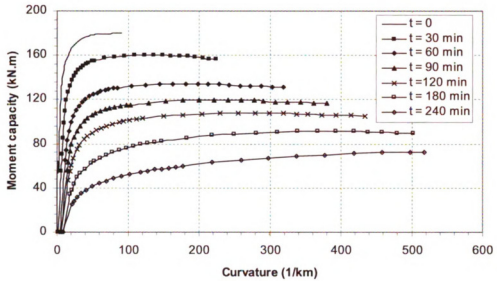

Figure 5.29 - Moment Curvature Curves at Mid-span of Beam B0 at Various Time Steps

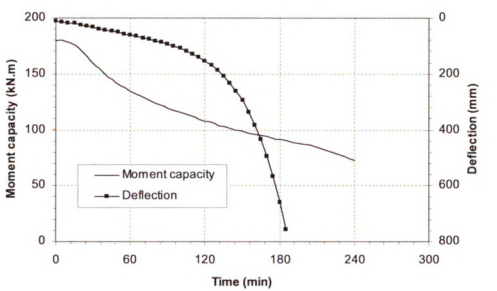

Figure 5.30 – Variation of Moment Capacity and Deflection for Beam B0 as a Function of Fire Exposure Time

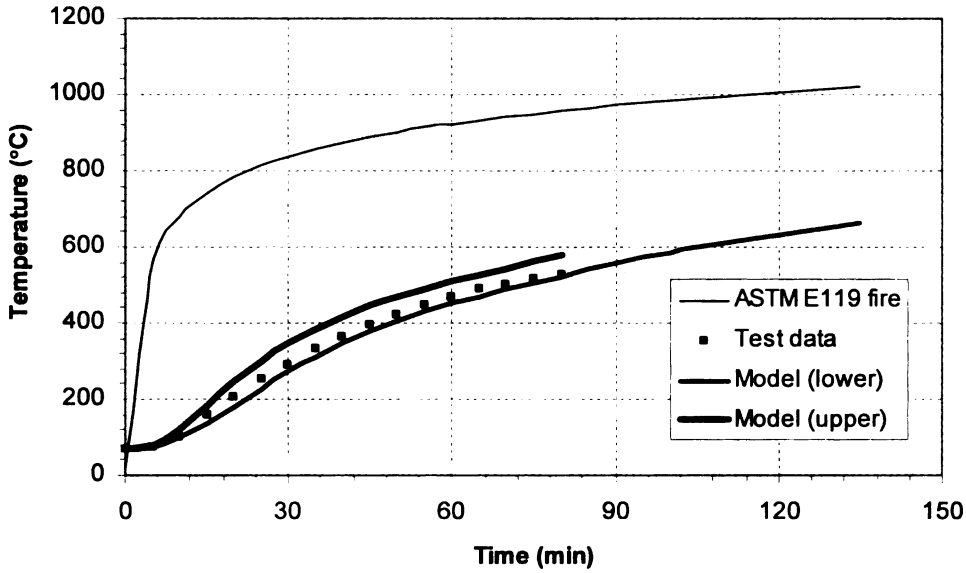

Figure 5.31 - Predicted and Measured Rebar Temperatures for Beam BL1

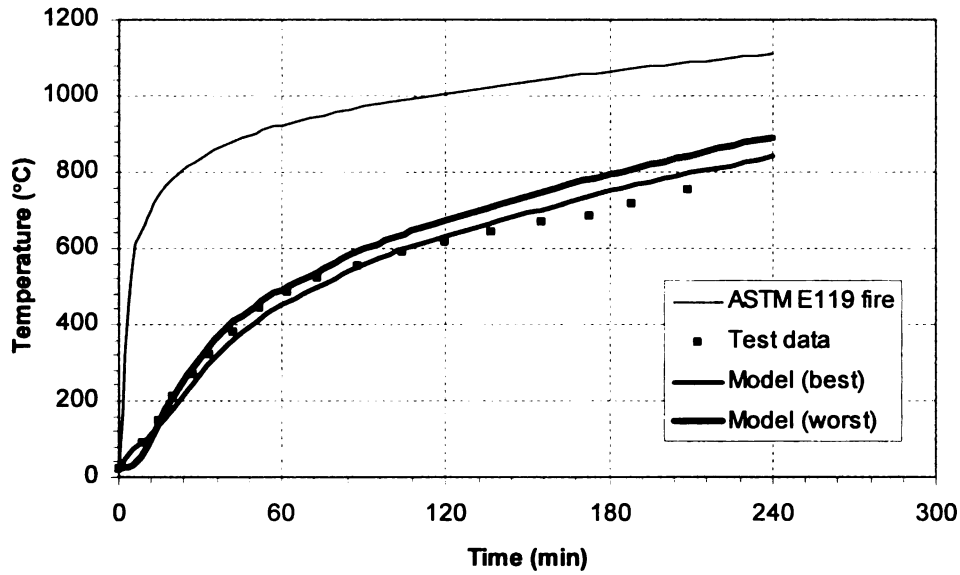

Figure 5.32 - Predicted and Measured Rebar Temperatures for Beam BL2

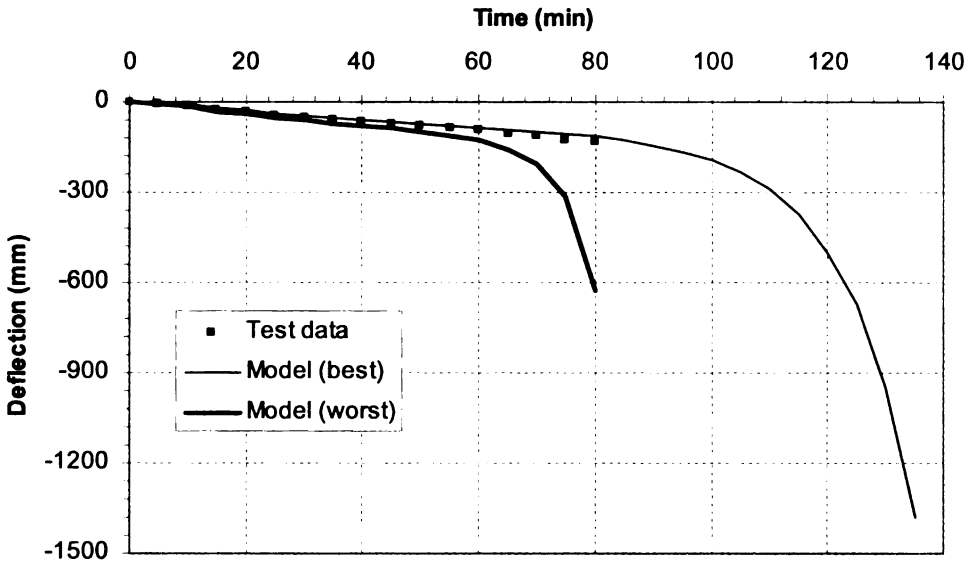

Figure 5.33 – Predicted and Measured Deflections for Beam BL1

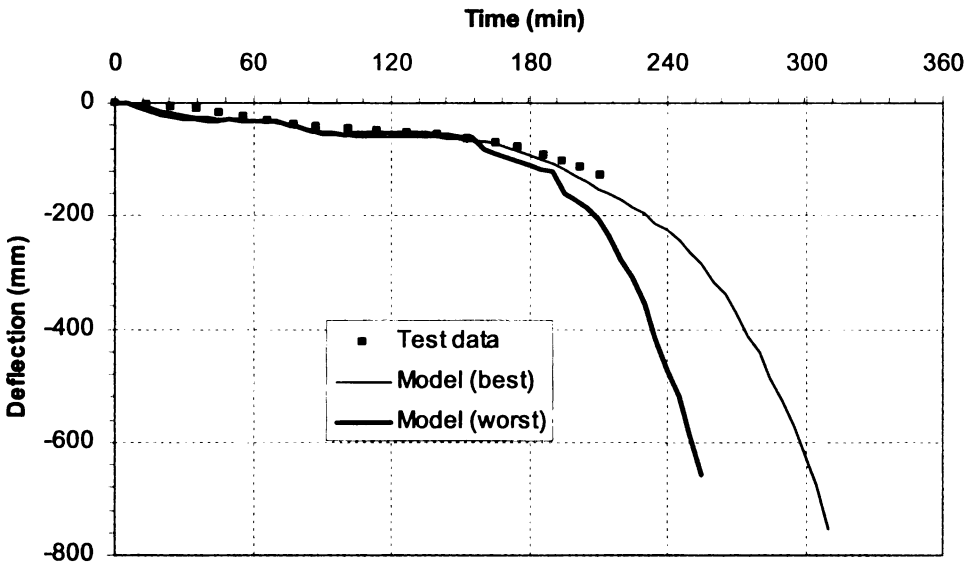

Figure 5.34 – Predicted and Measured Deflections for Beam BL2

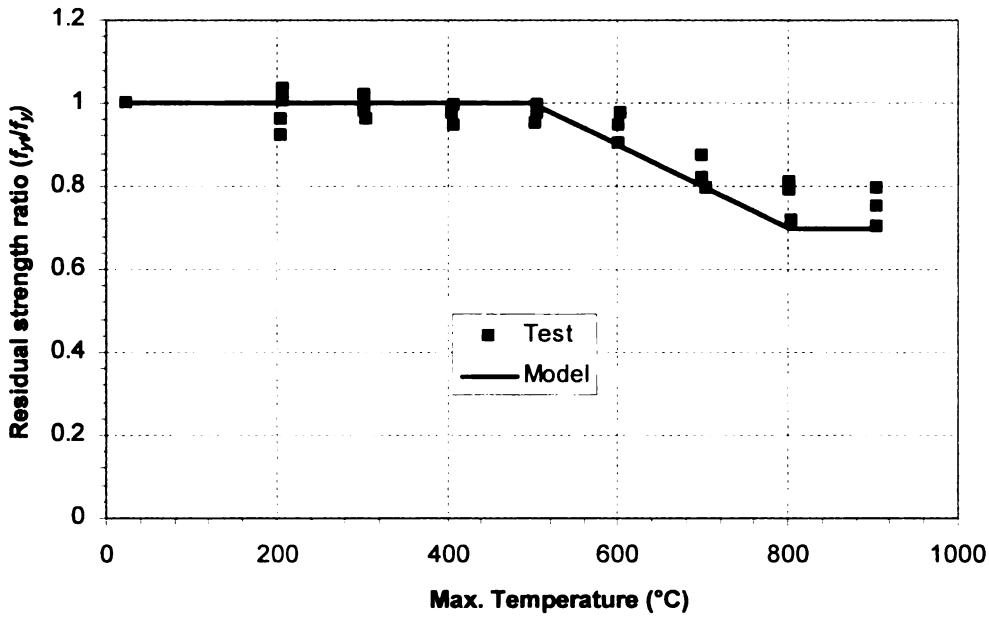

Figure 5.35 – Variation of residual strength of reinforcing steel as a function of temperature

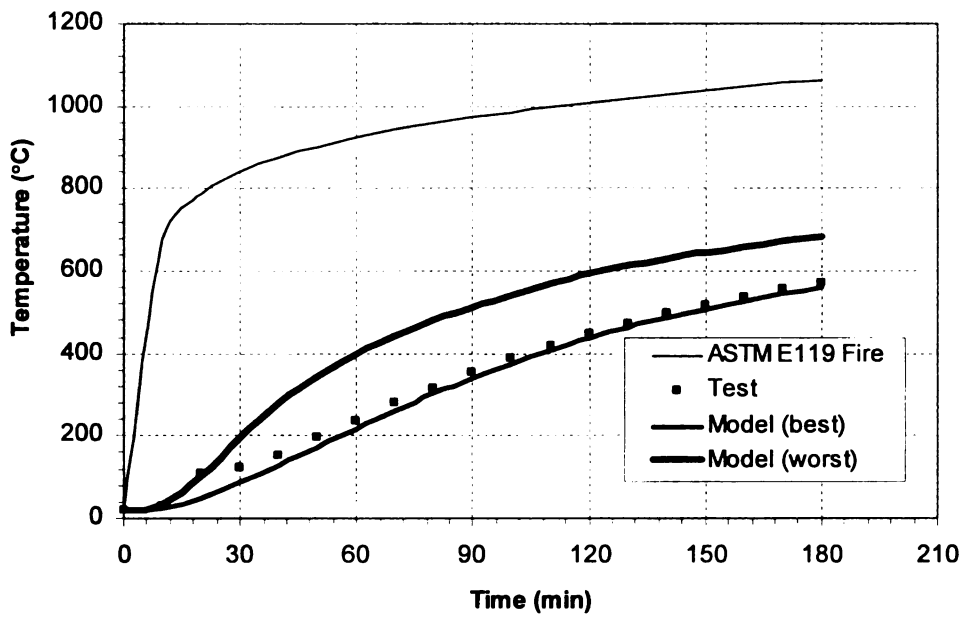

Figure 5.36 – Measured and Predicted Average Rebar Temperature as a Function of Time for Beam B1

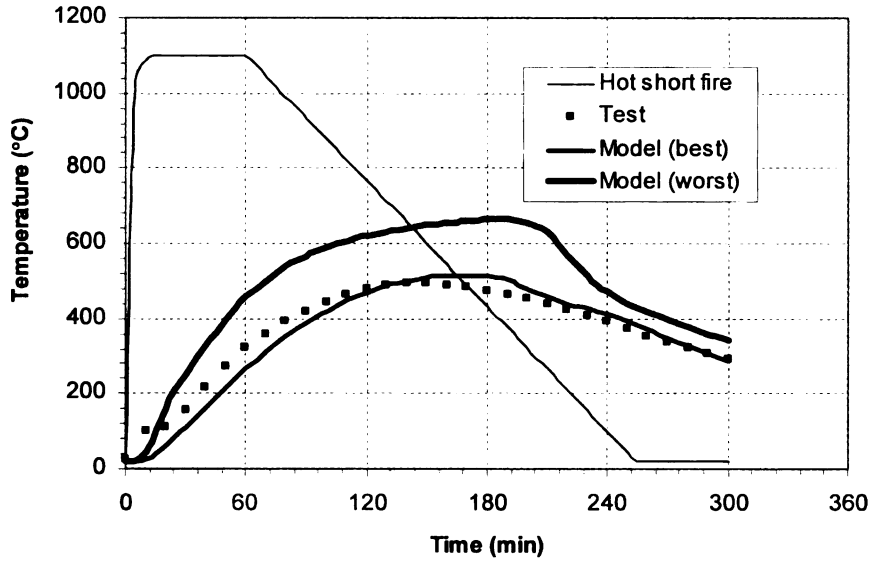

Figure 5.37 – Measured and Predicted Rebar Temperature as a Function of Time for Beam B2

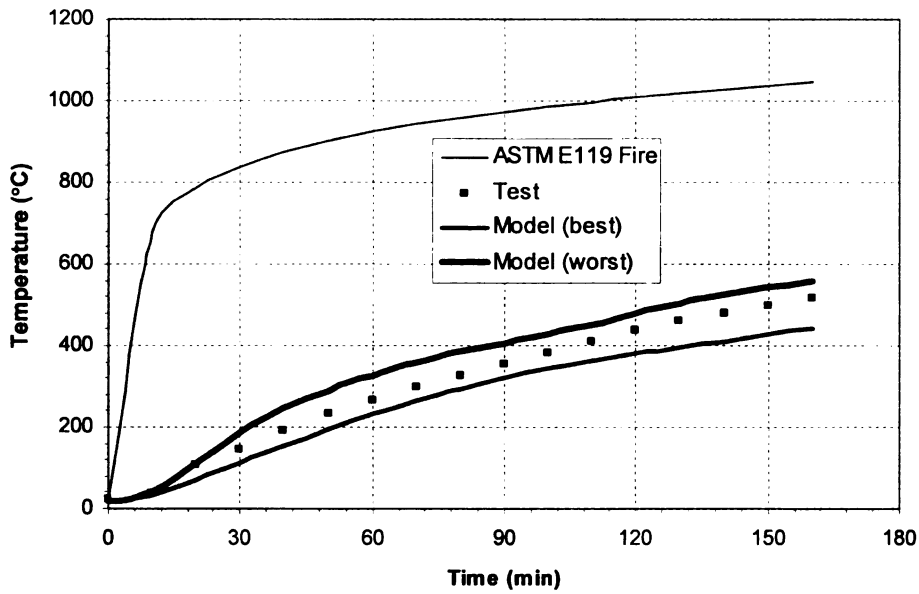

Figure 5.38 – Measured and Predicted Rebar Temperature as a Function of Time for Beam B3

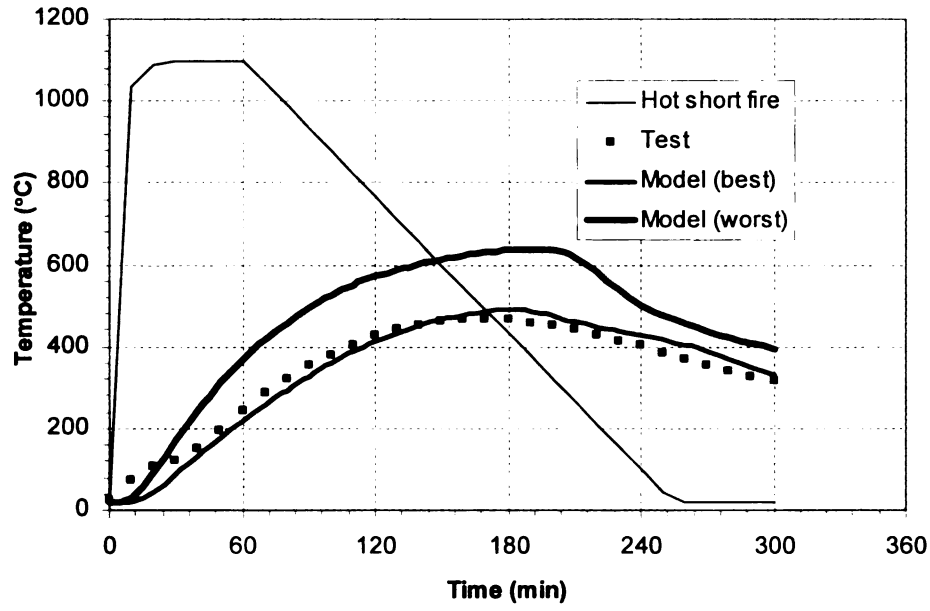

Figure 5.39 – Measured and Predicted Rebar Temperature as a Function of Time for Beam B4

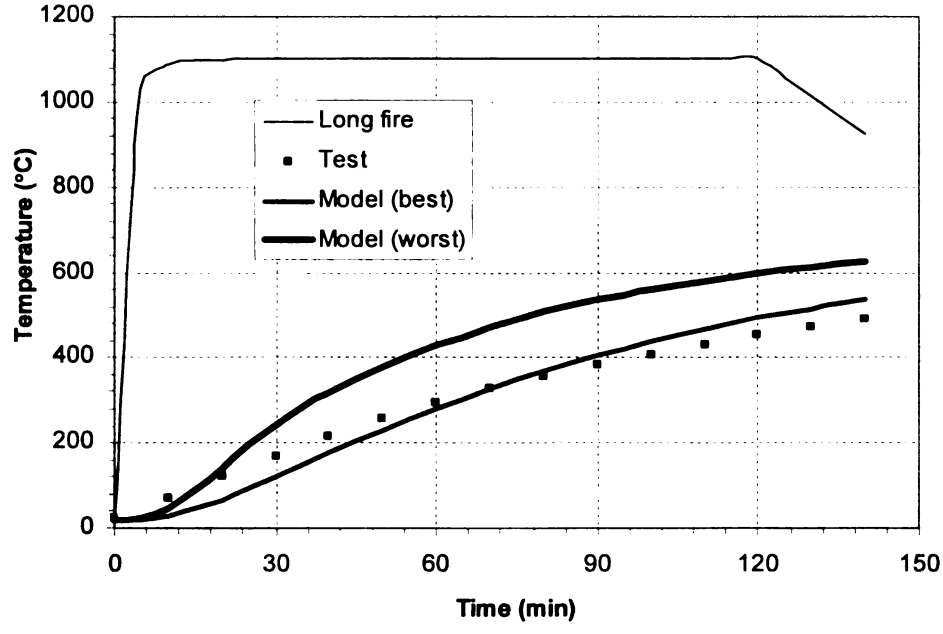

Figure 5.40 – Measured and Predicted Rebar Temperature as a Function of Time for Beam B5

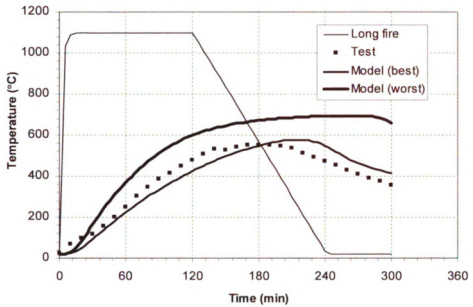

Figure 5.41 – Measured and Predicted Rebar Temperature as a Function of Time for Beam B6

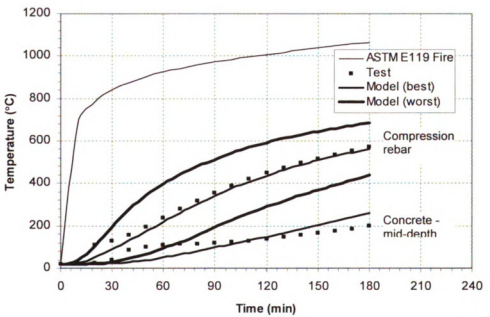

Figure 5.42 – Measured and Predicted Compression Rebar and Concrete Temperature as a Function of Time for Beam B1

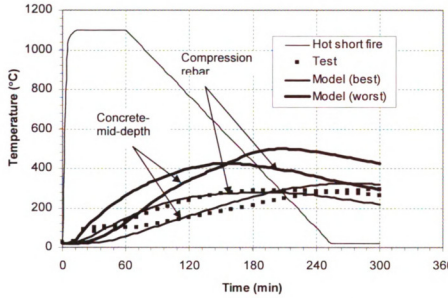

Figure 5.43 – Measured and Predicted Compression Rebar and Concrete Temperature as a Function of Time for Beam B2

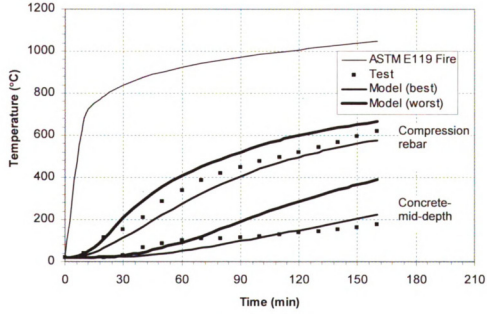

Figure 5.44 – Measured and Predicted Compression Rebar and Concrete Temperature as a Function of Time for Beam B3

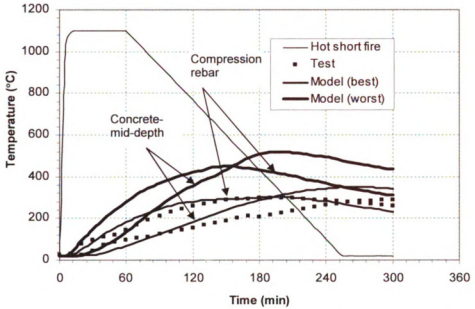

Figure 5.45 – Measured and Predicted Compression Rebar and Concrete Temperature as a Function of Time for Beam B4

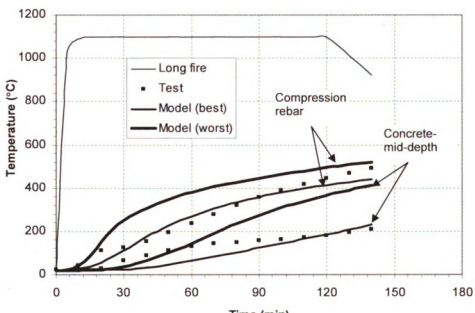

Figure 5.46 – Measured and Predicted Compression Rebar and Concrete Temperature as a Function of Time for Beam B5

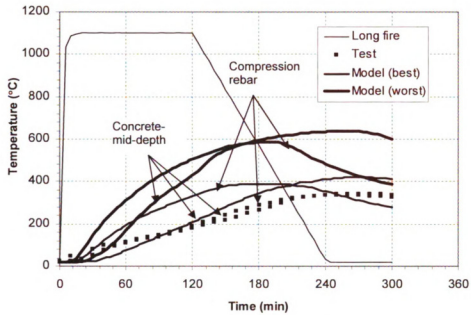

Figure 5.47 – Measured and Predicted Compression Rebar and Concrete Temperature as a Function of Time for Beam B6

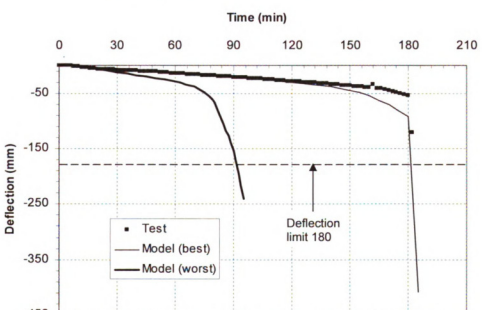

Figure 5.48 – Measured and Predicted Mid-span Defeclection as a Function of Time for NSC Beam B1

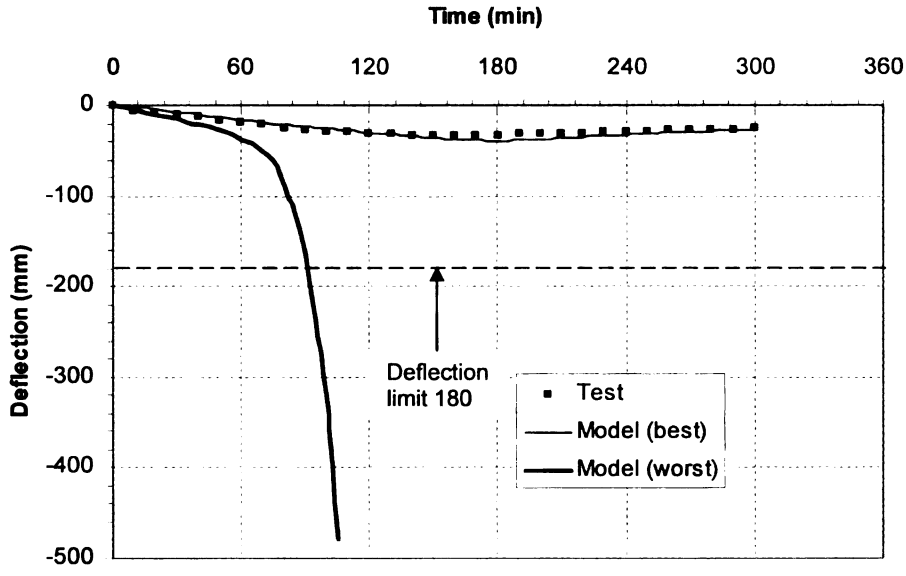

Figure 5.49 – Measured and Predicted Mid-span Defeclection as a Function of Time for NSC Beam B2

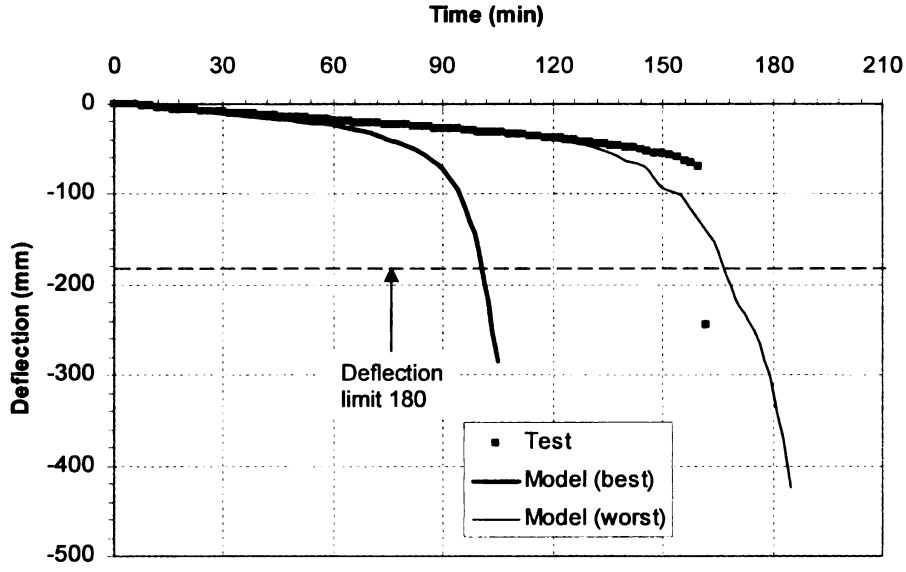

Figure 5.50 – Measured and Predicted Mid-Span Defeclection as a Function of Time for HSC Beam B3

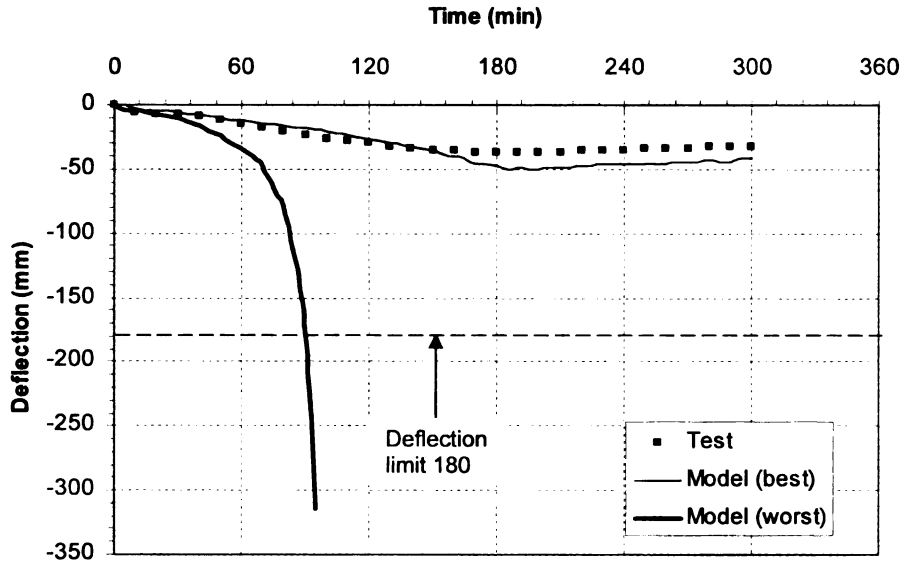

Figure 5.51 – Measured and Predicted Mid-span Defeclection as a Function of Time for HSC Beam B4

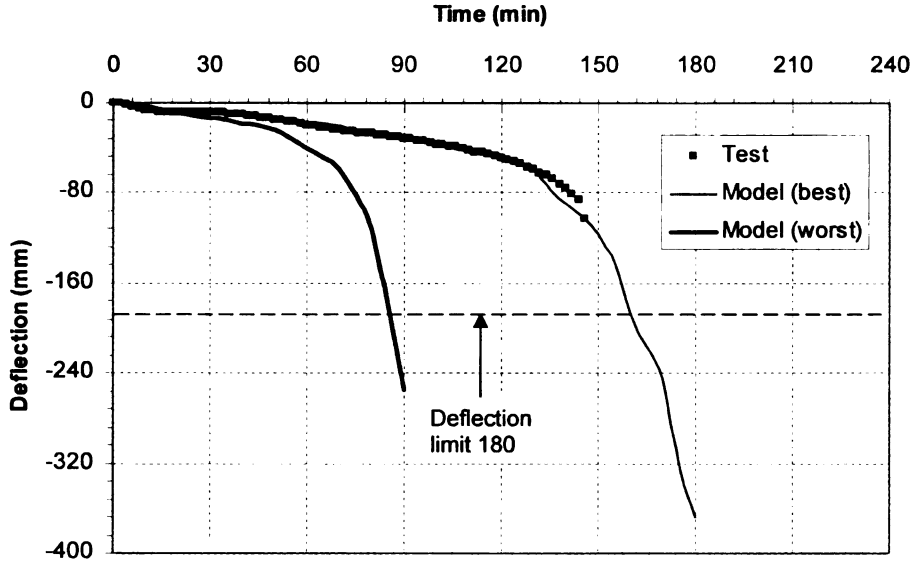

Figure 5.52 – Measured and Predicted Mid-span Defeclection as a Function of Time for HSC Beam B5

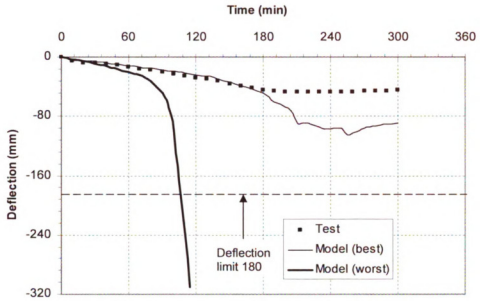

Figure 5.53 – Measured and Predicted Mid-span Defeclection as a Function of Time for HSC Beam B6

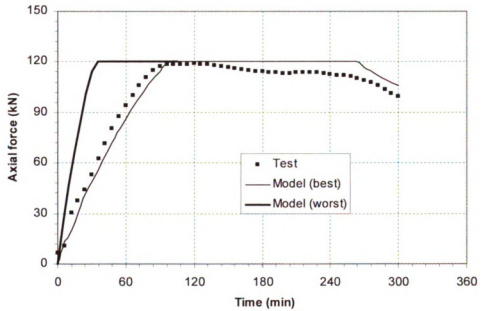

Figure 5.54 – Measured and Predicted Axial Restraint Force as a Function of Time for NSC Beam B2

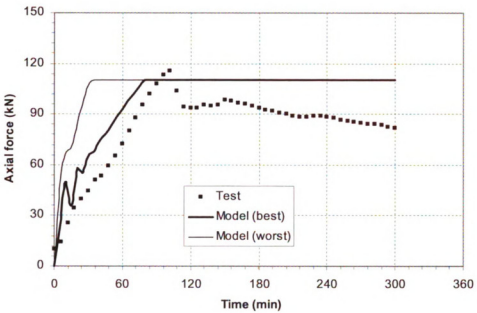

Figure 5.55 – Measured and Predicted Axial Restraint Force as a Function of Time for HSC Beam B6

Chapter 6

6. Parametric Studies

6.1 General

The numerical model presented in Chapter 4 is applied to investigate the effect of various parameters on the fire response of RC beams. The studied parameters are: section characteristics (including beams width and concrete cover thickness), load level, aggregate type, axial restraint stiffness, span-to-depth ratio, location of axial restraint force, rotational restraint, fire scenario, concrete strength, and failure criteria.

As illustrated in Chapter 2, there is large variation in high temperature properties for concrete and reinforcing steel. Thus, the parametric studies are conducted using the average material properties (obtained by averaging the worst and best case scenarios of material properties). The reason for using the average material properties is the fact that fire is a rare event, and therefore fire design is generally performed using the most likely expected (average) material properties (Buchanan 2002). Thus, it is reasonable to use the average high temperature properties to carry out the parametric studies. It should be noted

that the effect of the studied parameters on the fire resistance of RC beams is not significantly influenced by variation in the high temperature properties. Results from the parametric studies are presented in this chapter.

6.2 Factors Influencing Fire Resistance

A state-of-the-art review clearly indicates that several factors govern the fire response of RC beams. It was shown through qualitative parametric studies (Kodur and Dwaikat 2008b, Dwaikat and Kodur 2008a) that the main factors influencing the fire response of RC beams are:

- Sectional characteristics (beam width, concrete cover thickness and steel ratio),
- Load ratio,
- Aggregate type,
- Axial and rotational restraint stiffness,
- Span-to-depth ratio,
- Location of axial restraint,
- Fire scenario,
- Concrete strength,
- Failure criteria,

Detailed parametric studies were conducted to quantify the influence of each of the above factors on the fire resistance of RC beams and the results are presented in Section 6.4.

6.3 Numerical Studies

6.3.1 Beam Characteristics

For the parametric studies, RC beams with four different cross-sections are selected. The reinforcement ratio in these beams (ratio of area of tension steel to the effective area of the beam cross-section) is in the range of 0.6 to 1.7%, which lies within the minimum and maximum limits specified in ACI 318 (2008). The compressive strength of concrete is varied from 30 MPa to 100 MPa, while the yield strength of rebars is assumed to be 413 MPa (Grade 60 steel bars). Details of the characteristics of the four cross-sections of the beams are given in Table 6.1.

6.3.2Analysis Variables

The parameters varied in the analysis include four different concrete cross-sections, three load ratios (30%, 50% and 70%), two concrete types (NSC and HSC), two aggregate types (carbonate and siliceous aggregate), three span-to-depth ratios (8, 13, and 18), three degrees of axial restraint stiffness (0, 50 kN/mm and 200 kN/mm) and five locations (Y/H) of the axial restraint (0.3, 0.4, 0.5, 0.6 and 0.7). The location of axial restraint is measured from the top most fiber of the beam cross-section as a ratio of the total depth of the beam. Both rotationally restrained and unrestrained RC beams are used in the analysis. In addition, to investigate the effect of fire scenarios, some of the beams were analyzed under two standard fire exposures (ASTM E119a (2008) standard fire and ASTM E1529 (1993) hydrocarbon fire) and three design fire exposures (Fire I, Fire II and Fire III). The time temperature curves for the five fire scenarios are given in Figure 6.1.

Each of the analyzed beams is designated by five characters arranged from left to right as follows:

- Concrete type (N for NSC, and H for HSC),
- Aggregate type (S for siliceous aggregate and C for carbonate aggregate),
- Cross-section number (1, 2, 3 or 4 for the four sections detailed in Table 6.1),
- Support conditions (S for simply supported, A for axially restrained, R for rotationally restrained and AR for axially and rotationally restrained beams),
- Span-to-depth ratio (S representing small span-to-depth ratio of 8, M representing medium span-to-depth ratio of 13, and L representing large span-to-depth ratio of 18).

For example, designation NC2AM indicates a beam made of NSC with siliceous aggregate, of cross-section type '2', axially restrained, and has medium span-to-depth ratio of 13. A sixth character in the form of numeral is used in the designation of some beams, where the first five characters of the designation were repeated. More details on other parameters for the analyzed beams (such as load ratio, axial restraint stiffness and location of axial restraint) are presented in Table 6.2.

Each of the simply supported or axially restrained beams was discretized into 40 segments, while every rotationally restrained beam was discredited into 80 segments. The cross-section for each segment was idealized into elements such that the mesh size is 20 mm for NSC beams and 10 for HSC beams. Since spalling is a concern in HSC members a finer mesh was selected for HSC beams so as to obtain better spalling predictions. Details on the structural and cross-sectional discretization of beams are shown in Figure 6.2.

The analysis was carried out using the macroscopic finite element model, presented in Chapter 4, in 2.5 minute time increments till failure occurred in the beam. The failure time (fire resistance) for the analyzed beams is evaluated based on strength and two deflection limit states as discussed in Chapter 4. Results from parametric studies are utilized to illustrate the effect of different parameters on the overall fire response of RC beams.

6.4 Results of Parametric Studies

Results from the parametric studies are presented in Table 6.2 and Figures 6.3 to 6.20 where time-deflection curves for the analyzed beams are plotted. The effect of the studied parameters on the thermal response of the beam (rebar and concrete temperatures) is not presented here because many of these parameters such as load ratio, span-to-depth ratio and restraint do not influence the thermal response of the analyzed beams. The effect of each of the parameters on the fire response is discussed bellow.

6.4.1 Effect of Sectional Dimensions

The current practice of achieving required fire resistance in RC beams is through the provision of specified cover thickness to rebars and satisfying minimum sections dimensions (ACI 216.1 2007, ASCE/SFPE29 1999). The effect of section characteristics on the fire resistance of RC beams is investigated by analyzing a set of RC beams made of four cross-sections, namely, CS1, CS2, CS3 and CS4. A summary of the properties of these cross-sections is given in Table 6.1. Results from the analysis are shown in Figures 6.3 and 6.4 and in Table 6.2.

Figure 6.3 shows the variation of mid-span deflection as a function of fire exposure time for four RC beams, namely, NS1SM, NS2SM, NS3SM, and NS4SM, made of the four cross-sections. The four beams have three different concrete cover thicknesses and four widths as can be seen in Table 6.1. Results from the analysis plotted in Figure 6.3 illustrate that both concrete cover thickness and beam width have significant effect on the fire response of RC beams. The figure shows that the mid-span deflection of beam NS3SM is smaller than that of beam NS1SM throughout the fire exposure time. This can be attributed to the large width of beam NS3SM (as compared to beam NS1SM) which significantly reduces the heat transmission to the cross-section.

It can also be seen from Figure 6.3 that concrete cover thickness has significant influence on the response of RC beams exposed to fire. Beam NS4SM, despite having smaller width as compared to beam NS3SM, experienced smaller deflection particularly at later stages of fire exposure. This can be attributed to the larger concrete cover thickness for beam NS4SM (60 mm) as compared to that of beam NS3SM (40 mm). Increased concrete cover thickness decreases rebar temperature and therefore significantly reduces the deflection in RC beams as shown in Figure 6.3. This is because lower rebar temperature, resulting from increased concrete cover, is associated with smaller plastic and creep strains and also lesser deterioration of strength, which leads to reduced deflections in the beam. Similar trends are observed for beams NC1AM, NC2AM, NC3AM, and NC4AM which are axially restrained as can be seen in Figure 6.4.

Concrete cover thickness and beam width have significant influence on the fire resistance of RC beams based on three sets of failure criteria, as can be seen in Table 6.2. The table shows that increasing the beam width from 300 to 700 mm increases the fire resistance,

for strength failure criterion, by about 50 minutes. This is due to slower heat transmission to the concrete section, and thus smaller loss of strength, with increasing beam width. The results in the table also indicate that beam NS4SM, though has smaller width than beam NS3SM, has higher fire resistance due to its larger concrete cover thickness. Increasing concrete cover thickness decreases rebar temperature and reduces deflection and rate of deflection as can be seen in Figures 6.3 and 6.4.

6.4.2 Effect of Load Level

To investigate the effect of load on fire resistance, the beams were analyzed under three load ratios, namely, 30%, 50% and 70%. The load ratio is calculated as the ratio of the applied load under fire conditions to the capacity of the beam at room temperature computed as per ACI 318 (2008).

The effect of load ratio on the fire response of RC beams is illustrated in Figures 6.5 and 6.6 and Table 6.2. Figure 6.5 shows the variation of deflection with fire exposure time for three simply supported RC beams designated as NS1SS1, NS1SS2 and NS1SS3. It can be seen from Figure 6.5 that load level has significant influence on the deflection and the rate of deflection of RC beams. The figure shows that an increased load ratio increases deflection, as well as rate of deflection (significantly at later stages of fire exposure). This is because an increased load level causes early yielding of the steel reinforcement and thus increases the plastic and creep strains. This leads to lower stiffness in the beam and results in significant increase in deflection and rate of deflection.

Similar trends can be seen in Figure 6.6 which shows the variation of deflection with fire exposure time for three axially restrained beams (NC3AM1, NC3AM, and NC3AM2). However, Figure 6.6 shows that the rate of deflection (slop of time deflection curve) in

these three beams decreases at early stages of fire exposure time to a certain value then increases again. This reduction in the rate of deflection at early stages of fire exposure time can be attributed to the developed axial restraint force which produces a counteracting moment in a mechanism similar to arch action as discussed in Chapter 2. The counteracting moment reduces the effect of the applied load, which enhances the stiffness and decreases the deflection and rate of deflection of the beam. At later stages of fire exposure, the effect of the arch action becomes small due to the large degradation in the strength and stiffness of the constituent materials and thus the rate of deflection increases as can be seen from Figure 6.6.

Fire resistance values presented in Table 6.2 show that load level has a significant influence on the fire resistance of RC beams, predicted based on strength and deflection failure criteria. It can be seen that increased load level significantly reduces the fire resistance of RC beams. This can be attributed to the fact that a higher load level causes early softening and weakening of the constituent materials leading to early strength and stiffness reduction of the beam. It should be noted that current prescriptive approach is derived from standard fire tests where the load ratio is generally 50%. The results presented above illustrate that fire resistance, computed based on prescriptive approach, may not be conservative if the load ratio is higher than 50%.

6.4.3 Effect of Aggregate Type

Previous studies have shown that the type of aggregate in concrete influences the high temperature concrete properties and thus the fire resistance of RC members. The effect of aggregate type on the fire response of RC beams is illustrated in Figures 6.7 and 6.8 and Table 6.2. Figure 6.7 shows the variation of deflection with fire exposure time for simply

supported beams NS2SM and NC2SM, while Figure 6.8 shows the variation of deflection with fire exposure time for axially restrained beams NS4AM and NC4AM. Beams NC2SM and NC4AM are fabricated from carbonate aggregate (predominantly limestone) concrete, while beams NS2SM and NS4AM are fabricated from siliceous aggregate (predominantly quartz) concrete.

It can be seen from Figures 6.7 and 6.8 that the carbonate aggregate concrete beam attains much lower deflection throughout the fire exposure time. This is mainly because of the high thermal capacity of carbonate aggregate resulting from an endothermic reaction that occurs due to disassociation of dolomite in carbonate aggregate. This endothermic reaction, which occurs in 650-700°C temperature range, leads to the consumption of large amount of heat and significantly increases the specific heat which is about 10 times higher than that for siliceous aggregate concrete. In addition, carbonate aggregate concrete generally has lower thermal conductivity than that of siliceous aggregate concrete as can be seen when comparing Figure 5.11 to Figure 5.12. The high thermal capacity and the low thermal conductivity of carbonate aggregates results in lower temperature, and thus lower deflection. Therefore, the carbonate aggregate concrete beam has lower mid-span deflection than siliceous aggregate concrete beam.

The fire resistance values presented in Table 6.2 show that aggregate type has significant effect on the failure time of RC beams. It can be seen from Table 6.2 that the fire resistance of beams made with carbonate aggregate concrete is about 20% to 30% higher than that for beams made of siliceous aggregate concrete. This can be attributed to the high thermal capacity and low thermal conductivity of carbonate aggregate concrete

which reduces the temperature in the beam (made of carbonate aggregate concrete) and thus improve the fire response.

6.4.4 Effect of Span-to-depth Ratio

The effect of span-to-depth ratio on the fire response of RC beams is illustrated in Figure 6.9 which shows the variation of deflection with fire exposure time for three axially restrained beams (NS1AS, NS1AM and NS1AL) with different span-to-depth ratio. It can be seen from Figure 6.9 that the mid-span deflection in all beams increases with fire exposure time. However, the rate of increase in deflection is higher for beam with high span-to-depth ratio. This is mainly because of the reduced flexural stiffness of slender beams (having high span-to-depth), which are prone to buckling under increased axial restraint force that develops under fire exposure. Further, the reduced flexural stiffness of slender beams produces higher deflection at any fire exposure time. This will increase the secondary moments developed due to the P-δ effect (the axial force, P, and vertical deflection, δ, will lead to development of secondary moments) of the axial restraint force and will in turn cause even larger deflections ultimately leading to early failure of the beam.

Results from the analysis show that the fire resistance of unrestrained RC beams is not significantly affected by changing the span-to-depth ratio of the beam. This is because the span length has no effect on the moment capacity and the temperature distribution within the beam cross-section. Thus, maintaining the depth of the beam and changing its span length will not affect its fire resistance provided that the load level is maintained constant. Further, the large deflection and rate of deflection for longer beams are

associated with higher limits for deflection and rate of deflection as discussed in Chapter 4 (the limit for deflection is $L/20$ and is given by Eq. [4.75] for rate of deflection).

The fire resistance of restrained RC beams is significantly influenced by the span-to-depth ratio of the beam as can be seen from Table 6.2. Results in this table show that the fire resistance is considerably reduced by increasing the span-to-depth ratio. As an illustration, the fire resistance for the three beams (computed based on strength failure criteria) decreases from 200 minutes to 75 minutes when the span-to-depth ratio is increased from 8 to 18. This is mainly because slender beams are more susceptible to buckling under axial restraint force as discussed above. In general, the higher the span-to-depth ratio, the lower is the fire resistance provided that all other properties of the beam are maintained constant. It should be noted that the span-to-depth ratio is not considered in the current approach for evaluating the fire resistance of RC beams as discussed in Chapter 2. This may lead to unconservative fire resistance values for slender RC beams when the span-to-depth ratio is high.

6.4.5 Effect of Degree of Axial Restraint Stiffness

The effect of the degree of axial restraint on the fire response of RC beams can be gauged from the results predicted in Figure 6.10 and 6.11 and Table 6.2. Figure 6.10 shows the variation of deflection with fire exposure time for RC beams NS1SS2, NS1AS and NS1AS1 having span-to-depth ratio of 8, while Figure 6.11 shows the variation of deflection with fire exposure time for RC beams NS1SL1, NS1AL and NS1AL3 (with span-to-depth ratio of 18). The beams in each figure have an axial restraint stiffness of 0, 50, and 200 kN/mm, respectively, which represent typical values of axial restraint encountered in practice.

It can be seen from Figures 6.10 and 6.11 that the axial restraint stiffness significantly influence the deflection of RC beams exposed to fire. It can also be seen that the effect of axial restraint on RC beams exposed to fire is largely dependent on the span-to-depth ratio for beam. Figure 6.10 shows that for deep beams (low span-to-depth ratio), the deflection decreases for increased axial restraint stiffness at any stage of fire exposure. This is because the fire induced axial restraint force creates an arch action which leads to the development of a counteracting moment that reduces the effect of the applied loading (Dwaikat and Kodur 2008a). On the other hand, Figure 6.11 shows that for slender beams, the deflection increases for increased axial restraint stiffness at late stages of fire exposure. This is due to the P-δ effect which creates additional moments that increase the effect of the applied loading and thus increase deflections. Further, the low depth of the beam, compared to its span length, makes the developed arch action less efficient in reducing the deflection.

Results from the analysis presented in Table 6.2 show that the axial restraint stiffness has a significant effect on the fire resistance and its extent depends on the span-to-depth ratio of the beam. In general, the higher the axial restraint stiffness, the higher the fire induced axial restraint force. This produces buckling in the beam and thus lower fire resistance for slender beams with high span-to-depth ratio. However, for deep beams, increasing the axial restraint stiffness makes the arch action, developed under fire conditions, more effective and this in turn increases the fire resistance of the beam.

6.4.6 Effect of Location of Axial Restraint

The effect of the location of axial restraint on the fire response of RC beams is illustrated in Figure 6.12 and 6.13 and Table 6.2. Five positions of axial restraint (Y/H), namely, 0.3,

0.4, 0.5, 0.6, and 0.7 were used in the analysis. The definition of Y and H can be seen in Figure 6.12.

Figure 6.12 shows variation of deflection with fire exposure time for RC beams NS1AS1, NS1AS2, NS1AS, NS1AS4, and NS1AS5 having span-to-depth ratio of 8, while Figure 6.13 shows the variation of deflection with fire exposure time for RC beams NS1AL1, NS1AL2, NS1AL, NS1AL4, and NS1AL5 having span-to-depth ratio of 18.

It can be seen from Figures 6.12 and 6.13 that the location of axial restraint significantly influence the deflection of RC beams exposed to fire, particularly for deep beams (with low span-to-depth ratio). It can also be seen that the effect of location of axial restraint on the response of RC beams exposed to fire is largely dependent on the span-to-depth ratio for beam. Figure 6.12 shows that for deep beams (with low span-to-depth ratio) the deflection decreases when the position of the axial restraint is shifted downward (increasing Y/H) at any stage of fire exposure. This is because of the arch action, developed due to the axial restraint force, which becomes more efficient with the axial restraint force shifted downward. Figure 6.12 also shows that the deflection for beam NS1AS5 (for which the location of axial restraint is at 0.7 times the beam depth) increases at early stages of fire exposure and then decreases to reach a minimum value at about 300 minutes. This reduction is followed by increase in deflection at later stages of fire exposure until failure. This trend can be explained by the arch action, discussed above. At early stages of fire exposure, the developed axial restraint force is small and thus the arch action does not significantly reduce the effect of the applied loading. However, the developed axial restraint force increases with fire exposure time making the arch action more efficient in overcoming the effect of the applied loading and this in turn

reduces the deflection of the beam. At later stages of fire exposure, the axial restraint force decreases due to the large reduction in the stiffness of the beam leading to a reduced effect of the arch action and thus to increased deflections.

Figure 6.13 shows that for slender beams, the deflection decreases when the position of axial restraint is shifted downward at early stages of fire exposure. However, at late stages of fire exposure time and by shifting the axial restraint downward, the deflection increases to a maximum value and decreases again. The figure shows that the maximum deflection occurs at later stages of fire exposure and thus the minimum failure time are obtained when the axial restrain is at the geometrical centroid of the beam cross-section (Y/H =0.5). This can be attributed to the combined effect of the arch action and the P-δ effect as discussed in Section 6.4.5. At early stages of fire exposure, the fire induced axial force (P) and the deflection (δ) in the beam are small and thus the P-δ effect is small. Therefore, the response of the beam is predominantly controlled by the arch action which becomes more efficient when the location of the axial restraint is moved downward and this in turn reduces the deflection of the beam. However, despite the fact that the effect of the arch action is small when $Y/H < 0.5$, the developed axial force in this case is relatively small to cause flexural buckling of the beam at later stages of fire exposure. On the other hand, when $Y/H > 0.5$, the effect of the arch action is significant and dominates the behavior of the beam. Therefore, the deflection in the beam is smaller at later stages of fire exposure time. When Y/H is close to 0.5, the developed axial force is sufficiently large to cause early buckling in the beam as can be seen from Figure 6.13.

Results presented in Table 6.2 show that the position of axial restraint has a significant effect on the fire resistance of RC beams and the extent of influence depends on the span-

to-depth ratio. For deep beams, shifting the axial restraint downward makes the arch action, developed under fire condition, more effective and this will in turn increase fire resistance. However, for slender beams, minimum fire resistance is obtained when the axial restraint is at the geometrical centroid of the beam cross-section ($Y/H = 0.5$). This is mainly due to the combined effect of the arch action and the P-δ effect as discussed above.

6.4.7 Effect of Rotational Restraint

The effect of the rotational restraint on the fire response of RC beams can be gauged by looking at the results presented in Figure 6.14 and 6.15 and Table 6.2. The support conditions for the analyzed beams are assumed to be rotationally unrestrained and rotationally restrained. Figure 6.14 shows the variation of deflection with fire exposure time for beams NS2SM and NS2RM (simply supported and rotationally restrained, respectively), while Figure 6.15 shows the variation of deflection with fire exposure time for beams NS4AM and NS4ARM, which are axially, and axially and rotationally restrained, respectively.

Figures 6.14 and 6.15 shows that rotational restraint significantly reduces the deflection for both simply supported and axially restrained beams throughout the fire exposure duration. This can be attributed to the moment redistribution that occurs between span (positive moment) and support (negative moment) sections. This moment redistribution increases the strength and stiffness of the beam, which reduces the deflection and improves the fire response at any fire exposure time.

The fire resistance of the four beams is tabulated in Table 6.2. The table shows that rotational restraint significantly increases the fire resistance of RC beams. As an

illustration, the fire resistance of rotationally restrained beam NS2RM is about 150 minutes higher than that for simply supported beam NS2SM. This can be attributed to the moment redistribution (under fire exposure conditions) taking place between the support and the mid-span moments, which increases the capacity of the beam. Further, under fire exposure, the negative moment capacity at the beam supports decreases with relatively lower rates when compared to the span moment capacity. This is because the tension rebars at support sections are relatively at farther depths from the fire exposed surface of the beam. Thus, the temperatures in these rebars are much lower and hence the strength loss is minimal.

Table 6.2 also shows that deflection and rate of deflection limit states are not likely to be exceeded for rotationally, and axially and rotationally restrained RC beams. This is because of the influence of the developed arch action and support moments which significantly reduce the deflection and rate of deflection of the beams.

6.4.8 Effect of Fire Scenario

To investigate the effect of fire scenario on the response of RC beams, ten RC beams were analyzed under two standard fire scenarios; namely, ASTM E119a (2008) standard fire and ASTM E1529 (1993) hydrocarbon fire, and three design fire scenarios; namely Fire I, Fire II, and Fire III. There is no decay phase in the time temperature curves of the standard fire scenarios. However, in realistic fires (represented by the three design fires), there always exist a decay phase, since the amount of fuel or ventilation runs out leading to burn out of fire.

The parametric fire time-temperature curve proposed in Eurocode 1 (2002) and the recent modifications suggested by Feasey and Buchanan (2002) are selected to represent the

design fire scenarios. According to Eurocode 1, the design fire consists of a growth and a decay phase. Feasey and Buchanan (2002) shows that both the growth and decay phases of the fire are influenced by compartment properties such as the fuel load, ventilation opening and wall linings.

To develop the three design fire scenarios, a fire is assumed to occur in a room with dimensions of 6 m x 4 m x 3 m. Three values of fuel load, and opening dimensions are also assumed. More details on the properties of the room for the three fires are shown in Table 6.3. The values were assumed in such a way that Fire I represents a severe design fire whose temperatures exceeds 1200°C, Fire II represents a small design fire whose temperature reaches 700°C, and Fire III represents a moderate design fire. Fire I represents a typical (real) fire in a library or storage room where large amount of combustible materials and sufficient ventilation are available. Fire II and Fire III represent typical (real) fire in a residential room with small and reasonable amount of combustible material and ventilation, respectively. The time-temperature curves for the two standard fire scenarios and the three design fire scenarios are shown in Figure 6.1.

Figure 6.16 shows the variation of deflection with fire exposure time for five simply supported RC beams, namely, NC1SL1, NC1SL2, NC1SL3, NC1SL4, and NC1SL5, under ASTM E119 standard fire, ASTM E1529 hydrocarbon fire, Fire I, Fire II and Fire III, respectively. It can be seen from Figure 6.16 that the deflection and the rate of deflection increase with time for the four beams at early stages of fire exposure. However, Figure 6.16 shows reduction (recovery) in deflection for three beams exposed to the design fires at later stages of fire exposure. This is because of the presence of decay phase in design fires in which the beam starts cooling and recovers part of its strength and

stiffness. Figure 6.16 also shows that beam NC1SL2 exposed to hydrocarbon fire experiences higher deflection, particularly at later stages of fire exposure as compared to beam NC1SL1 (exposed to ASTM E119 standard fire). This is due to the steep increase in the temperature of the hydrocarbon fire at early stages of fire exposure (as can be seen in Figure 6.1), which increase the rebar and concrete temperature and thus increases the deflection of the beam.

Similar trends are observed in Figure 6.17 for axially restrained beams NC1AS1, NC1AS2, NC1AS3, NC1AS4 and NC1AS5 under ASTM E119 standard fire, ASTM E1529 hydrocarbon fire, Fire I, Fire II and Fire III, respectively. However, the difference in deflections between beam NC1AS2 (exposed to hydrocarbon fire) and beam NC1AS1 (exposed to ASTM E119 standard fire) becomes small at later stages of fire exposure as can be seen from Figure 6.16. This can be attributed to the fact that after about 225 minutes the temperature for the ASTM E119 fire becomes higher than that of the hydrocarbon fire as shown in Figure 6.1. The higher temperature of the ASTM E119 fire increases the rebar and concrete temperatures and thus the deflection of the beam.

Results from the analysis show that the fire exposure has significant effect on the fire resistance of RC beams, calculated based on different failure criteria (see Table 6.2). It can be seen, from Table 6.2, that the lowest fire resistance is obtained for the beams exposed to the hydrocarbon fire, and it is about 35 minutes lower than that for the simply supported beam under the ASTM E119 standard fire exposure. This is due to the high increase in fire temperature for the hydrocarbon fire as can be seen in Figure 6.1. Table 6.2 also shows that one out of the six beams exposed to design fire attains failure, which was based on deflection (or rate of deflection) failure criteria. It can also be noted that the

beam failing under design fire exposure is simply supported. However, none of the beams exposed to design fire exposure, and axially restrained, attained failure based on the strength and deflection failure criteria. Hence, in spite of the severe conditions assumed for design fire (Fire I), failure is attained only under simply supported conditions. This result shows that in many applications, the fire resistance values computed based on standard fire scenarios, may be conservative if the resulting fires have a decay phase, similar to the ones used in this study.

6.4.9 Effect of Concrete Strength and Spalling

To investigate the effect of concrete strength (HSC or NSC) and fire induced spalling, six HSC and NSC beams designated as NS1SM, HS1SM, NS1AM1, HS1AM, NS1RM, and HS1RM, were analyzed. The permeability at the top side (k_{top}) is assumed to be 10^{-16} m^2 and 10^{-20} m^2 for NSC and HSC beams, respectively. The spatial variation of permeability is assumed to follow Eq. [4.51] presented in Chapter 4 and its calibration in Chapter 5. The depth to the neutral axis under service loads (x in Eq. [4.51]) was computed as per ACI 318 for NSC and HSC beams. For the analyzed beams, the spalling depth (total thickness of concrete layer that spall off) is assumed not to exceed the concrete cover thickness. This is in agreement with what has been observed in previous fire resistance tests on concrete beams and columns, including the fire test presented in Chapter 3 (Dwaikat and Kodur 2009, Park et al. 2007). The analysis shows that no fire induced spalling occurs in NSC beams, while significant spalling (most of which is on the upper sides of the beam as discussed in Chapter 3 and Chapter 5) occurs in HSC beams. Results from the analysis are given in Figures 6.18, 6.19, and 6.20 and Table 6.2.

Figure 6.18 shows the effect of concrete strength and spalling on the mid-span deflection of simply supported RC beams. It can be seen that concrete strength and spalling have minor influence on the overall fire response of simply supported RC beams. This can be attributed to the fact that the fire response of simply supported RC beams is generally governed by the temperature of tension rebars which is not significantly influenced by concrete strength and fire induced spalling. In general, the moment capacity of an RC beam is governed by the area and the yield strength of tension reinforcement. Under fire conditions, and due to the fact that the area of steel remains constant, the reduction of the moment capacity of the beam mainly results from the degradation in the strength of the tension reinforcement which is directly related to rebar temperature. Due the spatial variation of permeability, spalling generally occurs in the upper part of the beam as observed in the fire tests presented in Chapter 3. Thus, spalling in the upper side of the beam does not have significant effect on the temperature of tension reinforcement (which is located at the bottom part of the beam cross-section for simply supported beams.

However, Figure 6.19 shows that concrete strength and spalling have significant effect on the deflection of axially restrained RC beams. The mid-span deflection in the HSC beam (which experiences severe spalling) is higher than that for NSC beam at later stages of fire exposure time. This increase in deflection for HSC beams results from two factors: the faster degradation of strength in the case of HSC and the occurrence of spalling in HSC beams due to the low permeability and high compactness of HSC. Spalling reduces the cross-sectional area of the concrete, and thus the moment capacity and stiffness, particularly for axially restrained beams, where the behavior is not governed by only the

rebar temperature. This results in higher deflection and early failure in axially restrained HSC beams.

Figure 6.20 shows the effect of concrete strength and spalling on the deflection of rotationally restraint RC beams. It can be seen that concrete strength and fire induced spalling significantly increase the deflection throughout the fire exposure time. This can be attributed to the fact that spalling reduces the concrete cover thickness for top reinforcement which is associated with a significant increase in temperature of top rebars leading to a large reduction in the negative (support) moment capacity of the beam. The reduction in support moment capacity significantly decreases the strength and stiffness of the beam leading to larger deflection and early failure as can be seen from Figure 6.20.

Concrete strength and spalling has significant effect on the fire resistance of rotationally and axially restrained RC beams as can be seen from Table 6.2. As an illustration, the fire resistance of rotationally restrained beam NS1RM (made of NSC) is about 300 minutes, whereas the fire resistance of beam HS1RM (made of HSC) is only 120 minutes. The reduction in the fire resistance of an HSC beam results from the faster degradation of strength and the occurrence of spalling in the HSC beam as discussed above. Spalling reduces the concrete cover thickness and beam cross-section, and thus the moment capacity and stiffness of the beam. This results in early failure and lower fire resistance in HSC beams.

However, the effect of concrete strength on the fire resistance of simply supported RC beams is minor as can be seen from Table 6.2. As an illustration, HSC concrete beam HS1SM has fire resistance of about 10 minutes lower that of NSC beam NS1SM. The small effect of concrete strength and spalling on the fire resistance can be attributed to the

fact that the fire resistance of simply supported beams is mainly governed by rebar temperature (provided that load ratio is maintained constant) which is not significantly affected by concrete strength or spalling.

6.4.10 Effect of Failure Criteria

The fire resistance for all analyzed beams was computed according to three sets of failure criteria, namely, strength, deflection and rate of deflection failure criteria, and is tabulated in Table 6.2. Rebar temperature failure criterion is not considered in the analysis because this failure criterion is prescriptive and does not represent the actual failure of the beam. Further, rebar temperature failure criteria does not take into consideration high temperature mechanical properties of the constituent materials, load ratio, support conditions and fire induced spalling.

Deflection and rate of deflection failure criteria predicts smaller fire resistance values than those predicted by strength failure criterion for many of the analyzed beams as can be seen from Table 6.2. Although, actual failure of an RC beam occurs when the strength limit state is reached, deflection and rate of deflection may be important in many applications to maintain the integrity of the structure so as to facilitate the fire fighters work, and to safely evacuate the occupants before the collapse of the structure. Therefore, under some fire scenarios, deflection or rate of deflection failure criterion may govern the failure of RC beams and govern their fire resistance. As explained earlier, ASTM E119 does not specify deflection or rate of deflection failure criterion. However, such deflection and rate of deflection limit states are specified in BS 476 (1987).

Thermal failure criterion, which is often used, is clearly insufficient to define the failure of RC beams because it does not consider important factors such as load ratio that may

significantly influence the fire response of the beam. It should be noted that the current fire resistance provisions in codes such as ACI 216.1 and Eurocode 2 are mainly based on thermal failure criterion, and this may not lead to realistic fire resistance of RC beams, especially under varying load levels.

6.4 Summary

This chapter presents results of parametric studies to illustrate the influence of various factors on the fire response of RC beams. The studied parameters are: section characteristics, load ratio, aggregate type, axial restraint stiffness, span-to-depth ratio, location of axial restraint, rotational restraint, fire scenario, concrete strength and spalling, and failure criteria. Data from parametric studies indicates that fire scenario, load ratio, span-to-depth ratio, location of axial restraint and rotational restraint have significant influence on the fire response of RC beams. The parameters that have moderate influence are: sectional dimensions (concrete cover thickness and beam width), aggregate type (carbonate or siliceous aggregate), degree of axial restraint, concrete strength and spalling, and failure criteria. Results from the parametric studies are utilized in Chapter 7 to develop guidelines for evaluating fire resistance of RC beams.

Table 6.1 – Properties for Concrete Cross-sections used in the Analysis

Property	Cross-section #			
	1	2	3	4
Cross-section (mm)	300 × 900	400 × 800	700 × 400	600 × 600
Reinforcement for simply supported and axially restrained	2 ϕ 14 mm top bars	2 ϕ 14 mm top bars	3 ϕ 14 mm top bars	3 ϕ 14 mm top bars
	5 ϕ 20 mm bottom bars	3 ϕ 35 mm bottom bars	6 ϕ 20 mm bottom bars	8 ϕ 20 mm bottom bars
Reinforcement for rotationally restrained beams	5 ϕ 20 mm top bars	3 ϕ 35 mm top bars	6 ϕ 20 mm top bars	8 ϕ 20 mm top bars
	4 ϕ 20 mm bottom bars	3 ϕ 30 mm bottom bars	4 ϕ 20 mm bottom bars	5 ϕ 20 mm bottom bars
f'_c (MPa) (for NSC beams)	40	60	30	50
f'_c (MPa) (for HSC beams)	100	100	100	100
f_y (MPa)	413	413	413	413
Concrete cover thickness (mm)	40	60	40	50

Table 6.2 – Summary of the Fire Resistance Values for the Analyzed Beams

Studied parameter	Beam designation*	LR (%)	Y/H	k_r (kN/mm)	Fire resistance based on failure criterion (in minutes)		
					Strength	Deflection	Rate of deflection
Section characteristics	NS1SM	50	0.5	0	135	123	115
	NS2SM	50	0.5	0	215	192	189
	NS3SM	50	0.5	0	183	165	166
	NS4SM	50	0.5	0	233	217	218
	NC1AM	50	0.5	50	143	NF	138
	NC2AM	50	0.5	50	228	227	223
	NC3AM	50	0.5	50	195	NF	192
	NC4AM	50	0.5	50	253	NF	249
Load ratio	NS1SS1	30	0.5	0	168	160	143
	NS1SS2	50	0.5	0	135	128	115
	NS1SS3	70	0.5	0	108	105	93
	NC3AM1	30	0.5	50	258	NF	254
	NC3AM	50	0.5	50	195	NF	192
	NC3AM2	70	0.5	50	145	NF	NF
Aggregate type	NS2SM	50	0.5	0	215	192	189
	NC2SM	50	0.5	0	283	245	244
	NS4AM	50	0.5	50	198	NF	194
	NC4AM	50	0.5	50	253	NF	249
Span-to-depth ration	NS1AS	50	0.5	50	200	NF	194
	NS1AM	50	0.5	50	110	NF	106
	NS1AL	50	0.5	50	75	74	70
Degree of axial restraint	NS1SS2	50	0.5	0	135	128	115
	NS1AS	50	0.5	50	200	NF	194
	NS1AS1	50	0.5	100	210	NF	206
	NS1SL1	50	0.5	0	135	117	115
	NS1AL	50	0.5	50	75	74	70
	NS1AL3	50	0.5	100	63	61	56
Location of axial restraint	NS1AS1	50	0.3	50	123	NF	115
	NS1AS2	50	0.4	50	143	NF	137
	NS1AS	50	0.5	50	200	NF	194
	NS1AS4	50	0.6	50	378	NF	373
	NS1AS5	50	0.7	50	588	NF	582
	NS1AL1	50	0.3	50	98	96	91
	NS1AL2	50	0.4	50	90	88	83
	NS1AL	50	0.5	50	75	74	70
	NS1AL4	50	0.6	50	80	NF	77
	NS1AL5	50	0.7	50	110	NF	106
Rotational restraint	NS2SM	50	0.5	0	215	192	189
	NS2RM	50	0.5	0	363	NF	NF
	NS4AM	50	0.5	50	198	NF	194
	NS4ARM	50	0.5	50	498	NF	NF

Table 6.2 (Continued) – Summary of the Fire Resistance Values for the Analyzed Beams

Studied parameter	Beam designation*	LR (%)	Y/H	k_r (kN/mm)	Fire resistance based on failure criterion (in minutes)		
					Strength	Deflection	Rate of deflection
Fire scenario	NC1SL1	50	0.5	0	170	146	149
	NC1SL2	50	0.5	0	133	113	113
	NC1SL3	50	0.5	0	NF	105	105
	NC1SL4	50	0.5	0	NF	NF	NF
	NC1SL5	50	0.5	0	NF	NF	NF
	NC1AS1	30	0.5	200	428	NF	425
	NC1AS2	30	0.5	200	425	NF	423
	NC1AS3	30	0.5	200	NF	NF	NF
	NC1AS4	30	0.5	200	NF	NF	NF
	NC1AS5	30	0.5	200	NF	NF	NF
Concrete type and spalling	NS1SM	50	0.5	0	135	123	113
	HS1SM	50	0.5	0	130	118	105
	NS1AM1	50	0.5	200	98	NF	95
	HS1AM	50	0.5	200	80	NF	75
	NS1RM	50	0.5	0	318	307	298
	HS1RM	50	0.5	0	120	NF	NF

N/H – HSC/NSC S/C – siliceous/carbonate aggregate 1/2/3/4 – cross-sectional size (refer to Table 6.1 for cross-sectional sizes)
S/A/R/AR – simply suppurated/axially restrained/rotationally restrained/axially and rotationally restrained
S/M/L – small/medium/large span-to-depth ratio.

Table 6.3 - Compartment Characteristics used to Generate Design Fire Scenarios

Design Fire	Lining material	Thermal capacity of lining material ($W.s^{0.5}/m^2.K$)	Opening dimension (m)	Fire load (MJ/m^2 floor area)
Fire I	Gypsum board	488	2.25 × 1.5	1200
Fire II	Concrete	1900	2.85 × 1	400
Fire III	Concrete + gypsum board	1200	2.15 × 1	1000

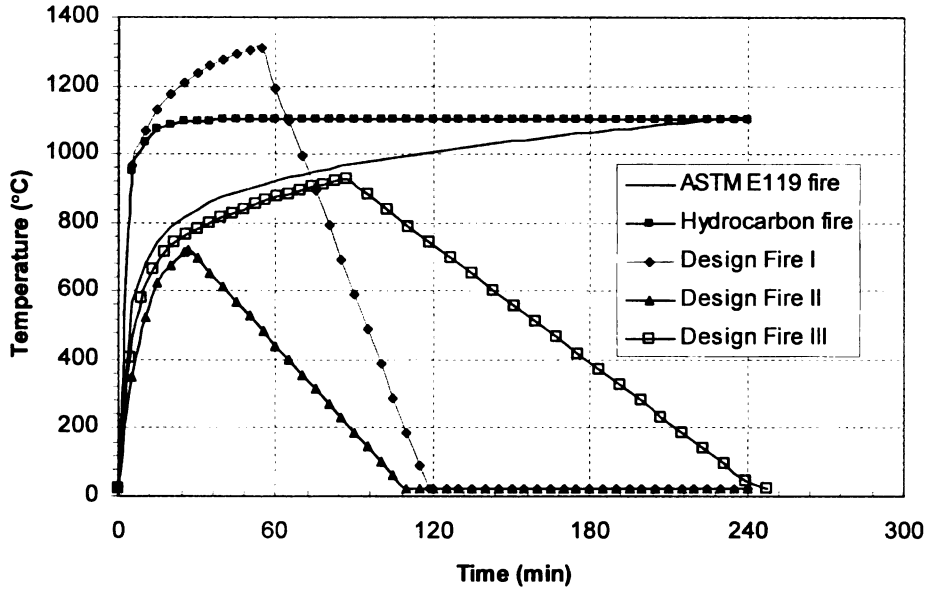

Figure 6.1 – Time-temperature Curves for Fire Scenarios used in the Analysis

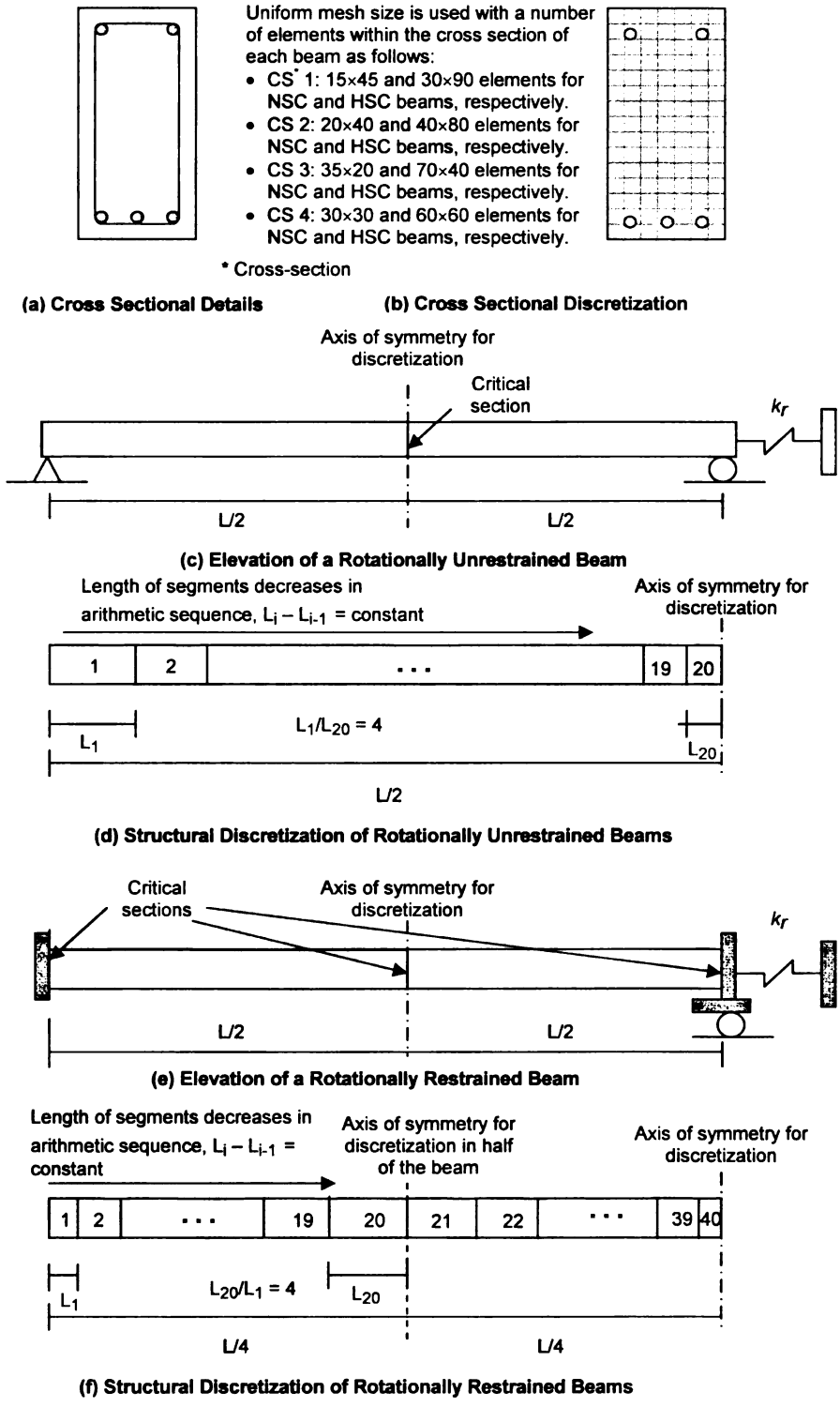

Figure 6.2 – Structural and Cross-sectional Discretization of the Analyzed Beams

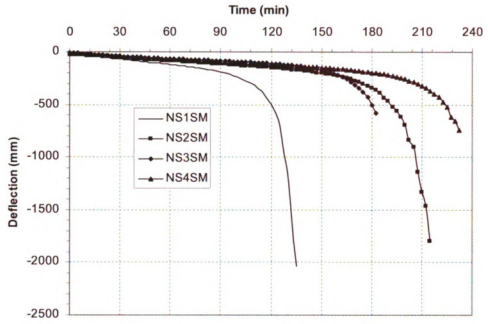

Figure 6.3 – Effect of Section Characteristics on the Deflection of Simply Supported RC Beams Exposed to Fire

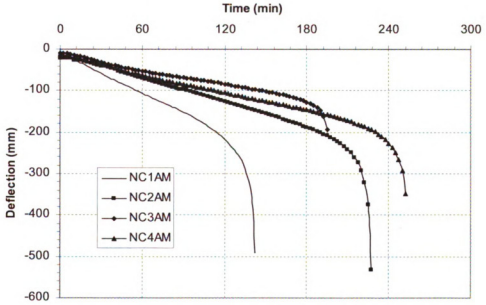

Figure 6.4 – Effect of Section Characteristics on the Deflection of Axially Restrained RC Beams Exposed to Fire

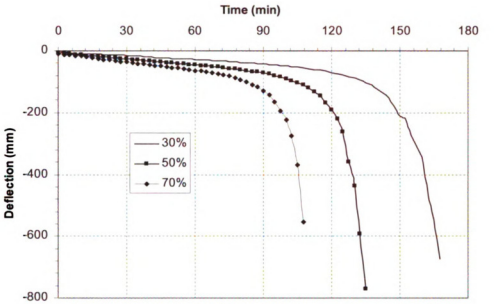

Figure 6.5 – Effect of Load Ratio on the Deflection of Simply Supported RC Beams Exposed to Fire

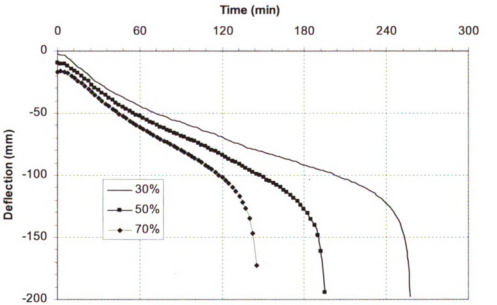

Figure 6.6 – Effect of Load Ratio on the Deflection of Axially Restrained RC Beams Exposed to Fire

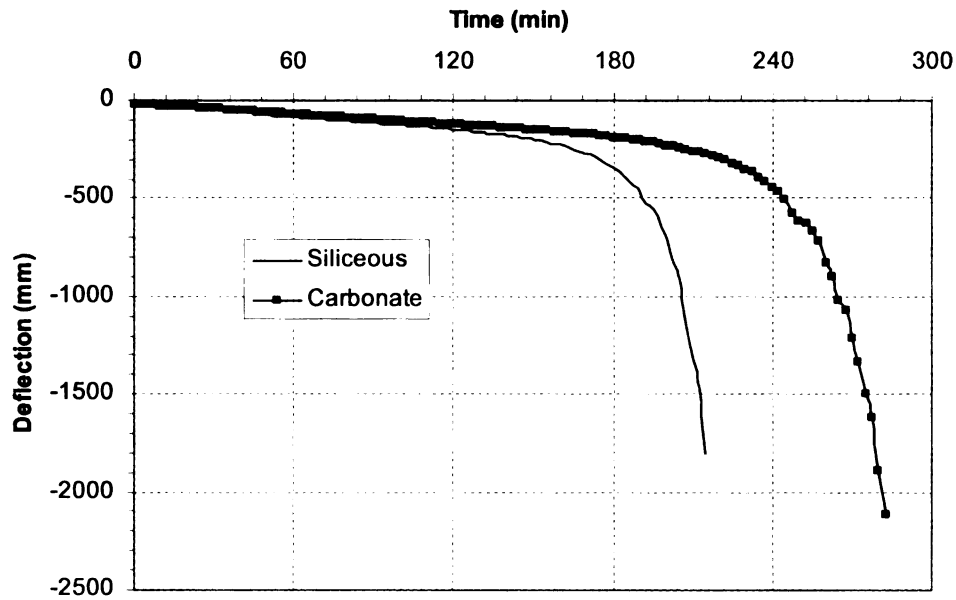

Figure 6.7 – Effect of Aggregate Type on the Deflection of Simply Supported RC Beams Exposed to Fire

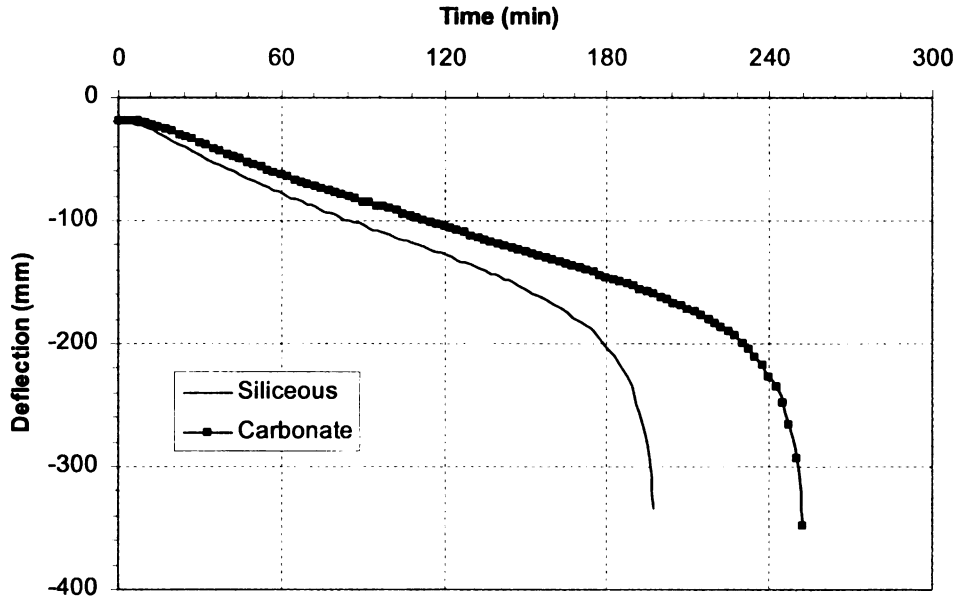

Figure 6.8 – Effect of Aggregate Type on the Deflection of Axially Restrained RC Beams Exposed to Fire

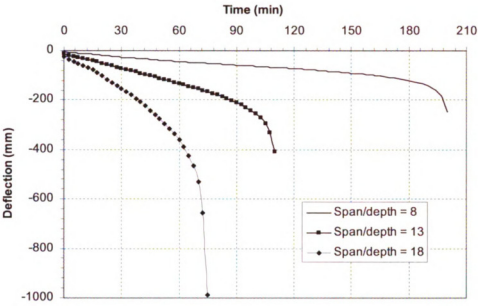

Figure 6.9 – Effect of Span-to-depth Ratio on the Deflection of Axially Restrained RC Beams Exposed to Fire

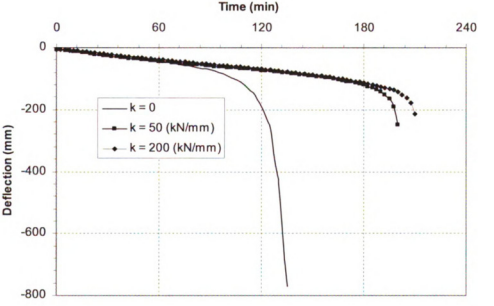

Figure 6.10 – Effect of Axial Restraint Stiffness on the Deflection of RC Beams Exposed to Fire (Span-to-depth Ratio = 8)

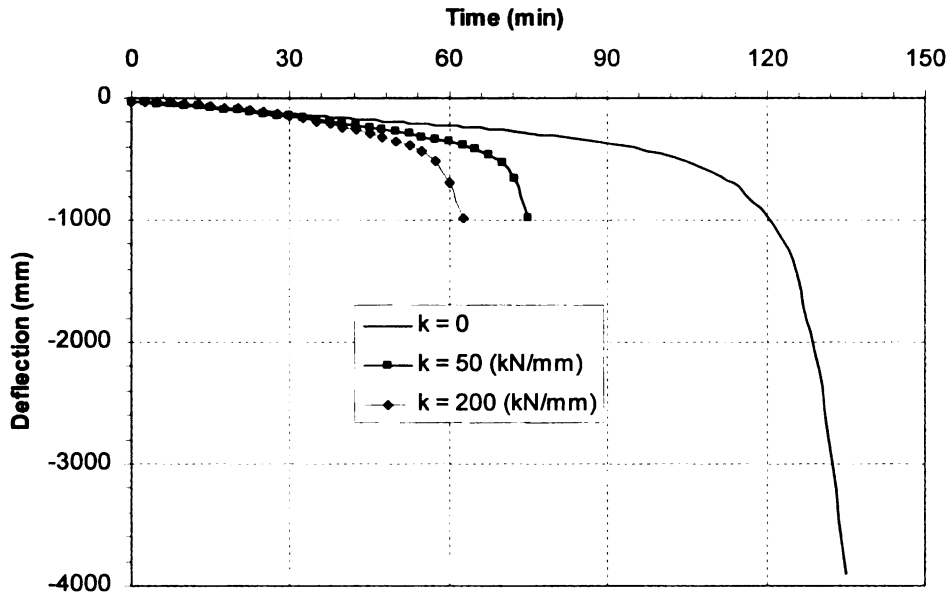

Figure 6.11 – Effect of Axial Restraint Stiffness on the Deflection of RC Beams Exposed to Fire (Span-to-depth Ratio = 18)

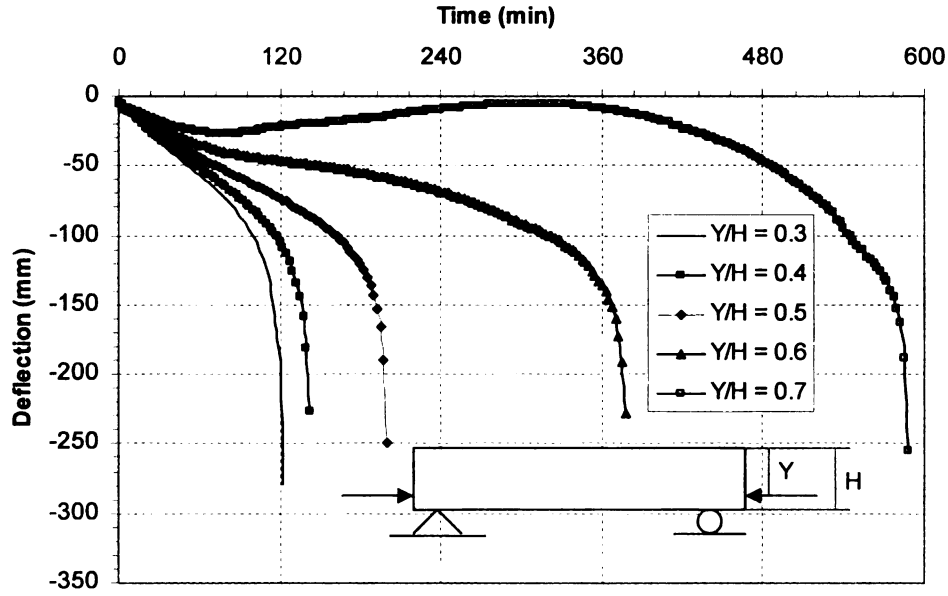

Figure 6.12 – Effect of Location of Axial Restrained on the Deflection of RC Beams Exposed to Fire (Span-to-depth Ratio = 8)

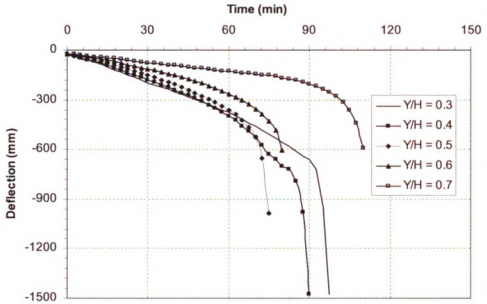

Figure 6.13 – Effect of Location of Axial Restrained on the Deflection of RC Beams Exposed to Fire (Span-to-depth Ratio = 18)

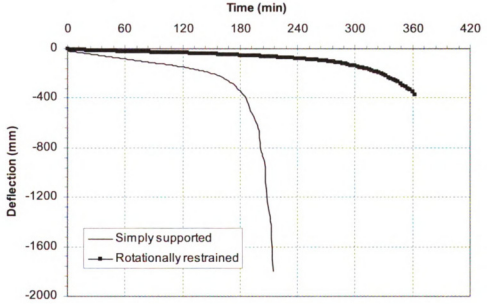

Figure 6.14 – Effect of Rotational Restraint on the Deflection of Simply Supported RC Beams Exposed to Fire

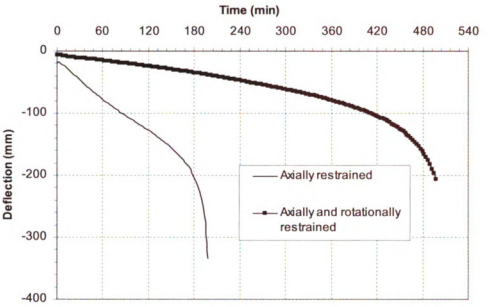

Figure 6.15 – Effect of Rotational Restraint on the Deflection of Axially Restrained RC Beams Exposed to Fire

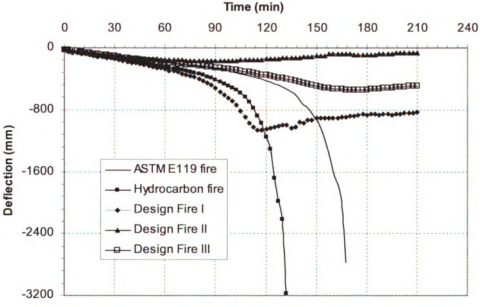

Figure 6.16 – Effect of Fire Scenario on the Deflection of Simply Supported RC Beams Exposed to Fire

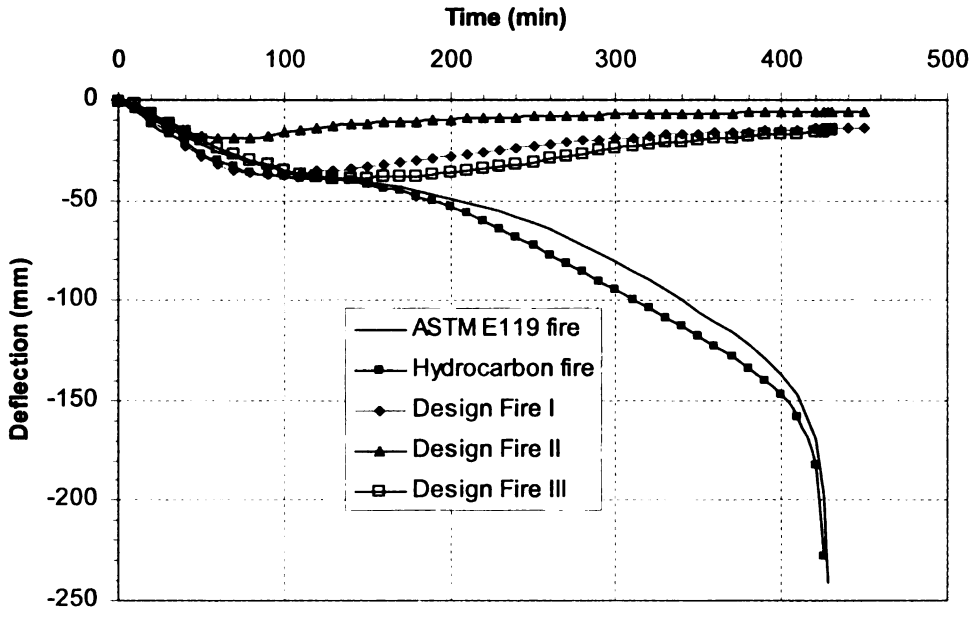

Figure 6.17 – Effect of Fire Scenario on the Deflection of Axially Restrained RC Beams Exposed to Fire

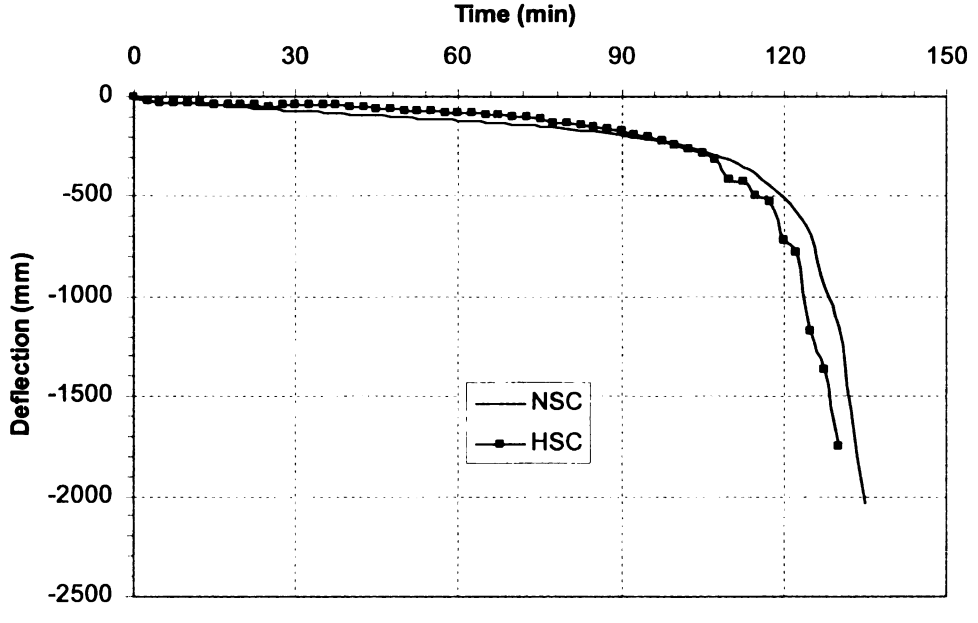

Figure 6.18 – Effect of Concrete Strength on the Deflection of Simply Supported RC Beams Exposed to Fire

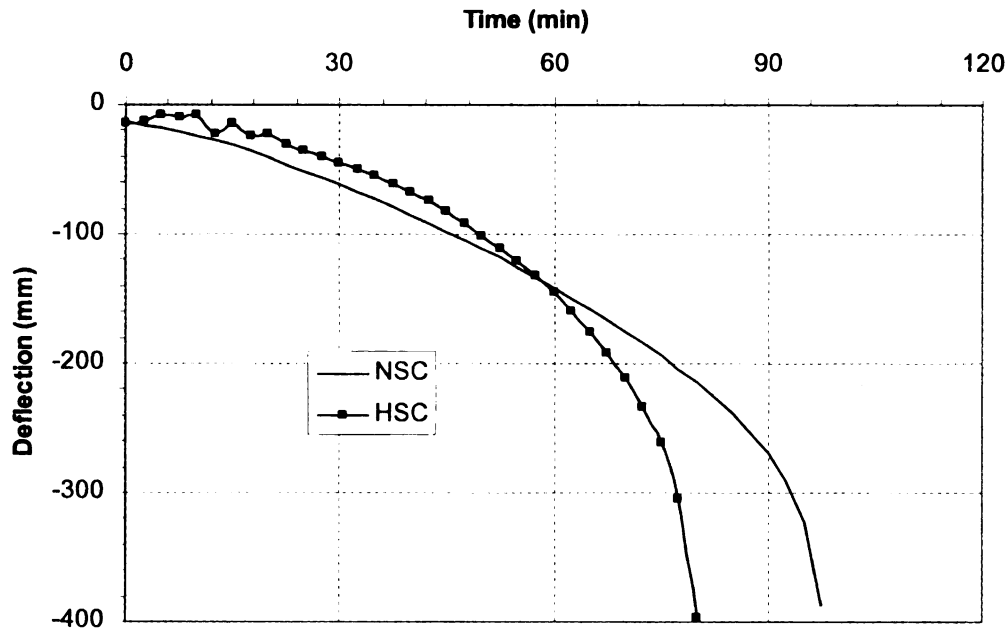

Figure 6.19 – Effect of Concrete Strength on the Deflection of Axially Restrained RC Beams Exposed to Fire

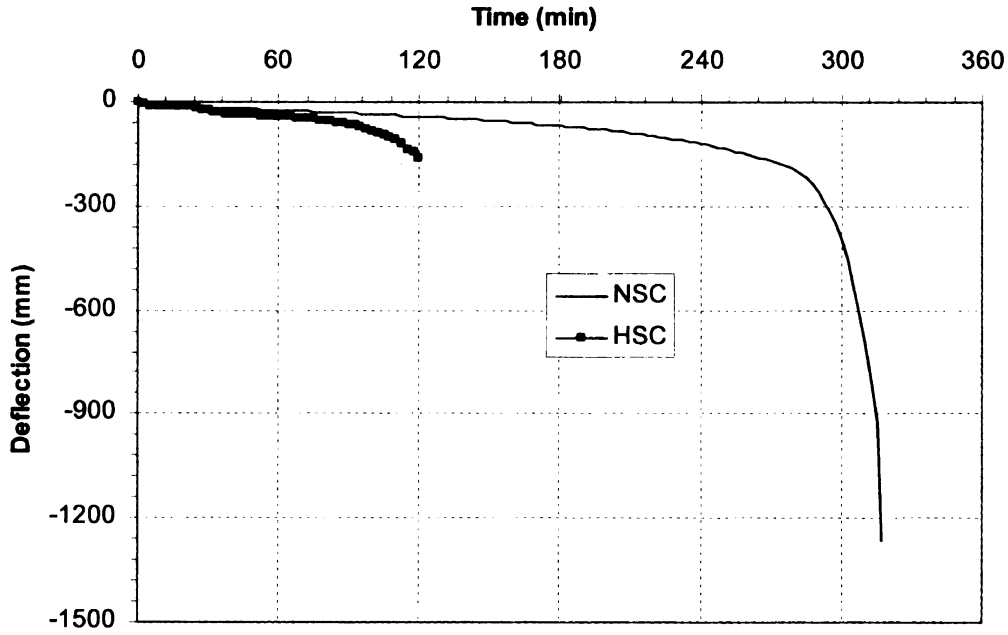

Figure 6.20 – Effect of Concrete Strength on the Deflection of Rotationally Restrained RC Beams Exposed to Fire

Chapter 7

7. Design Approach

7.1 General

As illustrated in Chapter 2, the current approaches for evaluating fire resistance of RC beams are prescriptive and do not account for critical factors that govern the response. To overcome some of these drawbacks, a rational approach is developed for predicting the fire resistance of RC beams. The approach comprises two main steps, namely, an empirical equation for evaluating fire resistance of an RC beam under standard fire exposure and establishing time equivalency between standard and design fire exposure. The proposed approach is derived based on results from the parametric studies presented in Chapter 6. The development of the simplified equation and time equivalency approach is illustrated in this Chapter. The validity of the proposed approach is established by comparing the fire resistance predictions with values from numerical studies as well as from fire resistance tests. Predictions from the proposed equation are also compared with

fire resistance estimates from current codes of practice. The applicability of the approach to design situations is illustrated through a numerical example.

7.2 Methodology for Evaluating Fire Resistance

7.2.1 Factors Governing Fire Resistance

Data from parametric studies presented in Chapter 6 indicate that the main factors that strongly influence fire resistance of RC beams are fire scenario, load ratio, span-to-depth ratio, location of axial restraint, and rotational restraint. Factors that have a moderate influence on the fire resistance of RC beams are sectional dimensions (concrete cover thickness and beam width), aggregate type (carbonate or siliceous aggregate), degree of axial restraint, concrete strength and spalling, and failure criteria.

An empirical equation, which accounts for various significant parameters, is developed for predicting the fire resistance of RC beams. For deriving such an equation, results from the parametric studies presented in Chapter 6 are utilized. Development of an empirical equation for fire resistance is quite involved due to the large number of parameters and the interdependency among them. Details on the development of the empirical equation are presented in the following sections.

7.2.2 General Approach

An approach for evaluating fire resistance of RC beams is outlined. Contrary to the current prescriptive approaches, the goal of the proposed method is not to determine the fire resistance of an RC beam under design fire exposure, but to determine if an RC beam can survive in a design fire scenario. In general, the design approach involves two steps, namely:

- Evaluating the fire resistance of the RC beam (R) under standard fire exposures, using a simplified equation,
- Determining the time equivalent (t_e) under a design fire scenario utilizing equivalent energy concept, and then checking failure of the beam (under a design fire exposure) which is said to occur when:

$$t_e > R \quad \Rightarrow \quad \text{Failure} \qquad [7.1]$$

where:

R = fire resistance of RC beam, and

t_e = time equivalent.

The proposed approach is carried out by giving full consideration to critical parameters, including fire scenario, load ratio, restraint effects, and failure criteria (key parameters for performance-based fire safety design as discussed in Chapter 2), that influence the fire resistance of RC beams. Critical parameters (such as section characteristics, load ratio, axial restraint, rotational restraint, span-to-depth ratio, and aggregate type) are accounted for in deriving the fire resistance equation under standard fire exposure. In the second step fire scenario is accounted for in evaluating the time equivalent.

7.3 Equation for Fire Resistance under Standard Fire

In the proposed design approach, the first step is to evaluate the fire resistance of an RC beam under standard fire exposure. This is achieved in a two sub-step process wherein fire resistance is first estimated based on thermal considerations and then correction factors are applied to account for all relevant factors influencing fire resistance.

- The first step is to estimate an initial value of the fire resistance, R_0. An initial value of fire resistance can be computed based on the thermal response of the beam by applying rebar temperature failure criteria. However, since fire resistance provisions in current codes and standards (such as ACI 216.1, Eurocode 2 and AS 3600) are mainly derived based on rebar temperature failure criteria, it is reasonable to estimate R_0 based on the tabulated fire resistance in these codes. To develop a base value for estimating R_0, twenty simply supported RC beams were analyzed. The beams were assumed to be made of four cross-sections given in Table 6.1. For each cross-section, five values of concrete cover thickness to rebar, namely, 30, 40, 50, 60 and 70 mm, were assumed in the analysis. The fire resistance for the analyzed beams is computed based on rebar temperature failure criteria as well as using the prescriptive provisions in three codes of practice (ACI 216.1, Euocode 2 and AS 3600). The results are plotted in Figure 7.1. It can be seen from the figure that the fire resistance computed based on ACI 216.1 is higher than the predicted value (from the numerical model) for most of the analyzed beams. It can also be seen that ACI 216.1 predicts the same fire resistance for many of the beams having different concrete cover thickness and cross-sectional dimensions. It should also be noted that ACI 216.1 specifies a fire resistance rating at a large time increment (1, 2, 3, and 4 hours) and may not provide reliable fire resistance with finer time increments. Thus, ACI 216.1 may not provide a reasonable estimate for R_0.

Figure 7.1 also shows that the Eurocode 2 and Australian code predictions are similar. However, the Australian code provisions specify different combinations of concrete cover thickness and beam widths to obtain a required fire resistance rating. Further, similar to ACI 216.1, Eurocode 2 provisions specify fire resistance rating at relatively large time increment (30 minutes) compared to the Australian code. Thus, the graph in the Australian code, reproduced in Figure 7.2, is selected to obtain an initial estimate of fire resistance, R_0. It should be noted that R_0 is an estimate and any graph similar to that in Figure 7.2 can be applied.

- The second step in computing fire resistance is to apply modification factors to estimated R_0 values to account for other critical factors that influence fire resistance of the beam. Three modification factors are to be applied, namely:
    - A 'structural factor' to account for the influence of support conditions (simply supported (SS), axially restrained (AR), eccentrically axially restrained (ER), rotationally restrained (RR), and rotationally and axially restrained (FR)), load ratio, location of axial restraint, and span-to-depth ratio.
    - An 'aggregate factor' to account for the influence of aggregate (siliceous or carbonate) in concrete.
    - A 'strength factor' to account for the influence of concrete strength and spalling.

Data from the parametric studies presented in Chapter 6 are used to establish these modification factors. In these parametric studies, about 900 NSC beams with four RC

cross-sections, and two aggregate types were analyzed. This produced 8 section-aggregate combinations.

Three values of span-to-depth ratio (8, 13, and 18), three values of load ratio (30%, 50% and 70 %), three values of axial restraint stiffness (0, 50 kN/mm and 200 kN/mm), and five values of the location of the axial restraint (0.3, 0.4, 0.5, 0.6 and 0.7) were used in the analysis. In addition, a number of HSC beams were analyzed to estimate the modification factors that account for concrete type and spalling. The HSC beams had the same characteristics as NSC beams except for concrete strength.

Results from the analysis are used to derive the fire resistance of beams based on strength, deflection, and rate of deflection limit states. The minimum failure times computed based on these three limit states is considered to be the fire resistance of the beam. The computed fire resistance values of the analyzed beams are utilized to develop a relationship for the three modification factors using regression analysis. The fire resistance data for the analyzed NSC beams, made of siliceous aggregate concrete, is used to establish relationships for the structural factor. The rest of the data is used to compute the aggregate and strength factors. Analysis results of the beams were randomly divided into two sets of which one set is used for regression analysis (calibration) and the other set is used for verification (validation).

Results from the regression analysis indicate that the fire resistance of an RC beam can be expressed as:

$$R = \phi_{st}\phi_{ag}\phi_{cs}R_0 \qquad [7.2]$$

where:

R = fire resistance of RC beam,

R_0 = initial estimate of fire resistance obtained from Figure 7.2,

ϕ_{st} = structural modification factor,

ϕ_{ag} = aggregate modification factor, and

ϕ_{cs} = strength modification factor.

Preliminary regression analysis indicates that ϕ_{st} mainly depends on support conditions, load ratio, axial restraint stiffness, location of axial restraint, span-to-depth ratio, and section characteristics. Based on the relationship between ϕ_{st} and these parameters, five empirical relationships were developed for the five support conditions (SS, AR, ER, RR and FR). For each support condition, the empirical relationships were developed such that its predictions had minimal variation from the values predicted by the finite element model. Regression analysis was carried out using statistical software 'SPSS' to find functions that accurately fit the data for different support conditions. It was found that the residuals from the regression analysis are not uniformly distributed for AR and ER beams. Thus, transformation (logarithmic) is used for predicted and simulated values to reduce the non-uniformity of the residuals for these two cases (AR and ER). The regression analysis is repeated for AR and ER with the transformed values to find the functions that best fit the data. The obtained functions for the five support conditions were then simplified to arrive at the following equations:

$$\phi_{SS} = 1.4 - LR - 0.02\psi_0 \qquad [7.3]$$

$$\phi_{AR} = 0.9\phi_{SS} - 0.2\left(\frac{L}{H} - 14\right)(0.1 + ax) \qquad [7.4]$$

ϕ_E

ϕ_R

ϕ_F

wh

ϕ_{SS}

ϕ_{1R}

ϕ_{ER}

ϕ_{RR}

ϕ_{FR}

ψ_0 =

ρ =

SF =

χ =

LR =

L =

H =

Y =

secti

$$\phi_{ER} = 0.8\begin{cases} 0.8\phi_{AR} + 0.2, & \frac{Y}{H} < 0.6 \\ \phi_{AR} + \left(18 - \frac{L}{H}\right)\left(\frac{Y}{H} - 0.6\right) & \frac{Y}{H} \geq 0.6 \end{cases} \quad [7.5]$$

$$\phi_{RR} = \phi_{SS} + 3 - 3.7LR \quad [7.6]$$

$$\phi_{FR} = \phi_{RR} + 0.5\phi_{AR}^2 \quad [7.7]$$

where:

ϕ_{SS} = structural factor for SS beams,

ϕ_{AR} = structural factor for AR beams,

ϕ_{ER} = structural factor for ER beams,

ϕ_{RR} = structural factor for RR beams,

ϕ_{FR} = structural factor for FR beams,

ψ_0 = section characteristic factor $= \frac{\chi}{SF\rho}$,

ρ = steel ratio = area of tension steel/effective area of cross-section,

SF = section factor (1/m) = heated parameter/ cross-sectional area,

χ = number of corner bars/total number of bars,

LR = load ratio,

L = span of the beam,

H = total depth of the beam,

Y = location of axial restraint measured from the top most fibers of the beam cross-section,

$$ax = \frac{k_r L}{E_c b H},$$

k_r = axial restraint stiffness,

b = beam width, and

E_c = modulus of elasticity of concrete.

The simulated values of the structural factor (computed from the actual data assuming ϕ_{ag} and ϕ_{cs} to be 1.0 for siliceous aggregate and NSC, respectively) are plotted against the predicted values from the best fit equations in Figures 7.3 to 7.7. The trends in these figures show that the best fit equation is sufficiently accurate in predicting the structural parameters. The coefficient of determination was found to be 0.95, 0.72, 0.79, 0.92 and 0.73 for the five equations, see Figures 7.3 to 7.7. The low coefficient of determinations for AR, ER and FR support conditions can be attributed to the large number of influencing parameters and the interactions among these parameters. Accounting for such a large number of parameters will make the equation very complex and unsuitable for design purposes.

The residuals (difference between structural modification factors computed from the numerical model and predicted values) are plotted versus predicted values in Figures 7.8 to 7.12 for the five support conditions. It can be seen that the residuals are almost uniformly distributed throughout the predicted range of structural parameters. This indicates that the equations for modification factors are not biased in predicting the values of fire resistance.

The second modification factor (ϕ_{ag}) is derived to take into account the influence of aggregate type. In practice, two types of aggregate are most commonly used in the concrete mix, namely, siliceous and carbonate. In the regression analysis, siliceous aggregate concrete is taken as the base line and hence its aggregate factor is 1.0. Results from parametric studies presented in Chapter 6 indicate that beams made of carbonate aggregate concrete have 20-30% higher fire resistance than those made of siliceous aggregate concrete. Further, previous studies on RC structural members have shown that members made of carbonate aggregate concrete have 10-20% higher fire resistance than those made of siliceous aggregate concrete (Kodur 2003a). Thus, for carbonate aggregate concrete, the aggregate factor is selected to be 1.2.

The simulated fire resistance values for carbonate aggregate RC beams are plotted versus the predicted values in Figure 7.13. It can be seen from the figure that the predicted fire resistance values match well with the simulated values, and are conservative for most of the carbonate aggregate concrete beams. The predicted fire resistance values are unconservative for only a few beams which generally have fire resistance values that are very close to the simulated values. This indicates that the proposed approach is capable of predicting the fire resistance of carbonate aggregate RC beams with sufficient accuracy for practical purposes.

The third modification factor (ϕ_{cs}) in the fire resistance equation is to account for the influence of concrete strength and fire induced spalling. In the regression analysis, the value of the material modification factor is assumed to be 1.0 for NSC beams. Results from parametric studies presented in Chapter 6 indicate that rotationally unrestrained (SS, AR and ER) HSC beams have 5-25% lower fire resistance than NSC beams. The results

also show that rotationally restrained (RR and FR) HSC beams have 40-60% lower fire resistance than NSC beams. Previous studies of RC beams and columns have shown that HSC members have 20-30% lower fire resistance than those made of NSC (Kodur and McGrath 2003, Dwaikat and Kodur 2009). Thus, for HSC beams (with compressive strength higher than 70 MPa as discussed in Chapter 1) the values 0.8 and 0.5 were selected for rotationally unrestrained and restrained beams, respectively. The reason for selecting two different values is that concrete strength (and spalling) has a large influence on the fire resistance of RR and FR beams as discussed in Chapter 6. The values are selected in such away that the fire resistance predictions for most of the analyzed HSC beams is conservative.

The simulated fire resistance values (using the computer program) for HSC beams are plotted against the predicted values (based on Eq. [7.2]) in Figure 7.14. The predicted fire resistance values are in good agreement with the simulated values and are conservative for most of the analyzed beams. Also, the fire resistance predictions are unconservative for only few HSC beams and the predicted fire resistance values for these beams are very close to the simulated values. This indicates that the proposed approach generally results in sufficiently accurate fire resistance predictions of HSC beams.

7.4 Establishing Fire Resistance under Design Fires

7.4.1 Time Equivalent

The fire resistance performance of a beam under a design fire exposure can be related to its fire resistance under standard fire exposure (R) provided a time equivalency is established between standard and design fire scenarios. The state-of-the-art review

presented in Chapter 2 illustrated that there are few time equivalent methods and empirical formula for RC members (beams). It was also shown in Chapter 2 that the time equivalent values predicted by existing methods and empirical formulae are generally unconservative and have an appreciable variation for the case of RC beams. Thus, the current methods for evaluating time equivalency for RC beams may not be fully reliable. To overcome this problem, a reliable, conservative semi-empirical approach for establishing time equivalency is presented (Kodur et al. 2009b).

7.4.2 Development of Time Equivalent Methodology

7.4.2.1 Approach

The proposed methodology for establishing time equivalency between standard and design fire scenarios is based on the concept of equivalent energy. The energy based concept is better suited than the equivalent area or equivalent (maximum) temperature approach since the equal energy concept assumes that the fire severity, and thus the fire resistance, depends on the amount of energy transferred to the beam. Accordingly, two fires will have the same fire severity if they transfer the same amount of energy to an RC beam. The amount of energy transferred to an RC beam exposed to fire is related to the heat flux on the fire exposed boundaries of the beam, which involves heat transfer through convection and radiation. The convection and radiation heat flux on the boundary of an RC beam exposed to fire can be given by the following two formulae, respectively (Buchanan 2002):

$$q_{con} = h_{con}(T_f - T_c) \qquad [7.8]$$

$$q_{rad} = \sigma\varepsilon(T_f^4 - T_c^4) \qquad [7.9]$$

where:

q_{con} = convective heat flux (W/m^2),

q_{rad} = radiative heat flux (W/m^2),

h_{con} = convective heat transfer coefficient (W/m^{2}K),

T_f = fire temperature (K),

T_c = temperature on surface of boundary (K),

σ = Stefan-Boltzmann constant (5.67×10^{-8} W/m^{2}K^4) and

ε = emissivity.

Equation [7.9] can be written as:

$$q_{rad} = \sigma\varepsilon(T_f{}^2 + T_c{}^2)(T_f + T_c)(T_f - T_c) \qquad [7.10]$$

Since the temperature on the exposed surface (T_c) is generally close to the fire temperature (T_f), the radiation heat flux can be approximated as:

$$q_{rad} \approx 4\sigma\varepsilon T_f{}^3(T_f - T_c) \qquad [7.11]$$

Thus, the total heat flux can be written as:

$$q = q_{con} + q_{rad} \approx h_{con}(T_f - T_c) + 4\sigma\varepsilon T_f{}^3(T_f - T_c) \qquad [7.12]$$

Assuming $T_f - T_c = \alpha\ T_f$, (where α is a dimensional constant), Eq. [7.12] can be written as:

$$q \approx \alpha(4\sigma\varepsilon T_f{}^4 + h_{con}T_f) \qquad [7.13]$$

The error involved in the above assumption is generally small due to the fact that the exposed surface temperature (T_c) is close to the fire temperature (T_f) and can be assumed 90% of it (ASCE Manual 1992).

Thus, the amount of energy transfer to an RC beam under fire exposure can be approximated by the following formula:

$$E_t = \int qAdt \approx \int A\alpha(4\sigma\varepsilon T_f{}^4 + h_{con}T_f)dt \qquad [7.14]$$

where:

A = area of boundary exposed to fire, and

E_t = total energy.

Since both A and α are assumed to be constant, they can be taken outside the integral in Eq. [7.14] and hence:

$$E_t = \alpha A\int(4\sigma\varepsilon T_f{}^4 + h_{con}T_f)dt \qquad [7.15]$$

The total energy, E_t, represents the energy bound by the time-temperature curve of a given fire exposure. The total energy in Eq. [7.15] can also be computed by the following equation:

$$E_t = \alpha A \text{ (Area under heat flux curve } (\frac{q}{\alpha}) \text{ integral over time)} \qquad [7.16]$$

Thus, using the equivalent energy principle, a design fire will have the same severity as that of the standard fire if:

$$E_d = E_s \qquad [7.17]$$

where:

E_s = total energy under the heat flux ($\frac{q}{\alpha}$) curve of the standard fire, and

E_d = total energy under the heat flux ($\frac{q}{\alpha}$) curve of the design fire.

The equivalent time can be computed by equating the total area under the heat flux ($\frac{q}{\alpha}$) curve for the design fire with the area under the heat flux ($\frac{q}{\alpha}$) curve for the standard fire as shown in Figure 7.15 (for the ASTM E119 standard and design fires). To arrive at equivalency, first the total area under the heat flux curve for the design fire (area B in Figure 7.15) is computed. The area under the heat flux of a standard fire (area A in Figure 7.15) is computed at various time steps. According to the proposed time equivalent method, the time at which area A (which varies as a function of time) equals area B is the time equivalent of the design fire.

7.4.2.2 Simplification

The area under the heat flux curve for both standard and design fires can be computed by applying the trapezoidal rule (any spread sheet software such as Excel can be used). However, for design fires whose time-temperature curves are established based on Eurocode 1 (2002), a more simplified approach can be used to compute the area under the heat flux curve. The area under the heat flux curve can be divided into two parts (A_1 and A_2) which represents the area under the ascending heat flux curve and the area under the descending heat flux curve as shown in Figure 7.16, respectively.

According to Eurocode 1, the fire temperature in the ascending branch (heating phase) can be given by the following expression:

$$T_f = 1325\left(1 - 0.324e^{-0.2t^*} - 0.204e^{-1.7t^*} - 0.472e^{-19t^*}\right) + 293 \quad [7.18]$$

where:

$t^* = \Gamma t$,

Γ = time modification factor,

$$\Gamma = \left(\frac{F_v/0.04}{b/1900}\right),$$

b = thermal inertia (J/m^2.K.s$^{0.5}$),

F_v = ventilation factor (m$^{0.5}$),

t = time (hours), and

T_f = fire temperature (K).

Thus, the heat flux ($\frac{q}{\alpha}$) in the heating phase of a Eurocode design fire can be written as:

$$\frac{q}{\alpha} = (4\sigma\varepsilon T_f{}^4 + h_c T_f) = \Phi\left(t^*\right) \quad [7.19]$$

in which $\Phi\left(t^*\right)$ represents a function of t^*.

Hence, A_1 can be computed by the following expression:

$$A_1 = \int_0^{t_d} \frac{q}{\alpha} dt = \int_0^{t_d} (4\sigma\varepsilon T_f{}^4 + h_c T_f)\, dt \quad [7.20]$$

where t_d = burning duration of fire (hours).

Equation [7.20] can be written as:

$$A_1 = \frac{1}{\Gamma} \int_0^{\Gamma t_d} \Phi\left(t^*\right) dt^* \quad [7.21]$$

The integration in Eq. [7.21] can be estimated by using the following empirical expression (which is derived based on regression analysis as shown in Figure 7.17):

$$\int_0^{\Gamma t_d} \Phi\left(t^*\right) dt^* \approx \begin{Bmatrix} 10(\Gamma t_d)^{1.5} & \Gamma t_d < 10 \\ 48.6(\Gamma t_d) - 175 & \Gamma t_d \geq 10 \end{Bmatrix} \qquad [7.22]$$

Substituting Eq. [7.22] in Eq. [7.21] leads to the following expression:

$$A_1 \approx \begin{Bmatrix} \dfrac{10(\Gamma t_d)^{1.5}}{\Gamma} & \Gamma t_d < 10 \\ 48.6(t_d) - \dfrac{175}{\Gamma} & \Gamma t_d \geq 10 \end{Bmatrix} \qquad [7.23]$$

For the cooling phase, the fire temperature (K) can be written as:

$$T_f = T_{\max} - r\left(t - t_d\right) \qquad [7.24]$$

where T_{max} = maximum fire temperature (K), and r = cooling rate (K/minute).

Thus, A_2 can be computed as follows:

$$A_2 = \int_{t_d}^{t_t} \frac{q}{\alpha} dt = \int_{t_d}^{t_t} (4\sigma\varepsilon T_f{}^4 + h_{con} T_f)\, dt \qquad [7.25]$$

where t_t = total duration of the fire.

However, $dT_f = -r\, dt$ or $dt = -\dfrac{dT_f}{r}$

Hence, Eq. [7.25] can be written as:

$$A_2 = \frac{-1}{r} \int_{T_{\max}}^{T_0} (4\sigma\varepsilon T_f{}^4 + h_{con} T_f)\, dT_f \qquad [7.26]$$

or

$$A_2 = \frac{4\sigma\varepsilon}{5r}\left(T_{\max}^5 - T_0^5\right) + \frac{h_{con}}{2r}\left(T_{\max}^2 - T_0^2\right) \qquad [7.27]$$

substituting $\varepsilon = 0.5$ and $h_{con} = 25$ W/m^2.K, and changing units from Watts (W) into Mega Watts (MW), Eq. [7.27] can be written as:

$$A_2 = \frac{0.4\sigma\left(T_{\max}^5 - T_0^5\right) + 12.5\left(T_{\max}^2 - T_0^2\right)}{r} \times 10^{-6} \qquad [7.28]$$

Thus, the total area (A_d) under the heat flux curve for a Eurocode design fire can be computed by the following formula:

$$A_d = A_1 + A_2 \qquad [7.29]$$

The area under the heat flux of the ASTM E119 (or ISO 834) standard fire curve can also be estimated empirically using the following expression (see Figure 7.18):

$$A_S \approx \left(\frac{t_S}{11.5}\right)^{1.41} \qquad [7.30]$$

where A_S = the area under the heat flux curve of ASTM E119 standard fire, and t_S = time at which the area under the heat flux curve is being evaluated (min).

Hence, to estimate the time equivalency, the following expression has to be satisfied:

$$A_S = A_d \qquad [7.31]$$

Substituting Eq. [7.30] in Eq. [7.31], the time equivalency (in minutes) can be estimated by the following formula:

$$t_e \approx 11.5 A_d^{0.7} \qquad [7.32]$$

where A_d is computed from Eq. [7.29].

In summary, estimating the time equivalency for a Eurocode design fire involves the following three steps:

- Compute A_1 using Eq. [7.23].

- Calculate A_2 using Eq. [7.28] and then compute A_d through substitution in Eq. [7.29].
- Estimate the time equivalency (in minutes) using Eq. [7.32].

For other design fire curves, estimating the time equivalency involves the following two steps:

- Compute the area under the heat flux curve of the design fire using any of the numerical integration procedures such as the trapezoidal rule.
- Estimate the time equivalency (in minutes) using Eq. [7.32].

7.4.2.3 Calibration

To improve the accuracy of the proposed method in predicting the time equivalent, the time equivalent predictions were calibrated against time generated by Kodur et al. (2009b). It was found that there exists a linear correlation between the ratio of the two time equivalent values, predicted by the finite element method and the equal energy method ($t_{e(FE)}/\ t_{e(energy)}$), and Γt_d^2 of the design fire. Based on the relationship between ($t_{e(FE)}/\ t_{e(energy)}$) and Γt_d^2, an equation was developed whose predictions had a minimal variation from the values predicted by the finite element model. Linear regression analysis was carried out using statistical software 'SPSS' (2007) to find the function that accurately fit the data. It was found that the residuals for the regression are not uniformly distributed. Therefore, a logarithmic transformation is used for the time equivalent values from finite element analysis and from the equal energy method to reduce the non-uniformity of the residuals. The regression analysis is repeated with the transformed

values to find the function that best fit the data. This function was then simplified to arrive at the following expression:

$$t_{e(FE)} = \left(1.2 - 0.01\Gamma t_d^2\right) t_{e(energy)} \qquad [7.33]$$

where:

$t_{e(FE)}$ = time equivalent computed from finite element analysis using maximum deflection method,

$t_{e(energy)}$ = time equivalent computed from equivalent energy method, and

t_d = burning duration of design fire (hours).

Figure 7.19 shows the simulated values of the transformed time equivalent, t_e, (computed from numerical model) versus the predicted t_e values from the best fit equation. The figure shows that the equation is sufficiently accurate in predicting the values of t_e. The coefficient of determination was found to be 0.97. The residuals (difference of transformed simulated and predicted t_e values) are plotted versus predicted transformed t_e in Figure 7.20. It can be seen that the residuals are uniformly distributed throughout the predicted range of t_e. This suggests that the equation is not biased in predicting the value of t_e. Thus, the actual time equivalent of a design fire can be estimated using Eq. [7.33].

7.5 Validation of Proposed Approach

The validity of the proposed approach in evaluating fire resistance of RC beams is established by comparing the predictions from the proposed approach with results from

numerical studies (using the computer model developed in Chapter 4) and from fire resistance tests for both standard and design fire scenarios.

7.5.1 Standard Fire

The proposed fire resistance equation is validated by comparing predictions from the proposed equation with simulated values from the detailed analysis using the numerical model presented in Chapter 4. For this validation, results for the second set of beams (different than the one used for regression analysis) was used. The comparison is illustrated in Figure 7.21 for beams with different support conditions (SS, AR, ER, RR and FR). In the figure, the 'safety limit' line represents the boundary where the predictions from proposed equation coincide with the simulated values. Any prediction above the 'safety limit' line indicates that the proposed expression overestimates the fire resistance and hence is unconservative.

It can be seen in Figure 7.21 that the predictions from the proposed equation compare well with the simulated values (using the numerical model), and are conservative for most of the beams. The predicted fire resistance values are unconservative for only few beams, most of which have fire resistance higher than 3 hours. Also, some predictions from the equation are highly conservative mostly for fire resistance beyond 3 hours. This may not be a major drawback since in most practical applications fire resistance ratings of 1 to 3 hours is required for RC beams. Therefore, it is deemed that the proposed equation is capable of predicting the fire resistance of RC beams with a sufficient degree of accuracy.

The validity of the equation is also established by comparing the predictions from the proposed equation with measured fire resistance from tests. Seven beams (five of which

are selected from the literature; the remaining two are beams B1 and B3 were used in the validation. The seven beams include four simply supported and three rotationally restrained beams. The properties of the RC beams together with measured values of fire resistance (as reported from fire tests), are provided in Table 7.1. Figure 7.22 shows the comparison of the predicted and measured fire resistance (using the proposed expression) to the measured fire resistance values. As before, the 'safety limit' line in this figure represents the boundary where the predictions from proposed equation coincide with the test measurements.

It can be seen in Figure 7.22 that the predictions from the proposed equation compare well with the test results, and are conservative for most of the beams. Also, the predictions from the equation are highly conservative for beams B1 and B3 tested as part of this study. This is mainly because the actual high temperature material properties for these two beams are close to the best case scenario, while the average high temperature material properties are used for developing the fire resistance equation. This may not be a major drawback since in many practical applications, due to the lack of information on high temperature material properties, fire resistance equations that were developed based on average material properties are generally used. Overall, the fire resistance equations, derived in this thesis, seem to produce reasonable fire resistance predictions for the seven tested beams.

7.5.2 Design Fire

The validity of the proposed energy-based time equivalent approach is established by comparing the time equivalent predictions from this approach with those obtained from finite element analysis for 90 beam-fire combinations. Data for this validation are

generated by analyzing beams with four different concrete cross-sections (described in Table 6.1), three load levels, fourteen design fire scenarios (which represent typical fire exposures in a building compartment), three span-to-depth ratios, and three values of axial restraint stiffness. All beams, except beams B78 through B90, were assumed to be made of NSC. Beams B78 to B90 were assumed to be made of HSC with compressive strength 100 MPa. More details on the characteristics of the analyzed beams are given in Table 7.2. The time-temperature curves for the fire scenarios used in the analyses are shown in Figure 7.23. The main results from the analysis are summarized in Table 7.2 and Figure 7.24.

Figure 7.24 shows the comparison of the predicted time equivalent (using the proposed method) with the simulated values from finite element analysis. As before, the 'safety limit' line in this figure represents the boundary where the predictions from the proposed method coincide with the simulated values. Data points above the 'safety limit' line indicate unconservative predictions.

It can be seen in Figure 7.24 that the predictions from the proposed method compare well with the simulated values, and are conservative for most of the beams. The predicted time equivalent values are unconservative for a few beams. In these cases the predicted values are close to the simulated values. Comparing Figure 7.24 with Figure 2.9, it can be seen that the time equivalents computed for the proposed method show less variation than those predicted by other methods. Thus, the proposed equal energy method can be considered as a reliable tool for the estimation of the time equivalent for design fires.

7.5.3 Comparison with Current Codes

To further evaluate the proposed approach, fire resistance predictions from Eq. [7.2] are compared to those obtained from code provisions for eleven RC beams. Seven of the selected beams are the ones used in the validation against fire tests results, and the remaining four represent typical RC beams used in practice. Details on the properties of the eleven beams are given in Table 7.1. Figure 7.25 shows a comparison of the fire resistance obtained from current provisions in ACI 216.1 (2007), Eurocode 2 (2004) and AS 3600 (2001), with those predicted by the proposed equation (Eq. [7.2]). The ACI code overestimates the fire resistance (significantly) for most of the RC beams. This is mainly due to the fact that ACI provisions employ large time increments for fire resistance ratings. These ratings are mostly based on concrete cover thickness requirements and minimum section dimensions, but do not fully account for important factors such as load ratio, span-to-depth ratio, and axial restraint effects. However, ACI 216.1 underestimates the fire resistance for the two rotationally restraint beams. This can be attributed to the fact that the tabulated fire resistance in ACI 216.1 does not properly account for the rotational restraint effect since the definition of support conditions (restrained or unrestrained) is not clearly addressed in the code provisions. Thus, it is not clear wither the restrained case refers to rotationally restrained, axially restrained or both rotationally and axially restrained.

It can be seen from Figure 7.25 that the Eurocode predictions are also unconservative for most of the beams, particularly axially restrained slender beams (with high span-to-depth ratio) and beams with high load ratios because these important parameters are not accounted for in the Eurocode. However, despite the fact that Eurocode specifications

account for rotational restraint, the fire resistance predictions based on that code are overly conservative for some cases (particularly rotationally restrained beams). This can be mainly attributed to the fact that Eurocode 2 does not account for the interdependent influence of load ratio and rotational restraint on the fire resistance of RC beams.

Figure 7.25 also shows that the Australian code predictions are similar to those from Eurocode 2 for all beams. This can be attributed to the fact the fire resistance provisions in both AS 3600 and Eurocode 2 are derived based on concrete cover thickness and beam width, and do not account for other governing parameters such as load ratio, restraint and span-to-depth ratio. Overall, the proposed equation provides better predictions of fire resistance than the current code estimates since it accounts for critical governing parameters.

7.6 Design Applicability

7.6.1 Design Procedure

The proposed approach can be conveniently applied for evaluating the fire performance of RC beams in design situations using the following procedure:

- Develop an initial estimate of fire resistance (R_0) based on the concrete cover thickness and beam width.
- Compute the structural modification factor using Eqs. [7.3], [7.4], [7.5], [7.6] or [7.7] based on the boundary conditions of the beam.
- Determine the aggregate and material modification factors.
- Apply modification factors to R_0 and compute fire resistance (R) of the beam using Eq. [7.2], for a standard fire exposure.

- Compute the time equivalent (by equating the area under the heat flux curve of a design fire with that of a standard fire) to estimate fire resistance under the design fire. This may require the use of a spread sheet computer program.
- For Eurocode design fires, the time equivalent can be obtained as follows:
  - Compute the area under the heat flux curve of the design fire using those expressions:

$$A_d = A_1 + A_2 \qquad [7.29]$$

$$A_1 \approx \begin{cases} \dfrac{10(\Gamma t_d)^{1.5}}{\Gamma} & \Gamma t_d < 10 \\ 48.6(t_d) - \dfrac{175}{\Gamma} & \Gamma t_d \geq 10 \end{cases} \qquad [7.23]$$

$$A_2 = \frac{0.4\sigma\left(T_{\max}^5 - T_0^5\right) + 12.5\left(T_{\max}^2 - T_0^2\right)}{r} \times 10^{-6} \qquad [7.28]$$

  - Compute the time equivalent using the following equation:

$$t_e \approx 11.5 A_d^{0.7} \qquad [7.32]$$

- Once the time equivalent is evaluated either using a spread sheet computer program or the simplified approach (for Eurocode fires), apply the modification factor for the computed time equivalent (based on the energy method):

$$t_{e(FE)} = \left(1.2 - 0.01\Gamma t_d^2\right) t_{e(energy)} \qquad [7.33]$$

- Check the failure of the beam using the following expression:

  time equivelant > Fire resistance $\Rightarrow$ Failure

Application of these steps for evaluating the fire resistance of RC beams is illustrated through a worked example in the following section.

7.6.2 Design Example

To illustrate the applicability of the proposed approach in a design situation, the procedure is applied to evaluate the fire resistance of an RC beam. Details on the properties of the beam are shown in Figure 7.26. The fire resistance calculations from the proposed equation are carried out for two support conditions, namely, simply supported and axially restrained with axial restraint stiffness 300 kN/mm (300,000 kN/m). The results from the proposed equation are compared with fire resistance values from current codes and standards. The beam is also checked (using the proposed method) for sustaining failure under design fire, Fire I, shown in Figure 7.23 (T_{max} = 1314 °C, t_d = 0.867 hours, decay rate = 17.54 °C/min, and Γ = 15.16). Details of the calculations are given in Appendix D.

The fire resistace of this beam under standard fire exposure was evaluated based on the proposed equation using the following steps:

- Based on the concrete cover thickness and beam width, the initial standard fire resistance (R_0) was found from Figure 7.2 to be 157 minutes.
- The fire resistance for simply supported and axially restrained beams was computed using the following two equations, respectively:

  For simply supported beam, $R = \phi_{SS}\phi_{ag}\phi_{cs}R_0$

  For axially restrained beam, $R = \phi_{AR}\phi_{ag}\phi_{cs}R_0$

  where: ϕ_{SS} and ϕ_{AR} can be computed from Eqs. [7.3] and [7.4], respectively, and ϕ_{ag} and ϕ_{cs} were selected to be 1.2 and 1.0 for the carbonate aggregate NSC.

- The fire resistance was found to be 153 minute and 204 minutes for simply supported and axially restrained beams, respectively.

The fire resistance is also evaluated based three widely used codes of practice, namely, ACI 216.1, Eurocode 2 and Australian code (AS 3600). Detailed calculations of fire resistance are given in Appendix D. A summary of the results is given in Table 7.3. It can be seen from the table that there is a large variation in the fire resistance computed as per current code provisions. It can also be seen that the proposed equation predicts a conservative fire resistance for the simply supported beam compared to the three codes of practice. This reveals that current codes may not be fully conservative under some scenarios.

However, under a design fire exposure (Fire I in Figure 7.23), the time equivalent (t_e) of the design fire computed using Eqs. [7.23], [7.28], [7.29], [7.32] and [7.33] was found to be 182 minutes. This value of the time equivalent is higher by about 16% than the fire resistance of the simply supported beam (under standard fire exposure) which implies failure of the simply supported beam under the given design fire scenario. However, the time equivalent is less than the fire resistance of axially restrained beams and thus failure does not occur in that beam under the given design fire scenario. Detailed calculations of the time equivalent are given in Appendix D.

7.6.3 Limitations

The proposed equation expresses fire resistance as a function of structural and material parameters, and thus offers a convenient way for evaluating fire resistance. Since the proposed equation is based on results from numerical studies, it is necessary to set limits of applicability on the parameters such that they are within the range of values used for

developing the equation. Overall, the proposed equation is valid for the following range of variables:

- Fire resistance (R) duration: 1 – 5 hours.
- Type of fire exposure: ASTM E119 standard fire, equivalent standard fire scenarios such as ISO 834 standard fire, or any design fire that follows the specifications of Eurocode 1 (2002) (or SFPE (2004)).
- Span-to-depth ratio: 8 – 18.
- Specified 28 day compressive strength (f'_c): 30 – 100 MPa.
- Axial restraint ratio (ax): 0 – 50%.
- Tension steel ratio (ρ): 0.7 – 1.7%
- Location of axial restraint (Y/H): 0.3 – 0.7.
- Aggregate type: Siliceous and carbonate aggregate
- Section characteristics factor (ψ_0): 2.8 – 10.5

7.7 Summary

The development of an approach for evaluating the fire resistance of RC beams is presented in this chapter. The approach is derived based on detailed parametric studies presented in Chapter 6 and comprises two main steps: evaluating the fire resistance under standard fire exposure and establishing time equivalency between standard and design fire scenarios. The approach accounts for various parameters that have a significant influence on the fire resistance of RC beams such as fire scenario, load ratio, support conditions and span-to-depth ratio. The validity of the proposed approach is established by comparing predictions with results from detailed finite element analysis and fire tests.

The proposed method provides a simple, rational approach for computing the fire resistance of an RC beam exposed to standard or design fire scenarios. The approach facilitates a rational methodology for achieving desired fire resistance by varying parameters such as beam dimensions, length and load. The applicability of the proposed equation in a design simulation is illustrated through a solved numerical example. The proposed equation provides a better estimate of fire resistance than those predicted by current codes of practice.

Table 7.1 – Properties of Beams used in Equation Validation and Comparison with Current Codes

Beam Designation	B1	B3	BD1	BL1	BL2	BL3	BL4	BCS1	BCS2	BCS3	BCS4
Description	tested by Dwaikat and Kodur (2009)		tested by Dotreppe and Franssen (1985)	tested by Lin et al (1981)				analyzed beams using the numerical model			
Cross-section	254 × 406		200 × 600	305 × 355				300 × 900	400 × 800	700 × 400	600 × 600
Length (m)	3.66		6.5	6.1				11.7	14.4	3.2	10.8
Reinforcement	3 ϕ 19 mm bottom bars		3 ϕ 22 mm bottom bars	4 ϕ 19 mm bottom bars				5 ϕ 20 mm bottom bars	3 ϕ 35 mm bottom bars	6 ϕ 20 mm bottom bars	8 ϕ 20 mm bottom bars
	2 ϕ 13 mm top bars		2 ϕ 12 mm top bars	2 ϕ 19 mm top bars	6 ϕ 19 mm bottom bars			2 ϕ 14 mm top bars	2 ϕ 14 mm top bars	3 ϕ 14 mm top bars	3 ϕ 14 mm top bars
f'_c (MPa)	52.2	91	15*	30				40	60	30	50
f_y (MPa)	450	450	300*	435.8				413	413	413	413
Loading ratio	0.54	0.54	0.263*	0.42				0.7	0.5	0.5	0.3
Concrete cover thickness (mm)	40	40	40	25 (bottom)				40	60	40	50
				38 (side)							
Aggregate type	Carbonate		Siliceous*	Carbonate				Siliceous			
Support conditions**	SS			RR				SS	AR with ax =		
									27.60%	9.10%	19.80%
Measured fire resistance (min)	180	160	80	120	236	183	271	Not applicable			

* Values based on correspondence (Franssen 2006)

** SS = simply supported, RR = rotationally restrained, AR = axially restrained, ax = ratio of axial restraint stiffness to the axial stiffness of the beam.

Table 7.2 – Summary of the Time Equivelant Values for the Analyzed Beams

Beam	Cross-section #	LR	LH	*Y/H*	ax (%)	Support	Aggregate	Fire	t_e (min)	
									FE Analysis	Proposed Method
B1	1	0.5	18	0.5	0.0	AR	C	Fire I	156	161
B2	1	0.3	13	0.3	7.8	AR	C	Fire I	146	161
B3	1	0.3	13	0.5	0.0	FR	C	Fire I	143	161
B4	1	0.5	18	0.5	10.8	FR	C	Fire I	147	161
B5	1	0.7	8	0.5	19.1	FR	C	Fire I	148	161
B6	1	0.5	18	0.5	0.0	AR	C	Fire II	51	48
B7	1	0.7	8	0.7	4.8	AR	C	Fire II	45	48
B8	1	0.3	13	0.3	7.8	AR	C	Fire II	42	48
B9	1	0.3	8	0.5	19.1	AR	C	Fire II	46	48
B10	1	0.3	13	0.5	0.0	FR	C	Fire II	34	48
B11	1	0.5	18	0.5	10.8	RR	C	Fire II	37	48
B12	1	0.7	8	0.5	19.1	FR	C	Fire II	42	48
B13	2	0.5	18	0.5	0.0	AR	C	Fire III	121	128
B14	2	0.7	8	0.7	3.1	AR	C	Fire III	119	128
B15	2	0.3	13	0.3	5.0	AR	C	Fire III	118	128
B16	2	0.3	8	0.5	12.3	AR	C	Fire III	121	128
B17	2	0.3	13	0.5	0.0	FR	C	Fire III	110	128
B18	2	0.5	18	0.5	6.9	FR	C	Fire III	113	128
B19	2	0.7	8	0.5	12.3	FR	C	Fire III	117	128
B20	2	0.7	8	0.7	3.1	AR	C	Fire IV	169	167
B21	2	0.3	13	0.3	5.0	AR	C	Fire IV	167	167
B22	2	0.3	8	0.5	12.3	AR	C	Fire IV	171	167
B23	2	0.3	13	0.5	0.0	FR	C	Fire IV	156	167
B24	2	0.5	18	0.5	6.9	FR	C	Fire IV	156	167
B25	2	0.7	8	0.5	12.3	FR	C	Fire IV	151	167
B26	3	0.3	18	0.5	0.0	AR	C	Fire V	238	246
B27	3	0.5	8	0.7	2.3	AR	C	Fire V	224	246
B28	3	0.3	13	0.3	3.7	AR	C	Fire V	237	246
B29	3	0.5	18	0.5	5.1	FR	C	Fire V	227	246
B30	3	0.7	8	0.5	9.1	FR	C	Fire V	232	246
B31	3	0.5	18	0.5	0.0	AR	C	Fire VI	119	127
B32	3	0.7	8	0.7	2.3	AR	C	Fire VI	116	127
B33	3	0.3	13	0.3	3.7	AR	C	Fire VI	109	127
B34	3	0.3	8	0.5	9.1	AR	C	Fire VI	112	127
B35	3	0.3	13	0.5	0.0	FR	C	Fire VI	116	127
B36	3	0.5	18	0.5	5.1	FR	C	Fire VI	112	127
B37	3	0.7	8	0.5	9.1	FR	C	Fire VI	114	127
B38	4	0.5	18	0.5	0.0	AR	C	Fire VII	115	107
B39	4	0.7	8	0.7	2.2	AR	C	Fire VII	117	107
B40	4	0.3	13	0.3	3.6	AR	C	Fire VII	113	107

Table 7.2 (Continued) – Summary of the Time Equivelant Values for the Analyzed Beams

Beam	Cross-section #	LR	LH	*Y/H*	ax (%)	Support	Aggregate	Fire	t_e (min)	
									FE Analysis	Proposed Method
B41	4	0.3	8	0.5	8.8	AR	C	Fire VII	115	107
B42	4	0.3	13	0.5	0.0	FR	C	Fire VII	105	107
B43	4	0.5	18	0.5	4.9	FR	C	Fire VII	106	107
B44	4	0.7	8	0.5	8.8	FR	C	Fire VII	109	107
B45	4	0.5	18	0.5	0.0	AR	C	Fire VIII	124	138
B46	4	0.7	8	0.7	2.2	AR	C	Fire VIII	124	138
B47	4	0.3	13	0.3	3.6	AR	C	Fire VIII	121	138
B48	4	0.3	8	0.5	8.8	AR	C	Fire VIII	121	138
B49	4	0.3	13	0.5	0.0	FR	C	Fire VIII	123	138
B50	4	0.5	18	0.5	4.9	FR	C	Fire VIII	123	138
B51	4	0.7	8	0.5	8.8	FR	C	Fire VIII	124	138
B52	1	0.5	18	0.5	0.0	AR	S	Fire IX	92	99
B53	1	0.7	8	0.7	4.8	AR	S	Fire IX	77	99
B54	1	0.3	13	0.3	7.8	AR	S	Fire IX	89	99
B55	1	0.5	18	0.5	10.8	FR	S	Fire IX	103	99
B56	1	0.7	8	0.5	19.1	FR	S	Fire IX	104	99
B57	3	0.5	18	0.5	0.0	AR	S	Fire X	55	63
B58	3	0.7	8	0.7	2.3	AR	S	Fire X	56	63
B59	3	0.3	13	0.3	3.7	AR	S	Fire X	55	63
B60	3	0.3	8	0.5	9.1	AR	S	Fire X	56	63
B61	3	0.3	13	0.5	0.0	FR	S	Fire X	51	63
B62	3	0.5	18	0.5	5.1	FR	S	Fire X	52	63
B63	3	0.7	8	0.5	9.1	FR	S	Fire X	53	63
B64	2	0.5	18	0.5	0.0	AR	S	Fire XI	60	67
B65	2	0.7	8	0.7	3.1	AR	S	Fire XI	63	67
B66	2	0.3	13	0.3	5.0	AR	S	Fire XI	60	67
B67	2	0.3	8	0.5	12.3	AR	S	Fire XI	65	67
B68	2	0.3	13	0.5	0.0	FR	S	Fire XI	53	67
B69	2	0.5	18	0.5	6.9	FR	S	Fire XI	57	67
B70	2	0.7	8	0.5	12.3	FR	S	Fire XI	60	67
B71	4	0.5	18	0.5	0.0	AR	C	Fire XII	82	83
B72	4	0.7	8	0.7	2.2	AR	C	Fire XII	82	83
B73	4	0.3	13	0.3	3.6	AR	C	Fire XII	81	83
B74	4	0.3	8	0.5	8.8	AR	C	Fire XII	83	83
B75	4	0.3	13	0.5	0.0	FR	C	Fire XII	76	83
B76	4	0.5	18	0.5	4.9	FR	C	Fire XII	79	83
B77	4	0.7	8	0.5	8.8	FR	C	Fire XII	80	83
B78	1	0.5	18	0.5	0.0	AR	S	Fire XIII	86	91
B79	1	0.3	13	0.3	7.8	AR	S	Fire XIII	74	91
B80	1	0.3	8	0.5	19.1	AR	S	Fire XIII	81	91

Table 7.2 (Continued) – Summary of the Time Equivelant Values for the Analyzed Beams

Beam	Cross-section #	LR	LH	*Y/H*	ax (%)	Support	Aggregate	Fire	t_e (min)	
									FE* Analysis	Proposed Method
B81	1	0.3	13	0.5	0.0	FR	S	Fire XIII	71	91
B82	1	0.5	18	0.5	10.8	FR	S	Fire XIII	73	91
B83	1	0.7	8	0.5	19.1	FR	S	Fire XIII	82	91
B84	4	0.5	18	0.5	0.0	AR	C	Fire XIV	65	56
B85	4	0.7	8	0.7	2.2	AR	C	Fire XIV	62	56
B86	4	0.3	13	0.3	3.6	AR	C	Fire XIV	62	56
B87	4	0.3	8	0.5	8.8	AR	C	Fire XIV	63	56
B88	4	0.3	13	0.5	0.0	FR	C	Fire XIV	49	56
B89	4	0.5	18	0.5	4.9	FR	C	Fire XIV	43	56
B90	4	0.7	8	0.5	8.8	FR	C	Fire XIV	46	56

The symbols and abbreviation in Table 7.2 are defined as: LR = load ratio, LH = span-to-depth ratio, *Y/H* = ration of location of axial restraint (from the top most fibers) to the full depth of the beam, *ax* = axial restraint stiffness ratio, FR = axially and rotationally restraint, AR = axially restraint, S = siliceous aggregate concrete, and C= carbonate aggregate concrete. * Finite element

Table 7.3 – Prediction of Fire Resistance Values for Analyzed Beam using Proposed Method and Different Codes

Support Conditions	Fire Resistance (min)			
	Proposed Equation	ACI	Eurocode	Australian Code
Simply supported	153	240	156	157
Axially restrained	204	>240	NA*	NA

* Not applicable

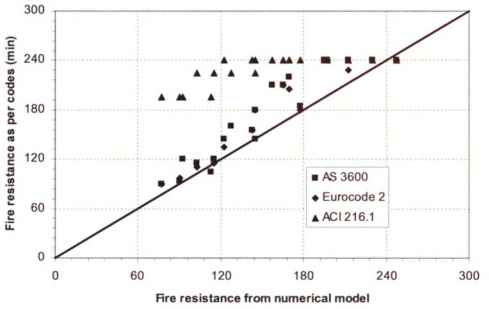

Figure 7.1 – Initial Estimates of Fire Resistance (in Minutes) based on Beam Width and Concrete Cover Thickness (R_0)

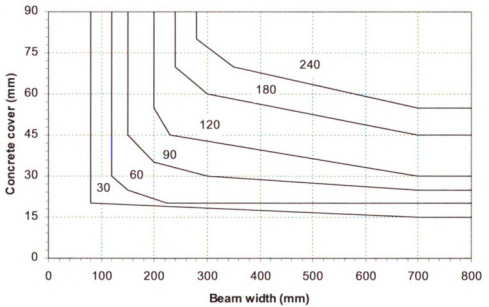

Figure 7.2 – Initial Estimates of Fire Resistance (minutes) based on Beam Width and Concrete Cover Thickness (R_0) (Reproduced from AS 3600 (2001))

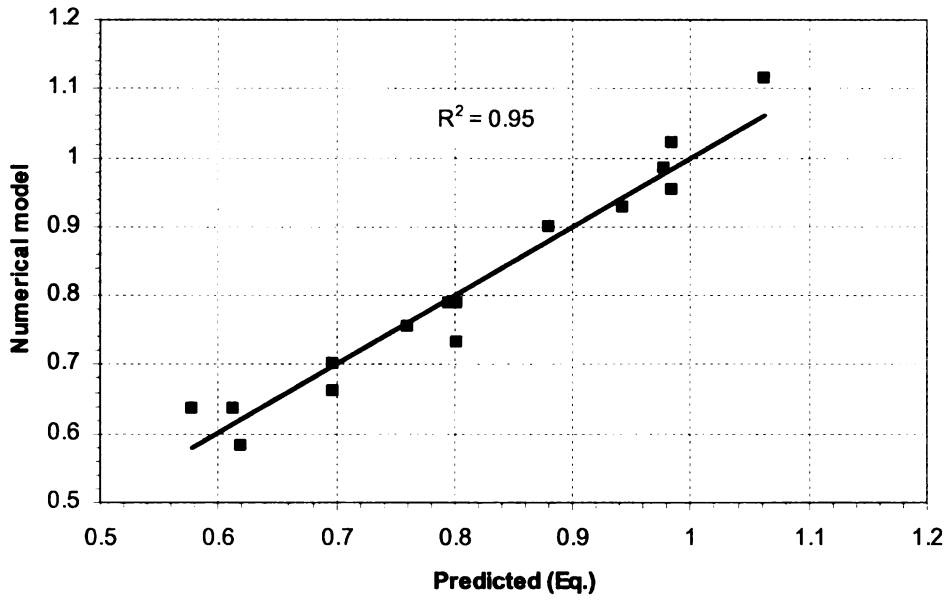

Figure 7.3 – Simulated versus Predicted Values of Structural Factor (ϕ_{SS})

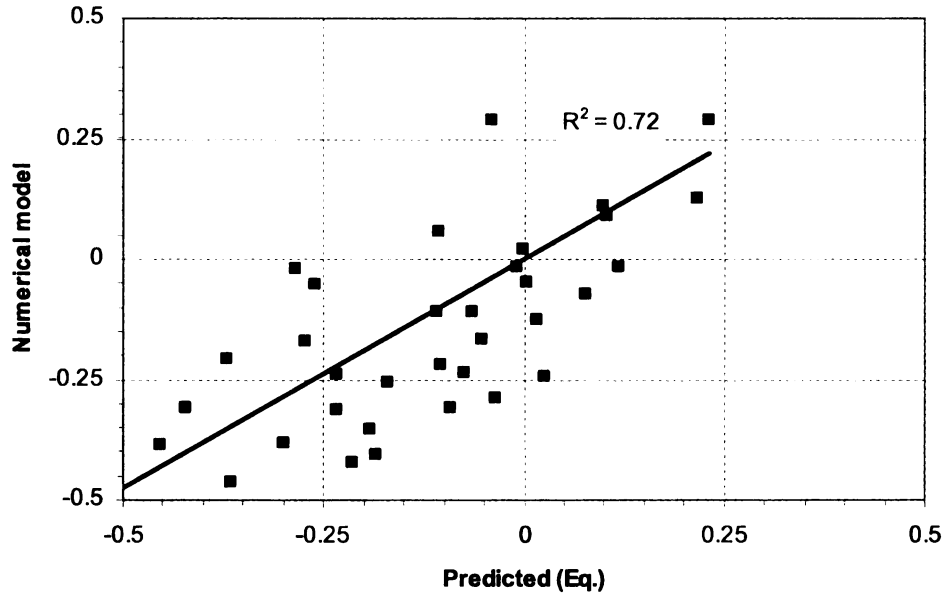

Figure 7.4 – Simulated versus Predicted Values of Structural Factor (LN(ϕ_{AR}))

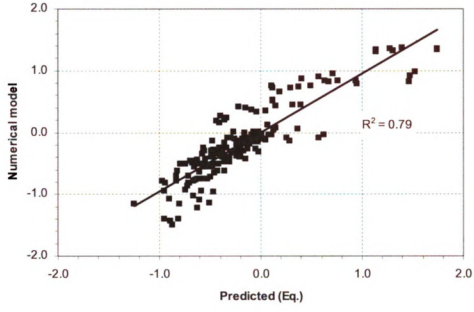

Figure 7.5 – Simulated versus Predicted Values of Structural Factor (LN(ϕ_{ER}))

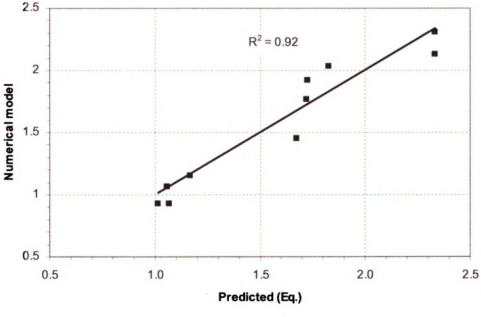

Figure 7.6 – Simulated versus Predicted Values of Structural Factor (ϕ_{RR})

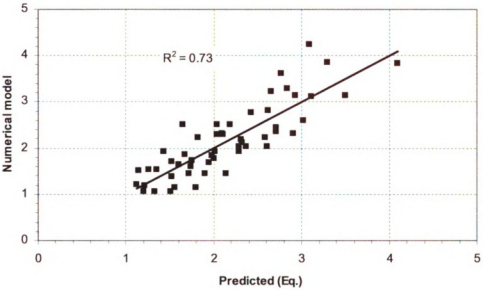

Figure 7.7 – Simulated versus Predicted Values of Structural Factor (ϕ_{FR})

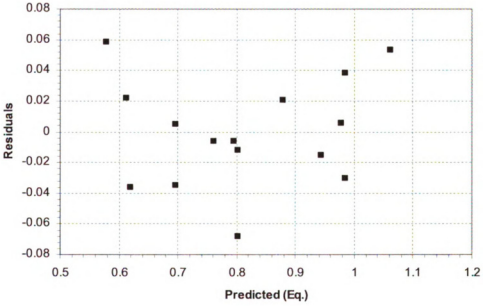

Figure 7.8 – Residual versus Predicted Values of Structural Factor (ϕ_{SS})

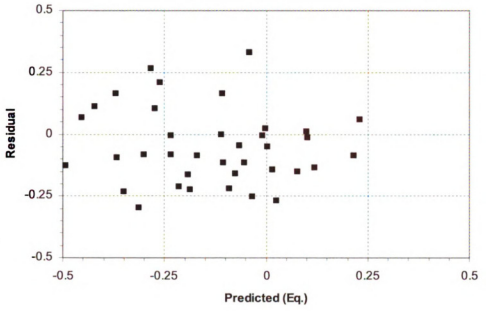

Figure 7.9 – Residual versus Predicted Values of Structural Factor (LN(ϕ_{AR}))

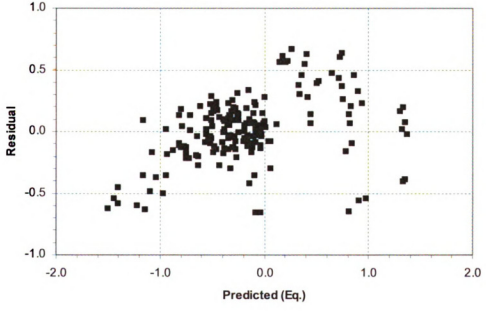

Figure 7.10 – Residual versus Predicted Values of Structural Factor (LN(ϕ_{ER}))

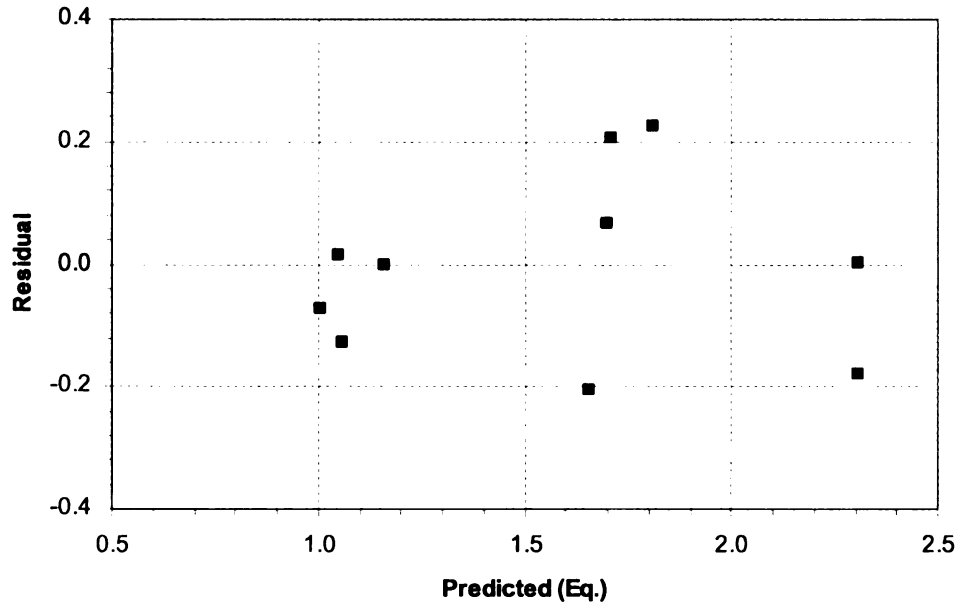

Figure 7.11 – Residual versus Predicted Values of Structural Factor (ϕ_{RR})

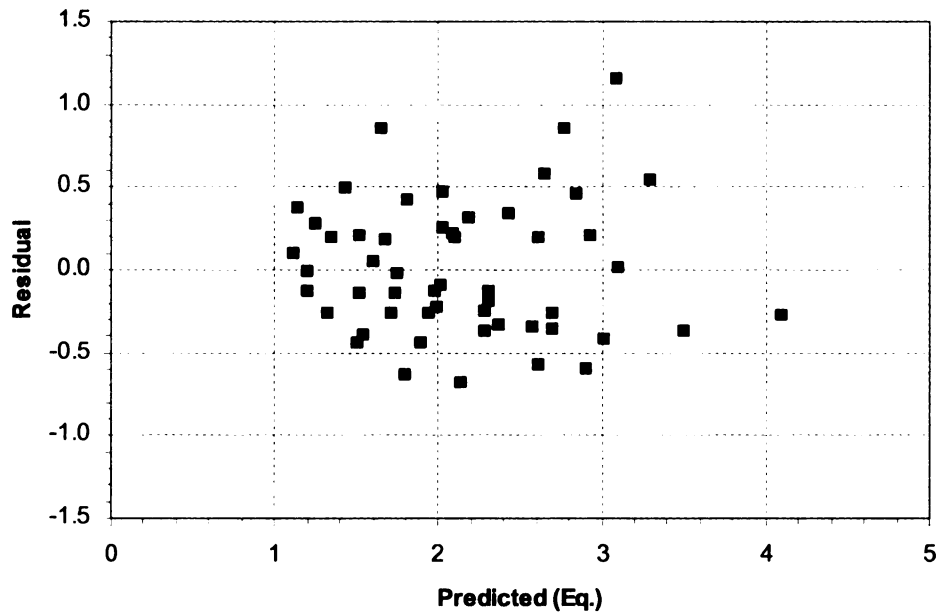

Figure 7.12 – Residual versus Predicted Values of Structural Factor (ϕ_{FR})

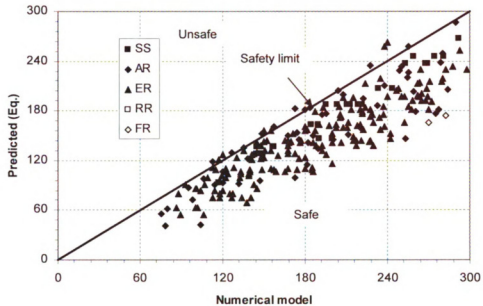

Figure 7.13 – Simulated versus Predicted Fire Resistance (in Minutes) for RC Beams Made of Carbonate Aggregate Concrete

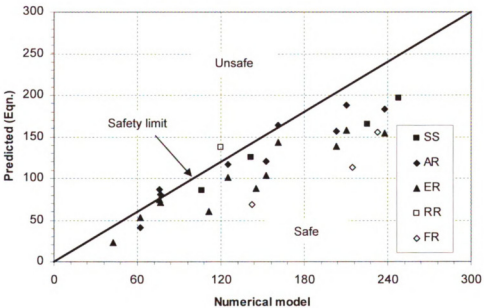

Figure 7.14 – Simulated versus Predicted Fire Resistance (in Minutes) for HSC Beams

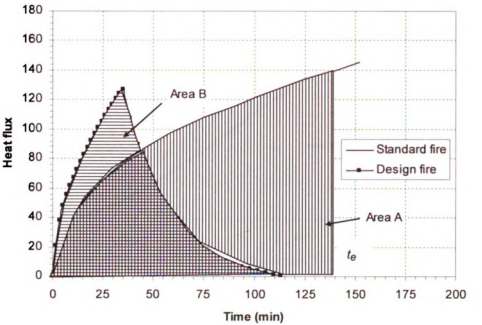

Figure 7.15 – Equivalent Energy Concept for Standard and Design Fires

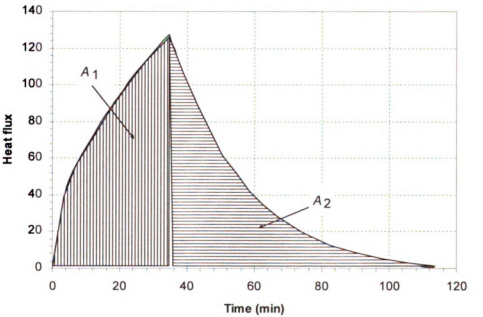

Figure 7.16 – The Areas under the Ascending and the Descending Heat Flux curve for a Design Fire

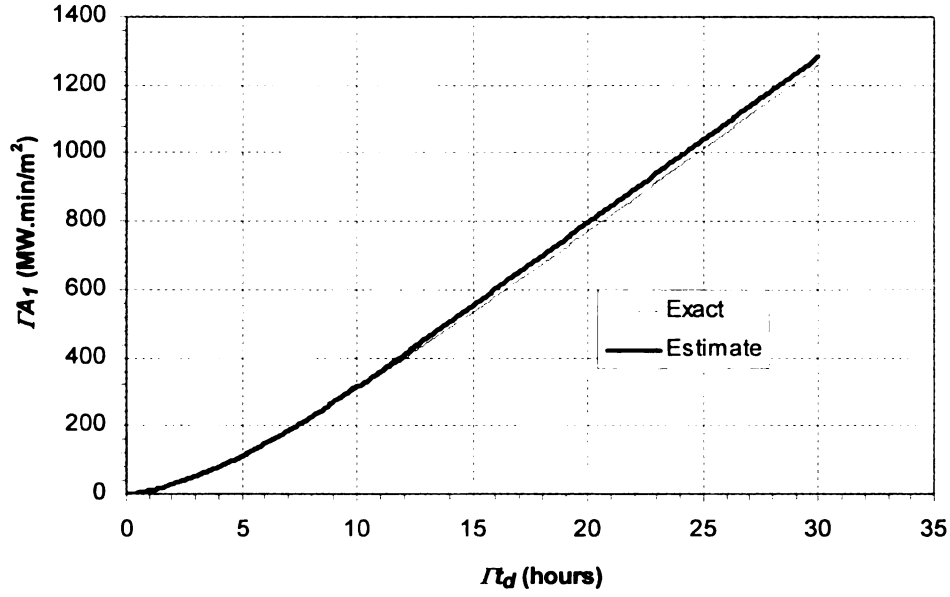

Figure 7.17 – Best Fitting for the Areas under the Ascending Heat Flux curve for a Design Fire

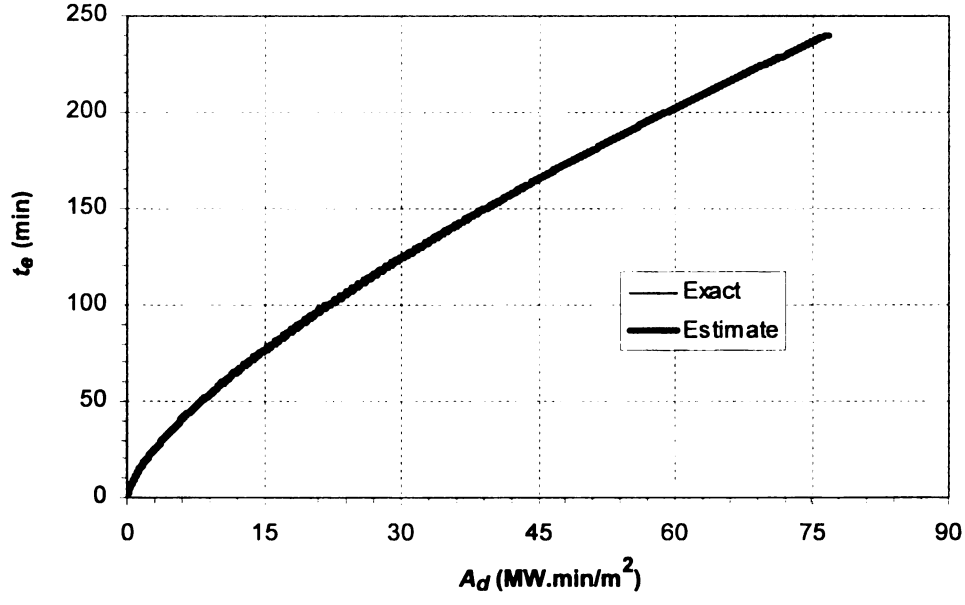

Figure 7.18 – Best Fitting for the Areas under the Heat Flux curve for ASTM E119 Standard Fire

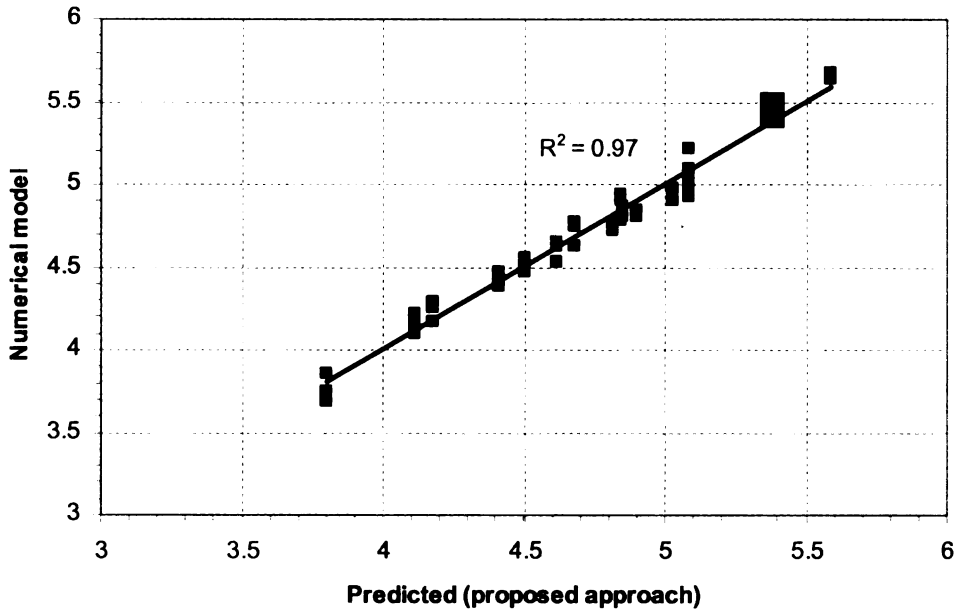

Figure 7.19 – Simulated versus Predicted Values of LN(t_e)

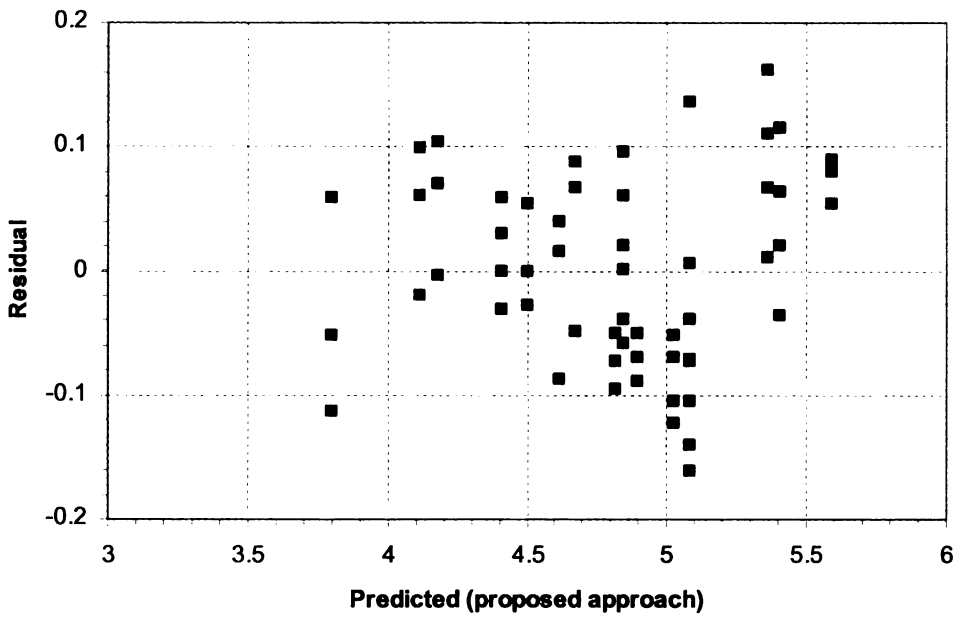

Figure 7.20 – Residual versus Predicted Values of LN(t_e)

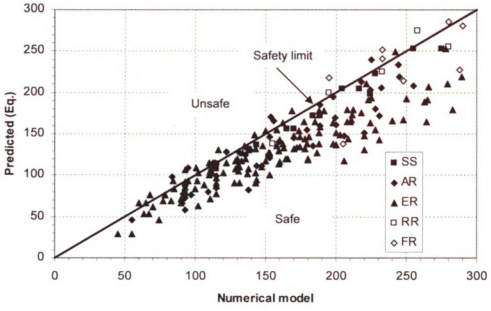

Figure 7.21 – Simulated versus Predicted Fire Resistance (in Minutes) for RC Beams

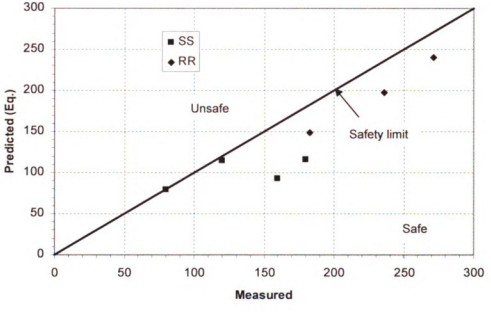

Figure 7.22 – Measured versus Predicted Fire Resistance (in Minutes) for HSC Beams

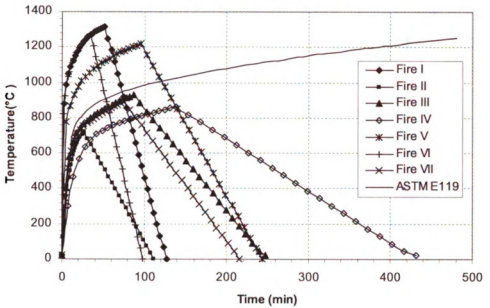

(a) Fires I to VII and ASTM E119

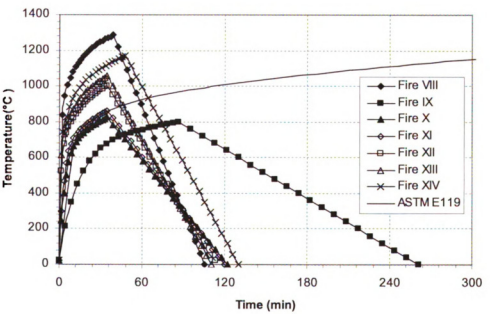

(b) Fires VIII and XIV and ASTM E119

Figure 7.23 – Time-temperature Curves for Design Fire Scenarios used in the Analysis

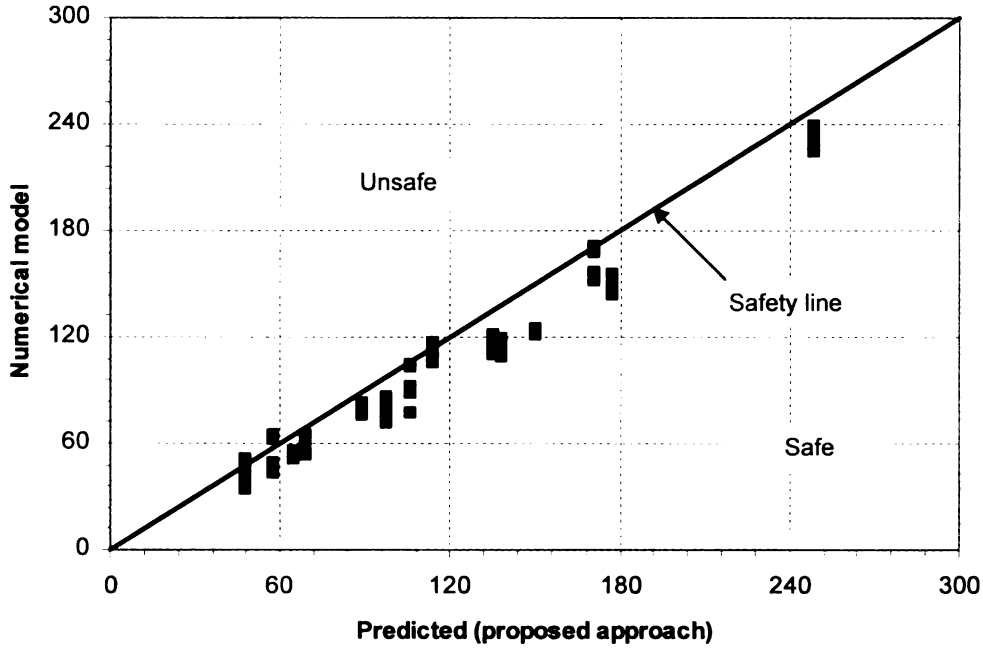

Figure 7.24 – Simulated versus Predicted Time Equivalent (in Minutes)

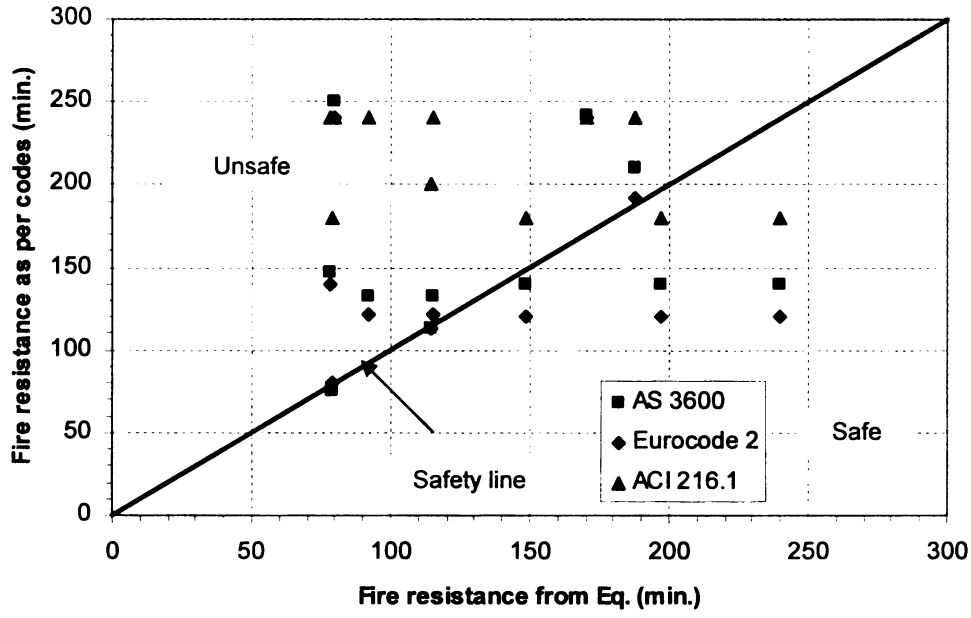

Figure 7.25 – Comparison of Fire Resistance Predicted from Proposed Equation with Provisions in Current Codes

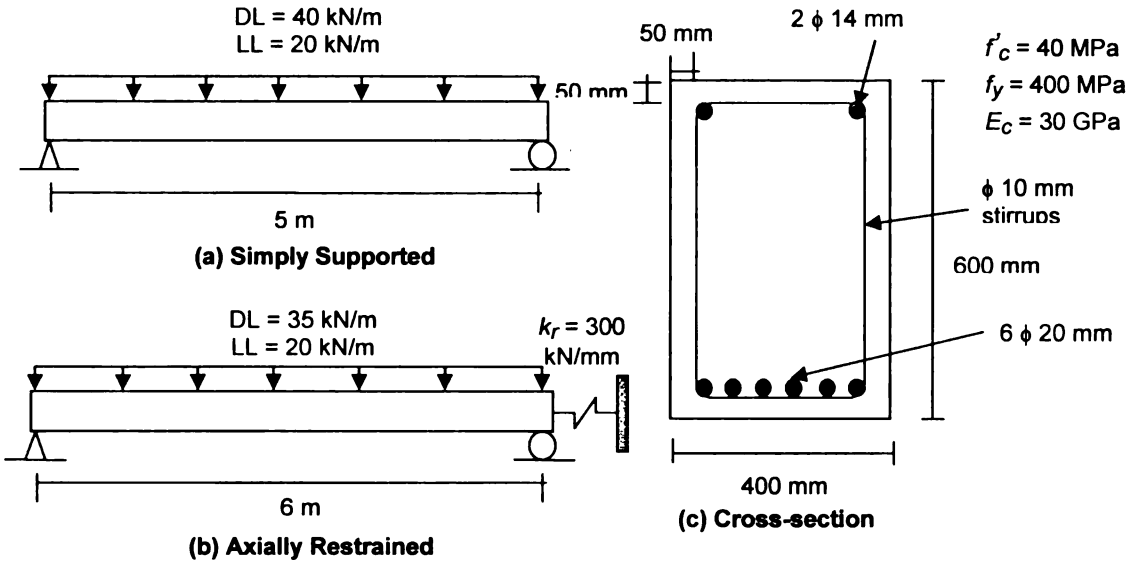

Figure 7.26 – Cross-section and Elevation of RC Beam used in the Worked Example

Chapter 8

8. Conclusions and Recommendations

8.1 General

The structural response of RC beams under fire conditions was investigated in this study. A numerical model was developed for tracing the response of RC beams under realistic fire, loading and restraint conditions. The model is based on a macroscopic finite element approach and uses time-dependent moment-curvature relationships to trace the response of the beam from the pre-fire stage to failure under fire conditions. All of the critical factors, namely, high temperature material properties, fire induced spalling, different strain components, and the fire induced restraint effect that have significant influence on the fire response of RC beams are incorporated in the model. For validating the numerical model, fire tests on six RC beams were conducted under varying fire, concrete strength, load level, and restraint conditions. Data from fire tests was used to validate the numerical model for various parameters such as temperatures, deflections, spalling, and fire resistance. The numerical model was applied to conduct parametric studies to

quantify the influence of various factors on the fire response of RC beams. Finally, data from parametric studies was utilized to develop a two-step rational design approach for evaluating the fire resistance of RC beams. In the first step, the fire resistance of the beam under standard fire exposure is evaluated. In the second step, a new equivalency approach is derived based on the equal energy concept and used to evaluate the fire resistance of RC beams under design fire exposure. The proposed design approach accounts for significant parameters that govern the fire response of RC beams, and thus provides better fire resistance estimates as compared to current code provisions.

8.2 Key Findings

Based on the information presented in this thesis, the following are the key conclusions:

- There is very limited information on the fire performance of RC beams, especially under design fires and realistic loading scenarios. The current fire resistance provisions, developed based on limited fire tests under "standard fire scenarios", are prescriptive and do not facilitate a rational approach for evaluating the fire resistance.
- The moment-curvature based macroscopic finite element model is capable of predicting the response of RC beams, in the entire range from the pre-fire stage to collapse under fire conditions. The model accounts for all critical factors governing the fire response of RC beams. In addition, the model is capable of simulating the response of beams under any given fire, loading and restraint scenarios.
- Fire resistance tests on six RC beams provide unique data on the behavior of NSC and HSC beams under realistic fire, load, and restraint scenarios.

- Results from parametric studies, as well as data from fire resistance tests, indicate that fire scenario, load ratio, span-to-depth ratio, location of axial restraint and rotational restraint have a significant influence on the fire response of RC beams. Concrete cover thickness, beam width, aggregate type, axial restraint stiffness, and concrete strength and spalling have a moderate influence on the fire response of beams. Strength of reinforcement and ratio of tension steel do not significantly influence the fire resistance of RC beams. Specifically:
    - Higher load level, higher span-to-depth ratio, or increased extent of spalling reduces the fire response of RC beams.
    - Increased beam width, increased concrete cover thickness, and increased rotational restraint lead to higher fire resistance of RC beams.
    - The effect of the degree of restraint and location of axial restraint on the fire resistance is dependent on the span-to-depth ratio of the beam. Generally, fire resistance is higher when the axial restraint is shifted downward below the centroidal axis of the beam.
    - The type of fire exposure has a significant effect on the fire resistance of RC beams and no failure occurs in RC beams under most design fire scenarios.
    - The fire resistance of HSC beams is lower than that of NSC beams with brittle failure occurring in HSC beams.
    - Concrete permeability has a significant influence on fire induced spalling and thus the fire resistance of RC beams. HSC, due to low permeability, is more prone to fire induced spalling than NSC and the extent of spalling

increases with higher load levels and under an increased degree of axial restraint.

- RC beams made with carbonate aggregate have higher fire resistance than those made with siliceous aggregate.
- The strength and the deflection limit states provide a realistic failure assessment in RC beams under fire conditions. The rebar temperature limit state, often used due to its ease of application, may not provide a realistic assessment of failure.

- The proposed fire resistance equation for standard fire exposure and the energy-based approach for establishing equivalency under design fire exposure account for critical governing parameters and thus is capable of predicting the fire resistance of NSC and HSC beams under realistic fire, loading and support conditions.
- In the proposed approach, the fire resistance is expressed in terms of commonly used design parameters and therefore the fire resistance calculations can be generally integrated into structural design.
- The proposed approach provides better fire resistance predictions than those obtained from current code provisions.

8.3 Recommendations for Future Research

While this study has advanced the state-of-the-art with respect to fire response of RC beams, further research is required to fully characterize the complex behavior of concrete members under fire exposure. The following are some of the key recommendations for further research in this area:

- The moment-curvature based microscopic finite element numerical model, presented here, can be extended to other concrete structures such as beams with different cross-sectional shapes (T, I, and inversed-T concrete sections), prestressing effects, and FRP-strengthening. This can be achieved by extending thermal and structural sub-models to account for different cross-sectional types, prestressing effect, and high temperature properties of FRP and insulation material. The numerical procedures should be enhanced to account for shear and bond effects, since these factors may be critical for prestressed and FRP-strengthened concrete beams.
- The macroscopic finite element model can be further advanced by incorporating coupling between hydro-thermal and structural models. Such advancement enables the model to consider the influence of mechanical response (such as stresses, and cracking) on the hydro-thermal analysis and spalling predictions in concrete.
- The current constitutive models for high temperature material properties of concrete and steel (including high temperature creep strain in concrete and reinforcing steel, and also transient strain in concrete), particularly in the cooling phase, are not sufficiently accurate. Improvements in such constitutive models will help to enhance the accuracy of the model predictions under design fire scenarios.
- The currently available constitutive relationships for high temperature permeability and porosity of concrete are not sufficiently reliable. Such

constitutive relationships are crucial to improve the accuracy of spalling predictions, which can be critical in HSC beams.

- Strain gage measurements would have been a useful source of data to fully validate the model under combined effects of applied load and fire, and to quantify the different strain components under fire exposure. The high temperature strain gages currently available in the market do not provide reliable measurements under fire exposure, and thus there is a need for developing reliable high temperature strain gages.

8.4 Research Impact

The current approach of evaluating fire resistance through standard fire tests on full-scale RC beams is expensive, time consuming and has a number of drawbacks. An alternative is to use calculation methods for predicting fire resistance. However, such calculation methods are not widely available at present. Further, the current fire resistance provisions in codes and standards (ACI 216.1 2007, Eurocode 2 2004) are prescriptive and do not account for realistic conditions such as loading, fire, restraint, and spalling effects. Thus, the current design approaches are not applicable for undertaking performance-based design which provides rational and cost-effective fire safety solutions.

The proposed numerical model and design approach provide a convenient way of obtaining fire resistance of RC beams, and thus can be used for estimating fire resistance in lieu of full-scale standard fire resistance tests. The numerical model can be utilized for studying the detailed fire response of RC beams under fire conditions. The proposed design approach can be applied to evaluate fire resistance under realistic fire, loading and restraint scenarios. The proposed equation expresses fire resistance in terms of structural

parameters, and thus the approach is attractive for incorporation in codes and standards. In summary, the use of the proposed approach can facilitate a rational fire resistance design under a performance-based code environment. Such a rational design approach will contribute to reduced loss of life and property damage in fire incidents.

Appendix A

A.1 Material Properties

Table A.1 – Constitutive Relationships for High Temperature Properties of Concrete

	Normal strength concrete – [ASCE Manual (1992)]
Stress-strain relationships	$$\sigma_c = \begin{Bmatrix} f'_{c,T}\left[1-\left(\frac{\varepsilon-\varepsilon_{\max,T}}{\varepsilon_{\max,T}}\right)^2\right], & \varepsilon \le \varepsilon_{\max,T} \\ f'_{c,T}\left[1-\left(\frac{\varepsilon_{\max,T}-\varepsilon}{3\varepsilon_{\max,T}}\right)^2\right], & \varepsilon > \varepsilon_{\max,T} \end{Bmatrix}$$ $$f'_{c,T} = \begin{Bmatrix} f'_c & ,20\,°C \le T \le 450\,°C \\ f'_c\left[2.011-2.353\left(\frac{T-20}{1000}\right)\right] & ,450\,°C < T \le 874\,°C \\ 0 & ,\ 874\,°C < T \end{Bmatrix}$$ $$\varepsilon_{\max,T} = 0.0025+\left(6.0T+0.04T^2\right)\times 10^{-6}$$
Thermal Capacity	Siliceous Aggregate Concrete: $$\rho c = \begin{Bmatrix} 0.005T+1.7 & 20\,°C \le T \le 200\,°C \\ 2.7 & 200\,°C < T \le 400\,°C \\ 0.013T-2.5 & 400\,°C < T \le 500\,°C \\ 10.5-0.013T & 500\,°C < T \le 600\,°C \\ 2.7 & 600\,°C < T \end{Bmatrix}$$ Carbonate Aggregate Concrete: $$\rho c = \begin{Bmatrix} 2.566 & 20\,°C \le T \le 400\,°C \\ 0.1765T-68.034 & 400\,°C < T \le 410\,°C \\ 25.00671-0.05043T & 410\,°C < T \le 445\,°C \\ 2.566 & 445\,°C < T \le 500\,°C \\ 0.01603T-5.44881 & 500\,°C < T \le 635\,°C \\ 0.16635T-100.90225 & 635\,°C < T \le 715\,°C \\ 176.07343-0.22103T & 715\,°C < T \le 785\,°C \\ 2.566 & 785\,°C < T \end{Bmatrix}$$

Table A.1 (Continued) – Constitutive Relationships for High Temperature Properties of Concrete

	Normal strength concrete – [ASCE Manual (1992)]
Thermal Conductivity	Siliceous Aggregate Concrete: $k_c = \begin{Bmatrix} -0.000625T + 1.5 & 20\,°C \le T \le 800\,°C \\ 1.0 & 800°C < T \end{Bmatrix}$ Carbonate Aggregate Concrete: $k_c = \begin{Bmatrix} 1.355 & 20\,°C \le T \le 293\,°C \\ -0.001241T + 1.7162 & 293\,°C < T \end{Bmatrix}$
Thermal Strain	All types: $\varepsilon_{th} = \left[0.004\left(T^2 - 400\right) + 6(T - 20)\right] \times 10^{-6}$

Table A.1 (Continued) – Constitutive Relationships for High Temperature Properties of Concrete

	High strength concrete – [Kodur et al. (2004)]
Stress-strain relationships	$$\sigma_c = \begin{cases} f'_{c,T}\left[1-\left(\dfrac{\varepsilon_{\max,T}-\varepsilon}{\varepsilon_{\max,T}}\right)^{H}\right] & \varepsilon \le \varepsilon_{\max,T} \\ f'_{c,T}\left[1-\left(\dfrac{30(\varepsilon-\varepsilon_{\max,T})}{(130-f'_c)\varepsilon_{\max,T}}\right)^{2}\right] & \varepsilon > \varepsilon_{\max,T} \end{cases}$$ $$f'_{c,T} = \begin{cases} f'_c[1.0-0.003125(T-20)] & T<100°C \\ 0.75f'_c & 100°C \le T \le 400°C \\ f'_c[1.33-0.00145T] & 400°C < T \end{cases}$$ $$\varepsilon_{\max,T} = 0.0018 + \left(6.7f'_c + 6.0T + 0.03T^2\right)\times 10^{-6}$$ $$H = 2.28 - 0.012f'_c$$
Thermal Capacity	Siliceous Aggregate Concrete: $$\rho c = \begin{cases} 0.005T + 1.7 & 20\,°C \le T \le 200\,°C \\ 2.7 & 200\,°C < T \le 400\,°C \\ 0.013T - 2.5 & 400\,°C < T \le 500\,°C \\ -0.013T + 10.5 & 500\,°C < T \le 600\,°C \\ 2.7 & 600\,°C < T \le 635\,°C \end{cases}$$ Carbonate Aggregate Concrete: $$\rho c = \begin{cases} 2.45 & 20\,°C \le T \le 400\,°C \\ 0.026T - 12.85 & 400\,°C < T \le 475\,°C \\ 0.0143T - 6.295 & 475\,°C < T \le 650\,°C \\ 0.1894T - 120.11 & 650\,°C < T \le 735\,°C \\ -0.263T + 212.4 & 735\,°C < T \le 800\,°C \\ 2 & 800\,°C < T \le 1000\,°C \end{cases}$$

Table A.1 (Continued) – Constitutive Relationships for High Temperature Properties of Concrete

	High strength concrete – [Kodur et al. (2004)]
Thermal Conductivity	Siliceous Aggregate Concrete: $k_c = 0.85(2 - 0.0011T) \quad 20°C < T \leq 1000°C$ Carbonate Aggregate Concrete: $k_c = \begin{Bmatrix} 0.85\,(2 - 0.0013T) & 20\,°C \leq T \leq 300\,°C \\ 0.85(2.21 - 0.002T) & 300\,°C < T \end{Bmatrix}$
Thermal Strain	All types: $\varepsilon_{th} = \left[0.004\left(T^2 - 400\right) + 6(T - 20)\right] \times 10^{-6}$

Table A.1 (Continued) – Constitutive Relationships for High Temperature Properties of Concrete

	Normal strength and high strength concrete – [Eurocode 2 (2004)]
Stress-strain relationships	$$\sigma_c = \frac{3\varepsilon f'_{c,T}}{\varepsilon_{c1,T}\left(2 + \left(\frac{\varepsilon}{\varepsilon_{c1,T}}\right)^3\right)} \quad , \varepsilon \leq \varepsilon_{cu1,T}$$ **For $\varepsilon_{c1(T)} < \varepsilon \leq \varepsilon_{cu1(T)}$, the Eurocode permits the use of linear as well as nonlinear descending branch in the numerical analysis.** **For the parameters in this equation refer to Table A2**
Thermal Capacity	Specific heat (J/kg°C) $c = 900$, for $20°C \leq T \leq 100°C$ $c = 900 + (T - 100)$, for $100°C < T \leq 200°C$ $c = 1000 + (T - 200)/2$, for $200°C < T \leq 400°C$ $c = 1100$, for $400°C < T \leq 1200°C$ Density change (kg/m^3) $\rho = \rho(20°C)$ = *Reference density* for $20°C \leq T \leq 115°C$ $\rho = \rho(20°C)\,(1 - 0.02(T - 115)/85)$ for $115°C < T \leq 200°C$ $\rho = \rho(20°C)\,(0.98 - 0.03(T - 200)/200)$ for $200°C < T \leq 400°C$ $\rho = \rho(20°C)\,(0.95 - 0.07(T - 400)/800)$ for $400°C < T \leq 1200°C$ *Thermal Capacity* $= \rho \times c$

Table A.1 (Continued) – Constitutive Relationships for High Temperature Properties of Concrete

		Normal strength and high strength concrete – [Eurocode 2 (2004)]
Thermal Conductivity	*All types*	Upper limit: $k_c = 2 - 0.2451\,(T/100) + 0.0107\,(T/100)2$ *for* $20°C \leq T \leq 1200°C$ Lower limit: $k_c = 1.36 - 0.136\,(T/100) + 0.0057\,(T/100)2$ *for* $20°C \leq T \leq 1200°C$
Thermal Strain	*Siliceous aggregate*	$\varepsilon_{th} = -1.8\times10^{-4}+9\times10^{-6}T+2.3\times10^{-11}T^3$ *for* $20°C \leq T \leq 700°C$ $\varepsilon_{th} = 14\times10^{-3}$ *for* $700°C < T \leq 1200°C$
	Carbonate aggregate	$\varepsilon_{th} = -1.2\times10^{-4}+6\times10^{-6}T+1.4\times10^{-11}T^3$ *for* $20°C \leq T \leq 805°C$ $\varepsilon_{th} = 12\times10^{-3}$ *for* $805°C < T \leq 1200°C$

Table A.2. Values for the Main Parameters of the Stress-strain Relationships of NSC and HSC at Elevated Temperatures (Eurocode 2)

T °C	NSC						HSC		
	Siliceous Agg.			Calcareous Agg.			$f'_{c,T} / f'_c(20°C)$		
	$\frac{f'_{c,T}}{f'_c(20°C)}$	$\varepsilon_{c1,T}$	$\varepsilon_{cu1,T}$	$\frac{f'_{c,T}}{f'_c(20°C)}$	$\varepsilon_{c1,T}$	$\varepsilon_{cu1,T}$	Class 1	Class 2	Class3
20	1	0.0025	0.02	1	0.0025	0.02	1	1	1
100	1	0.004	0.0225	1	0.004	0.023	0.9	0.75	0.75
200	0.95	0.0055	0.025	0.97	0.0055	0.025	0.9	0.75	0.70
300	0.85	0.007	0.0275	0.91	0.007	0.028	0.85	0.75	0.65
400	0.75	0.01	0.03	0.85	0.01	0.03	0.75	0.75	0.45
500	0.6	0.015	0.0325	0.74	0.015	0.033	0.60	0.60	0.30
600	0.45	0.025	0.035	0.6	0.025	0.035	0.45	0.45	0.25
700	0.3	0.025	0.0375	0.43	0.025	0.038	0.30	0.30	0.20
800	0.15	0.025	0.04	0.27	0.025	0.04	0.15	0.15	0.15
900	0.08	0.025	0.0425	0.15	0.025	0.043	0.08	0.113	0.08
1000	0.04	0.025	0.045	0.06	0.025	0.045	0.04	0.075	0.04
1100	0.01	0.025	0.0475	0.02	0.025	0.048	0.01	0.038	0.01
1200	0	-	-	0	-	-	0	0	0

Table A.3 – Constitutive Relationships for High Temperature Properties of Reinforcing Steel

	ASCE Manual (1992)
Stress-strain relationships	$$\sigma_s = \begin{cases} \dfrac{f(T,0.001)}{0.001}\varepsilon_s & \varepsilon_s \le \varepsilon_p \\ \dfrac{f(T,0.001)}{0.001}\varepsilon_p + f(T,\varepsilon_s - \varepsilon_p + 0.001) - f(T,0.001) & \varepsilon_s > \varepsilon_p \end{cases}$$ $$f(T,x) = 6.9(50 - 0.04T)\left[1 - \exp\left((-30 + 0.03T)\sqrt{x}\right)\right]$$ $$\varepsilon_p = 4 \times 10^{-6} f_{y,20}$$ where: σ_s and ε_s = stress (MPa) and strain in steel reinforcement, respectively, and $f_{y,20}$ is the yield strength of reinforcing steel (MPa) at room temperature.
Thermal Strain	$$\varepsilon_{ths} = \left[0.004\left(T^2 - 400\right) + 6(T - 20)\right] \times 10^{-6} \qquad T < 1000°C$$

Table A.3 (Continued) – Constitutive Relationships for High Temperature Properties of Reinforcing Steel

	Eurocode 2 (2004)
Stress-strain relationships	$$\sigma_s = \begin{cases} \varepsilon_s E_{s,T} & \varepsilon_s \le \varepsilon_{sp,T} \\ f_{sp,T} - c + (b/a)\left(a^2 - (\varepsilon_{sy,T} - \varepsilon_s)^2\right)^{0.5} & \varepsilon_{sp,T} < \varepsilon_s \le \varepsilon_{sy,T} \\ f_{sy,T} & \varepsilon_{sy,T} < \varepsilon_s \le \varepsilon_{st,T} \\ f_{sy,T}\left(1 - \dfrac{\varepsilon_s - \varepsilon_{st,T}}{\varepsilon_{su,T} - \varepsilon_{st,T}}\right) & \varepsilon_{st,T} < \varepsilon_s \le \varepsilon_{su,T} \\ 0.0 & \varepsilon_s > \varepsilon_{su,T} \end{cases}$$ Parameters $$\varepsilon_{sp,T} = \frac{f_{sp,T}}{E_{s,T}} \quad \varepsilon_{sy,T} = 0.02 \quad \varepsilon_{st,T} = 0.15 \quad \varepsilon_{su,T} = 0.2$$ Functions $$a^2 = (\varepsilon_{sy,T} - \varepsilon_{sp,T})\left(\varepsilon_{sy,T} - \varepsilon_{sp,T} + \frac{c}{E_{s,T}}\right)$$ $$b^2 = c(\varepsilon_{sy,T} - \varepsilon_{sp,T})E_{s,T} + c^2$$ $$c = \frac{(f_{sy,T} - f_{sp,T})^2}{(\varepsilon_{sy,T} - \varepsilon_{sp,T})E_{s,T} - (f_{sy,T} - f_{sp,T})}$$ **Values of $f_{sp,T}$, $f_{sy,T}$ and $E_{s,T}$ can be obtained from Table A.4**
Thermal Strain	$$\varepsilon_{ths} = \begin{cases} 1.2\times10^{-5}T + 0.4\times10^{-8}T^2 - 2.416\times10^{-4} & 20°C \le T < 750°C \\ 1.1\times10^{-2} & 750°C \le T < 860°C \\ 2\times10^{-5}T - 6.2\times10^{-3} & 20°C \le T < 750°C \end{cases}$$

Table A.4. Values for the Main Parameters of the Stress-strain Relationships of Reinforcing Steel at Elevated Temperatures (Eurocode 2)

Steel Temperature T (°C)	f_{yT} / f_y	f_{sp} / f_y *	E_{sT} / E_s *
20	1	1	1
100	1	1	1
200	1	0.807	0.9
300	1	0.613	0.8
400	1	0.42	0.7
500	0.78	0.36	0.6
600	0.47	0.18	0.31
700	0.23	0.075	0.13
800	0.11	0.05	0.09
900	0.06	0.0375	0.0675
1000	0.04	0.025	0.045
1100	0.02	0.0125	0.0225
1200	0	0	0

* f_y and E_s are yield strength and modulus of elasticity at room temperature

Appendix B

B.1 Design of Beams

This appendix summarizes the design calculations using ACI 318 (2008) provisions for an NSC beam and an HSC beam. The cross-section, shear force diagram, and bending moment diagram for the tested beams are shown in Figure B.1. The design calculations are presented in the following two sections.

B.1.1 Normal Strength Concrete Beam

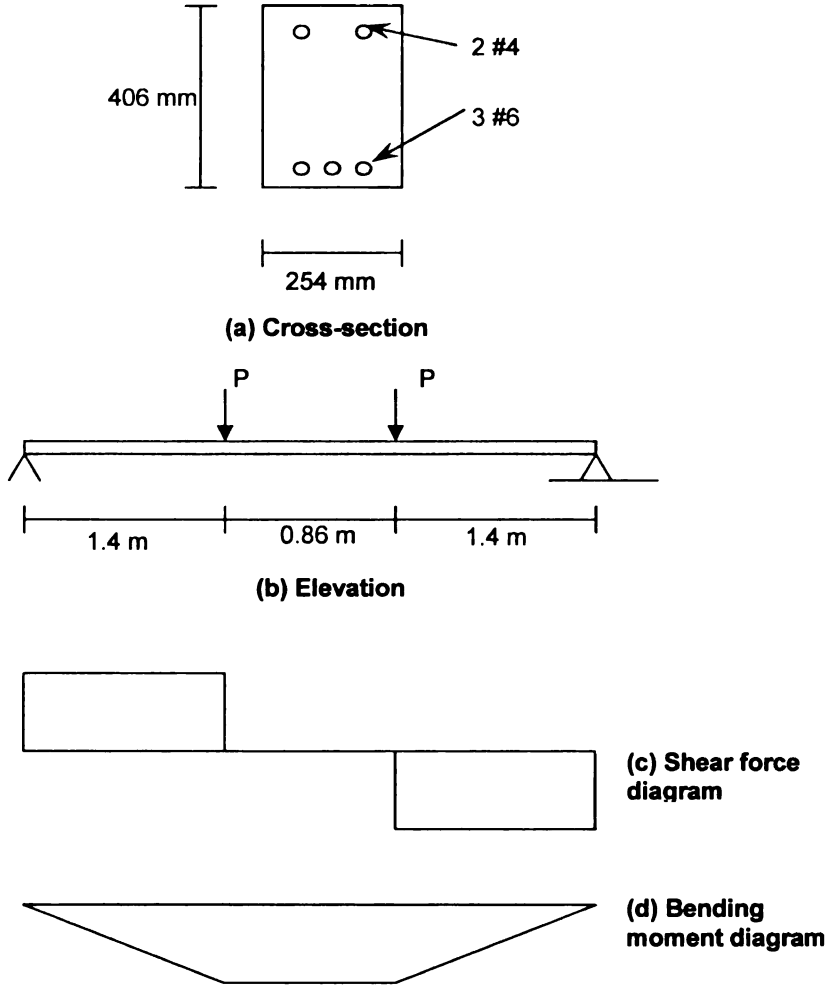

Figure B.1 – Cross-section, Elevation, Shear Force Diagram, and Bending Moment Diagram for Tested Beams

$f'_c = 41.3\,\text{MPa}$ $f_y = 413\,\text{MPa}$

Neglecting the area of steel in the compression zone:

The tensile area of steel A_s = 855 mm^2

Clear concrete cover = 38 mm

h = 406 mm b = 254 mm

d = 352.4 mm

$a = 39.6\,\text{mm}$

$a = \beta_1 c$

Hence, $\beta_1 = 0.75$

Therefore, $c = \dfrac{39.6}{0.75} = 52.8\,\text{mm}$

Strain in tensile steel can be calculated by interpolation as follows:

$$\varepsilon_t = \frac{0.003}{c}(d-c) = \frac{0.003}{52.8}(352.4-52.8) = 0.017 > 0.005$$

Hence, $\phi = 0.9$

Check minimum reinforcement:

$\rho_{min} = 0.0039$

$$\rho = \frac{A_s}{bd} = 0.00955 > \rho_{min}$$

The moment capacity of the beam is

$$M_n = A_s f_y\left(d - \frac{a}{2}\right) = \frac{855 \times 413 \times \left(352.4 - \dfrac{39.6}{2}\right)}{10^6} = 117\,\text{kN.m}$$

$M_n = 1.4P_n$

$P_n = 83.9$ kN and $P_u = 75.5$ kN

Design for shear:

The ultimate shear force is at distance *d* from the face of the support:

$V_u = P_u = 75.5$ kN

Required nominal shear strength:

$\phi = 0.75$

$$V_n = \frac{V_u}{\phi} = \frac{75.5}{0.75} = 100.7\,\text{kN}$$

The concrete shear strength is:

$$V_c = 0.16\sqrt{f_c'}b_w d = \frac{0.16\sqrt{41.3} * 254 * 352.4}{1000} = 92\,\text{kN}$$

The required shear strength obtained by shear reinforcement must be:

$V_n > V_c$

$V_S = V_n - V_C = 100.7 - 92 = 8.7\,\text{kN}$

$$V_{s\,min} = max\begin{Bmatrix} 0.344b_w d \\ 0.06\sqrt{f_c'}b_w d \end{Bmatrix} = 35\,\text{kN}$$

Use minimum shear reinforcement

The required shear reinforcement will be found to be

$$\frac{A_v}{s} = 0.237\,\text{mm}$$

Using #2 stirrups

The area of each leg is 31.6 mm^2

Hence, A_v =2×31.6 = 63.2 mm^2

The required spacing will be:

$$s = \frac{63.2}{0.237} = 267\ \text{mm} \le \frac{d}{2} = \frac{352.4}{2} = 176.2\,\text{mm}$$ ***(ACI 318 11.5.4.1)***

Hence, use #2 stirrups 150 mm c/c

Check deflection:

The gross moment of inertia (neglecting the compressive and tensile steel) can be calculated as:

$$I_g = \frac{bh^3}{12} = 1.416 \times 10^9 \text{ mm}^4$$

The cracked moment of inertia (neglecting the compressive steel) can be calculated as follows:

$$E_s = 210 \text{ GPa}$$

$$E_c = 4730\sqrt{f_c'} = 30.4 \text{ GPa}$$

$$n = \frac{E_s}{E_c} = 6.9$$

$$x = \frac{\sqrt{(nA_s)^2 + 2bdnA_s} - nA_s}{b} = 106.9 \text{ mm}$$

$$I_{cr} = \frac{bx^3}{3} + nA_s(d-x)^2$$

$$I_{cr} = 0.459 \times 10^9 \text{ mm}^4$$

The modulus of rupture is:

$$f_r = 0.6\sqrt{f_c'} = 3.86 \text{ MPa}$$

The cracking moment is

$$M_{cr} = \frac{f_r I_g}{y_t} = 26.9 \text{ kN.m}$$

The effective moment of inertia will be:

Assume M_a to be $0.7M_u$, then

$M_a = 0.7 \times 117 \times 0.9 = 73.71$ kN.m

$$I_e = \left(\frac{M_{cr}}{M_a}\right)^3 I_g + \left[1 - \left(\frac{M_{cr}}{M_a}\right)^3\right] I_{cr} \le I_g$$

$I_e = 0.506 \times 10^9 \text{ mm}^4$

Hence, the deflection of the beam will be:

$$\delta = \frac{M}{2E_c I_e}\left(\frac{L^2}{4} - \frac{a^2}{3}\right) = 6.5 \text{ mm}$$

B.1.2 High Strength Concrete Beam

$f'_c = 100 \text{ MPa}$ $f_y = 413 \text{ MPa}$

Neglecting the area of steel in the compression zone:

The tensile area of steel A_s = 855 mm^2

Clear concrete cover = 38 mm

h = 406 mm b = 254 mm

d = 352.4 mm

$a = 16.4 \text{ mm}$

$a = \beta_1 c$

Hence, $\beta_1 = 0.65$

Therefore, $c = \frac{39.6}{0.65} = 25.2 \text{ mm}$

Strain in tensile steel can be calculated by interpolation as follows:

$$\varepsilon_t = \frac{0.003}{c}(d - c) = \frac{0.003}{25.2}(352.4 - 25.2) = 0.039 > 0.005$$

Hence, $\phi = 0.9$

Check minimum reinforcement:

$\rho_{min} = 0.006$

$$\rho = \frac{A_s}{bd} = 0.00955 > \rho_{min}$$

The moment capacity of the beam is

$$M_n = A_s f_y \left(d - \frac{a}{2} \right) = \frac{855 \times 413 \times \left(352.4 - \frac{16.4}{2} \right)}{10^6} = 121.6 \text{ kN.m}$$

$$M_n = 1.4 P_n$$

$$P_n = 86.8 \text{ kN} \qquad \text{and } P_u = 78.1 \text{ kN}$$

Design for shear:

The ultimate shear force is at distance *d* from the face of the support:

$$V_u = P_u = 78.1 \text{ kN}$$

Required nominal shear strength:

$$\phi = 0.75$$

$$V_n = \frac{V_u}{\phi} = \frac{78.1}{0.75} = 104.2 \text{kN}$$

The concrete shear strength is:

$$V_c = 0.16\sqrt{f_c'} b_w d = \frac{0.16\sqrt{100} * 254 * 352.4}{1000} = 165 \text{kN}$$

The required shear strength obtained by shear reinforcement must be:

$$V_n < V_c \qquad V_n > \frac{V_c}{2}$$

Use minimum shear reinforcement

$$V_{S\,min} = max\begin{Bmatrix} 0.344 b_w d \\ 0.06\sqrt{f_c'} b_w d \end{Bmatrix} = 53.7 \text{ kN}$$

The required shear reinforcement may be calculated by

$$\frac{A_V}{s} = 0.369 \text{mm}$$

Using #2 stirrups

The area of each leg is 31.6 mm^2

Hence, A_v =2*31.6 = 63.2 mm^2

The required spacing will be:

$$s = \frac{63.2}{0.369} = 171 \text{ mm}$$

Hence, use # 2 stirrups 150 mm c/c

Check deflection:

The gross moment of inertia (neglecting the compressive and tensile steel) can be calculated as:

$$I_g = \frac{bh^3}{12} = 1.416 \times 10^9 \text{ mm}^4$$

The cracked moment of inertia (neglecting the compressive steel) can be calculated as follows:

$$E_S = 210 \text{GPa}$$

$$E_C = 4730\sqrt{f_c'} = 47.3 \text{ GPa}$$

$$n = \frac{E_s}{E_c} = 4.4$$

$$x = \frac{\sqrt{(nA_s)^2 + 2bdnA_s} - nA_s}{b} = 88.8 \text{ mm}$$

$$I_{cr} = \frac{bx^3}{3} + nA_s(d-x)^2$$

$$I_{cr} = 0.323 \times 10^9 \text{ mm}^4$$

The modulus of rupture is:

$$f_r = 0.6\sqrt{f_c'} = 6 \text{ MPa}$$

The cracking moment is

$$M_{cr} = \frac{f_r I_g}{y_t} = 41.9 \text{ kN.m}$$

The effective moment of inertia will be:

Assume M_a to be $0.7M_u$, then

$M_a = 0.7 \times 121.6 \times 0.9 = 76.6$ kN.m

$$I_e = \left(\frac{M_{cr}}{M_a}\right)^3 I_g + \left[1 - \left(\frac{M_{cr}}{M_a}\right)^3\right] I_{cr} \leq I_g$$

$$I_e = 0.501 \times 10^9 \text{ mm}^4$$

Hence, the deflection of the beam will be:

$$\delta = \frac{M}{2E_c I_e}\left(\frac{L^2}{4} - \frac{a^2}{3}\right) = 4.4 \text{ mm}$$

B.2 Load Calculations

This appendix summarizes the load calculations using ACI 318 (2008) provisions for an NSC beam and an HSC beam, which were tested in the experimental program. The shear force diagram and bending moment diagram for the tested beams are shown in Figure B.2. The load calculations are presented in the following two sections.

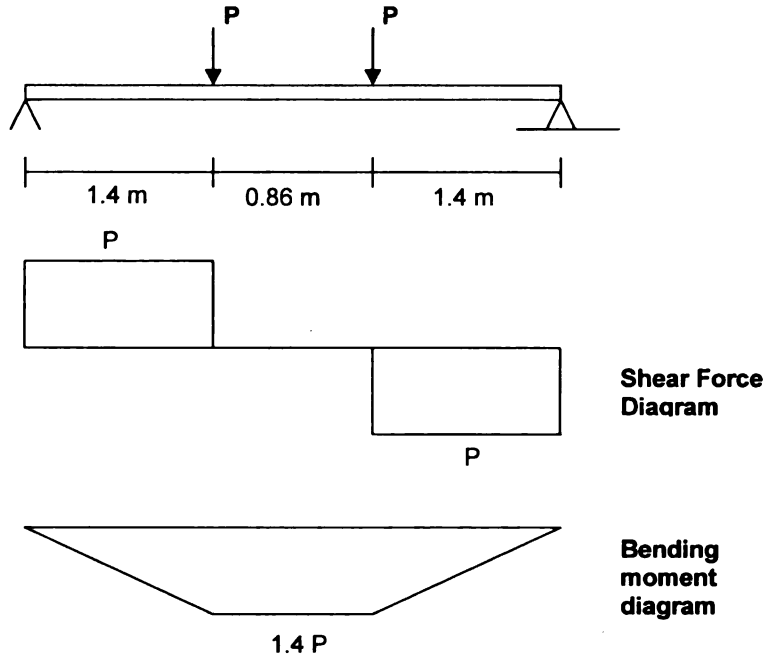

Figure B.2 – Shear Force Diagram and Bending Moment Diagram for Tested Beams

B.2.1 Normal Strength Concrete Beam

$f_c' = 58.2\,\text{MPa}$ $f_y = 450\,\text{MPa}$

Neglecting the area of steel in the compression zone:

The tensile area of steel $A_s = 855\ \text{mm}^2$

Clear concrete cover = 38 mm

$h = 406$ mm $b = 254$ mm

$d = 352.4$ mm

$a = 30.6\,\text{mm}$

$a = \beta_1 c$

Hence, $\beta_1 = 0.65$

Therefore, $c = \frac{30.6}{0.65} = 47.1\,\text{mm}$

Strain in tensile steel can be calculated by interpolation as follows:

$$\varepsilon_t = \frac{0.003}{c}(d-c) = \frac{0.003}{47.1}(352.4-47.1) = 0.019 > 0.005$$

Hence, $\phi = 0.9$

Check minimum reinforcement:

$\rho_{\min} = 0.0042$

$$\rho = \frac{A_s}{bd} = 0.00955 > \rho_{\min}$$

The moment capacity of the beam is

$$M_n = A_s f_y\left(d - \frac{a}{2}\right) = \frac{855 \times 450 \times \left(352.4 - \frac{30.6}{2}\right)}{10^6} = 129.7\,\text{kN.m}$$

The nominal load can be calculate as follows

$M_n = 1.4P_n$

$P_n = 92.7$ kN

The load ratio is defined as the ratio of applied load under fire conditions to the capacity of the section at room temperature (Buchanan 2002). Accordingly, the load ratio is given as:

$$LR = \frac{50}{92.7} \times 100\ \% = 54\%$$

B.2.2 High Strength Concrete Beam

$f_c' = 106.5\,\text{MPa}$ $\qquad$ $f_y = 450\,\text{MPa}$

Neglecting the area of steel in the compression zone:

The tensile area of steel $A_s = 855\ \text{mm}^2$

Clear concrete cover = 38 mm

$h = 406$ mm $\qquad b = 254$ mm

$d = 352.4$ mm

$a = 16.7$ mm

$a = \beta_1 c$

Hence, $\beta_1 = 0.65$

Therefore, $c = \dfrac{16.7}{0.65} = 25.7\,\text{mm}$

Strain in tensile steel can be calculated by interpolation as follows:

$$\varepsilon_t = \frac{0.003}{c}(d-c) = \frac{0.003}{48.7}(352.4-48.7) = 0.038 > 0.005$$

Hence, $\phi = 0.9$

Check minimum reinforcement:

$\rho_{\min} = 0.0057$

$$\rho = \frac{A_s}{bd} = 0.00955 > \rho_{\min}$$

The moment capacity of the beam is

$$M_n = A_s f_y\left(d - \frac{a}{2}\right) = \frac{855 \times 450 \times \left(352.4 - \dfrac{16.7}{2}\right)}{10^6} = 132.4\,\text{kN.m}$$

The nominal load can be calculate as follows

$M_n = 1.4P_n$

$P_n = 94.5$ kN

Thus, the load ratio is given as:

$$LR = \frac{50}{94.5} \times 100\ \% = 53\%$$

For 60 kN load under fire the load ratio will be:

$$LR = \frac{60}{94.5} \times 100\ \% = 63\%$$

B.3 Stress Strain Curves for Reinforcing Steel

The stress strain relationships determined via testing for the tension reinforcement used in the tested beams are shown in Figure B.3.

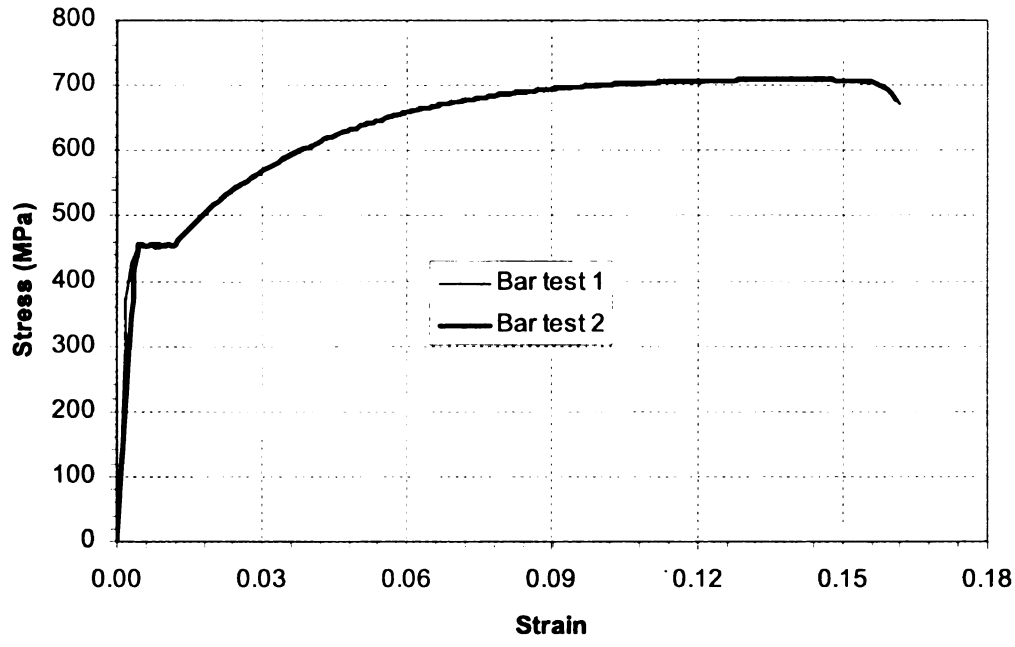

Figure B.3 – Stress Strain Curves for Steel Reinforcement used in the Tested Beams

B.4 Thermal Response

This appendix presents the temperatures measured at different locations in the tested beams. The thermocouples in each beam are classified based on their locations in the

beam into four sets, namely, unexposed surface thermocouples, exposed surface thermocouples, reinforcement thermocouples and concrete thermocouples. The reinforcement thermocouples measured the temperatures in compression and tension rebars. The temperatures measured by different groups of thermocouples in the six tested beams are plotted in Figures B.4 to B.27.

In all the tested beams, one thermocouple (TC13 in beam B5) was not recording temperature throughout the fire test. Two more thermocouples, namely, TC10 in beam B5 and TC8 in beam B6, were measuring nonsensical values (almost constant temperatures) throughout the fire exposure time. Further, a few of the thermocouples were measuring nonsensical temperatures particularly at later stages of fire exposure time. It should be noted that most of these thermocouples were in beams B5 and B6. The defects in the thermocouples used in these two beams can be attributed to the severe spalling which occurred at early stages of fire exposure in these beams. Overall, most of the thermocouples measured sensible temperatures throughout fire exposure time as can be seen from Figures B.4 to B.27.

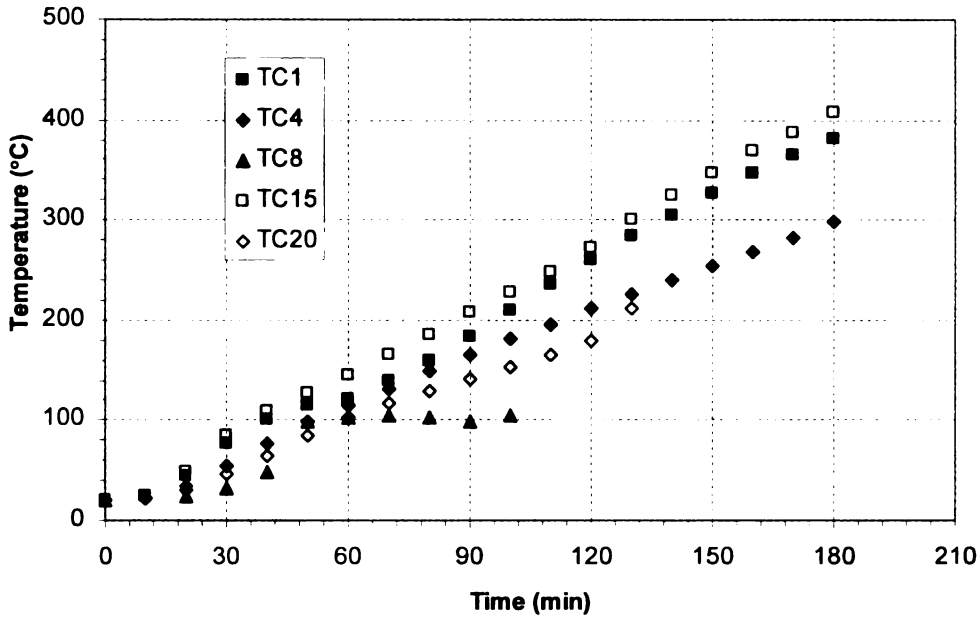

Figure B.4 – Measured Unexposed Surface Temperatures in RC Beam B1

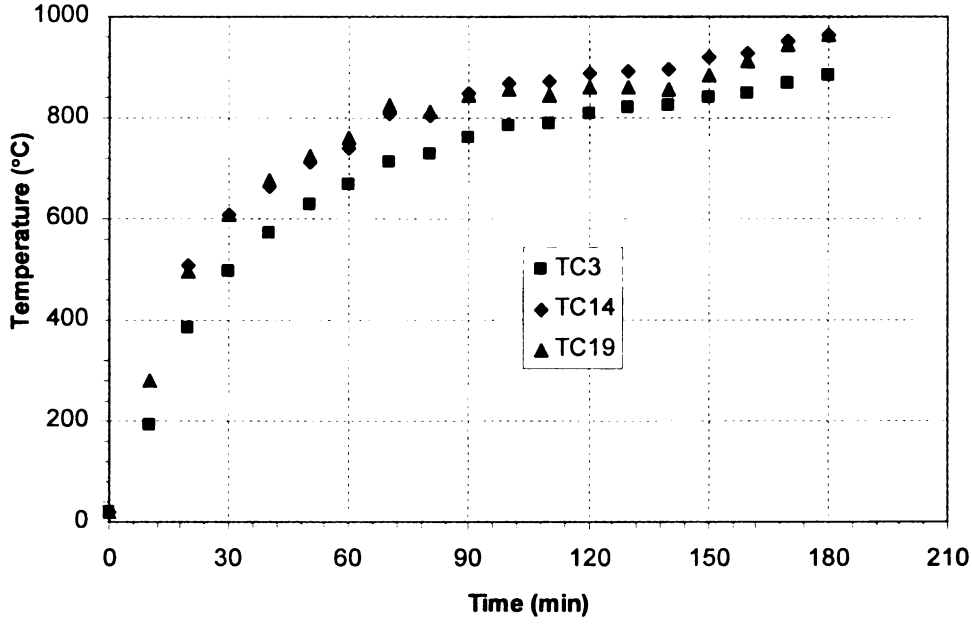

Figure B.5 – Measured Exposed Surface Temperatures in RC Beam B1

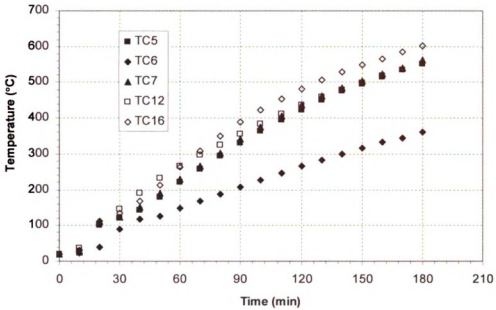

Figure B.6 – Measured Temperatures in Tension and Compression Rebars in RC Beam B1

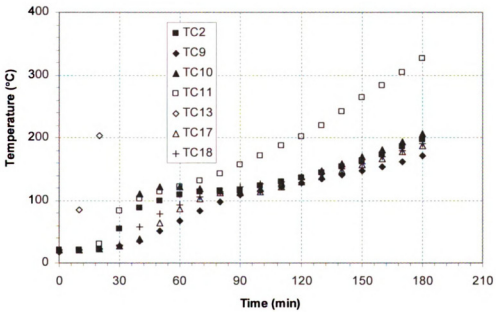

Figure B.7 – Measured Concrete Temperatures Beam B1

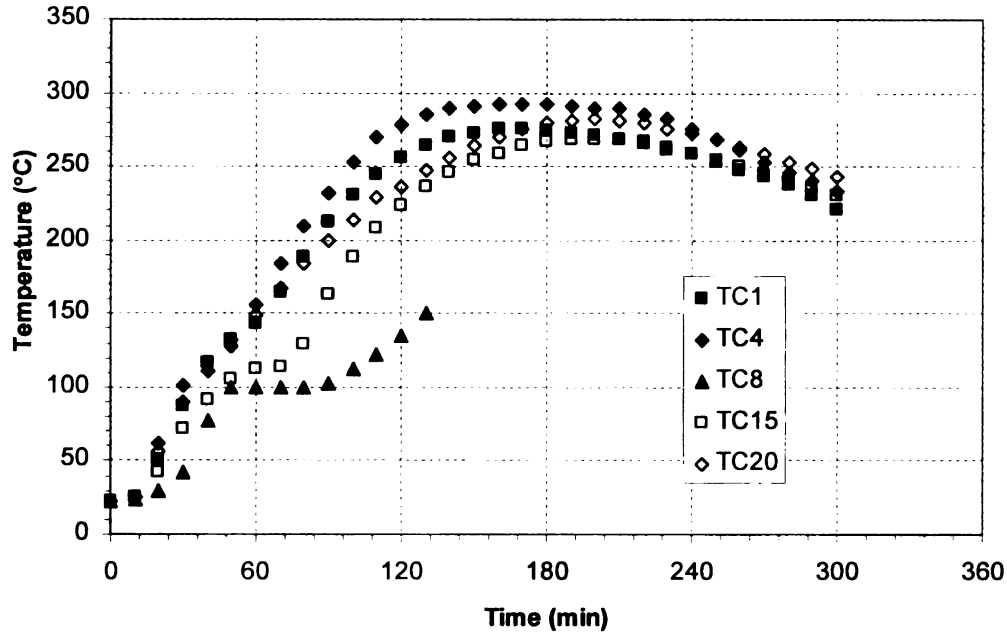

Figure B.8 – Measured Unexposed Surface Temperatures in RC Beam B2

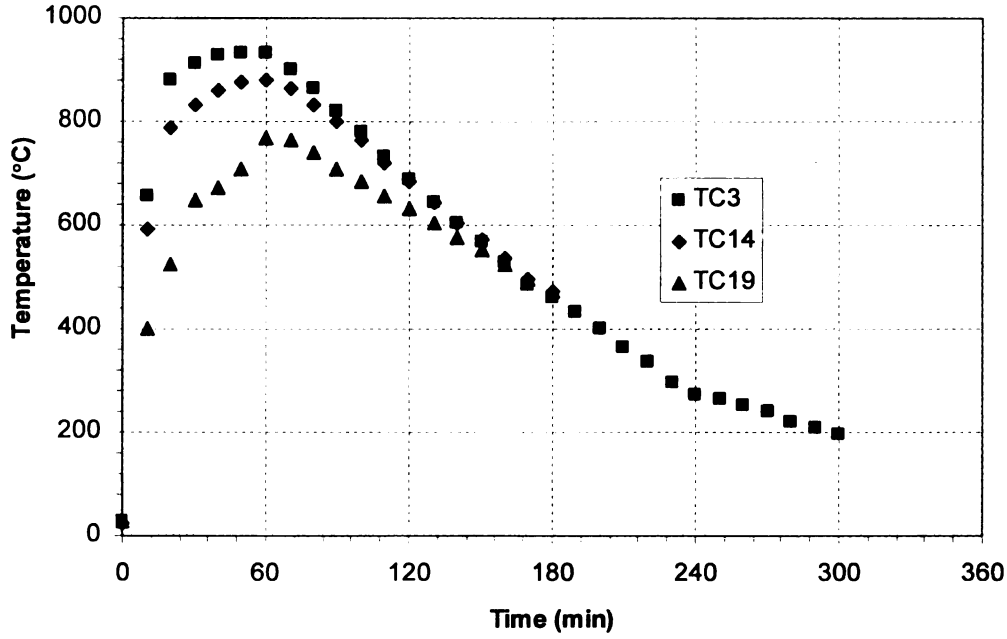

Figure B.9 – Measured Exposed Surface Temperatures in RC Beam B2

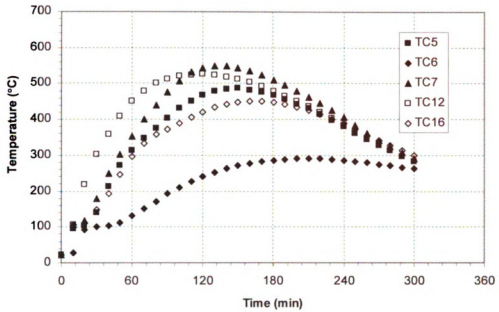

Figure B.10 – Measured Temperatures in Tension and Compression Rebars in RC Beam B2

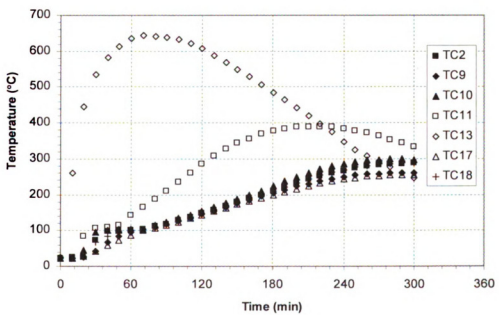

Figure B.11 – Measured Concrete Temperatures Beam B2

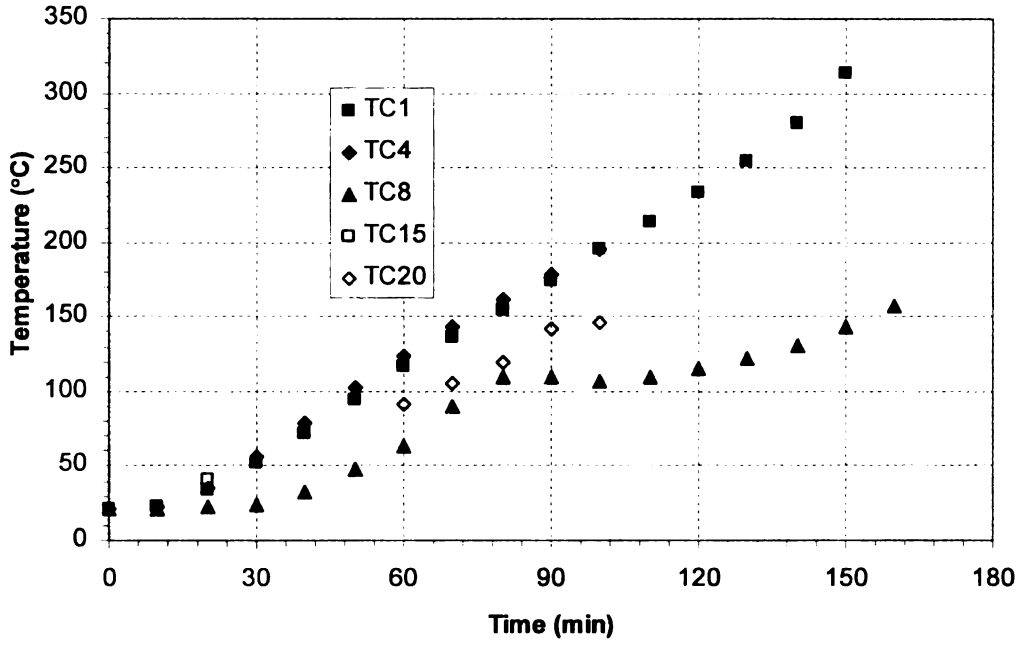

Figure B.12 – Measured Unexposed Surface Temperatures in RC Beam B3

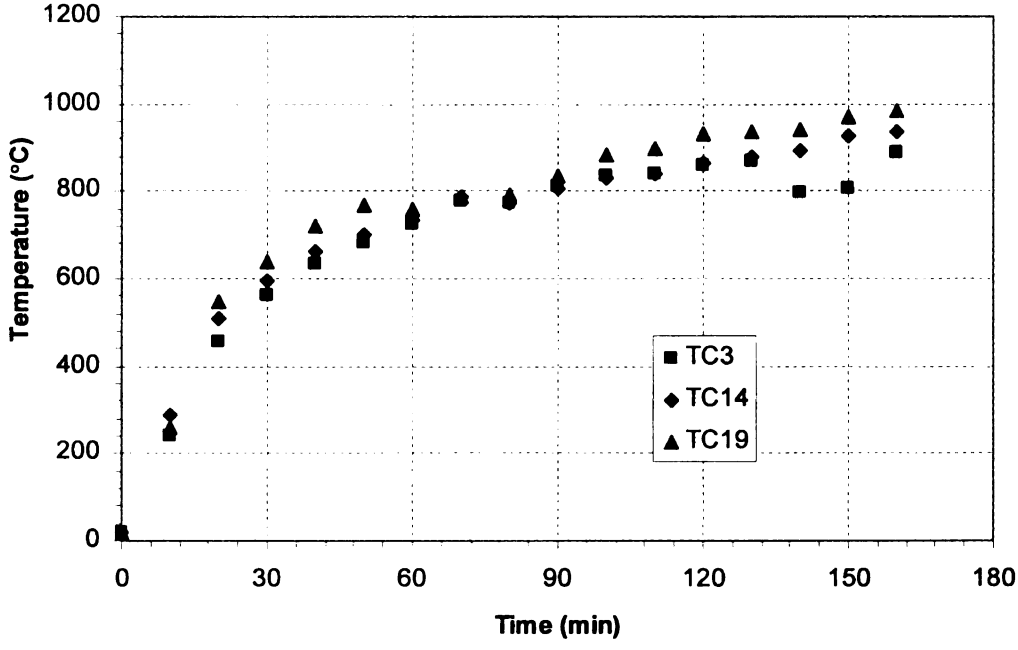

Figure B.13 – Measured Exposed Surface Temperatures in RC Beam B3

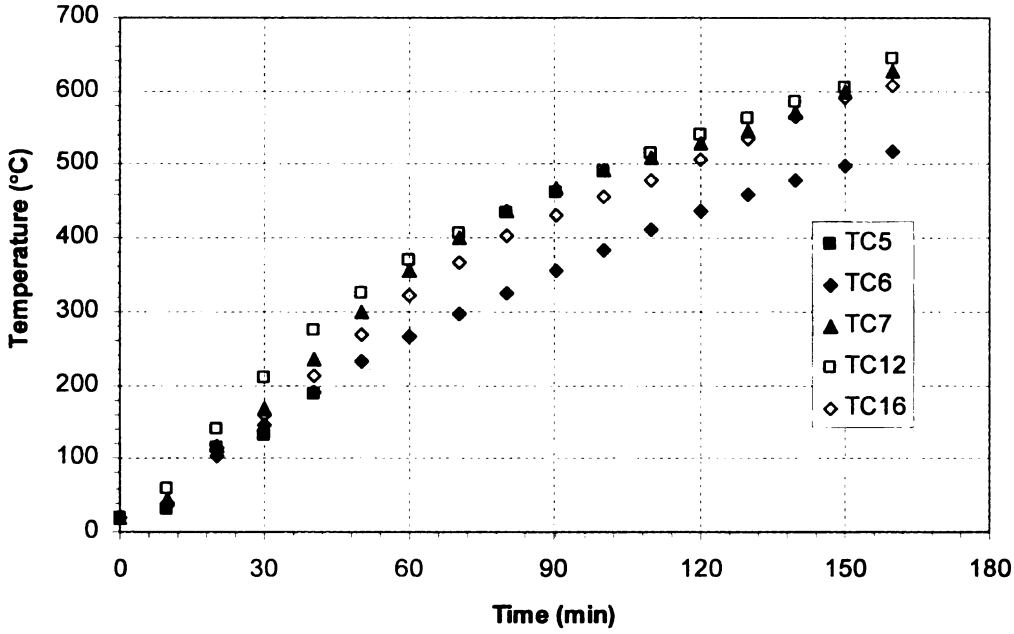

Figure B.14 – Measured Temperatures in Tension and Compression Rebars in RC Beam B3

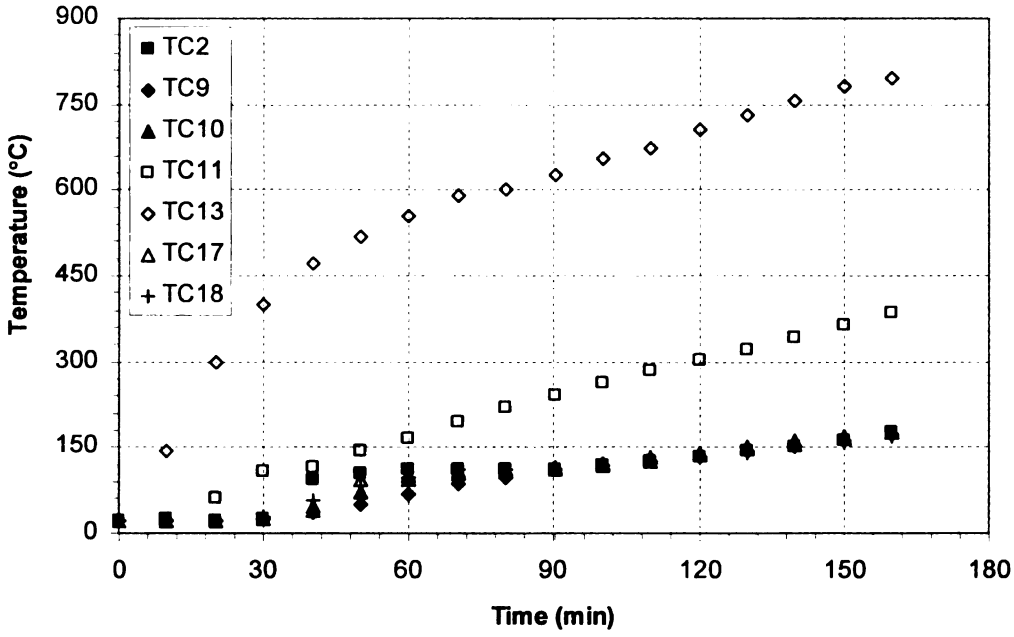

Figure B.15 – Measured Concrete Temperatures Beam B3

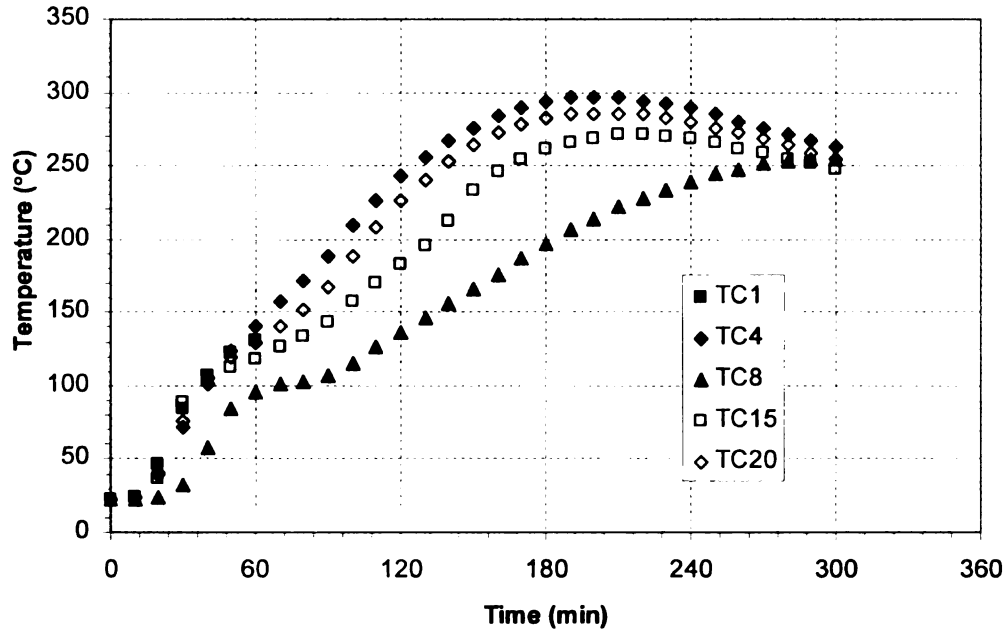

Figure B.16 – Measured Unexposed Surface Temperatures in RC Beam B4

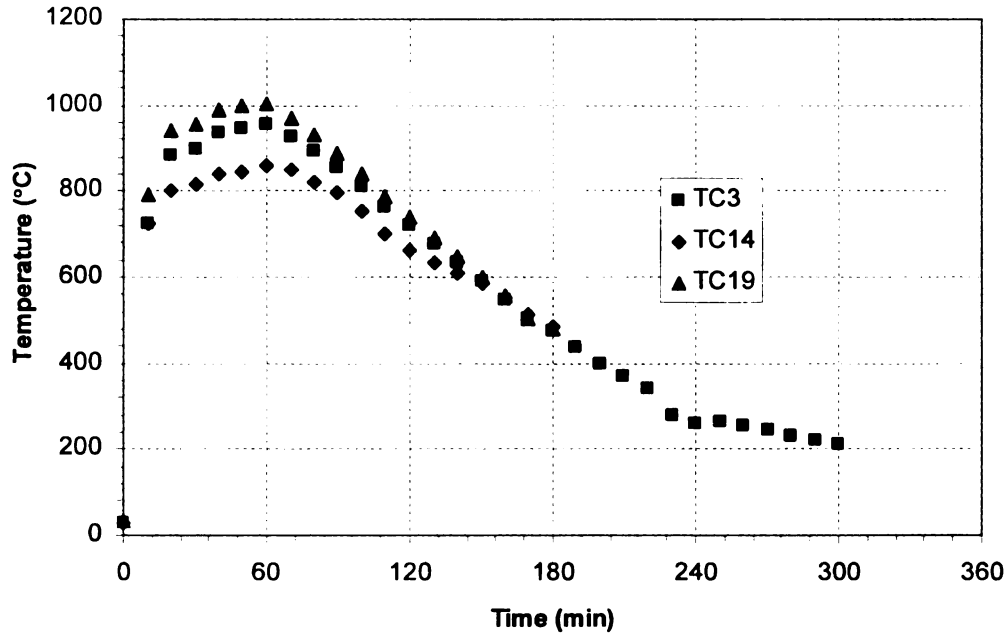

Figure B.17 – Measured Exposed Surface Temperatures in RC Beam B4

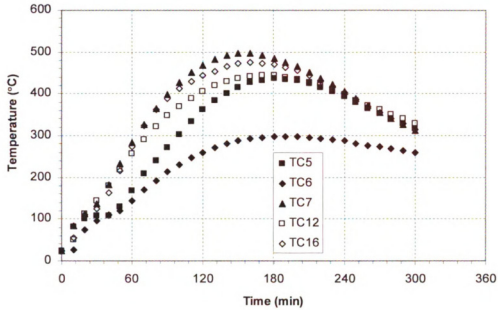

Figure B.18 – Measured Temperatures in Tension and Compression Rebars in RC Beam B4

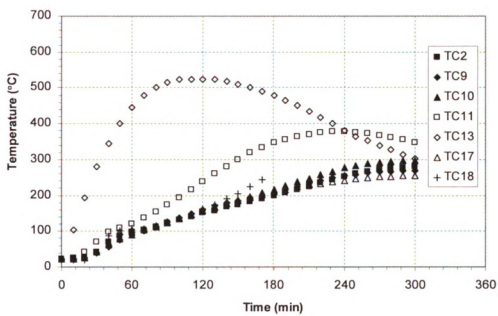

Figure B.19 – Measured Concrete Temperatures Beam B4

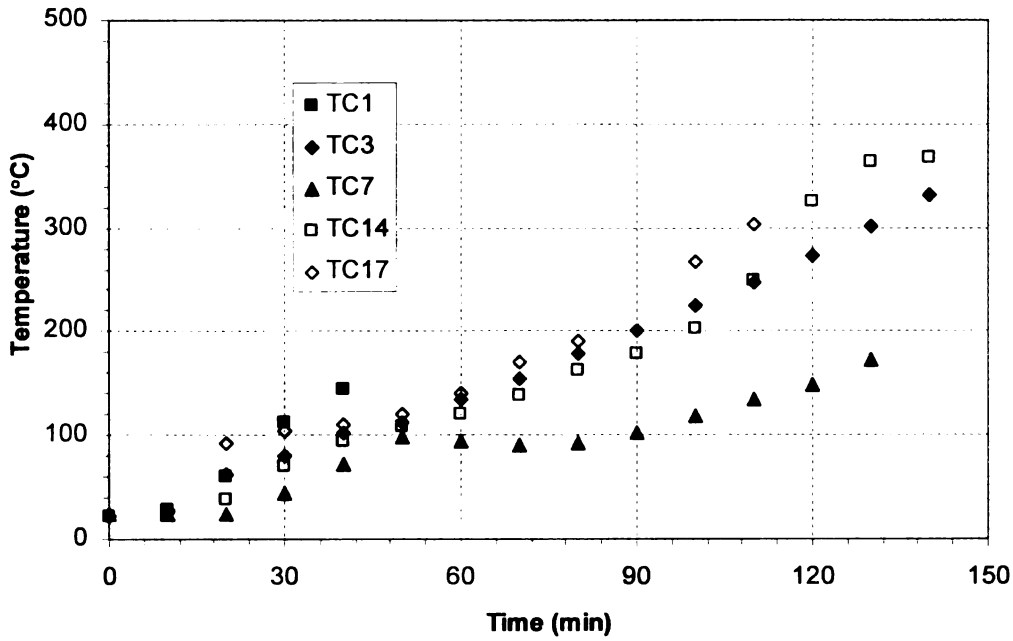

Figure B.20 – Measured Unexposed Surface Temperatures in RC Beam B5

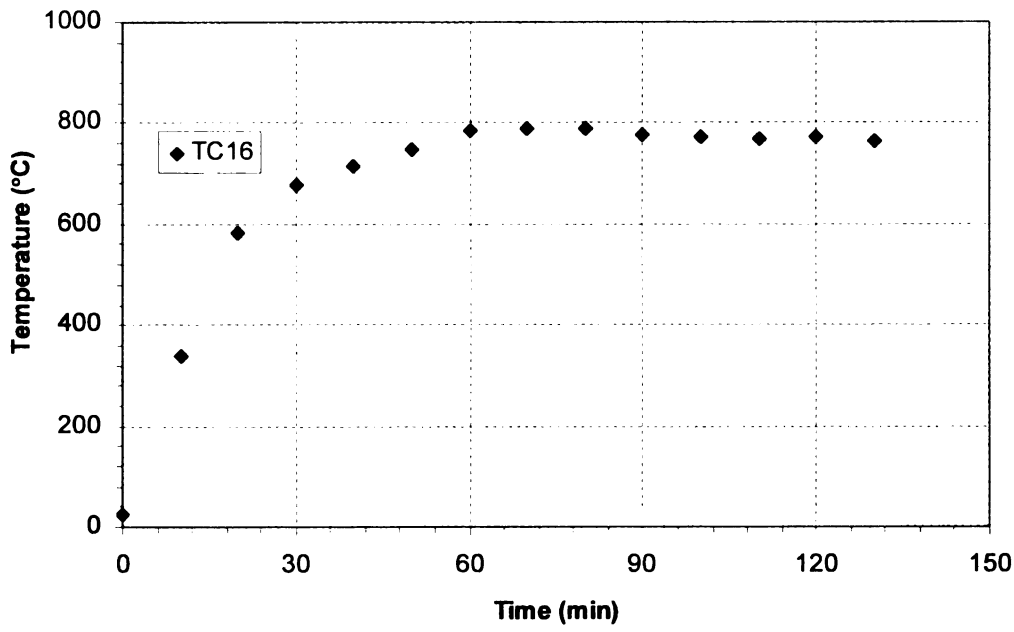

Figure B.21 – Measured Exposed Surface Temperatures in RC Beam B5

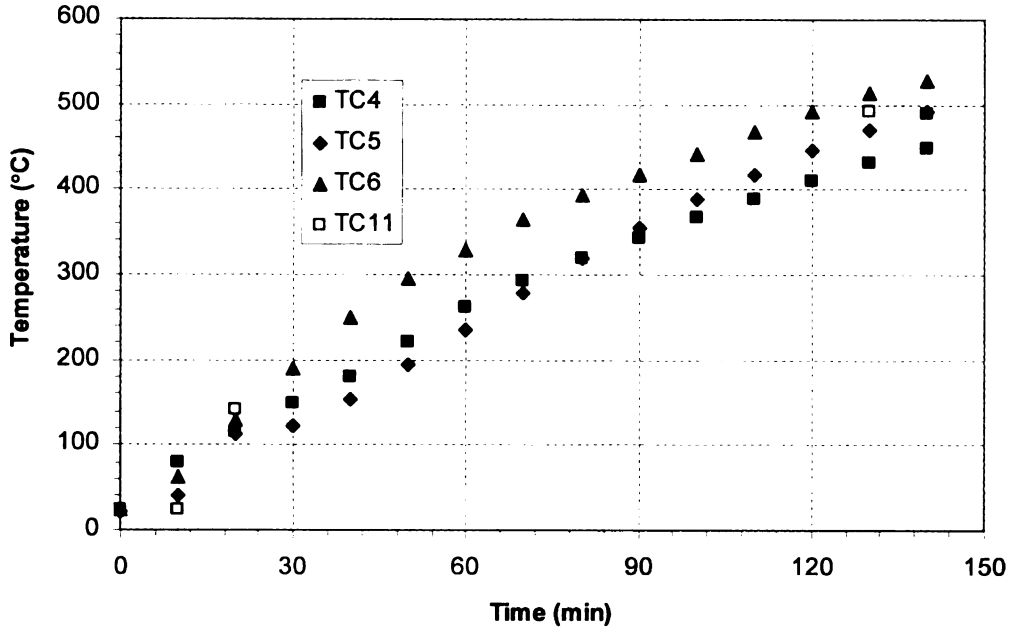

Figure B.22 – Measured Temperatures in Tension and Compression Rebars in RC Beam B5

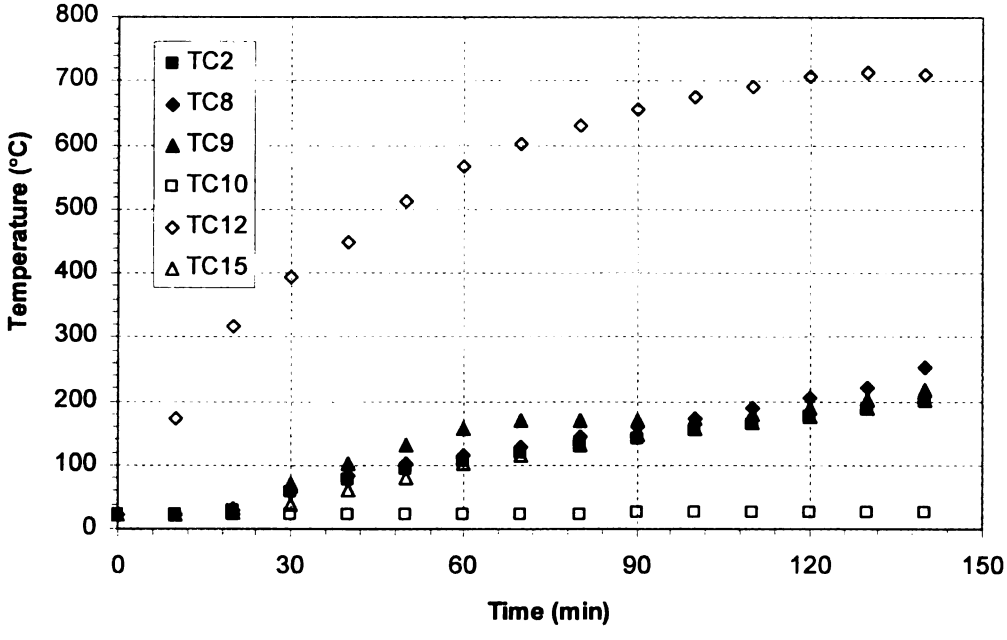

Figure B.23 – Measured Concrete Temperatures Beam B5

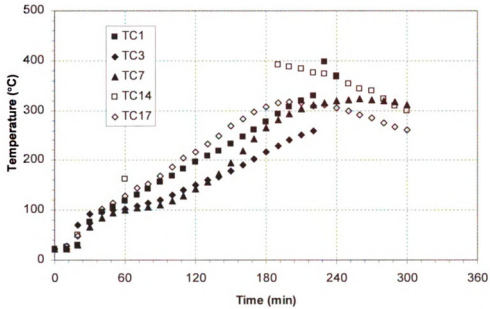

Figure B.24 – Measured Unexposed Surface Temperatures in RC Beam B6

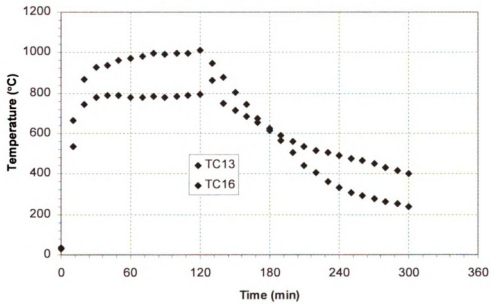

Figure B.25 – Measured Exposed Surface Temperatures in RC Beam B6

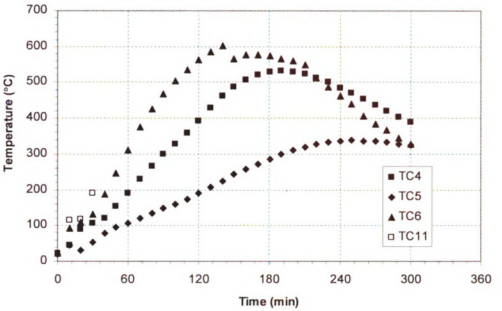

Figure B.26 – Measured Temperatures in Tension and Compression Rebars in RC Beam B6

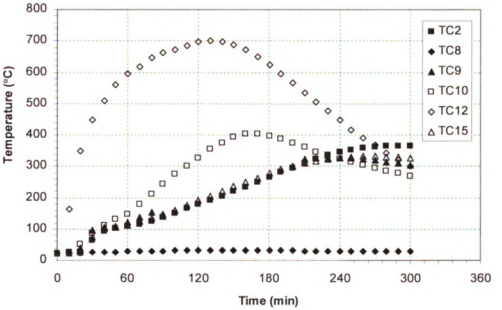

Figure B.27 – Measured Concrete Temperatures Beam B6

B.5 Strain Measurements

The measured strains in the compression reinforcement of the central section (section B in Figures 3.1(b) and 3.1(c)) and also in section A in Figure 3.1(b) for the six tested beams are shown in the following figures. It can be seen from Figures B.28 through B.30 that the recorded values of stain are nonsensical. This can be attributed to the unreliable nature of high temperature strain gages as discussed in Section 3.7.2.3.

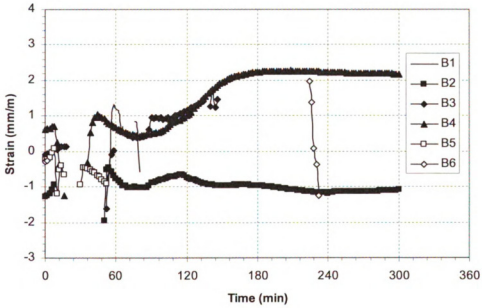

Figure B.28 – Measured Strain as a Function of Time in the Compression Reinforcement in the Central Section of the Tested Beams

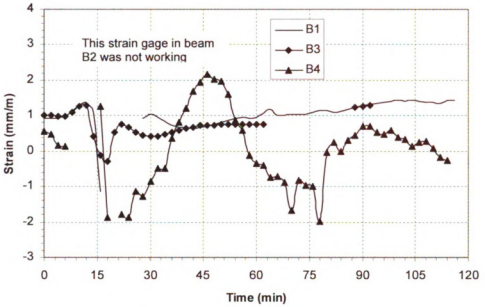

Figure B.29 – Measured Strain as a Function of Time in the Tension Reinforcement in Section A of the Tested Beams

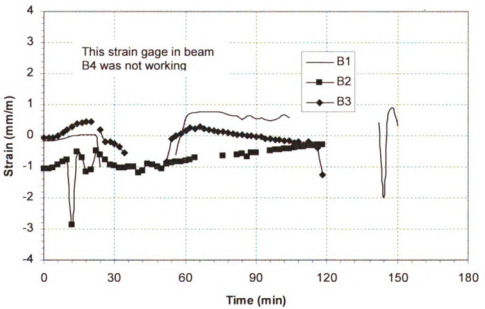

Figure B.30 – Measured Strain as a Function of Time in the Compression Reinforcement in Section A of the Tested Beams

Appendix C

C.1 Finite Element Formulation

To solve the heat and mass transfer problems, the cross-section of the beam segment is divided into rectangular elements as shown in Figure 4.3. Since the dependent variable (the variable to be computed) in the two problems is scalar, Q4 (four node) element is used in the analysis. Due to the nonlinearity of both problems, the integrations in Eqs. [4.40] through [4.42] are evaluated numerically using Gaussian quadrate integration technique. The vector of shape functions for Q4 element can be written as:

$$N = \begin{bmatrix} \frac{(1-s)(1-t)}{4} \\ \frac{(1+s)(1-t)}{4} \\ \frac{(1+s)(1+t)}{4} \\ \frac{(1-s)(1+t)}{4} \end{bmatrix} \qquad [C.1]$$

where: s and t = transformed coordinates as shown in Figure C.1.

The analysis is generally carried out using four Gauss points and the element stiffness matrix (K_e), mass matrix (M_e) and nodal heat or mass flux (F_e) are evaluated at every Gauss point. Those values of the element matrices at the four Gauss points are summed to form the element material property matrices which are used for the subsequent steps in the analysis.

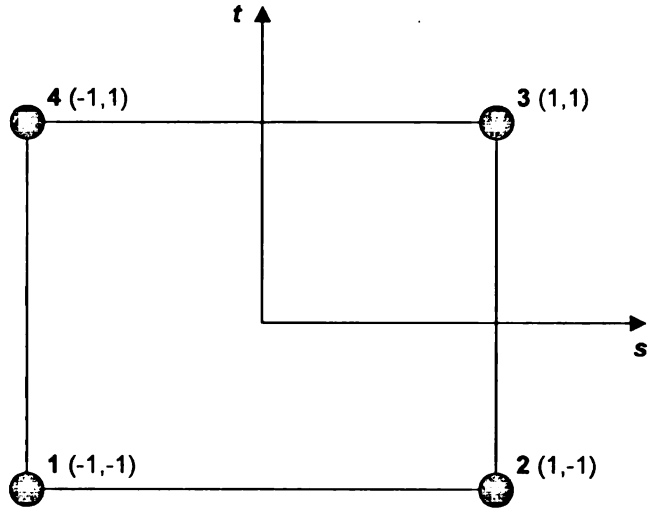

Figure C.1 – Q4 Element in Transformed Coordinates

Appendix D

Worked Example

D.1 Problem Statement

The analyzed beam has 400 mm × 600 mm rectangular cross-section and span length of 5 m. The beam is loaded with uniformly distributed dead load of 40 kN/m and live load of 20 kN/m. The calculations of the fire resistance of the beam using the proposed equation as well as three codes of practice (ACI 216.1, Eurocode2 and AS 2600) is detailed below.

D.2 Solution

Standard Fire Exposure

Compute R_0:

Concrete cover = 50 mm beam width = 400 mm $\Rightarrow R_0$ = 157 min.

Compute load ratio:

First compute the nominal room temperature load carrying capacity of the beam:

$$M_n = A_s f_y \left(d - \frac{A_s f_y}{1.7 f_c' b} \right)$$

$$A_s = \frac{6 \times 20^2 \times \pi}{4} = 1885 \text{ mm}^2$$

d = 600 – 50 – 20/2 = 540 mm

hence, $M_n = 1885 \times 400 \left(540 - \frac{1885 \times 400}{1.7 \times 40 \times 400} \right) \times 10^{-6} = 386.3 \text{ kN.m}$

The room temperature capacity from different codes will be very much similar due to the fact that the values of all strength reduction factors used in computing the room temperature capacity should be assumed 1.0.

$$w_n = \frac{8M_n}{L^2} = \frac{8 \times 386.3}{5^2} = 123.6$$

Load under fire = 1.2×40 + 0.5×20 = 58 kN/m

Load ratio = $LR = \frac{58}{123.6} = 0.47$

Calculate ψ_0:

$$\rho = \frac{6 \times 10^2 \pi}{400 \times 540} = 0.0087$$

$$\chi = \frac{2}{6} = 0.333$$

$$SF = \frac{2 \times 0.6 + 0.4}{0.6 \times 0.4} = 6.667 \text{ m}^{-1}$$

$$\psi_0 = \frac{0.333}{6.667 \times 0.0087} = 5.7$$

Standard fire resistance for simply supported RC beam (R_{SS}):

$Rss = \phi_{SS}\phi_{ag}\phi_{cs}R_0$

Carbonate aggregate, ϕ_{ag} = 1.2

NSC, ϕ_{cs} =1.0

$\phi_{SS} = (1.4 - 0.47 - 0.02 \times 5.7) = 0.816$

Hence, $Rss = 0.816 \times 1.2 \times 1 \times 157 = 153$ min.

Standard fire resistance for axially restrained RC beam (R_{AR}):

$$Rss = \phi_{AR}\phi_{ag}\phi_{cs}R_0$$

$$ax = \frac{kL}{AE} = \frac{300000 \times 5}{0.4 \times 0.6 \times 30 \times 10^6} = 0.2083$$

$$\frac{L}{H} = \frac{5}{0.6} = 8.333$$

$$\phi_{AR} = 0.9\phi_{SS} - 0.2\left(\frac{L}{H} - 14\right)(0.1 + ax)$$

$$\phi_{AR} = 0.9 \times 0.816 - 0.2(8.333 - 14)(0.1 + 0.2083) = 1.084$$

$$R_{AR} = 1.084 \times 1.2 \times 1 \times 157 = 204 \text{ min.}$$

Eurocode Method (Eurocode 2 2004)

Axis distance = 50 + 20/2 = 60 mm beam = 400

Based on Table 5.5 in Eurocode 2 (2004), the fire resitance of this beam is 156 min.

It should be noted that Eurocode 2 does not have clear guidance for evaluating the fire resistance of axially restrained beams.

Australian Code Method (AS 3600 2001)

Concrere cover = 50 mm beam width = 400 mm

Based on Figure 5.4.2 (A) in the Australian Code, the fire resitance for this beam is 157 min.

Similar to Eurocode 2 the Austrailian code does not have clear guidance for evaluating the fire resistance of axially restrained beams.

ACI Method (ACI 216.1 2007)

Concrete cover thickness = 50 mm beam width = 400 mm

Fire resistance for simply supported beam = 240 minutes

Fire resistance for axially restrained beam > 240 minutes

Design Fire Exposure

Compute total area under heat flux for design fire

$\Gamma t_d = 15.16 \times 0.867 = 13.14 > 10$

$$A_1 = \frac{10 \times (13.14)^{1.5}}{15.16} = 31.4 \text{ MW.min/m}^2.$$

$$A_2 = \frac{0.4\sigma\left(T_{\max}^5 - T_0^5\right) + 12.5\left(T_{\max}^2 - T_0^2\right)}{r} \times 10^{-6}$$

T_{max} = 1314°C = 1587 K

T_0 = 20°C = 293 K

$$A_2 = \frac{0.4 \times 5.67 \times 10^{-8}\left(1587^5 - 293^5\right) + 12.5\left(1587^2 - 293^2\right)}{17.54} \times 10^{-6}$$

$A_2 = 14.75 \text{ MW.min/m}^2$

$A_d = A_1 + A_2 = 31.4 + 14.75 = 46.15$ MW.min/m^2.

Compute time equivalent

$t_{e(energy)} = 11.5 A_d^{0.7} = 11.5 \times (46.15)^{0.7} = 168$ min.

$t_e = \left(1.2 - 0.01\Gamma t_d^2\right) t_{e(energy)} = \left(1.2 - 0.01 \times 15.16 \times 0.867^2\right) \times 168 = 182$ min.

Check failure

Simply supported beam	time equivelan > Fire resistance	⇒	failure
Axially restrained beam	time equivelan < Fire resistance	⇒	no failure

Summary

Based on the above calculation the fire resistance calculated from various codes and the proposed equation for standard fire exposure is shown in Table 7.3. For the given design

fire exposure, failure is predicted to occur in the simply supported beam and not to occur in the axially restrained beam.

References

1. ACI Committee 216.1-07 (2007), "Standard Method for Determining Fire Resistance of Concrete and Masonry Construction Assemblies", American Concrete Institute, Detroit.

2. ACI 318-2008 (2008), "Building Code Requirements for Reinforced Concrete", *ACI 318-08 and Commentary*, American Concrete Institute, Detroit, MI.

3. AISC (2005), "Steel Construction Manual 3rd Edition", American Institute of Steel Construction, Chicago, Illinois.

4. Anderberg, Y. (1997), "Spalling Phenomenon of HPC and OC", International Workshop on Fire Performance of High Strength Concrete, NIST SP 919, Gaithersburg, MD, pp. 69-75.

5. Anderberg Y., and Thelandersson S. (1976), "Stress and Deformation Characteristics of Concrete at High Temperatures, 2. Experimental Investigation and Material Behaviour Model", *Lund Institute of Technology*, Sweden.

6. AS 3600 (2001), "Concrete Structures", Committee BD-002, Australia.

7. ASCE manual No.78 (1992), "Structural Fire Protection", ASCE committee on fire protection, structural division, American Society of Civil Engineers, New York.

8. ASCE-07 (2005), "Minimum Design Loads for Buildings and Other Structures", American Society of Civil Engineers, Reston, VA.

9. ASCE/SFPE29 (1999), *Standard Calculation Method for Structural Fire Protection*, American Society of Civil Engineers, Reston, VA.

10. ASTM C1202 (1997), "Standard test method for electrical indication of concrete's ability to resist chloride ion penetration", *American Society for Testing and Materials*, West Conshohocken, PA.

11. ASTM Test Method E119-08a (2008), "Standard Methods of Fire Test of Building Construction and Materials", American Society for Testing and Materials, West Conshohocken, PA.

12. ASTM Test Method E1529 (1993), "Standard Test Methods for Determining Effects of Large Hydrocarbon Pool Fires on Structural Members and Assemblies", American Society for Testing and Materials, West Conshohocken, PA.

13. Balendran R.V., Abid Nadeem, Tayyab Maqsood, and Leung H.Y. (2003), "Flexural and Split Cylinder Strengths of HSC at Elevated Temperatures", Fire Technology, 39, pp. 47–61.

14. Baroghel-Bouny V., Mainguy M., Lassabatere T., and Coussy O. (1999), "Chatacterization and Identification of Equilibrium and Transfer Moisture Properties for Ordinary and High-Performance Cementations Materials", *Cement Concrete Research*, 29, pp. 1225-1238.

15. Bazant Z.P. (1997), "Analysis of Pore Pressure, Thermal Stress and Fracture in Rapidly Heated Concrete", International Workshop on Fire Performance of High Strength Concrete, NIST SP 919, Gaithersburg, MD, pp. 155-164.

16. Bazant Z.P., and Kaplan M.F. (1996), *Concrete at High Temperature*, Longman.

17. Bazant Z.P., and Thonguthai W. (1978), "Pore pressure and Drying of Concrete at High Temperature", *Journal of the Engineering Mechanics Division*, ASCE, 104(EM5), pp. 1059-1079.

18. 'BBC', http://news.bbc.co.uk/2/hi/europe/7610919.stm, September 11, 2008.

19. Bilodeau A., Kodur V.R., and Hoff G.C. (2004), "Optimization of the type and amount of polypropylene fibers for preventing the spalling of lightweight concrete subjected to hydrocarbon fire", *Cement & Concrete Composites*, Elsevier Ltd., 26(2), pp. 163 – 174.

20. Bisby 2003

21. BS 476-3:1987 (1987), "Fire Tests on Building Materials and Structures – Part 20: Method fro Determination of the Fire Resistance of Elements of Construction (General Principles) ", *BSi*, UK.

22. Buchanan A.H. (2002), *Structural Design for Fire Safety*, John Wiley & Sons Ltd., Chichester, England.

23. Campbell T.I., and Kodur V.R. (1990), "Deformation Controlled Nonlinear Analysis of Prestressed Concrete Continuous Beams", *PCI Journal*, PCI, pp. 42-55.

24. Castillo C., Durrani A. J. (1990), "Effect of Transient High Temperature on High-Strength Concrete", *ACI Materials Journal*, 87(1), pp. 47 – 53.

25. Chan S.Y.N., Peng G.F., and Anson M. (1999), "Fire Behavior of High-Performance Concrete Made with Silica Fume at Various Moisture Contents", *ACI Materials Journal*, 96(3), pp. 405 – 409.

26. Chang Y.F., Chen Y.H., Sheu M.S., and Yao G.C. (2006), "Residual stress–strain relationship for concrete after exposure to high temperatures", *Cement and Concrete Research*, 36, pp. 1999–2005.

27. Cheng F.P., Kodur V.R., and Wang T.C. (2005), "Stress-Strain Curves for High Strength Concrete at Elevated Temperatures", *Journal of Materials in Civil Engineering*, 16(1), pp. 84 – 94.

28. Cook R.D., Malkus D.S., Plesha M.E. and Witt R.J. (2003), *Concepts and Applications of Finite Element Analysis*, 4th edition, John Wiley & Sons, NY, USA.

29. Diederichs U., Jumppanen U. M., Penttala V. (1988), "Material properties of high strength concrete at elevated temperature", *IABSE 13th Congress*, Helsinki.

30. Diederichs U., Jumppanen U.M., and Schneider U. (1995), "High Temperature Properties and Spalling Behavior of High Strength Concrete". *Proceedings of Fourth Weimar Workshop on High Performance Concrete*, HAB Weimar, Germany, pp. 219-235.

31. Dotreppe J.C., and Franssen J.M. (1985), "The Use of Numerical Models for the Fire Analysis of Reinforced Concrete and Composite Structures", *Engineering Analysis*, CML Publications, 2(2), pp. 67-74.

32. Dwaikat M.B., and Kodur V.R. (2008a), "A Numerical Approach for Modeling the Fire Induced Restraint Effects in Reinforced Concrete Beams", *Fire Safety Journal*, 43(4), pp. 291-307.

33. Dwaikat M.B., and Kodur V.R. (2008b), "Hydrothermal Model for Predicting Fire Induced Spalling in Concrete Structural Systems ", in Press, *Fire Safety Journal.*

34. Dwaikat M.B., and Kodur V.R. (2009), "Response of Restrained Concrete Beams under Design Fire Exposure", *ASCE Journal of Structural Engineering*, in Press.

35. 'Dutchnews', http://www.dutchnews.nl/news/archives/2008/05/massive_fire_destroys_delfts_a.php, May 13, 2008.

36. Ellingwood B., and Lin T.D. (1991), "Flexure and Shear Behavior of Concrete Beams During Fire", *Journal of Structural Engineering*, ASCE, 117(2), pp. 440-458.

37. Eurocode 1 (2002), "EN 1991-1-2: Actions on Structures. Part 1-2: General Actions - Actions on Structures Exposed to Fire", European Committee for Standardization, Brussels, Belgium.

38. Eurocode 2 (2004), "EN 1992-1-2: Design of Concrete Structures. Part 1-2: General Rules - Structural Fire Design", European Committee for Standardization, Brussels, Belgium.

39. Feasey, R., and Buchanan, A.H. (2002), "Post Flash-over Fires for Structural Design", *Fire Safety Journal*, Vol 37, No 1, pp. 83-105.

40. Felicetti R., Gambarova P.G., Rosati G.P., Corsi F., and Giannuzzi G. (1996), "Residual mechanical properties of high-strength concretes subjected to high-temperature cycles", *Proceedings, 4th International Symposium on Utilization of High-Strength/High-Performance Concrete*, Paris, France, pp. 579-588.

41. FEMA (2002), "World Trade Center Building Performance Study: Data Collection", *Preliminary Observations, and Recommendations*, Federal Emergency Management Agency (FEMA), Federal Insurance and Mitigation Administration, Washington, DC.

42. FEMA (2008), *Firefighter Fatalities in the United States in 2007*, U.S. Fire Administration, FEMA, Washington DC, USA.

43. Fire Prevention (1997), "Channel Tunnel Fire Protection Measures Questioned after Fire on HGV Wagon", *Fire Prevention*, 296.

44. Flynn D. R. (1999), "Response of High Performance Concrete to Fire Conditions: Review of Thermal Property Data and Measurement Techniques", *NIST GCR 99-767*, MetSys Corportation, US.

45. Franssen, J.M. (2006), "Personal Communication on Fire Test Results for Reinforced Concrete Beams", June 1st.

46. Franssen J.M., Kodur V.K. R., and Mason J. (2004), *User Manual for SAFIR*, University of Liege, Belgium.

47. Fu Y. F., Wong Y. L., Poon C. S., and Tang C. A. (2005), "Stress–Strain Behaviour of High–Strength Concrete at Elevated Temperatures", *Magazine of Concrete Research*, 57(9), pp. 535-544.

48. Furumura T., Abe T., and Shinohara Y. (1995), "Mechanical Properties of High Strength Concrete at High Temperatures", *Proc. of 4th Weimar Workshop on High Performance Concrete: Material Properties and Design*, held at Hochschule für Architektur und Bauwesen (HAB), Weimar, Germany, pp. 237–254.

49. Gawin D., Majorana C.E., and Schrefler B.A. (1999), "Numerical Analysis of Hygro-thermic Behaviour and Damage of Concrete at High Temperature", *Magazine of Cohesive Frictional Material*, 4, pp. 37-74.

50. Gawin D., Pesavento F., Schrefler B.A. (2005), "Towards Prediction of the Thermal Spalling Risk through A multi-phase Porous Media Model of Concrete", *Computer Methods in Applied Mechanics and Engineering*, 195, pp. 5707-5729.

51. Hammer T. A. (1995), "High strength concrete phase 3, spalling reduction through material design", *SP6 Fire Resistance, Report 6.2*, SINTEF Structures and Concrete, STF70 A95024.

52. Han C., Hwang Y., Yang S., and Gowripalan N. (2005), "Performance of spalling resistance of high performance concrete with polypropylene fiber contents and lateral confinement", *Cement and Concrete Research*, Elsevier Ltd., 35(9), pp. 1747-1753.

53. Hansen P.A., and Jensen J. J. (1995), "High strength concrete phase 3, Fire resistance and spalling behavior of LWA Beams", *SP6 -Fire Resistance, Report 6.3*, SINTEF NBL -Norwegian Fire Research Laboratory, STF25 A95004.

54. Harada T., Takeda J., Yamane S., and Furumura F. (1972), "Strength, Elasticity and Thermal Properties of Concrete Subjected to Elevated Temperatures", *in International Seminar on Concrete for Nuclear Reactor*, ACI Special Publication 34(1), Paper SP34-21, American Concrete Institute, Detroit, pp. 377–406.

55. Harmathy T.Z. (1967), "A comprehensive Creep Model", *Journal of Basic Engineering*, 89(2), pp. 496-502.

56. Harmathy T.Z. (1969), "Simultaneous Moisture and Heat Transfer in Porous Systems with Particular Reference to Drying". *I & E C Fundamentals*, 8(1).

57. Harmathy T.Z. (1970), "Thermal properties of concrete at elevated temperatures", *ASTM Journal of Materials*, 5(1), pp.47-74.

58. Harmathy T.Z. (1971), "Moisture and Heat Transport with Particular Reference to Concrete", *National Council of Canada*, NRCC 12143.

59. Harmathy T.Z. (1993), "Fire Safety Design and Concrete", *Concrete Design and Construction Series*, Longman Scientific and Technical, UK.

60. Harmathy T.Z., and Allen L.W. (1973), "Thermal Properties of Selected Masonry Unit Concretes", *Journal of American Concrete Institute*, 70, 132–142

61. Hertz K. (1991), "Danish investigations on silica fume concretes at elevated temperatures", *Proceedings, ACI 1991 Spring Convention*, Boston, MA, March 17-21.

62. Hertz K.D. (2003), "Limits of Spalling of Fire-Exposed Concrete", *Fire Safety Journal*, 38, pp. 103-116.

63. Huang C.L. (1979), "Multi-Phase Moisture Transfer in Porous Media Subject to Temperature Gradient", *International Journal of Heat and Mass Transfer*, 22, pp. 1295-1307.

64. ISO 834-1975 (1975), "Fire resistance tests – elements of building construction. International Organization for Standardization".

65. JIS A1304 (2002), " Method for Fire Resistance Test for Structural Parts of Buildings", *Japanese Industrial Standards*, Japanese Standard Association, Japan

66. Kalifa P., Chene G., and Galle C. (2001), "High-Temperature Behavior of HPC with Polypropylene Fibers: From Spalling to Microstructure", *Cement and Concrete Research*, 31, pp. 1487-1499.

67. Kang S.W., and Hong S.G. (2004), "Analytical Method for the Behavior of a Reinforced Concrete Flexural Member at Elevated Temperatures", *Fire and Materials*, 28, pp. 227-235.

68. Kanema M., Noumowe A., Gallias J., and Cabrillac R. (2007), "Pearmeability and Mechanical Properties of Concrete at High Temperatures", *Concrete Under Sever Concditions: Environment & Loading*, CONSEC'07 Tours, France.

69. Karter M. J. (2008), "Fire Loss in the United States 2007", Fire Analysis and Research Division, National Fire Protection Association, MA, USA.

70. Khoury G.A. (1996), "Performance of Heated Concrete-Mechanical Properties", *Contract NUC/56/3604A with Nuclear Installations Inspectorate*, Imperial College, London.

71. Khoury G.A. (2006a), "Strain of heated concrete during two thermal cycles. Part 1: Strain over two cycles, during first heating and at subsequent constant temperature", *Magazine of Concrete Research*, 58(6), pp. 367 – 385.

72. Khoury G.A. (2006b), "Strain of heated concrete during two thermal cycles. Part 2: Strain during first heating and at subsequent thermal cycle", *Magazine of Concrete Research*, 58(6), pp. 387 – 400.

73. Khoury G.A. (2006c), "Strain of heated concrete during two thermal cycles. Part 3: Isolation of strain components and stain model development", *Magazine of Concrete Research*, 58(7), pp. 421 – 435.

74. Khoury G.A., Grainger B.N., and Sullivan P.J.E. (1985), "Strain of Concrete during Fire Heating to 600 °C", Magazine of Concrete Research, 37, pp. 195-215.

75. Kodur V.R. (1999), "Performance based fire resistance design of concrete-filled steel columns", *Journal of Constructional Steel Research Institute*, 51, pp. 21-36.

76. Kodur V.R. (2000), "Spalling in High Strength Concrete Exposed to Fire - Concerns, Causes, Critical parameters and Cures", *Proceedings: ASCE Structures Congress*, 1-8, Philadelphia, U.S.A.

77. Kodur, V.R. (2003a), "Fire resistance design guidelines for high strength concrete columns", *National Research Council of/ /Canada*, Institute for research in Construction, Internal Report No. 46116, pp. 1-11.

78. Kodur V.R. (2003b), "Fiber reinforcement for minimizing spalling in HSC structural members exposed to fire", *Innovations in Fibre-Reinforced Concrete for Value*, ACI Special Publication SP: 216, pp. 221-236.

79. Kodur V.R. (2007), "Design Strategies for Protecting Built Infrastructure against Fire Hazard", *Protect "2007" Conference – Whistler*, BC, Canada, pp. 1-11.

80. Kodur V.R, and Dwaikat M.B. (2008a), "Performance-Based Fire Safety Design of Reinforced Concrete Beams", *Journal of Fire Protection Engineering*, 17(3), pp. 293-320.

81. Kodur V.R., and Dwaikat M.B. (2008b), "Flexural Response of Reinforced Concrete Beams Exposed to Fire", *Structural Concrete*, 9(1), pp. 45-54.

82. Kodur V.R, and Harmathy T. Z. (2008), "Properties of building materials" Editor: DiNenno P.J., *SFPE Handbook of Fire Protection Engineering*, 4th edition, National Fire Protection Association, Quincy, MA, pp. 1.167-1.195.

83. Kodur V.R., and McGrath R.C. (2003), "Fire endurance of high strength concrete columns", *Fire Technology - Special Issue,* 39(1), pp. 73-87.

84. Kodur V.R., and Phan L. (2007), "Critical Factors Governing the Fire Performance of High Strength Concrete Systems", *Fire Safety Journal*, 42, pp. 482-488.

85. Kodur V.R., and Sultan M.A. (2003), "Effect of Temperature on Thermal Properties of High-Strength Concrete", *Journal of Materials in Civil Engineering*, 15(2), pp. 101-107.

86. Kodur V.R., Cheng F.P., and Wang T.C. (2003), "Effect of strength and fiber reinforcement on the fire resistance of high strength concrete columns", *ASCE Journal of Structural Engineering*, 129(2), pp. 253-259.

87. Kodur V.R., Dwaikat M.M.S., and Dwaikat M.B. (2008), "High Temperature Properties of Concrete for Fire Resistance Modeling of Structures", *ACI Material Journal*, 105(5), pp. 517-527.

88. Kodur V.R., Dwaikat M.B., and Raut, N. (2009a), "Macroscopic FE Model for Tracing the Fire Response of Reinforced Concrete Structures", *Engineering Structures*, in Press.

89. Kodur V.R., Pakala P., and Dwaikat M.B. (2009b), "Equivalent Fire Severity Approach for evaluating Fire Resistance of Reinforced Concrete Beams", Submitted to: *Fire Safety Journal.*

90. Kodur V. K. R., Wang T., and Cheng F. (2004), "Predicting the Fire Resistance Behavior of High Strength Concrete Columns", *Cement & Concrete Composites*, Elsevier Ltd., 26(2), pp. 141-153.

91. Kumar A. (2003), "Behaviour of RCC Beams after Exposure to Elevated Temperatures", *Journal of the Institution of Engineers (India): Civil Engineering Division*, 84(3), pp. 165-170.

92. Lau A., Anson M. (2006), "Effect of High Temperatures on High Performance Steel Fibre Reinforced Concrete", *Cement and Concrete Research*, 36, pp.1698-1707.

93. Lawson J.R., Phan L.T., and Davis F. (2000), "Mechanical Properties of High Performance Concrete After Exposure to Elevated Temperatures", *NISTIR 6475*, US.

94. Li M., Qian C.X., and Sun W. (2004), "Mechanical properties of high-strength concrete after fire", *Cement and Concrete Research*, Elsevier Ltd., 34(6), pp. 1001-1005.

95. Lie T.T., and Irwin R.J. (1993), "Method to Calculate the Fire Resistance of Reinforced Concrete Columns with Rectangular Cross-section", *ACI Structural Journal*, American Concrete Institute, 90(1), pp. 52-60.

96. Lie T.T., and Kodur V.R. (1995a), "Thermal Properties of Fibre-Reinforced Concrete at Elevated Temperatures", *IRC-NRC, Internal Report No. 683.*

97. Lie T.T., and Kodur V.R. (1995b), "Mechanical Properties of Fibre-Reinforced Concrete at Elevated Temperatures", *IRC-NRC, Internal Report No. 687.*

98. Lie T.T., and Kodur V.R. (1996), "Thermal and Mechanical Properties of Steel-Fibre-Reinforced Concrete at Elevated Temperatures", *Canadian Journal of Civil Engineering*, 23, pp. 511-517.

99. Lin T.D., Gustaferoo A.H., and Abrams M.S. (1981), "Fire Endurance of Continuous Reinforced Concrete Beams", *R&D Bulletin RD072.01B*, Portland Cement Association, IL, USA.

100. Lin T.D., and Ellingwood B. (1987), "Flexural and Shear Behavior of Reinforced Concrete Beams during Fire Tests", *NBS-GCR-87-536*, Portland Cement Association, IL, USA.

101. Meacham B.J., and Custer R.L.P. (1992), "Performance-Based Fire Safety Engineering: an Introduction of Basic Concepts", *Journal of Fire Protection Engineering*, 7(2), pp. 35-54.

102. Mindess S., Young J. F., and Darwin D. (2003), *Concrete*, 2nd Edt., Prentice Hall, Pearson Education Inc., Upper Saddle River, NJ 07458.

103. Morita T., Saito H., and Kumagai H. (1992), "Residual mechanical properties of high strength concrete members exposed to high temperature - part 1. Test on material properties", *Summaries of Technical Papers of Annual Meeting*, Architectural Institute of Japan, Niigata (in Japanese).

104. Nassif A. (2006), "Postfire full stress–strain response of fire-damaged concrete", *Fire and Materials*, 30, pp.323–332.

105. Naus D.J. (2006), "The Effect of Elevated Temperatures on Concrete Materials and Structures – A Literature Review", U.S. *Nuclear Regulatory Commission*, Office of Nuclear Regulatory Research, Washington, DC 20555-0001.

106. Nawy E.G. (2005), *Reinforced Concrete a Fundamental Approach*, 5th edition, Pearson Prentice Hall, NJ, USA.

107. NBCC (2005), "Fire and Structural Protection of Buildings", *National Building Code of Canada*, National Research Council, Canada.

108. Neves I. C., Rodrigues J. C., and Loureiro A. P. (1996), "Mechanical Properties of Reinforcing and Prestressing Steels after Heating," *Journal of Materials in Civil Engineering*, 8(4), 1996, pp. 189-194.

109. Neville A.M. (1996), *Properties of Concrete*, John Wiley & Sons, Inc., New York, USA.

110. Park C. K., Lee S. H., Kim G. D., and Lee H. K. (2007), "Effect of Tie Spacing and Section Size on Fire Resistance of High-Strength Concrete Column", *Concrete under Sever Conditions: Environment & Loading*, CONSEC'07, France.

111. Phan L.T. (1996), "Fire performance of high-strength concrete: A report of the state-of-the-art", *NISTIR 5934*, National Institute of Standard and Technology, Gaithersburg, MD.

112. Phan L.T. (2007), "Spalling and Mechanical Properties of High Strength Concrete at High Temperature", *Concrete under Sever Conditions: Environment & Loading*, CONSEC'07, France.

113. Phan L.T., Carino N.J. (2003), "Code Provisions for High Strength Concrete Strength - Temperature Relationship at Elevated Temperatures", *Materials and Structures*, 36(256), pp. 91-98.

114. Phan L.T., Lawson J.R., and Davis F.L. (2000), "Heating, spalling characteristics and residual properties of high performance concrete", *Fifteenth Meeting of the UJNR Panel on Fire Research and Safety*, Volume 2, NIST, USA.

115. Purkiss, J.A. (2007), "Fire Safety Engineering : Design of Structures", 2nd edition, Butterworth-Heinemann, UK.

116. Qian C., Wang H., Sun W., Guo Z., and Stroeven P. (2005), "Numerical calculations of vapor pressure in concrete exposed to fire", *Magazine of Concrete Research*, Thomas Telford Ltd., 57(3), pp. 179-184.

117. Saad M., Abo-El-Enein S. A., Hanna G. B., and Kotkata M. F. (1996), "Effect of temperature on physical and mechanical properties of concrete containing silica fume", *Cement & Concrete*, 26, pp. 669-675.

118. Sahota M.S., and Pagni P.G. (1979), "Heat and Mass Transfer in Porous Media Subjecte to Fire". *International Journal of Heat and Mass Transfer*, 22, pp. 1069-1081.

119. Saito H., Kumagai H., and Morita T. (1992), "Residual mechanical properties of high strength concrete members exposed to high temperature- Part 2. Test on reinforced concrete beams", *Summaries of Technical Papers of Annual Meeting,* Architectural Institute of Japan, Niigata.

120. Sanjayan G., and Stocks L. (1991), "Spalling of High Strength Concrete in Fire", *ACI Spring Convention*, Boston, MA.

121. Savva A., Manita P., and Sideris K.K. (2005), "Influence of elevated temperatures on the mechanical properties of blended cement concretes prepared with limestone and siliceous aggregates", *Cement & Concrete Composites*, Elsevier Ltd., 27(2), pp. 239 – 248.

122. Scheider U. (1988), "Concrete at High Temperatures – A General Review", *Fire Safety Journal*, 13, pp. 55-68.

123. Schneider U., and Herbst H.J. (1989), "Permeabiliteat und Prositaet von Beton bei hohen Temperaturen", *Deutscher Ausschuss fuer Stahlbeton*, 403, pp. 23-52.

124. SFPE (2004), "Fire Exposures to Structural Elements - Engineering Guide", Society of Fire Protection Engineers, Bethesda, MD, pp. 150.

125. Shi X., Tan T., Tan K., and Guo Z. (2004), "Influence of concrete cover on fire resistance of reinforced concrete flexural members", *Journal of Structural Engineering*, ASCE, 130(8), pp. 1225 – 1232.

126. Shin K.-Y. et al. (2002), "Thermo-Physical Properties and Transient Heat Transfer of Concrete at Elevated Temperatures", *Nuclear Engineering and Design 212*, pp. 233–241.

127. SPSS (2007), Polar Engineering and Consulting, Nikiski, AK 99635, USA.

128. Sullivan P.J.E. (2004), "A Probabilistic Method of Testing for the Assessment of Deterioration and Explosive Spalling of High Strength Concrete Beams in Flexure at High Temperature", *Cement & Concrete Composites*, Elsevier Ltd., 26(2), pp. 155 – 162.

129. Tenchev R., and Purnell P. (2005), "An application of damage constitutive model to concrete at high temperature and prediction of spalling", *International Journal of Solids and Structures*, Elsevier Ltd., 42(26), pp. 6550-6565.

130. Tenchev R.T., Li L.Y., Purkiss J.A., and Khalafallah B.H. (2001), "Finite Element Analysis of Coupled Heat and Mass Transfer in Concrete When It is in a Fire", *Magazine of Concrete Research*, Thomas Telford Ltd., 53(2), 2001, pp. 117-125.

131. Ulm F.J., Acker P., and Levy M. (1999), "Chunnel Fire. II: Analysis of Concrete Damage", *Journal of Engineering Mechanics*, 125(3), pp. 283-289.

132. Van Geem M.G., Gajda J., and Dombrowski K. (1996), "Thermal Properties of Commercially Available High Strength Concretes", *PCA R&D Serial No. 2031*, Portland Cement Association Skokie, IL, US.

133. Van Geem M. G., Gajda J., and Dombrowski K. (1997), "Thermal Properties of Commercially Available High Strength Concretes", *Cement, Concrete, & Aggregates*, 19, 38-53.

134. Wang Y.C., Wong P.M.H, and Kodur V.R. (2003), "Mechanical properties of fibre reinforced polymer reinforcing bars at elevated temperatures", *IRC – NRCC*, Report 46121.

135. William, B.B. (1990), *A first Course in the Finite Element Method*, Richard D. Irwin, INC., US.

136. Williams B.K. (2004), "Fire Performace of FRP-Strengthened Reinforced Concrete Flexural Memebers", *PhD Thesis*, Queen's University, Kongston, Ontario, Canada.

137. Witek A., Gawin D., Pesavento F., and Schrefler B.A. (2006), "Finite Element Analysis of Various Methods for Protection of Concrete Structures Against Spalling During Fire", *Computation Mechanics*, 39, pp. 271-292.

138. Xiao J., Xie M., and Zhang Ch. (2006), "Residual Compressive Behaviour of Pre-heated High-performance Concrete with Blast–furnace–slag", *Fire Safety Journal*, 41, pp. 91–98.